NON-LINEAR ANALYSIS OF INFILLED FRAMES

(PART TWO)

Vol 2.

By

Abolghasem Saneinejad

A

THESIS

Submitted to the Department of

Civil and Structural Engineering,

in partial fulfilment of the

requirements for the

Degree of

Doctor of Philosophy

UNIVERSITY OF SHEFFIELD

May, 1990

TABLE OF CONTENTS

PART ONE

CHAPTER 3 The Finite Element Technique 73

CHAPTER 5 Numerical Implementation and Programming

PART TWO

CHAPTER 6 Application of The Finite Element Analysis and Discussion 259

CHAPTER SIX

Application of The Finite Element Analysis and Discussion

6.1 Aims and Scope

This chapter deals with the analyse of a series of infill and frame combinations which are believed to be relevant for multi-storey buildings. For such analyses program 'NEPAL' has been used. As described in chapter 5, this program is written by the author particularly for the purpose of analysis of infilled frames emphasizing the requirements outlined in Table 2.2. The results of the analysis are presented in this chapter in a fairly detailed but concise fashion in order that useful discussions can be made.

6.2 Infill Size and Proportion

Fig 6.1 and Table 6.1 show the loading setup and the typical finite element subdivision layout and also the dimensions used in the analysis. As shown the infill consisted of a 140mm thick wall with three different sizes and proportions designated as; S for square, R for rectangular and B for big square. The finite elements along the boundary and within the corners of the wall were set smaller so that the high strain and stress gradients in the loaded corners can be simulated.

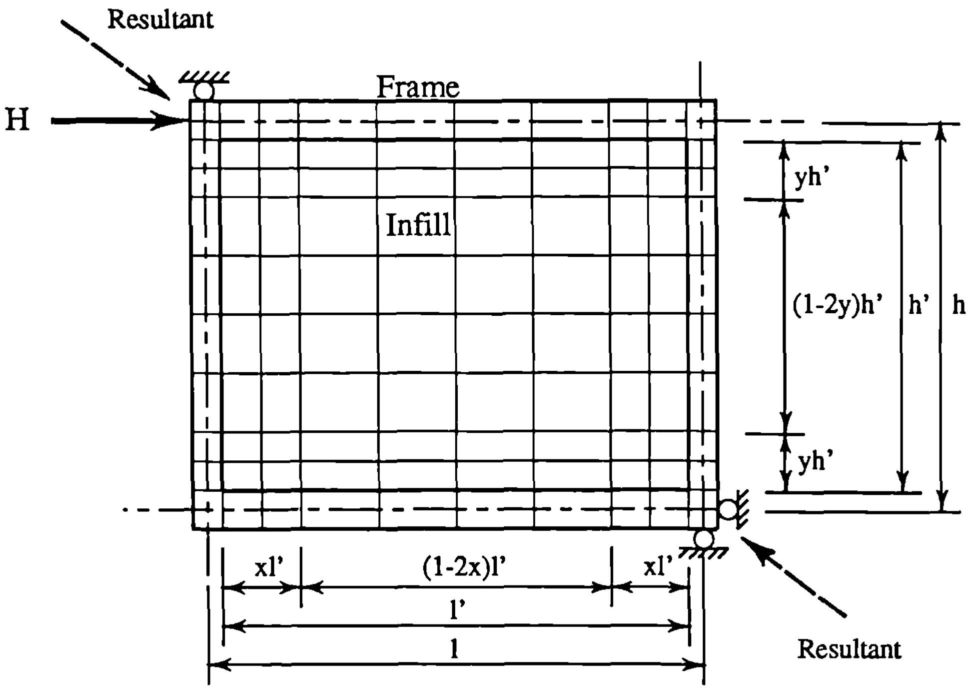

Figure 6.1 Infilled Frame under Diagonal Load

Table 6.1 F.E Subdivision and Dimensions of Infilling Walls

Infill Type	Length mm	Height mm	Thickness mm	Aspect Ratio	x/l' & y/h' Ratios
S	2709	2709	140	1.000	1/6
R	4743	2709	140	0.572	1/6
B	4743	4743	140	1.000	1/10

The frame, the infill and their interfaces were modelled using the newly developed beam, the 4-node isoparametric and the newly developed interface elements respectively. These elements are described in Chapter 3

6.3 Frame Members

Three types of beams and columns from the standard universal sections were chosen to represent weak, medium and strong beams and columns designated as 'W', 'M' and 'S' respectively. Table 6.2 summarizes the properties of these sections.

After running the program for a few infilled frames, it was found that the universal sections, alone, could not take the high shear forces developed in the loaded corners. Plasticity initiated at the centroid of the web well before the plastic resisting moment of the member has reached. Therefore adequate web stiffeners were combined with the standard universal sections. These arrangements are detailed in Table 6.2. The mechanical behaviour model of steel has been described in chapter 4.

6.4 Infill Material

The infill material was assumed to be uniform and proposed to have mechanical properties equivalent to those of blockwork, made of structural 140mm thick solid blocks with 15 N/mm2 nominal strength laid on designation (iii) mortar, BS5628. The assumed mechanical properties of infill are listed in Table 6.3. The mechanical behaviour model of the infill material has been described in chapter 4.

Table 6.2 Geometry and Mechanical Properties of Frame Members

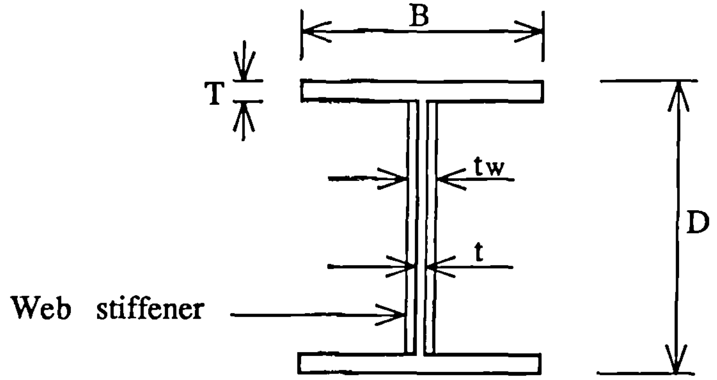

F_Y = 245 N/mm^2
E = 200 KN/mm^2

Main Section	Type	D mm	B mm	t mm	t_w mm	T mm	I cm^4	Z_e cm^3	Z_p cm^3	M_e KN.m	M_p KN.m	A cm
Beams												
UB 178x102x19	W	177.8	101.6	4.7	18.0	7.9	1797	202.1	254.5	49.5	62.4	45.25
UB 254x146x31	M	251.5	146.1	6.1	20.0	8.6	5852	465.4	579.7	114.0	142.0	71.99
UB 406x178x74	S	412.8	179.7	9.7	25.0	16.0	34151	1655	2047	405.4	501.6	152.7
Columns												
UC 152x152x23	W	152.4	152.4	6.1	30.0	6.8	1768	232	295.4	56.8	72.4	62.37
UC 254x254x73	M	254.0	254.0	8.6	35.0	14.2	13731	1081	1310	264.9	321.0	151.1
UC 356x368x177	S	368.3	372.1	14.5	40.0	23.8	63630	3455	4079	846.5	999.4	305.4

Table 6.3 Mechanical Properties of Assumed Infill Material

Initial modulus of elasticity,	E_o	18.5 KN/mm^2
Initial Poisson's ratio,	ν_o	0.175
Direct tencile strength,	σ_t	1.5 N/mm^2
Unconfined compressive strength,	σ_c	11.3 N/mm^2
Strain at peak unconfined uniaxial stress,	ε_c	0.00175
Factor A (see Section 4.5.3)		0.25
Factor R (see Section 4.6.4)		3.5
Factor $\overline{fbc}$ (see Section 4.5.2)		1.17
Co efficient of friction at crack surface		0.0
Crack dilatancy factor		1.5
Designated straining ratio at crushing		4.0

Table 6.4 Mechanical Properties of Frame-Infill Inteface

Normal stiffness	K_n	100000 N/mm^3
Shear stiffness	K_s	50000 N/mm^3
Tensile bond strength	σ_{tb}	0.05 N/mm^2
Shear bond strength	σ_{sb}	0.07 N/mm^2
Shear stiffness after debonding	K_{sru}	50 N/mm^3
Co efficient of friction	μ	0.64

6.5 Frame-Infill Interface

Table 6.4 lists the mechanical properties of the frame-infill interfaces. As seen these interfaces are given a very high shear and normal stiffness values , 50000 and 100000 N/mm3, when they are intact. When debonded they are assumed to have much lower shear stiffness, 50N/mm3, so that quick convergence can be achieved during deflection increments especially when a joint slip is involved. Considering the scale of the structure, this value is approximately equivalent to the value taken by Liauw[24] et al, Table 4.2. Taking higher values for shear stiffness did not make any significant change in the results, but slowed down the convergence of the solution .

No stiffness was allowed for a separated interface. The coefficient of friction of the interfaces was adopted from reference 77, Table 4.2. A fairly small bond strength was given to the interfaces, because infill normally loses its bond to the frame as a result of shrinkage and variation of temperature. The mechanical behaviour model of interfaces is discussed in chapter 4.

6.6 Infilled Frames Analysed

The following factors have been the major concerns in combining the frame and the infill for analysis.

i) Study of a group of infilled frames with the same beam but various column strengths.
ii) Study of the effect of the aspect ratio of the infill.
iii) Study of the effect of eliminating the frame-infill interface frictional resistance.

iv) Study of the effects of the relative stiffness and strength of the frame and the infill

Table 6.5 lists the chosen infilled frames for the analysis, based on the above needs. As seen all the infilling walls have been made of the assumed uniform material. Three frames with names ending with NF were analysed with assumption of no frictional strength and stiffness at the infill boundary interfaces.

The table also lists the values of stiffness and strength parameters defined by various authors; **λh** by Stafford Smith[12], **m** by Wood[20] and m1 to m3 by Liauw et al[25]. These parameters are described in chapter 2.

Table 6.5 Stiffness and Strength Parameters of The Infilled Frames Considered

Frame Type	i'/h'	λh	m_n	m	m_1	m_2	m_3
WMUR2, WMUR2NF	1.75	8.17	0.016	0.031	<u>0.154</u>	0.328	0.190
MMUR2,	1.75	4.90	0.031	0.068	0.276	0.378	<u>0.213</u>
SMUR2, SMUR2NF	1.75	3.34	0.031	0.068	0.433	0.378	<u>0.213</u>
SWUR2, SWUR2NF	1.75	3.25	0.013	0.027	0.417	0.250	<u>0.187</u>
WWUS2,	1.00	8.27	0.041	0.111	0.149	<u>0.143</u>	0.187
MWUS2	1.00	4.96	0.041	0.111	0.251	<u>0.143</u>	0.187
SWUS2	1.00	3.38	0.041	0.111	0.417	<u>0.143</u>	0.187
SSUS2,	1.00	3.65	0.329	1.266	0.496	0.406	<u>0.331</u>
WWUB2,	1.00	12.24	0.013	0.027	0.085	<u>0.082</u>	0.173

Notes;
Underlined m values denote the minimum values, ie the ones which applies in Liauw method
Letters conforming the Frame type name signify its column type, beam type, infill material and infill shape respectively from left to right as follows:
Column types; W= Week, M = Medium strength, S = Strong
Beam type; W= Week, M = Medium strength, S = Strong
Infill material; U = Uniform material (concrete), M = Masonry, O = Open(empty)
Infill shape; R = Rectangular, S = Square
Letters 'NF' at the end of a frame type denotes that the frame-infill interface is perfectly smooth, ie. no frictional stress develops at such interface.

6.7 Open Frames

In order to study the significance of the effects of the infill, the behaviour of the companion open frames needed to be studied.

Fig 6.2 shows a typical load deflection diagram resulting from finite element analysis of an open frame. As seen such a load deflection relation can be simulated by two straight lines representing the linear-elastic and perfect plastic behaviour of the frame material(steel).

Table 6.6 lists the elastic and plastic horizontal load capacity and also the corresponding deflections for the chosen frames resulting from the analysis. The designated names in this table contains 4 letters signifying column type, beam type, infill type (O=Open) and infill size and proportion listed in Table 6.5.

Table 6.6 also lists the calculated values of the horizontal load capacity of each frame using the limit analysis of plasticity[98]. As seen these values are fairly close to those obtained by the proposed finite element analysis . The computed plastic strength values, though, were about 5% lower than the computed ones. This may be due to the effects of shear and axial stresses and also the effect of the corner blocks which are ignored in the hand plastic analysis.

The open frame load-deflection diagrams are shown also in Figs 6.3 to 6.7 for the purposes of comparison with the load-deflection diagrams of the companion infilled frames.

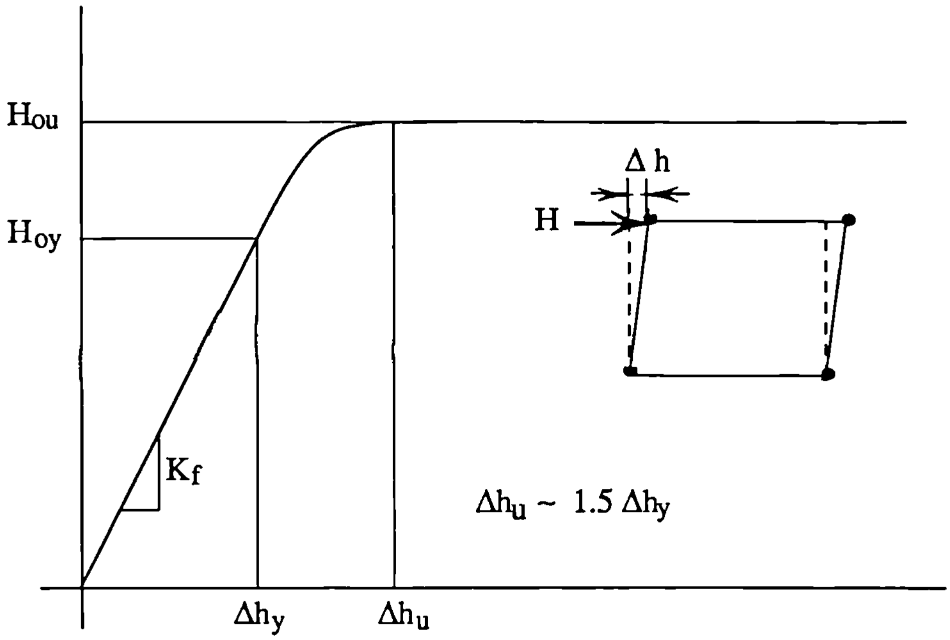

Figure 6.2 Typical Open Frame Load-Deflection Diagram

Table 6.6 Elastic and Plastic Horizontal Load Capacity of Open Frames

Frame	Finite Element				Limit Analysis	
	Δh_y mm	H_{oy} KN	H_{ou} KN	K_f KN/mm	H_{oy} KN	H_{ou} KN
WMOR2	36.33	86.9	102.3	2.4	84	107
MMOR2	30.64	165.8	192.2	5.41	168	209
SMOR2	24.68	166.3	199.7	6.74	168	209
SWOR2	32.56	76.7	88.1	2.35	73	92
WWOS2	38.3	72.8	86.8	1.90	73	92
MWOS2	22.0	78.5	90.0	3.57	73	92
SWOS2	18.52	79.9	94.0	4.31	73	92
SSOS2	16.85	607.2	707.0	36.03	598	740
WWOB2	115.3	43.5	50.0	0.38	42	52.6

N.B. In the Limit analysis of plasticity, $H_{ou} = 4\,Mp/h'$ and H_{oy} may be approximated as $H_{ou}\,Me/Mp$

6.8 Infilled Frames

6.8.1 General

This section deals with the presentation of the finite element analysis results for the horizontally loaded single bay infilled frames listed in Table 6.5. The frames were loaded monotonically using the deflection increment approach. As shown in Fig 6.1, the loading set up was so arranged that becomes equivalent to the diagonal loading.

The results generally consisted of the load-deflection and also the force and stress distribution diagrams within various parts of the structure at marked stages. Such results are classified and described in the following subsections.

6.8.2 Load-Deflection Diagrams

Figs 6.3 to 6.7 show the load-deflection diagrams of the infilled frames. The companion open and no-friction infilled frames are also shown in these figures in order that a direct comparison is possible. The term no-friction used here, refers to the same frame with assumption of perfectly smooth frame-infill interface, i.e. $\mu=0$. Full results are reported by the program at nominated stations in the analysis. These are described below and are indicated in Figs 6.3 to 6.7.

i) The point signified by "1" is defined to correspond approximately to 50% of the peak load. At this load stresses neither in the frame nor in the infill have reached the peak values, but separation and slip has occurred along significant parts of the frame-infill interface. This load level may also be considered as representing the maximum likely load occurring during the service usage of the structure.

ii) The point signified by "2" indicates the station at or close to the onset of the infill diagonal cracking.

iii) The points signified by "3", "4" and "5" refer to the station at or close to the peak, post peak and a point well beyond the peak load respectively.

In addition, the key events in the response are indicated as follows:

i) I refers to the load at which the infill material experiences the peak stress level in one or both loaded corners.

ii) F refers to the load at which frame initiates plasticity.

iii) C refers to the onset of diagonal cracking.

Figs 6.3 to 6.7 do not show the complete diagrams for open frames, because the deflection scale was set to suit the infilled frames deflection. The complete open frame load deflection diagrams can be determined from Tables 6.6 and Fig 6.2.

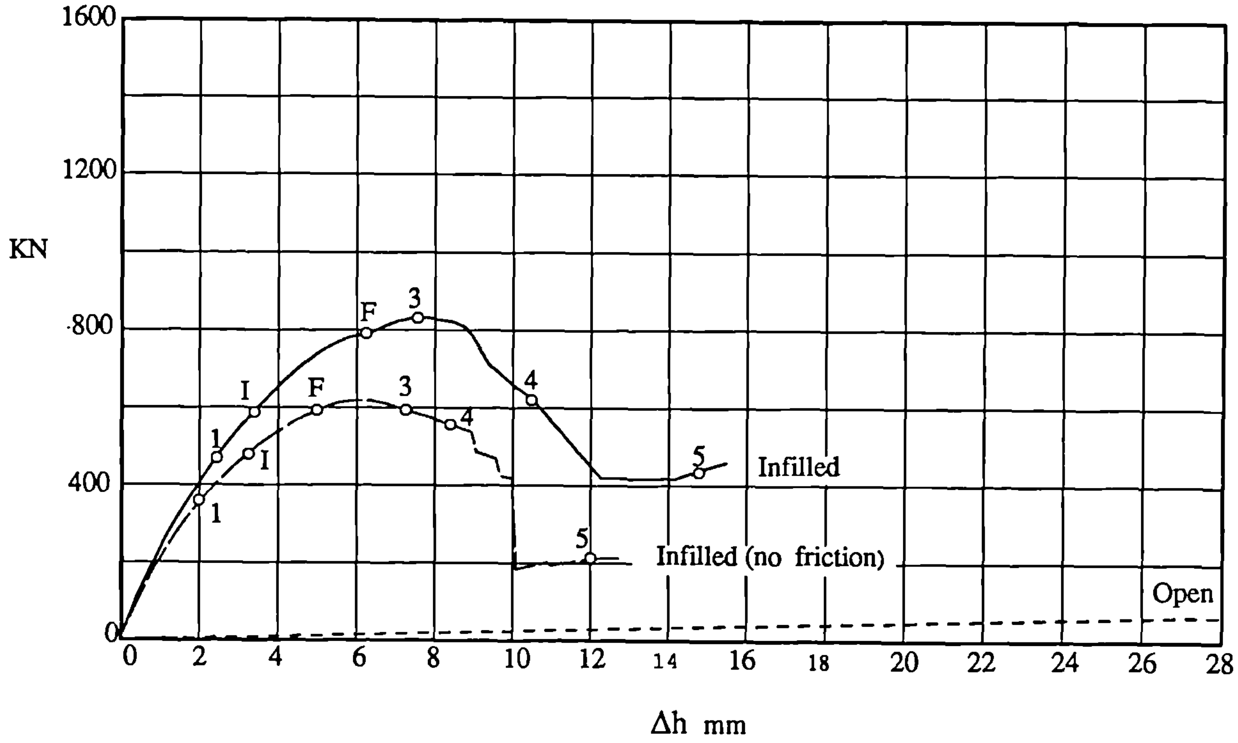

(a)

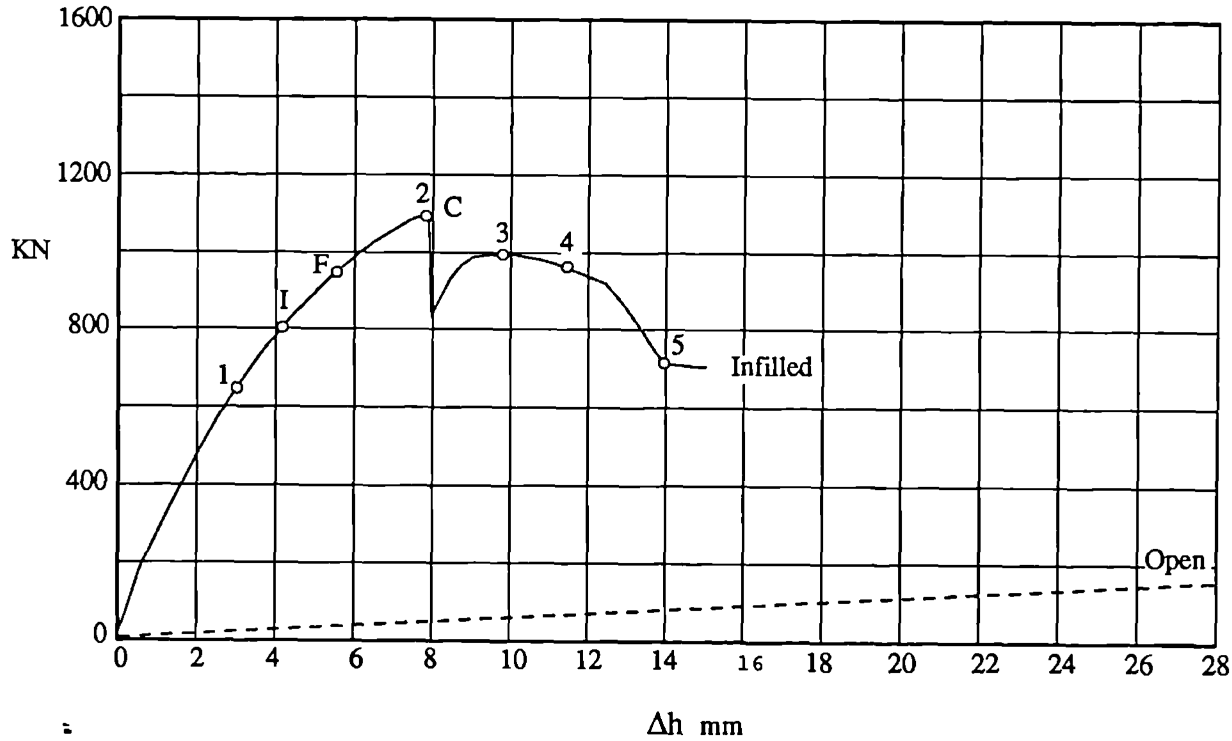

(b)

Figure 6. 3 Load-deflection Diagrams, Results of F.E Analysis;
a) Frames WMUR2 and WMUR2NF, b) Frame MMUR2

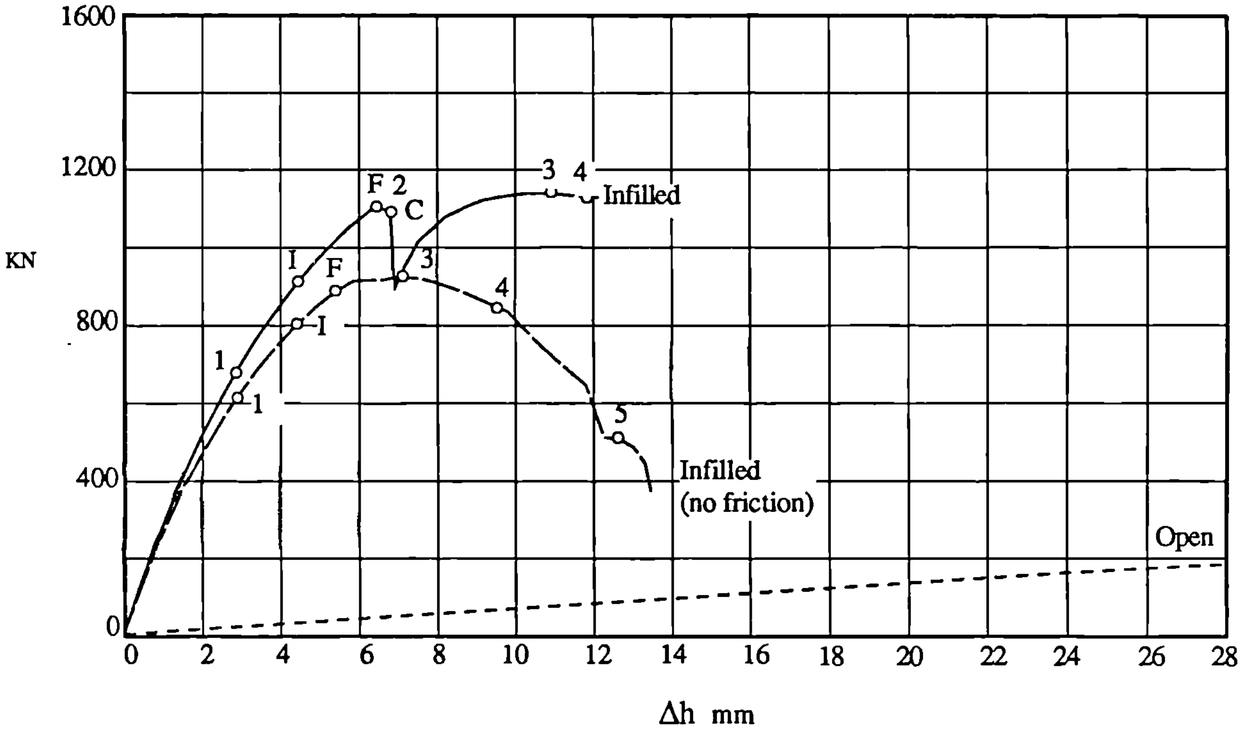

(a)

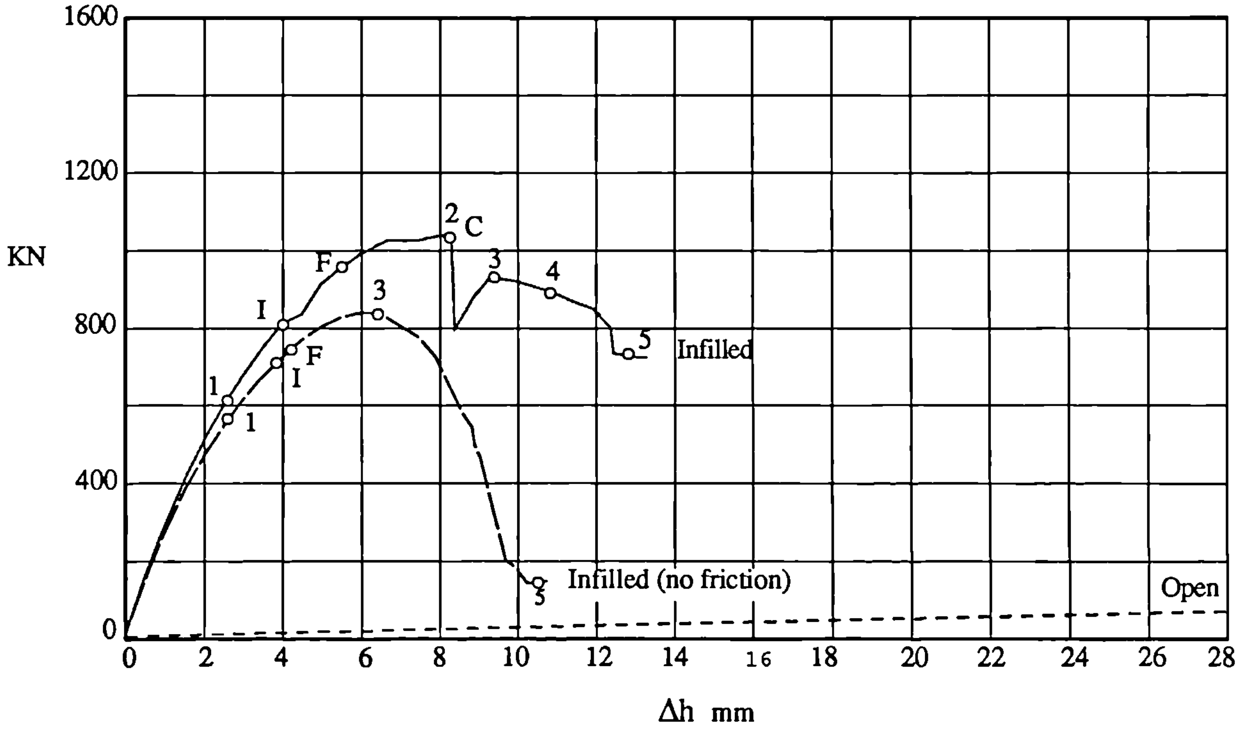

(b)

Figure 6.4 Load-deflection Diagrams, Results of F.E Analysis;
a) Frames SMUR2 and SMUR2NF, b) Frames SWUR2 and SWUR2NF

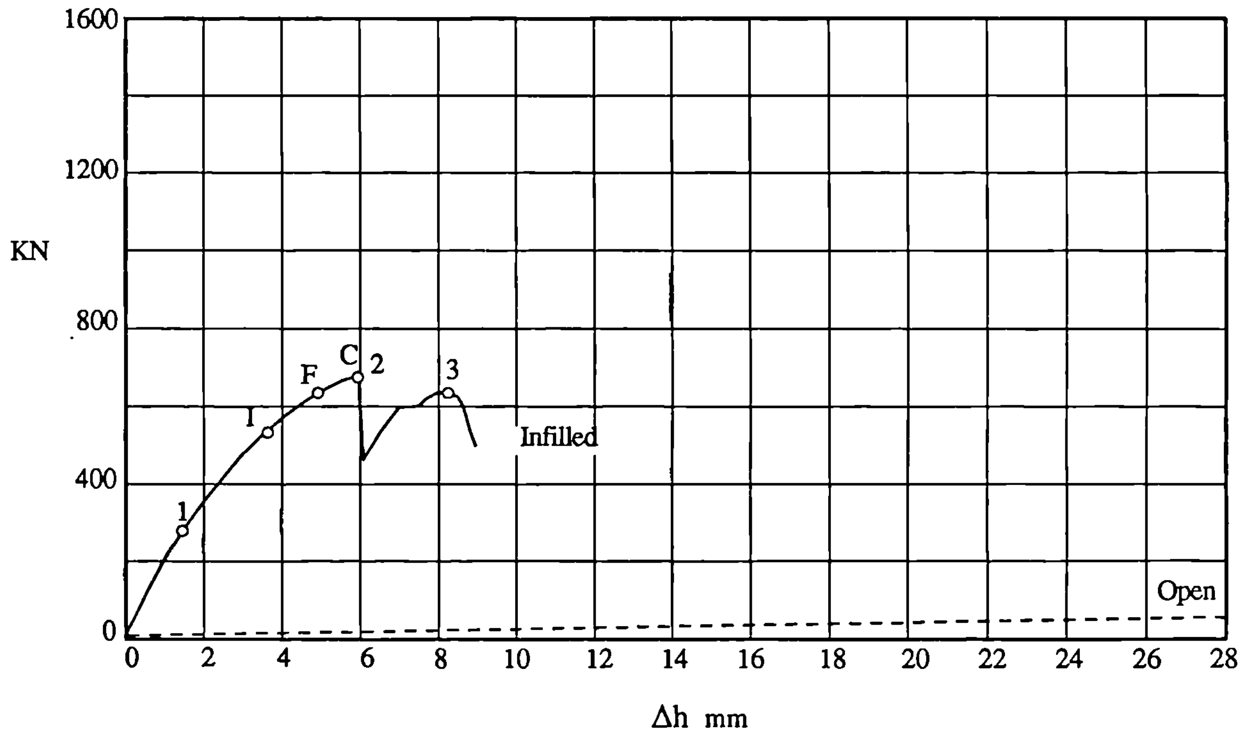

(a)

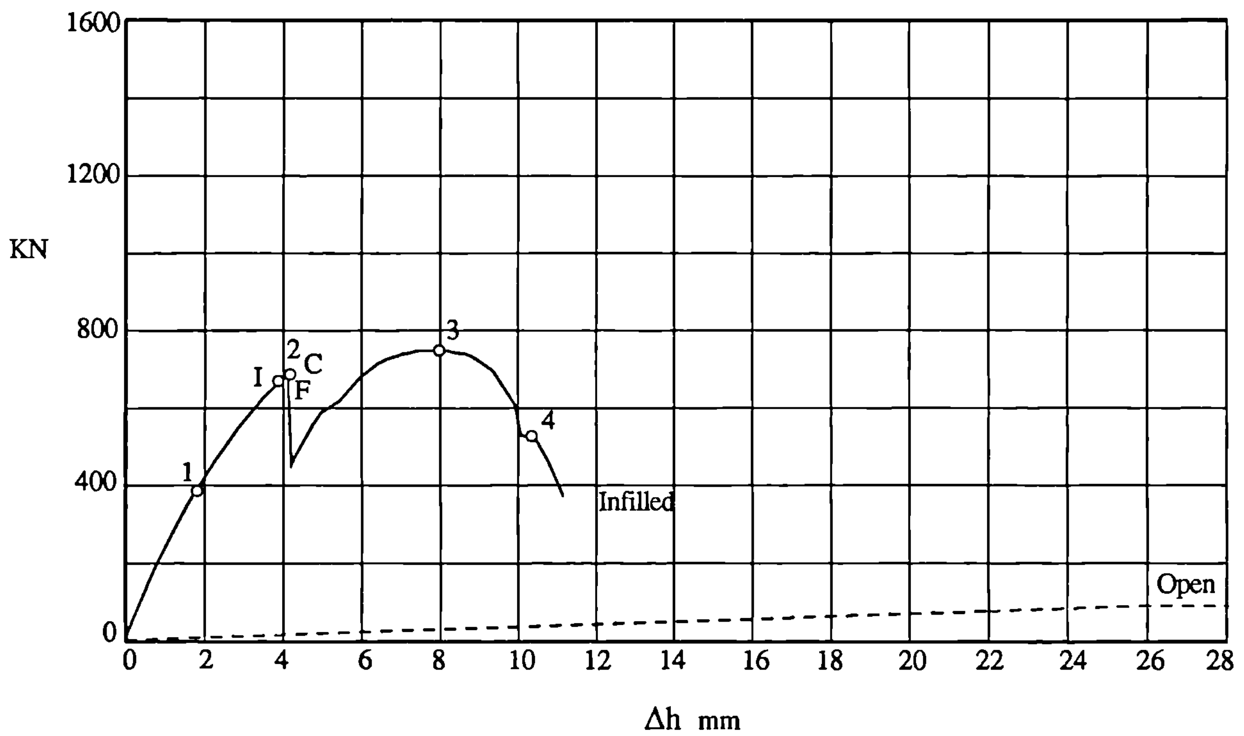

(b)

Figure 6.5 Load-deflection Diagrams, Results of F.E Analysis;
a) Frame WWUS 2 b) Frame MWUS 2

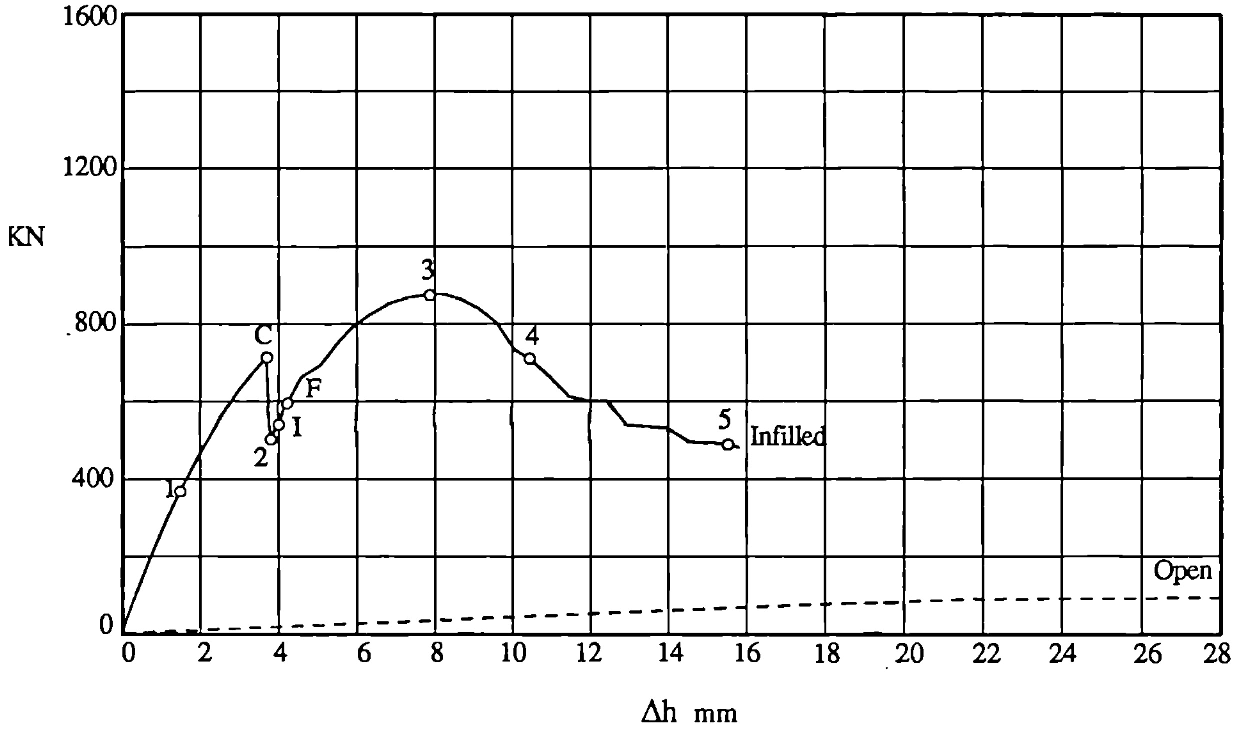

(a)

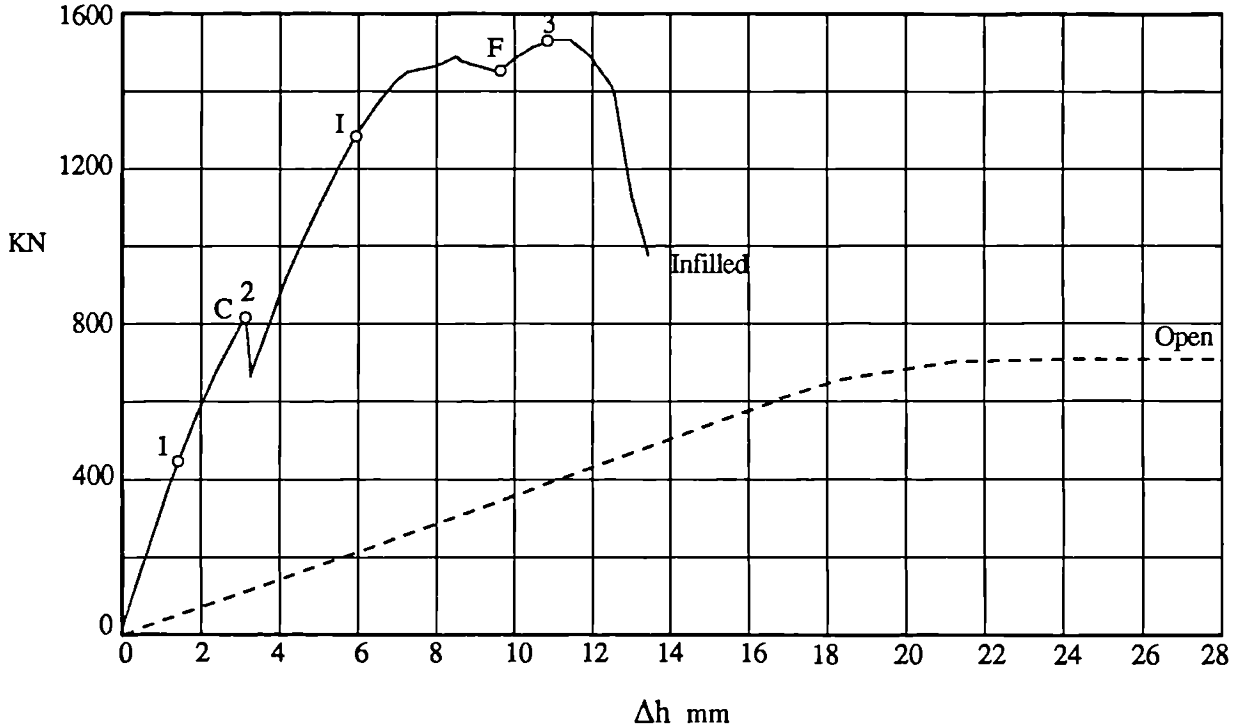

(b)

Figure 6.6 Load-deflection Diagrams, Results of F.E Analysis;
a) Frame SWUS2, b) Frame SSUS2

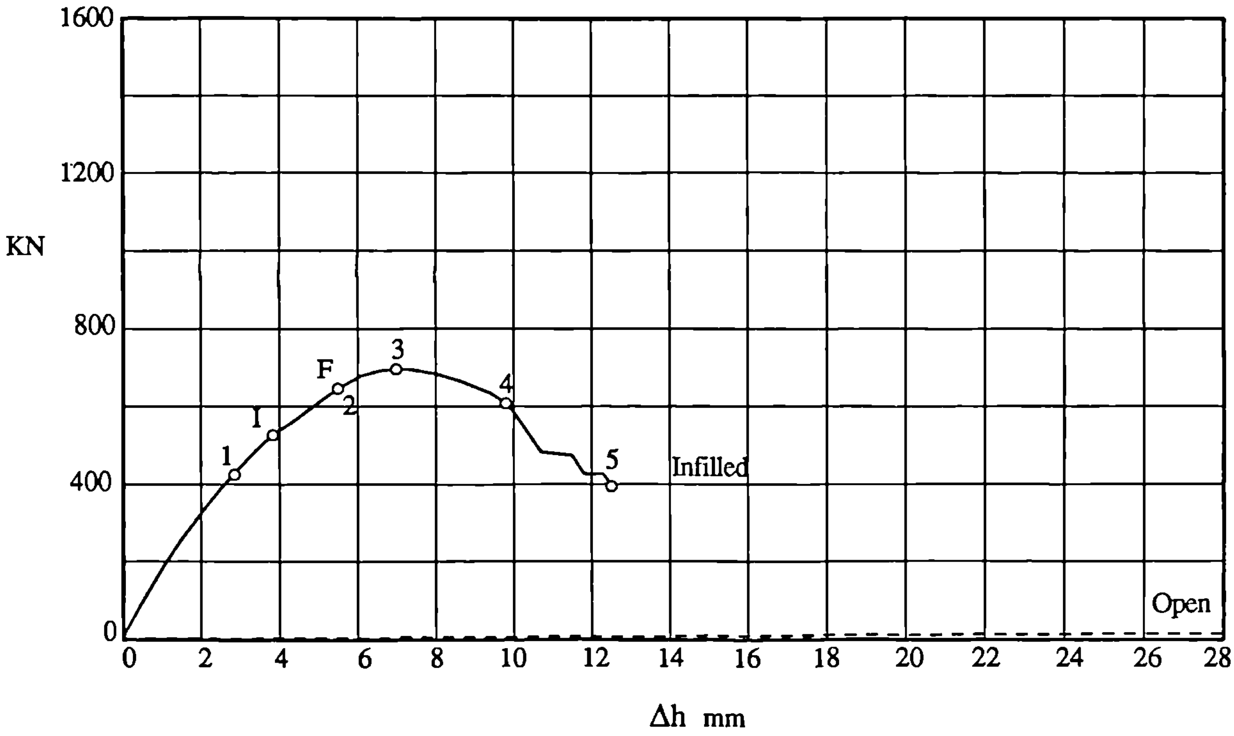

Figure 6.7 Load-deflection Diagrams, Results of F.E Analysis; Frame WWUB2

6.8.3 Frame Forces

Beams and columns were subjected to thrust, shear and bending moment. As shown typically in Figs 6.8(a) and 6.9(a) these forces were generally concentrated in the loaded corners. These figures refer to infilled frame MMUR2 at stations 1 and 3. i.e. at service and the peak loads respectively. The complete results for all the marked stations and for all the frames analysed are given in Appendix E.

6.8.4 Infill Stresses

The infills were subjected to biaxial compression concentrated in the loaded corners. The central area of the infills were, however, subjected to biaxial tension-compression.

Figs 6.8(b) and 6.9(b) show the infill principal stress contours before and after diagonal cracking, i.e. at stations 1 and 3 respectively.

Tables E.1 to E.12 in Appendix E summarize the stress values in the loaded corners and also at the centre of the infill at various stations for infilled frames analysed.

6.8.5 Frame-Infill Interaction

In all the frames analysed, frame-infill separation occurred at very early stages of loading. Contact, however remained in the loaded corners. The length of contact rapidly increased as either the non-linearity started within the infill, or plasticity initiated in the frame. This can be seen by comparing Fig 6.8(b) with Fig 6.9(b) which show the frame-infill contact stress distribution diagrams for frame MMUR2 at the service and peak loads. The complete results for all the chosen stations are given in Tables E.1 to E.12 in Appendix E for all the frames analysed.

The analyses showed that all the infilled frames developed considerable shear forces at the frame-infill interfaces in contact.

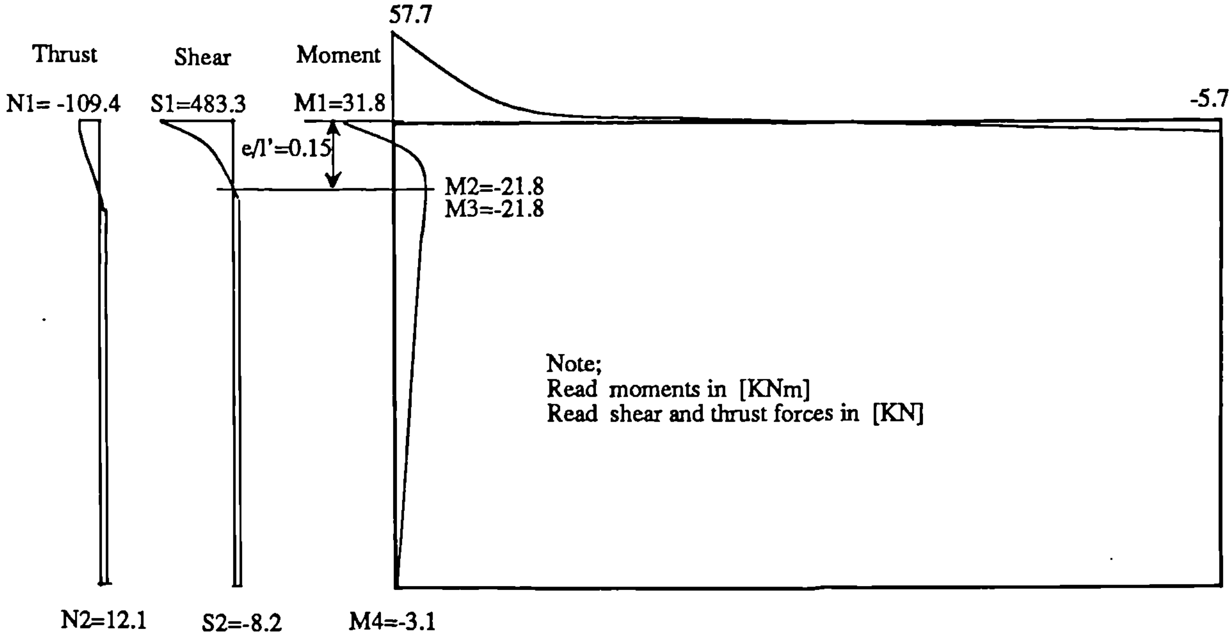

(a)

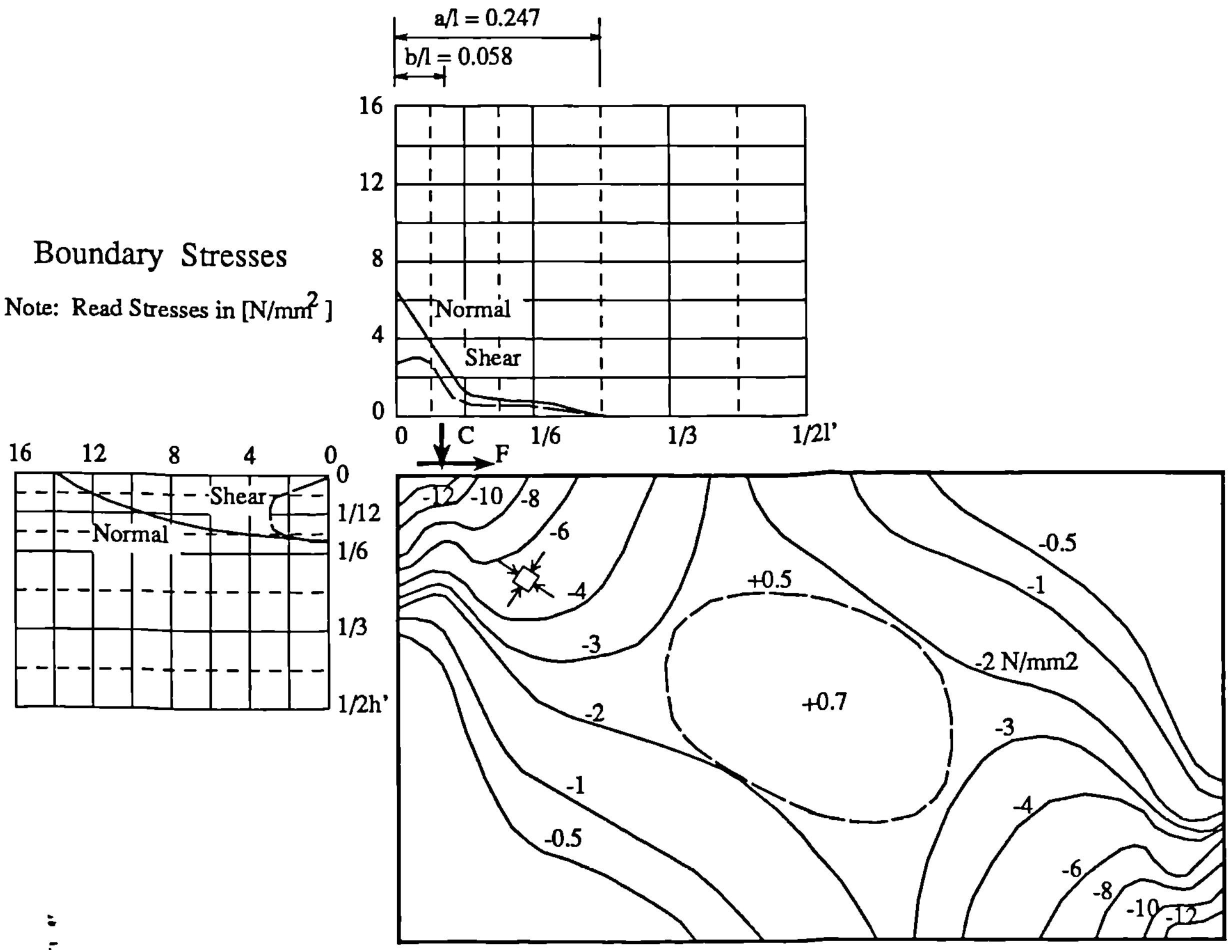

(b)

Figure 6.8 F.E Analysis Results of Infilled Frame 'MMUR2' at Working Stress Load level: (a) Frame Forces, (b) Infill Boundary and Internal Stresses.

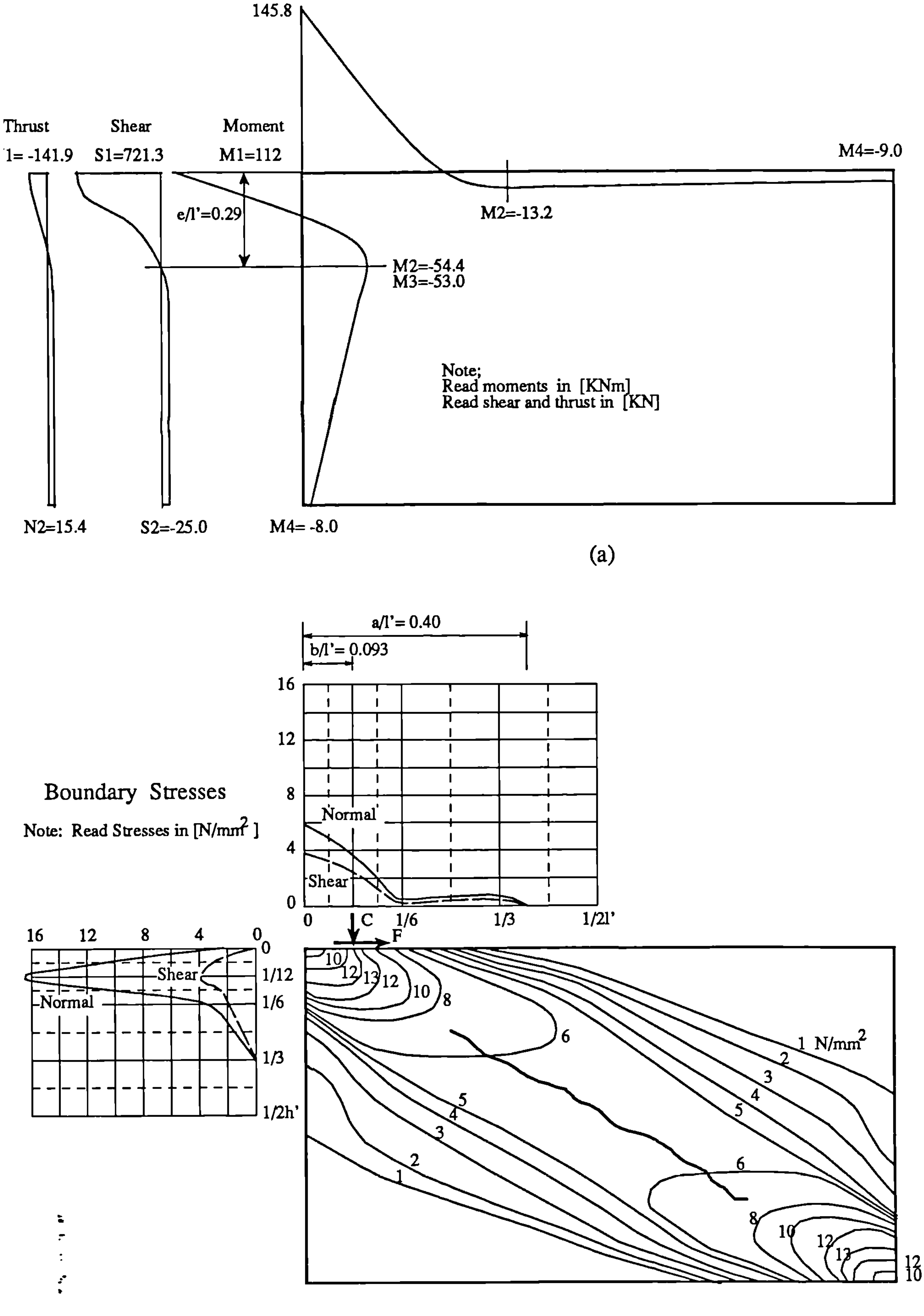

Figure 6.9 F.E Analysis Results of Infilled Frame 'MMUR2' at Peak Load : (a) Frame Forces, (b) Infill Boundary and Internal Stresses.

6.9 Discussion of Overall Behaviour of Infilled Frames

6.9.1 General

The graphical representations given in Section 5.5.5 and the results obtained from the finite element analyses, Tables E.1 to E.12, showed that apart from the state of the infill, the state of the frame can be classified with relation to the generalized load-deflection characteristics shown in Fig 6.10(a). These states are described in the following sections.

6.9.2 Elastic State

Up to a load close to the peak load the frame behaves in an elastic manner while the infill becomes non-linear in the loaded corners and remains linear elastic in the rest of the area. Infill/frame separation occurs, but contact remains at the loaded corners of the infill both at the beam and column interfaces. Normal stress at these interfaces increase as the diagonal load increments to higher levels. The length of contact and also the offset of the resultant of the normal stress, **b/h'**, remains nearly constant, Fig 6.10(b).

6.9.3 Elastoplastic State

As the load increases, the frame initiates plasticity at the loaded corners at a load close to the peak load. The position of this event on the load deflection diagrams is designated by letter F, Fig 6.10(a). From this point on, the state of the infilled frame can be called "Elastoplastic". Increasing further the load, leads to strain softening in the loaded corners of the infill and formation of two plastic hinges at the loaded corners of the frame followed by plastic rotation at these points. This trend continues up to point P on the load deflection diagram designating the peak load. The load-deflection diagram, Fig 6.10(a), thence follows a falling branch through to much higher deflections accompanied by infill crushing and increase in **b/h'** and also increase in the frame sagging (or hugging) bending moments.

6.9.4 Plastic State

Because difficulties arose in achieving convergence due to excessive non-linearities occurring in the materials, the finite element analyses were halted at a deflection about twice that at the peak load. However, the trend of the changes in the frame bending moments indicates formation of new plastic hinges at the unloaded corners and perhaps in the members of the frame, at a higher deflection. Formation of these additional plastic hinges turns the frame into a plastic collapse mechanism by which it would undergo perfect plasticity. This state can be referred to as the plastic state. Strong frames with weak infill also may eventually develop a load even higher than the initial peak load as shown in Fig 6.10(a). Such a case was not encountered in this work, but occurred in the tests carried out by Saneinejad(29) for an infilled frame with extremely strong frame.

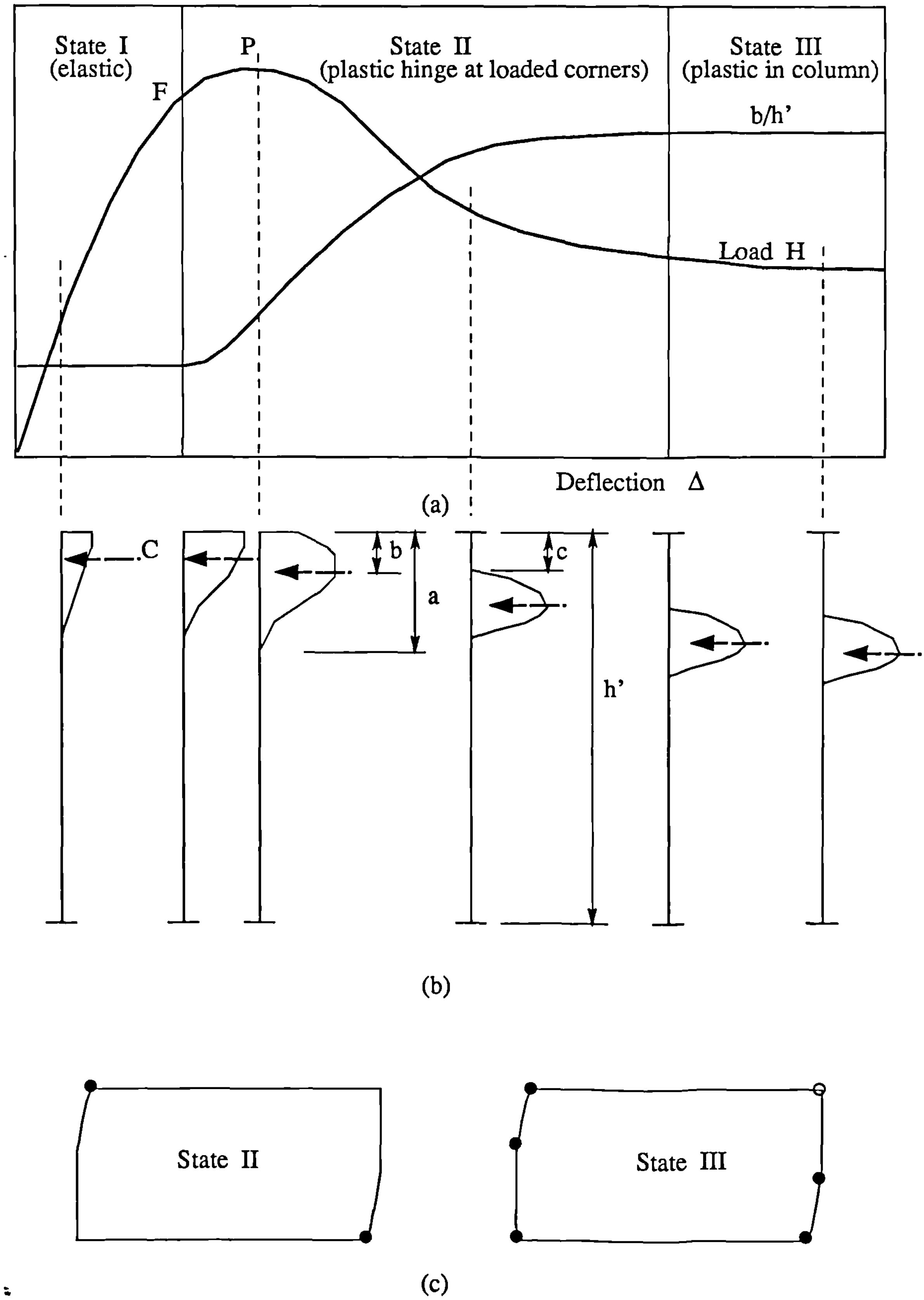

Figure 6.10 Typical Failure Stages of infilled Frames under Racking
a)Load-deflection Diagram (not to scale), b)Infill /Column interaction ,
c)Plastic hinge Development at different states.

6.9.5 Some Exceptions for Strong Frames

Infilled frames with adequately strong frame relative to the infill, may finally develop four plastic hinges at the corners. In this case the falling branch of the load-deflection diagram becomes rather sharp, as shown in Fig 6.6(b). The only example exhibiting this behaviour was the infilled frame SSUS2.

6.9.6 Comments

Stress in the loaded corners of the infill, while in the elastic state, can reach the compressive strength whereas the maximum stress within the frame at the same load level, is still below the yield point. This indicates that the repetition of a load as low as perhaps 70% of the peak load may lead to gradual deterioration of the infill at the loaded corners. This necessitates further tests or analysis allowing for cycling loads.

6.10 Discussion on Normal Force at Frame-infill Interface

6.10.1 General

The frame-infill normal stress diagram over the length in contact, had no consistent shape. Therefore it was decided to characterize its shape by an equivalent rectangular stress block so that the equivalent normal stress, σ_{nc} or σ_{nb}, and also the length of the equivalent stress block , $2b_c$ or $2b_b$ respectively, can be calculated. Table 6.7 lists these values for all the frames analysed. The factors affecting the equivalent stress block are described in the following sections.

Table 6.7 Normal Stress Distribution at Infill-frame Interface

$\sigma_{nc} = C_c/(2b_c t)$

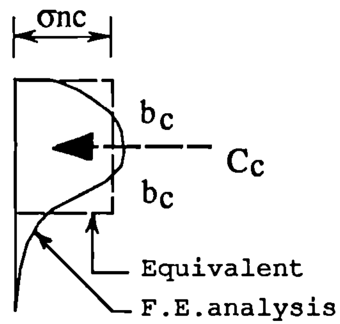

Column

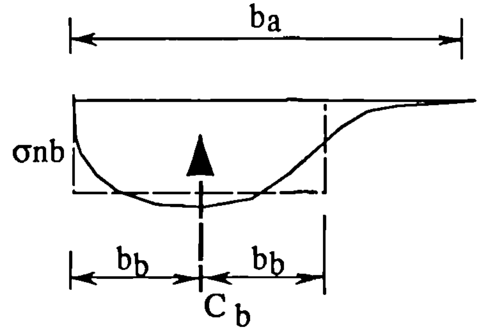

Beam

Frame	Column					Beam				
	C_c	a_c/h'	b_c/h'	σ_{nc}		C_b	a_b/l'	b_b/l'	σ_{nb}	σ_{nb0}
	KN			f.e	Eq7.13	KN			f.e.	Eq7.13
WMUR2*	568.3	0.126	0.067	11.2	10.6	398.1	0.424	0.075	4.00	7.57
MMUR2*	796.5	0.187	0.094	11.2	"	497.2	0.290	0.070	5.35	"
SWUR2*	900.1	0.19	0.10	11.7	"	351.9	0.112	0.041	6.47	"
MMUR2	746.3	0.33	0.10	9.6	"	447.9	0.402	0.093	3.60	"
SMUR2	1021.7	0.472	0.152	8.9	"	469.4	0.329	0.088	4.00	"
SWUR2	899.3	0.489	0.13	8.5	"	335.1	0.176	0.054	4.70	"
WWUS2*	420.8	0.145	0.06	8.7	7.57	429.8	0.161	0.068	8.33	"
WWUS2	414.2	0.162	0.085	6.4	"	416.0	0.496	0.098	5.60	"
MWUS2	540.4	0.747	0.116	6.1	"	419.7	0.381	0.098	5.60	"
SWUS2	728.0	0.523	0.142	6.8	"	400.9	0.300	0.099	5.30	"
SSUS2	925.4	0.547	0.295	4.1	"	1023.9	0.506	0.208	6.50	"
WWUB2	424.3	0.083	0.039	8.2	"	430.2	0.090	0.042	7.7	"
WMUR2NF	610.3	0.093	0.06	13.4	11.3	409.8	0.231	0.062	4.99	11.3
SMUR2NF	1038.9	0.289	0.109	12.6	"	524.7	0.162	0.057	6.94	"
SWUR2NF	948.0	0.199	0.093	13.4	"	475.0	0.090	0.035	10.23	"

* Maximum load occured at diagonal cracking load or infill did not crack.

6.10.2 Effect of Infill Aspect Ratio

Square infills developed almost equal normal stress at the interfaces with the beams and columns. Rectangular infills, however, transferred much of the resulting diagonal force to the columns rather than to the beams. This is because the projection of such a diagonal force on the normal of the column is greater than that of the beam. But the straight forward rule of dividing the diagonal force into components acting to the beam and column did not agree with the finite element analysis results.

6.10.3 Effect of Beam to Column Strength Ratio

As shown in table 6.7, variation of the equivalent normal stress at the beam interface, σ_{nb}, was strongly dependent on the beam/column strength ratio. However, the normal stress at the column interface, σ_{nc}, was almost unaffected by the beam/column strength ratio for both the square and rectangular infills.

6.10.4 Effect of Frame/Infill Strength Ratio

As seen in table 6.7, this parameter did not affect the normal stress at column interface σ_{nc}, but it had a significant effect on the normal stress at the beam interface, σ_{nb}. The length of the stress block, **2b**, increased as the strength of the adjacent frame member increased.

6.10.5 Effect of Diagonal Cracking

Diagonal cracking rapidly increased the lengths of contact, a_c and a_b, thus reducing by approximately 30% the equivalent normal stresses, σ_{nc} and σ_{nb} respectively, while the total normal forces at the interfaces remained almost constant. This can be verified by comparing the results of the identical frames, with and without an "*" in Table 6.7.

6.10.6 Effect of Coefficient of Friction

As seen in Table 6.7, the no-friction infilled frames developed significantly higher normal stresses both at the column/infill and at the beam/infill interfaces. This was much more effective for rectangular frames.

6.11 Discussion on Shear Force at Frame-infill Interface

All the infilled frames analysed were assumed to have a coefficient of friction, μ, equals to **0.64** at the frame-infill interfaces. The resulting total normal and shear forces acting to each frame member at the peak load, **C** and **F** respectively taken from Tables E.1 to E.12, are summarized in Table 6.8. Also listed in this table are the results of the analyses of three no-friction infilled frames for comparison.

Like the normal forces, the frictional forces are also dependent on infill aspect ratio, beam/column strength ratio, frame/infill strength ratio and infill cracking. It was found convenient to study the frictional forces only in relation to their corresponding normal forces leading to the following conclusions.

i) State of the beam-infill interface remains slipping, thus the maximum possible shear develops at the beam-infill interface. i.e:

$$F_b = \mu C_b \tag{6.1}$$

As seen in Table 6.8 this relation agreed with all the rectangular infilled frame analysis results with up to only 1% difference. However, for square infills the differences varied between 0 to 10%.

ii) Shear force at the column interface is strongly dependent on the aspect ratio of the infill. The following relation was found to be simple and also reasonably accurate for predicting the shear force at the infill-column interface:

$$F_c = \mu \left(\frac{h'}{l'}\right)^2 C_c \tag{6.2}$$

As shown in table 6.8, this relation gives F_c between 0 to 16% lower than the results obtained for rectangular infills and 0 to13% higher than the results obtained for square infills.

Analysis of frame SSUS2 led to a fairly high infill-column length of contact as a result of the high frame strength and stiffness. The frictional force at the column, F_c, was 32% less than given by Eq 6.2. As will be seen in Chapter 7 this discrepancy will be rectified by reducing the μ value to satisfy the equilibrium conditions preventing infill rigid body rotation.

Table 6.8 Shear Transferred at Frame-infill Interface

Frame	Column			Beam		
	Cc	Fc [KN]		Cb	Fb [KN]	
	[KN]	F.E	Eq 6.2	[KN]	F.E	Eq 6.1
WMUR2*	568.3	141.5	119.1	398.1	254.3	254.8
MMUR2*	796.5	186.8	167.0	497.2	317.8	318.2
SWUR2*	900.	218.0	188.6	351.9	225.0	225.2
MMUR2	746.3	157.3	156.4	447.9	286.5	286.6
SMUR2	1021.7	213.3	214.1	469.4	299.8	300.4
SWUR2	899.3	194.3	188.5	335.1	197.4	214.4
WWUS2	420.7	256.4	269.2	429.7	260.0	275.0
WWUS2	414.2	245.7	265.1	416.1	259.0	266.3
MWUS2	540.4	317.8	345.9	419.7	267.8	268.6
SWUS2	728.0	414.0	465.9	400.9	255.7	256.6
SSUS2	925.4	402.7	592.3	1023.9	621.0	655.3
WWUB2	424.3	268.4	271.6	430.2	272.0	275.3
WMUR2NF	610.3	0	0	409.8	0	0
SMUR2NF	1038.9	0	0	528.7	0	0
SWUR2NF	948.0	0	0	475.0	0	0

*Maximum load occured at diagonal cracking load or

6.12 Discussion on Infill Stress Distribution

6.12.1 General

Figs 6.8(b) and 6.9(b) show the infill stress contours for infilled frame MMUR2 at the working stress and at the peak loads respectively. As shown, two distinct stress combinations can be pointed out, typically, in the regions described in the following sections.

6.12.2 Loaded Corners

The loaded corners are subjected to highly variable biaxial compression extending over the area surrounded by the beam and column lengths of contact.

The ratio of the minor to major principal stress at the critical points within these regions, increases as the infill gradually becomes non-linear and the state of the infilled frame becomes elastoplastic. As shown in Tables E.1 to E.12, this ratio was between 0.2 to 0.4 for the critical points of the region at the peak load. These ratio limits together with the experimental results of helmut Kupfer[55], the Von Mises criterion and the proposed criterion, Eq4.31 are shown in Fig 6.11. As can be seen the peak of the most compressive principal stress must be at least 15% higher than the unconfined uniaxial compressive strength.

All the frames analysed in this study collapsed eventually as a result of failure of the infill material in the loaded corners. The straining ratio of infill (defined as the ratio of the biaxial strains at the most critical point in the loaded corner, to the biaxial strains corresponding to the biaxial peak stresses) may be interpreted as the degree of plasticity occurring in the infill at the peak load. As shown in Tables E.1 to E.12 this ratio was 2.2 to 2.6, for all the frames studied, except frame SSUS2, in which the above ratio was 1.43. This particular infilled frame had a very strong frame and consequently long lengths of contact at the beam and column interfaces.

6.12.3 Central Region

The central region of infill is subjected to nearly uniform biaxial tension and compression, directed nearly normal and parallel to the loaded diagonal of the infill respectively, Fig 6.8(b). The infill material behaves in linear elastic manner within this region.

The ratio of compressive to tensile principal stress remains almost constant during the process of loading until the onset of a diagonal cracking, Fig 6.9(b). As can be seen in Tables E.1 to E,12 and also Table 6.9, this ratio ranged from 2.44 to 3.57 for the frames analysed. The limits of this ratio are mapped on the biaxial stress coordinates together with the failure criteria of concrete as shown in Fig 6.11. It is interesting to note that because of the similarity of the behaviour the ratio of biaxial stresses at the centre of a concrete cylinder specimen subjected to the standard splitting test[39], also falls within the above fairly limited range. Therefore this standard test suits best examining the tensile failure of infill, i.e:

$$\sigma_1 \text{(at the cracking load)} = \text{tensile splitting strength}$$

The load deflection diagrams, Figs 6.3 to 6.7, show that the infill cracking load must not be considered as the ultimate load, but rather a load limit for serviceability considerations. This is because a diagonally cracked infill may withstand higher lateral loads through the diagonal struts formed after cracking.

Comparison of the load-deflection diagrams leads to the conclusion that the infill cracking load is not much affected by the frame strength but rather depends on the geometry and strength of the infill. As seen in Figs 6.3 to 6.6 and also as experimentally observed by Saneinejad[29], diagonal cracking is sudden, inducing an abrupt deflection.

Table 6.9 Stress Combination at Centre of Infill Resulted from Finite Element Analysis

Fram	σ	σ2	-σ1/σ2	σ1/σt
WMUR2	1.32	- 4.35	3.29	0.88
MMUR2	1.37	- 3.68	2.69	0.91
SMUR2	1.36	- 3.64	2.68	0.91
SWUR2	1.30	- 4.65	3.57	0.87
WWUS2	1.36	- 3.58	2.63	0.91
MWUS2	1.36	- 3.55	2.61	0.91
SWUS2	1.30	- 3.96	3.05	0.87
SSUS2	1.35	- 3.88	2.87	0.90
WWUB2	1.31	- 3.20	2.44	0.87

σ1 and σ2 denote the tensile and compressive principal stresses respectively. These stresses have been adapted from Tables 6.7 to 6.18 and adjusted to correspond Diagonal-cracking Load of the infill.

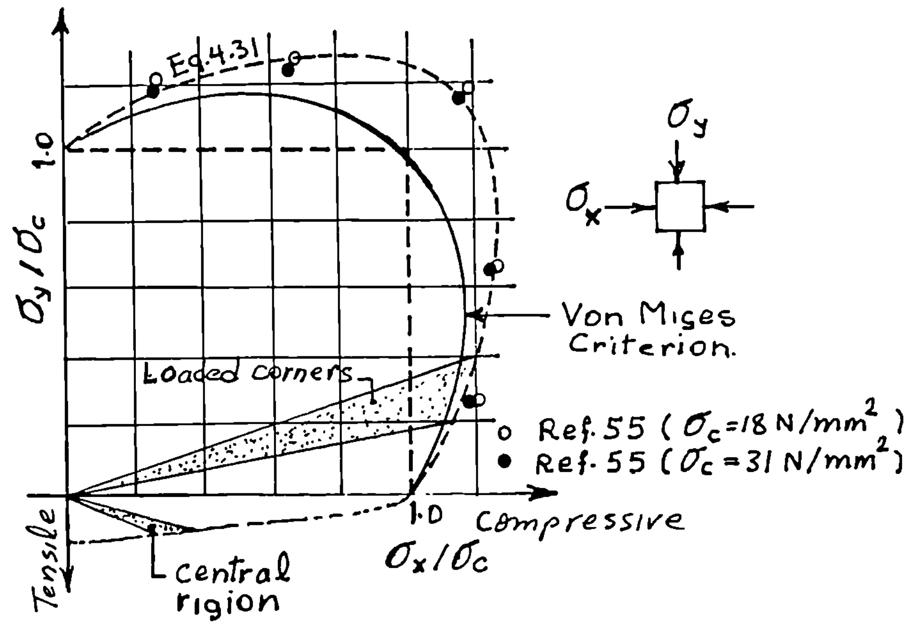

Figure 6.11 Biaxial Stress Combinations of Infill in Highly Stressed Regions Leading to Crushing or Cracking

6.13 Discussion on Frame Forces

6.13.1 General

As discussed in section 6.9, the frame remains in an elastic state up to a load close to the peak load. See symbol 'F' on the load-deflection diagrams in Figs 6.3 to 6.7. Two plastic hinges gradually form at the loaded corners before the peak load is reached. The frame forces at the peak load are discussed in the following sections.

6.13.2 Axial Forces

Development of shear stress at the frame-infill interface in the loaded corners produces significant axial force in the frame members, the no-friction frames developed almost no axial force in their members(see $\mathbf{N_1}$ in Table 6.10). Table 6.10 gives the ratio of $\mathbf{N_1}$ to the squash load, $\mathbf{N_p}$. As seen this ratio for the weak members of the frame is higher. Theoretically[98], the axial forces lowered the effective plastic resisting moment of the frame members only up to 7%. Notice that if the effect of non-diagonal loads produced as a result of service and lateral loads were included into the analysis, the total axial load would have been much higher.

Diagonal loads are defined here as the external horizontal and vertical in-plane loads acting on only the diagonally-compressed corners of the frame while keeping it in equilibrium. Non-diagonal loads, however, are defined as any other additional in plane loads such as the vertical service loads acting on the frame members while again keeping the frame in equilibrium. The infilled frames analysed in this study were all subjected to diagonal loads only. This was necessary to maintain a consistent condition in assessing the behaviour of the structure avoiding the effect of non-diagonal loads which may be arranged in different ways according to the actual needs.

In almost all the frames analysed, the axial load in the frame members at the unloaded corners, N_2, was insignificant, Table 6.10.

6.13.3 Shear Forces

Development of normal stress at the frame infill interface in the loaded corners produce significant shear force in the frame members. Table 6.10 lists 'S_1' and also the ratio of S_1/S_p, where S_1 denotes the maximum shear force produced in the frame member in question, and S_p signifies the maximum shear force that the same member would have resist if no bending moment presented.

As concluded by Horne et al[98], for $S_1/S_p<=0.5$ the shear force has no effect on the plastic resisting moment of the frame member under consideration and for $0.5<S_1<0.75$ such a reducing effect is in the range of only a few percent, and may thus be ignored. Once S_1/S_p approaches unity the member undergoes shear plasticity, no matter what the value of bending moment. Therefore, the possibility of shear plastic failure must be avoided in the analysis and design of the infilled frames.

In the present study, the frames computed had been made of the selected universal beams and columns with additional web stiffeners, Table 6.2, so as to avoid S_1/S_p

becoming greater that 0.75. However, as seen in Table6.10, there have still been few cases that S_1/S_p have exceeded this limit. This did not reduce the reserved plastic resisting moment of the frame members. Because the S_1/S_p ratios shown in Table 6.10, which are calculated for the very end of the frame members, were not used to examine the strength of the material of this end element. In the finite element analysis, which uses the analogy of the proposed beam elements, the values of axial and shear forces are assumed to be uniform along each beam element. These uniform stress values correspond to the centre of the element. In the very end element in the loaded corners of the frame, such uniform stress values are appreciably lower than the axial and shear forces at the very end of the element. Notice that the first series of the analysis using plain I sections (without shear stiffeners) led to frame shear plasticity and failure well before the plastic resisting moment of the frame members had been reached. Since such a behaviour was unacceptable from the design point of view, all such results were excluded from the comparison scheme.

Variation of shear force in the frames analysed, was such that the maximum shear occurred at the loaded end of the member and decreased rapidly between this end and the point of separation, Figs 6.8 and 6.9. The uniform shear force between the point of separation and the unloaded end of the members was insignificant, see the ratio S_2/S_1 in Table 6.10.

6.13.4 Bending Moment

The analyses showed, typically, that the peak load always follows the formation of the plastic hinges at the loaded corners. The ratio of strength or stiffness of the frame, relative to the infill do not change this trend.

As shown in Table 6.10, the bending moment at the unloaded corners, M_4, was generally so small such that it could be neglected unless the frame was very stiff. Infilled frame SSUS2 with a very stiff frame developed significant bending moment at the unloaded corners. This moment was still well below the plastic resisting moment of the weakest element approaching these corners. This indicates that if the frame was yet stiffer, it might have developed plastic hinges at the unloaded corners at the peak load.

Normal stress acting at the frame-infill interface produced sagging (or hogging) bending moment in the frame members, but in none of the infilled frames analysed did any plastic hinge occur between the corners of the frame at the peak load. The bending moment at the point of separation, M_3, is listed in Table 6.10 for all the frames analysed. As shown, this moment was generally below 25% of the plastic resisting moment of the frame member under consideration, no matter what the frame stiffness or strength.

The low sagging (or hogging) bending moment may be attributed to the limited plastic deformation (ductility) that the adjacent infill material could undergo while under high biaxial compression. As shown in Tables E.1 to E.12 in Appendix E, higher sagging (or hogging) bending moment would evelop in the frame members, only well after the peak load.

The preceding discussion in this section indicates hat all the previous finite element analyses that used a erfect plasticity or a perfect elasticity model for infill aterial might have led to misleading frame bending moments.

Table 6.10 Frame Thrust, Shear and Moment Distribution

Frames and Members		Thrust			Shear				Moment	
		N1	N2/N1	N1/Np	S1	|S2|	S2/S1	S1/Sp	M3/Mp	M4/Mpj
WMUR2*	C	104.4	0.350	0.068	560.2	8.0	0.014	**0.833**	**0.236**	0.026
	B	268.4	0.050	0.152	400.4	2.3	0.006	0.541	0.007	0.100
MMUR2*	C	144.8	0.290	0.039	769.5	27.0	0.007	0.589	**0.200**	0.033
	B	319.0	0.004	0.181	502.2	5.0	0.010	0.679	0.020	0.100
SWUR2*	C	219.1	0.005	0.029	843.5	56.6	0.067	0.389	**0.134**	0.170
	B	168.7	0.333	0.152	353.7	1.8	0.005	**0.752**	0.036	0.087
MMUR2	C	141.9	0.108	0.038	721.3	25.0	0.035	0.552	**0.165**	0.056
	B	270.0	0.061	0.153	446.5	1.3	0.003	0.604	0.091	0.064
SMUR2	C	206.6	0.027	0.028	931.0	87.7	0.094	0.430	**0.151**	0.178
	B	217.3	0.380	0.123	472.2	2.6	0.006	0.639	0.079	0.137
SWUR2	C	188.3	0.032	0.025	812.0	87.3	0.108	0.375	**0.132**	0.177
	B	114.4	0.726	0.103	335.9	0.8	0.002	0.714	0.037	0.085
WWUS2*	C	256.4	0.000	0.168	420.8	0.0	0.000	0.626	0.068	0.018
	B	258.7	0.005	0.234	429.0	0.7	0.002	**0.912**	**0.198**	0.052
WWUS2	C	234.5	0.063	0.153	407.3	6.7	0.016	0.606	0.068	0.018
	B	230.7	0.123	0.208	409.6	9.8	0.025	**0.870**	**0.198**	0.059
MWUS2	C	314.9	0.008	0.085	521.7	18.7	0.036	0.399	0.040	0.000
	B	225.0	0.190	0.203	412.5	7.3	0.017	**0.877**	**0.146**	0.006
SWUS2	C	428.2	0.033	0.057	690.4	37.6	0.054	0.319	0.069	0.332
	B	188.8	0.354	0.170	396.4	4.5	0.011	**0.842**	**0.176**	0.038
SSUS2	C	463.0	0.130	0.062	914.3	10.8	0.012	0.422	**0.166**	0.304
	B	609.9	0.018	0.163	1084.2	60.4	0.055	0.715	0.117	0.278
WWUB2	C	267.3	0.004	0.175	423.0	1.3	0.003	0.629	**0.067**	0.014
	B	270.7	0.005	0.244	429.1	1.1	0.003	**0.91**	0.062	0.014
WMUR2NF	C	52.6	1.000	0.034	601.6	8.7	0.014	**0.895**	**0.133**	0.034
	B	8.7	1.000	0.005	411.9	2.0	0.005	0.557	0.006	0.091
SMUR2NF	C	5.2	1.000	0.001	980.6	58.3	0.060	0.453	**0.137**	0.175
	B	58.3	1.000	0.033	530.0	5.2	0.010	0.717	0.029	0.117
SWUR2NF	C	0.4	1.000	0.000	893.0	55.0	0.060	0.412	**0.126**	0.112
	B	55.0	1.000	0.050	474.6	0.4	0.001	**1.009**	0.063	0.035

* Maximum load occured at diagonal-cracking load or infill did not crack.

NB: All axial loads are compressive.

Mp refers to the Plastic resisting moment of the element in question.

Mpj referes to the lesser of the plastic resisting moment of the frame members approaching the loaded corners.

CHAPTER SEVEN

Proposed Method of Analysis and Comparison

7.1 Introduction

7.1.1 General

As discussed in Chapter 2, Wood[20] used a perfect plasticity theory in developing a method of analysis based on four plastic collapse mechanisms at the peak load. In order to complete the work he adjusted the high resulting collapse load by imposing a penalty factor, γ_p , to reduce the infill compressive strength. Liauw[24], on the other hand, allowed for rather similar plastic collapse mechanisms and reduced the resulting high collapse load by neglecting the shear forces acting at the frame infill interfaces. As seen both methods tried to adjust (reduce) the infill strength so as to narrow the large gap between the theoretical and experimental results.

Contrary to the assumptions made in their methods, the finite element analysis results discussed in Chapter 6, proved that at the peak lateral load the frame has not developed a plastic collapse mechanism and still has considerable capacity to withstand higher stresses. The collapse however is merely due to compressive failure of the infill mainly at the loaded corners. Therefore should the solution to the problem be needing a penalty factor, such an adjustment must be imposed to the frame strength rather than the infill's. In other words the limit analysis of perfect plasticity[98,39] based on the lower and upper-bound theorems used in all the previous plastic analysis methods[20,22,24], may not be the most accurate approach to the analysis of infilled frames. This is because no plastic collapse mechanism exists at the peak load. As will be shown later in this chapter such a discrepancy between the existing plastic methods and the true behaviour of infilled frames leads to misleading predictions of shear and normal forces as well as the bending moments in the frame members.

Therefore a new method of analysis was developed by the author as described in this chapter. The method is based on a rational elastic and plastic analysis allowing for limited ductility for the infill, and thus limited deflection for the frame at the peak load. The method results in the necessary information for design purpose such as collapse load, cracking load, stiffness and deflection of the infilled frame and also shear, normal and bending moment diagrams of the frame members. The proposed method also allows for the major practical imperfections such as lack of fit and shrinkage of the infill. It is concluded that the effects of pin and semi-rigid joints at the column-beam connections can also be accommodated. Variations such as the aspect ratio of the infill and also beams having different strength and stiffness from those of the columns are accounted for in the proposed method. The results of the proposed method are compared with the results of the finite element analyses, experiments and other previous methods at the end of this chapter.

7.1.2 Basis of The Analysis

The finite element analysis results discussed in Chapter 6 showed that at the peak lateral load, the infilled frame failure initiated in the infill and collapse is merely due to excessive compressive strain accompanied by loss of strength (strain softening) at the loaded corners of the infill. The frame, however, at the peak load still has considerable capacity to withstand higher stresses and to develop additional plastic hinges in far later stages of loading. Therefore no distinct plastic collapse mechanism and thus, no upper-bound solution exists at the peak load.

In the absence of an upper-bound solution at the peak load, many lower-bound solutions can be imagined. i.e. many force distribution patterns can be proposed satisfying the equilibrium of the external and internal forces. In order to find a solution close to the exact one, the following facts were concluded from the work described in Chapter 6.

i) The strength of an infilled frame is mainly contributed by the infill. Increase in the lateral deflection of the infill accompanies a gradual increase in the lateral load up to only a limited deflection beyond which the infill gradually loses its strength at the loaded corners and the load falls due to limited infill ductility.

ii) Development of plastic hinges at the loaded corners of the frame precedes the peak load. However, this might not be the case for infilled frames having frame/infill strength and stiffness parameter beyond the range studied.

iii) Because of the limited infill ductility and thus limited frame deformation at the peak load the bending moment at the unloaded corners of the frame, rarely reaches the joint plastic resisting moment of the frame. The unloaded corner moment is negligible for infilled frames with weak or medium strength frames. The joint plastic resisting moment is defined as the least of the plastic resisting moments of the members meeting the joint and also their connections to the corner.

iv) The sagging or hogging bending moments in the frame members remain well below the plastic resisting moment of the member in question. These moments are nearly proportional to the plastic resisting moment of the corresponding frame members.

These conclusions led to definite solutions based on distinct elastoplastic deformation modes (instead of mechanisms used in the limit analysis) for different values of frame/infill strength and also stiffness ratios. The proposed analysis method will be described in the following sections.

7.2 Frame-infill Interaction

Fig 7.1(a) shows the frame-infill interaction forces for an infilled frame loaded diagonally up to the peak load. As discussed in chapter 6, the frame separates from the infill, but contact remains in the loaded corners to transfer the diagonal force to the infill. It is proposed that the frame-infill interactive forces are assumed to be distributed uniformly over the proposed lengths of contact, $\alpha_c h'$ and $\alpha_b l'$, resulting in uniform normal and shear contact stresses acting to the beams and columns designated by, σ_{nc}, σ_{nb}, τ_c and τ_b respectively. h' and l' denote the height and length of the infill respectively. Plastic hinges develop at the loaded corners of the frame. The moment diagram and also the forces acting on the left hand side column are shown in Figs 7.1(c) and 7.1(b) respectively. Similar forces act on the other members of the frame. M_{pj} designates the frame joint plastic resisting moment, which is defined as the least of the plastic resisting moment of the beam and column and their

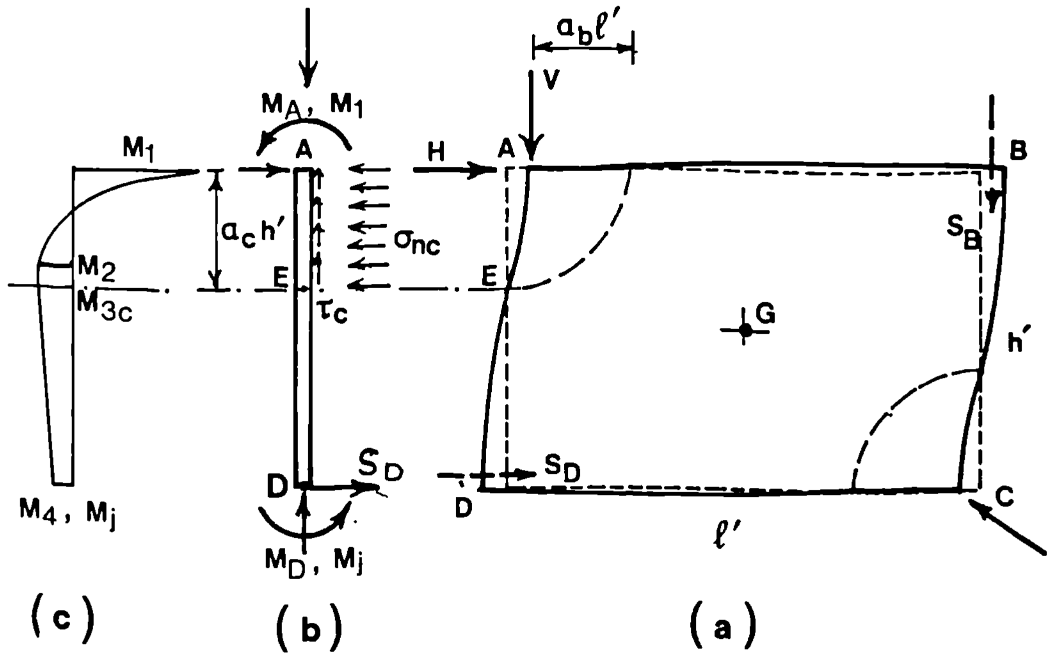

Figure 7.1 Proposed Frame-Infill Interaction Forces; a) wall, b) column, c) moment diagram

connections to the corner. α_c and α_b denote the ratios of the lengths of contact of the column and beam to the height and length of the infill respectively.

In order to calculate the frame bending moments it was found convenient to study the column and beam deformations separately. Fig 7.2(a) illustrates the lateral deflection of an infilled frame resulting from the flexibility of only columns of the frame and also deformation of the infill only in horizontal direction. The deflection produced by such a system may be signified by Δh_x. This deflection can be incorporated into an elastic analysis allowing for only the column end at the loaded corners to move and rotate, leading to the fixed end moment of this column written as:

$$M_{jc} = \frac{1}{2} M_{1c} + \frac{3E_cI_c}{h'^2} \Delta h_x - \frac{1}{8} \sigma_{nc} t h'^2 \alpha_c^2 (2-\alpha_c^2) \qquad (7.1)$$

Fig 7.2(c) shows the step oy step proceder to derive Eq 7-1

Similar deformation can be envisaged for the bottom beam, Fig 7.2(b), leading to its fixed end moment as:

$$M_{jb} = \frac{1}{2} M_{1b} + \frac{3E_bI_b}{l'^2} \Delta h_y - \frac{1}{8} \sigma_{nb} t l'^2 \alpha_b^2 (2-\alpha_b^2) \qquad (7.2)$$

where infill and beams are assumed to undergo only vertical deformation and the columns assumed to be extremely stiff. Δh_y denotes the vertical deflection of the infilled frame due to only beams flexibility. In the above analysis the eccentricity of the infill-frame frictional forces to their offset from neutral axis of the frame members were neglected for simplicity. The effects of these are insignificant

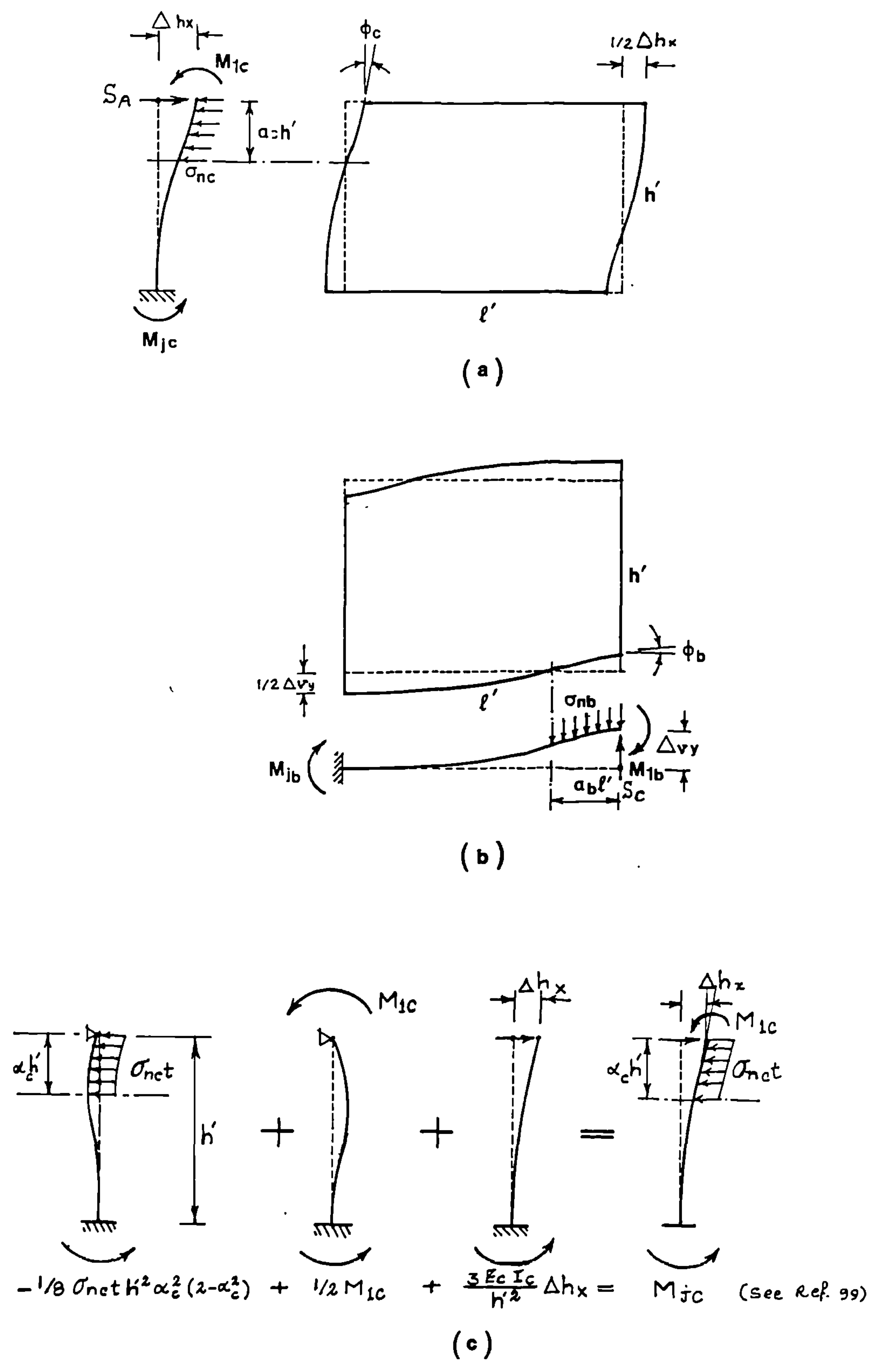

Figure 7.2 Deformation of Infilled Frames;
a) columns only, b) beams only, c) Forces distribution

in this calculation because the lever arms are small in relation to the lever arms for the normal forces.

Superposition of the above two systems gives the overall infilled frame deformation. This can be achieved by rotating the second system (clockwise) such that the bottom beam becomes horizontal. This results in the overall horizontal deflection as:

$$\Delta h = \Delta h_x + \Delta h_y (h'/l') \tag{7.3}$$

The fixed end moments are equal for equilibrium, therefore

$$M_{jb} = M_{jc} = M_j \quad \text{and} \quad M_{lc} = M_{lb} = M_l \tag{7.4}$$

Combination of Eqs 7.1 to 7.4 leads to the frame moment at the unloaded corners as follows:

$$M_j = \frac{1}{2} M_l + 3\Delta h_x \frac{K_c}{h'} - \frac{1}{8} A \tag{7.5}$$

and

$$\Delta h_x = \frac{(h'/24)(A-B) + K_b \Delta h}{K_c + K_b}$$

$$\Delta h_y = \frac{(l'/24)(B-A) + K_c \Delta h/K}{K_c + K_b}$$

where

$$A = \sigma_{nc} t h' 2\alpha_c^2 (2-\alpha_c^2)$$

$$B = \sigma_{nb} t l' 2\alpha_b^2 (2-\alpha_b^2)$$

$$K_c = \frac{E_c I_c}{h'} \quad \text{and} \quad K_b = \frac{E_b I_b}{l'}$$

Where E_c and E_b denote modulus of elasticity and I_c and I_b

designate the moment of inertia of columns and beams respectively. The finite element analysis results described in chapter 6 showed that at the peak load, plastic hinges developed at the loaded corners in all the frames studied. Therefore Eq 7.5 becomes:

$$M_j = \frac{1}{2}M_{pj} + 3\Delta h_x \frac{K_c}{h'} - \frac{1}{8}A \tag{7.6}$$

The above elastic analysis for the exceptional case when $M_1 < M_{pj}$ will be dealt with later in Section 7.14. Eq 7.6 involves the stiffness and strength of the frame and infill materials. Solution of this equation requires determining the length-of-contact ratios, α_c and α_b, and the racking deflection of the frame at the peak load, Δh. These parameters are highly indeterminate. The study of the finite element analysis and also the conclusion made in the previous section, provided grounds to propose some constant values to make the above parameters determined. These are discussed in the following sections.

7.3 Frame-infill Contact Lengths

Equations of equilibrium of the left hand side column and the top beam, Fig 7.1, can be written and solved for the shear forces at points D and B respectively leading to:-

$$\begin{aligned} S_D &= \sigma_{nc} t(\alpha_c h')\left(\frac{\alpha_c}{2}\right) - \frac{M_{pj}+M_j}{h'} \\ S_B &= \sigma_{nb} t(\alpha_b l')\left(\frac{\alpha_b}{2}\right) - \frac{M_{pj}+M_j}{l'} \end{aligned} \tag{7.7}$$

The regularities observed in the magnitude of the sagging or hogging moment produced in the frame members described in section 6.13.4, leads to the proposed following approximate but convenient relations to estimate the shear forces at the unloaded corners.

$$S_D = \left(\beta_c M_{pc} - M_j\right)/h'$$
$$S_B = \left(\beta_b M_{pb} - M_j\right)/l' \tag{7.8}$$

Where β_c and β_b are constant factors yet to be determined. If either of them become unity the frame member in question would have developed a plastic hinge due to excessive sagging or hogging bending moment. As discussed earlier, becaus of limited ductility of infill material such a plastic hinge may not occur. Therefore β values take values less than unity. A single constant value of 0.2 ,referred to as β was found to be a reasonable value for β_c and β_b when the infill is made of concrete.

Substituting for S_D and S_B from Eqs 7.8 into Eqs 7.7 leads to the lengths of contact as:-

$$\alpha_c = \sqrt{\frac{2M_{pj} + 2\beta_c M_{pc}}{\sigma_{nc} t h'^2}}$$

$$\alpha_b = \sqrt{\frac{2M_{pj} + 2\beta_b M_{pb}}{\sigma_{nb} t l'^2}} \tag{7.9}$$

Notice that M_j vanished during the above derivation. This permits the length of contact to be calculated independently

7.4 Infill Boundary Stresses

Fig 7.3 shows the proposed typical uniform stress and force distribution at the frame/infill interface. As discussed in section 6.11 at the peak lateral load the following relations agreed well with the F.E. analysis results:

$$F_c = \mu K^2 C_c \qquad \text{and} \qquad F_b = \mu C_b$$

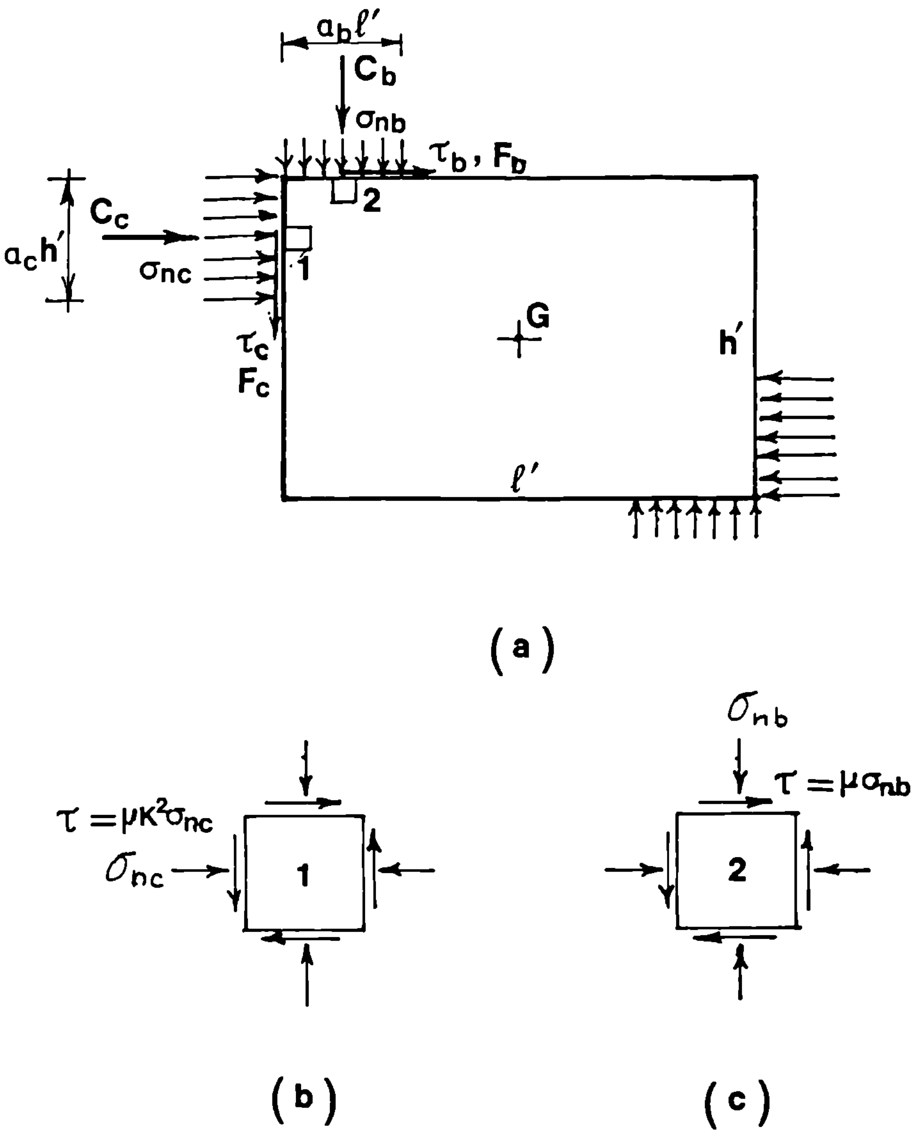

Figure 7.3 Proposed Infill Boundary Stresses; a) boundary stresses, b) at column interface c) at beam interface

where $K=h'/l'$ and μ denotes the co-efficient of friction of the infill-frame interface. C_c and C_b designate the total normal forces and F_c and F_b denote the total frictional forces acting over the contacted regions of the infill-column and beam interfaces respectively. Since the areas of application of the friction and normal stresses are assumed to be identical, the above relations can be written also in terms of the boundary stresses as follows:

$$\tau_c = \mu K^2 \sigma_{nc} \qquad \text{and} \qquad \tau_b = \mu \sigma_{nb} \tag{7.10}$$

At the peak load, the infill stress approaches the failure surface. As shown in fig 6.11 Von Mises criterion suits concrete under biaxial compressions and leads to a simple manipulation, its general format for in plane stresses becomes(39):

$$\sigma_x^2 + \sigma_y^2 - \sigma_x\sigma_y + 3\tau_{xy}^2 = f_c2$$

The second and third terms of this equation would vanish if the minor compressive stress takes a value equals to either zero or the major compressive stress. Therefore if only the major compressive stress is known, this criterion can be safely reduced to:

$$\sigma_n^2 + 3\tau^2 = f_c^2 \tag{7.11}$$

where f_c denotes the effective uniaxial compressive strength of the infill material given as;

$$f_c = K_1 \text{ x (compressive strength of infill)} \tag{7.12}$$

Factor K_1 has been proposed to adjust the standard compressive strength (either f_c' or fcu or the unconfined compressive strength, σ_c, used throughout this work) to the effective strength accounting for the following effects:

i) Errors due to the assumption of uniform stress block
ii) Reserve of strength because of using a simplified Von Mises criterion in biaxial compression(see Fig 6.11).
iii) Difference between the standard compressive strength and the effective uniaxial compressive strength for this particular structure.

A value of unity for K_1 gave results that agreed well with the F.E. analysis and also various experimental results from different sources examined at the end of this chapter provided the unconfined compressive strength, σ_c, has been taken (see also Section 7.19.5 for the choice of variable K_1 value). Combining Eq 7.11 with Eq 7.10 leads to the proposed infill normal stresses acting on the columns and beams, respectively, in the loaded corners as follows:

$$\sigma_{nc} = \frac{f_c}{\sqrt{1+3\mu_c{}^2K^4}}$$
$$\sigma_{nb0} = \frac{f_c}{\sqrt{1+3\mu_b{}^2}} \tag{7.13}$$

Subscripts **c** and **b** refer to the column and beam respectively

Failure of the infill in the loaded corners does not have to occur at the beam and column interfaces simultaneously. Comparison of the above proposed stresses and the F.E. analysis results, Table 6.7, showed that all the rectangular infills failed because of excessive σ_{nc} alone. Therefore the calculated value for σ_{nb}, signified as σ_{nb0}, should be regarded as only its upper limit value. The value of σ_{nb} can be derived by applying the condition to prevent rigid body rotation of the infill panel, ie:

$$C_c(h'-\alpha_c h') - F_c l' - C_b(l'-\alpha_b l') + F_b h' = 0 \qquad (7.14)$$

The external forces acting on the infill, Fig 7.3, can be written as:

$$\begin{aligned} C_c &= \sigma_{nc} t(\alpha_c h') \;, \quad & F_c &= \tau_c t(\alpha_c h') \\ C_b &= \sigma_{nb} t(\alpha_b l') \;, \quad & F_b &= \tau_b t(\alpha_b l') \end{aligned} \qquad (7.15)$$

Substituting for these forces, Eq 7.14 leads to:

$$\sigma_{nb}\alpha_b(1-\alpha_b-\mu_b K) - \sigma_{nc}\alpha_c K^2(1-\alpha_c-\mu_c K) = 0 \qquad (7.16)$$

Solving Eq 7.16 for σ_{nb} gives:

$$\sigma_{nb} = \sigma_{nc}K^2\left(\frac{\alpha_c}{\alpha_b}\right)\frac{1-\alpha_c-\mu_c K}{1-\alpha_b-\mu_b K}$$

Combining the above equation with Eqs 7.9 leads to α_b as:

$$\alpha_b = \frac{1-\mu_b K}{1+A} > 0 \qquad (7.17)$$

where

$$A = \frac{1-\alpha_c-\mu_c K}{\alpha_c} \cdot \frac{M_{pj}+\beta_c M_{pc}}{M_{pj}+\beta_b M_{pb}}$$

Now Eq 7.9 can be solved for σ_{nb} resulting in:

$$\sigma_{nb} = \frac{2M_{pj}+2\beta_b M_{pb}}{tl'^2\alpha_b^2} < \sigma_{nbo} \qquad (7.18)$$

where

$$\sigma_{nb0} = \frac{f_c}{\sqrt{1 + 3\mu_b^2}}$$

The value of α_b resulting from Eq 7.17 was positive for all the frames analysed and is therefore very unlikely to become negative. Value of σ_{nb}, however, may exceed σ_{nb0} especially for square infills. This is not physically possible because it implies a stress exceeding the infill failure stress and this will be discussed later in section 7.12.

It must be noted that for a uniform frame where M_{pc} equals M_{pb} and β_c equals β_b and also μ_c equals μ_b, Eq 7.17 reduces to:

$$\alpha_c = \alpha_b$$

7.5 Lateral Deflection

Comparison of the load-deflection diagrams of the infilled frames studied, Fig 6.3 to 6.7, led the author to assume that the infill deflection at the peak load is proportional to the following parameters.

i) The reference diagonal band width of the infill, w', first introduced by Mainstone[9] (see section 2.2 and Fig 2.1b), where:

$$w' = 2h'\cos\theta \qquad (7.19)$$

ii) A function relating to both the beam and the column length of contact ratios, α_c and α_b. The following function was found appropriate for this purpose.

$$q = \sqrt[3]{\alpha_c^2+\alpha_b^2} \qquad (7.20)$$

iii) The infill failure strain reference, ε_u, proposed as:

$$\varepsilon_u = K_e\varepsilon_c$$

where ε_c denotes the infill strain corresponding to its peak unconfined compressive strength.

These assumptions lead to the infilled frame lateral deflection at the peak load proposed as:

$$\Delta h = qw'\varepsilon_u$$

A K_e value of 2.75 gave results that agreed well with the finite element analysis results.

The effect of the expansion and contraction of the infill such as changes in temperature, shrinkage, and lack of fit on the horizontal deflection, may now be calculated by a simple manipulation in terms of their equivalent horizontal and vertical strains ε_{xr} and ε_{yr}. Inclusion of these residual strains leads to the following expression for total lateral deflection of the panel as:

$$\Delta h = 2k_e\varepsilon_c h'\cos\theta \sqrt[3]{\alpha_c^2+\alpha_b^2} - \varepsilon_{xr}l' - \varepsilon_{yr}h'\tan\theta \qquad (7.21)$$

where an expansive strain is regarded as +ve. Deflection values calculated using this equation will be compared with some experimental results from different sources later in this chapter. In the above simple analysis the effect of the axial deformation of the frame members resulting from non-diagonal loads (section 6.13.2) has not been included. Such additional deflections can be incorporated separately in the overall frame analysis.

7.6 Frame Bending Moments

As discussed in Section 7.2, occurrence of the plastic hinges at the loaded corners always preceded the peak load in the frames analysed. Therefore bending moment at these corners equals the plastic resisting moment of the joint, M_{pj}. However the conditions leading to $M_1 < M_{pj}$ at the peak load is discussed in Section 7.17 as an exceptional case. At the other corners the frame develops a smaller bending moment, M_j, which now can be calculated from Eq 7.6 using the proposed values of α and σ_n and also Δh calculated from Eqs 7.9, 7.13, 7.17, 7.18 and 7.21. In most cases in finite element analysis, M_j became so small that it could be easily neglected(see Table 6.10). However, the infilled frame SSUS2 with a fairly stiff frame relative to the infill, developed a significant bending moment at its unloaded corners. This moment was still well below the plastic resisting moment of the joint in question. It may, therefore, be concluded that the stiffer the frame is relative to the infill, the higher the bending moment at the unloaded corners becomes. These characteristics are well reflected in the proposed Eq 7.6.

7.7 Frame Forces

Fig 7.4 shows all the horizontal forces acting on the frame leading to the frame horizontal forces. Similarly vertical forces lead to the vertical frame forces. The resulting frame forces at the peak load are summarized in Table 7.1. The unloaded end shear forces of the beams and columns, S_D and S_B, are given by Eq 7.7. The external forces, C_c, C_b, F_c and F_b, and also the bending moment at the unloaded corners, M_j, are given by Eqs 7.15 and Eq 7.6 respectively.

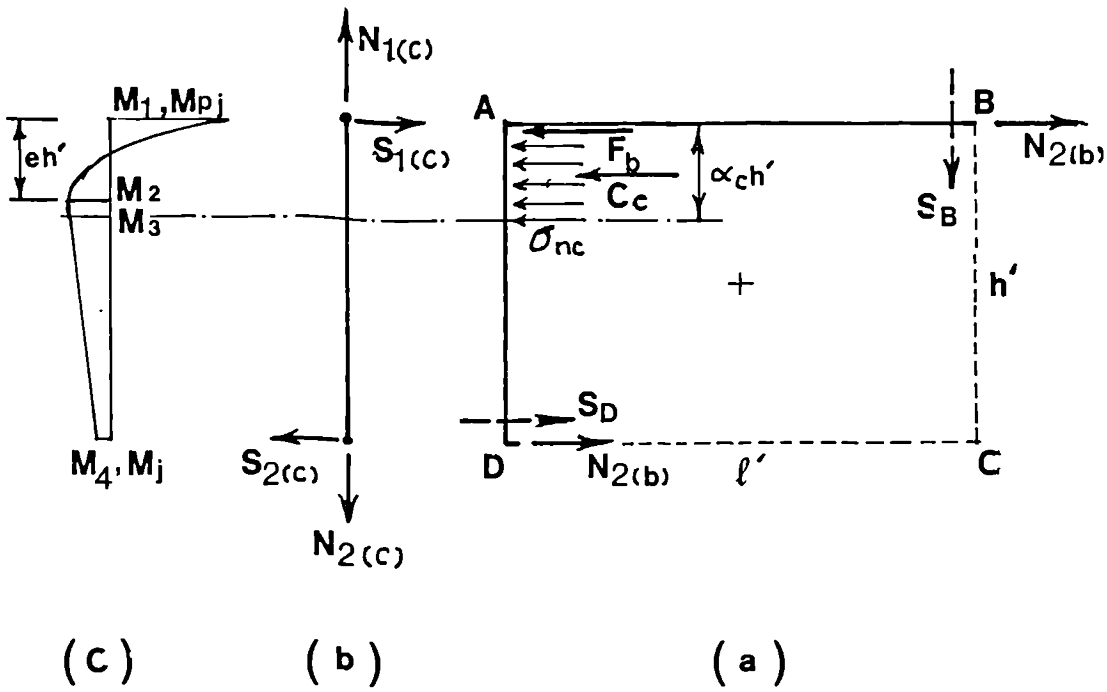

Figure 7.4 Frame forces; a) Horizontal Forces Equilibrium, b) Column forces, c) Column Bending Moment Diagram

Table 7.1 Frame Forces

Force	Column	Beam
Normal	$N_1 = S_B - F_c$ $N_2 = S_B$	$N_1 = S_D - F_b$ $N_2 = S_D$
Shear	$S_1 = C_c - S_D$ $S_2 = -S_D$	$S_1 = C_b - S_B$ $S_2 = -S_B$
Moment	$M_1 = -M_{pj}$ $M_2 = 0.5(eh')S_1 - M_{pj}$ where: $eh' = S_1/(\sigma_{nc}t)$ $M_3 = S_D(1-\alpha_c)h' + M_j$ $M_4 = M_j$	$M_1 = -M_{pj}$ $M_2 = 0.5el'S_1 - M_{pj}$ where: $el' = S_1/(\sigma_{nb}t)$ $M_3 = S_B(1-\alpha_b)l' + M_j$ $M_4 = M_j$

Notes: a) M_2 is valid only when $e<\alpha$ has been ensured.
b) subscripts **1** and **2** used with **N** and **S** Designate the member end at the loaded and unloaded corners respectively.
c) Notice that a negative axial force specifies compression.
d) M_{pj} is to be replaced by the smaller value given in Section 7.15 for very weak infill.

7.8 Peak Horizontal Load

From Fig 7.4, the proposed peak load becomes:

$$H_c = C_c + F_b - 2N_{2\,(beam)} \tag{7.22}$$

It must be noted that infilled frames with a strong frame, relative to the infill, under increasing deflections eventually undergo a mechanism and develop a plastic load well after the infill compressive failure. If the frame is extremly strong, such a plastic load could exceed the load estimated by Eq 7.22 leading to the peak load given by:

$$H_{uf} = \frac{4M_{pj}}{h'} \tag{7.23}$$

7.9 Modes of Displacement and Failure

7.9.1 Frame Failure

At the peak lateral load the frame normally develops plastic hinges at only the loaded corners. The bending moment at the other corners, M_j, remains well below M_{pj}. In an infilled frame having an extremly strong frame, the calculated M_j from Eq 7.6 may possibly exceed M_{pj}. In such a case new plastic hinges must have developed at the unloaded corners and the mode of failure of the frame may be referred to as "Shear mode" (S). A frame with shear mode of failure develops a mechanism at the peak load which is coincident with the infill failure. The possible combination of frame and infill failure modes are classified in section 7.9.3.

7.9.2 Infill Failure

Generally the mode of failure of the infill at the peak lateral load must be regarded as "Corner Crushing" (CC). In this mode, the stronger or stiffer the frame member is, the higher the length of contact becomes. But there is an upper limit for this length. Imagine an infilled frame with an extremly strong frame subjected to lateral load to the peak level, Fig 7.6. If the small diagonal infill contraction and expansion developed at the central area of the infill, are ignored the racking deformation of the infill can be attributed to only deformation of the loaded corners of the infill. The horizontal displacement of the infill at the loaded corners, **AA'** and **C'C**, induced by contraction of the infill, permits the beams to move over and produce a gap, **BB′** and **D′D**, between the opposite column and the infill in the unloaded corners such that **AA′=BB′** and **DD′=CC′**. Because of the symmetry of the loaded corners **AA′=C′C**, combination of these equations leads to **AA′=D′D** and **BB′=C′C** and consequently **AE=DE** and, thus, **AE=0.5h′**. Therefore the length of contact would not exceed half the length of the corresponding side of the infill.

When the length of contact of either the column or beam approaches this limit the mode of failure of the infill may be referred to as "Diagonal Compression" (DC), because the biaxial compression zones of the infill have expanded to the maximum size along the infill diagonal. In an infilled

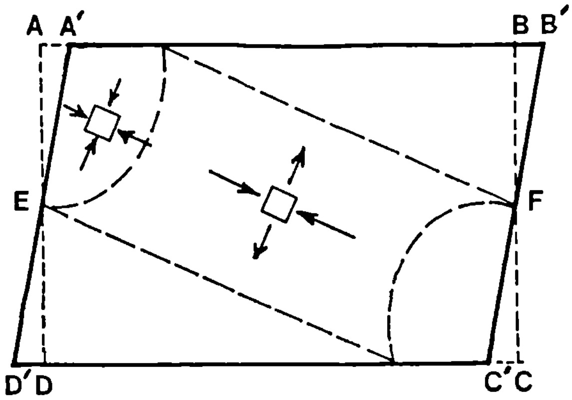

Figure 7.5 Upper Limit for Length of Contact

frame undergoing DC mode the ratio of the length of the proposed rectangular interface stress block to the corresponding side dimension of the infill, can generally be written as:

$$\alpha_i = 0.5K_2 \tag{7.24}$$

where K_2 is an adjusting factor to cater for the errors due to the proposed simple rectangular stress block and i denotes either column or beam as the case may be. As will be shown later, K_2 equals to $2/3$ was found to give results that agree well with the finite element results for the practical range of stress and stiffness of infill material. This leads to $\alpha_i=1/3$.

For an infilled frame with α_c becoming greater than $0.5K_2$, thus DC mode, the value of β_c must be adjusted to correspond to $\alpha_c=0.5k_2$. Substituting for the value of α_c from Eq 7.24 into Eq 7.9 leads to:

$$\underset{(new)}{\beta_c} = \frac{(1/8)K_2^2\sigma_{nc}th'^2 - M_{pj}}{M_{pc}} < \underset{(old)}{\beta_c} \tag{7.25a}$$

Similar adjustment must be carried out for β_b to correspond to $\alpha_b=0.5K_2$, should the β_b becomes greater than $0.5K_2$. Substituting for α_b from Eq 7.24 into Eq 7.17 and solving for β_b leads to:

$$\underset{(new)}{\beta_b} = \frac{1}{M_{pb}}\left[\frac{S}{P}(M_{pj}+\beta_c M_{pc}) - M_{pj}\right] < \underset{(old)}{\beta_b} \tag{7.25b}$$

where

$$S = \frac{1-\alpha_c-\mu_c}{\alpha_c} \quad \text{and} \quad P = \frac{1-\mu_b K}{0.5K_2} - 1$$

Notice that the above adjustments are independent of each other. A proposed chart for calculating α_c and also adjusting β_c will be described in section 7.13.

7.9.3 Infilled Frame Failure

Sections 7.9.1 and 7.9.2 described the requirements for frame and infill failure modes respectively. Infilled frame failure modes can now be categorized by combining these modes as shown diagrammatically in Fig 7.6 and as defined below;

i) Corner Crushing (CC), referred to infill corner crushing with presence of no frame plastic mechanism.

ii) Diagonal Compression (DC), referred to infill diagonal compression failure with presence of no frame plastic mechanism.

iii) Sheared Corner Crushing (SCC), referred to infill corner crushing with presence of frame shear plastic mechanism.

iv) Sheared Diagonal Compression (SDC), referred to infill diagonal compression failure with presence of frame shear plastic mechanism.

Modes CC and DC normally involve flexural failure of the frame with single plastic hinges at the loaded corners. Modes SCC and SDC involve plastic hinges at all four corners of the frame, but these two latter modes were not encountered in the infilled frames studied in this work. They may possibly occur only in infilled frames with extremely strong frame and infills with very low modulus of elasticity and high ductility, i.e. high ε_c value.

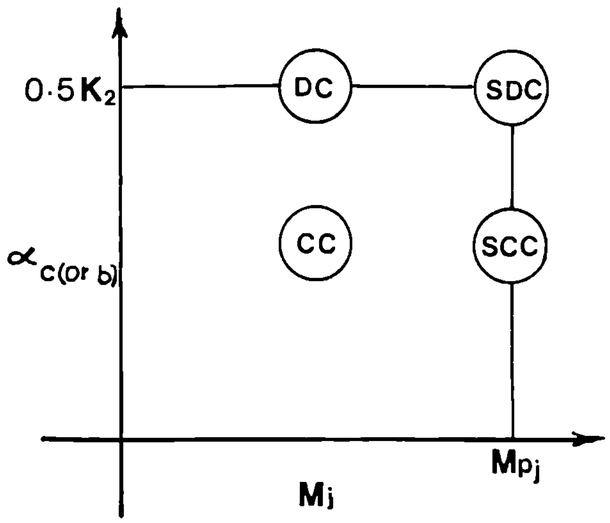

Figure 7.6 Graphical Representation of Failure Modes

7.10 Cracking Load

Cracking of the infill has been studied in Section 6.12.3. As discussed the cracking strength of the infill is proportional to the following parameters:

i) Tensile splitting strength, $\mathbf{f_t'}$, which was proved to be the best cracking strength reference for this particular type of structure.

ii) Infill geometry represented by the infill effective diagonal band area, $\mathbf{A = w't}$ (see Eq 7.19). Note that this parameter has been taken also by Mainstone[9] for the same purpose.

Introducing an adjusting factor, $1/2k_t$, these lead to the infill diagonal cracking load as;

$$R_t = (1/2)k_t w' t f_t' \qquad (7.26)$$

The multiplier **1/2** is incorporated only for convenience in later manipulation. Converting R_t into its horizontal component, Eq 7.26 leads to the cracking load of the infill as:

$$H_{ti}=(1/2)K_t w' t f_t' \cos\theta \qquad (7.27)$$

Mainstone[9] suggested almost the same formula as Eq 7.27 for cracking load using the compressive strength of the infill as the strength reference and related Kt to the frame/infill stiffness parameter, λh. Variation of λh only changes the length of contact of the frame and the infill at the loaded corners[9]. Comparison of the load-deflection diagrams of the infilled frames with different λh value, WWUS2 and SWUS2 in Figs 6.5 and 6.6, leads to the conclusion that for infilled frames with $\lambda h>3.4$ the Saint Venant's Principle[38] applies to the cracking strength of the infill. i.e. the centre of the infill which is the point where cracking starts, is sufficiently far from the regions where the external loads are applied, so that the cracking load is not affected by the way the load is distributed over the loaded corners. Therefore K_t can be taken a constant value. Substituting for w' from Eq 7.19, Eq 7.27 leads to the proposed infill cracking load as:

$$H_{ti} = k_t f_t' h' \cos^2\theta \tag{7.28}$$

In order to verify the value of K_t, one may study the elastic analysis of a cube under diagonal load carried out by Davis et al (described by Chen[59]). This analysis led to the diagonal strength of the cube in terms of the tensile strength of the material as;

$$Q = \frac{\pi}{1.6\sqrt{2}} t w' f_t'$$

This also gave results fairly close to the limit analysis of plasticity[59]. This relation can be converted into the horizontal component of the load and written in a fashion that can be compared with Eq 7.28, as:

$$H_{ti} = 2.78\ f_t' t h' \cos^2\theta$$

Comparison of this equation and Eq 7.28 leads to K_t equals to 2.78. The finite element analysis results agreed safely and well with the Eq 7.28 with kt taken as 2.70 which is only 3% lower than the theoretical value. As will be shown later, this constant value leads to a more comparable and consistent cracking load than given by the empirical equations of Mainstone[9].

To the infill cracking load, Eq 7.28, the frame contribution must be added. This combination (see Fig 7.4) leads to the cracking load of the infilled frame as:

$$H_t = 2.70 f_t' t h' \cos^2\theta - 2N_{2b}' \tag{7.29}$$

where N_{2b}' denotes the beam axial force (comp., -ve.) at the unloaded corners at the onset of cracking. The frame forces may be assumed to be nearly proportional to the horizontal load. Therefore N_{2b}' can be calculated as:

$$N_{2b}' = \left(\frac{H_t}{H_c}\right) N_{2b} \qquad (7.30)$$

where N_{2b} denotes the beam axial force at the peak load and at the unloaded corner. Substituting for N_{2b}' from Eq 7.30 and also substituting for N2(b) from Table 7.1 into Eq 7.29 leads to:

$$H_t = 2.70 f_t' t h' \cos^2\theta (1+Q) \qquad (7.31)$$

where the frame contribution ratio, Q, is written as:

$$Q = \frac{-2S_D}{C_c + F_b} \qquad (7.32)$$

S_D can be obtain from Eq 7.7 and C_c and F_b are listed in Eqs 7.15. It must be noted that the value of the frame contribution ratio, Q, may take a positive or a negative value. If Q takes a small positive or negative value, it may be neglected. When Q takes a negative and significant value it may not be neglected. This implies that α_c is rather high (see Eq 7.7). As discussed earlier in this section a frame with a long length of contact (i.e low λ_h) withstands a higher cracking load, because the diagonal load has been distributed over a large area of corners. The beneficial effect of such a reserve strength may be assumed to compensate for the effect of the negative **Q** value and, thus, both the effects may be neglected. As shown later in this chapter the cracking loads calculated neglecting the negative **Q** values improved significantly.

7.11 Stiffness

The secant stiffness of an infilled frame to a particular load level can be written as:

$$K = \frac{H}{\Delta h}$$

This equation can be written for the peak load as:

$$K_C = \frac{H_C}{\Delta h} \tag{7.33}$$

where Δh is given by Eq 7.21. The load deflection diagrams, Figs 6.3 to 6.7, show that the secant stiffness of an infilled frame within its linear elastic range of loading, is approximately twice as high as its secant stiffness at the peak load i.e.

$$K_0 = \frac{2H_C}{\Delta h} \tag{7.34}$$

7.12 Special cases with Sq are Infills

As concluded in section 7.4 the normal stress at the beam interface, σ_{nb}, may not exceed ı s maximum possible value, σ_{nb0}. This is not physically possible because it implies that a stress exceeding the infill failure stress at the beam infill interface. If however the calculated value of σ_{nb} exceeds σ_{nb0}, it must be taken equal to σ_{nb0}. This requires that either β_b or β_c to be adjusted so that the infill equilibrium is maintained.

Assuming β_c remains unchanged, β_b must be adjusted. Solving Eq 7.16 for α_b leads to:

$$\alpha_b = \frac{1-\mu_b K}{2} \pm \sqrt{\left(\frac{1-\mu_b K}{2}\right)^2 - P_b} \tag{7.35}$$

where

$$P_b = \left(\frac{\sigma_{nc}}{\sigma_{nb0}}\right) K 2\alpha_c (1-\alpha_c-\mu_b K)$$

Now β_b can be calculated from Eq 7.9 as:

$$\beta_b = \frac{0.5\sigma_{nb0} t l'^2 \alpha_b^2 - M_{pj}}{M_{pb}} \tag{7.36}$$

The largest β_b value that also is less than the old β_b value must have led to the true solution.

If, however, none of the calculated βb values satisfies the above condition, β_b must be taken equal to its original value and β_c is to be adjusted. Solving Eq 7.16 for α_c leads to:

$$\alpha_c = \frac{1-\mu_c K}{2} \pm \sqrt{\left(\frac{1-\mu_c K}{2}\right)^2 - P_c} \tag{7.37}$$

where

$$P_c = \left(\frac{\sigma_{nb0}}{\sigma_{nc}}\right)\left(\frac{\alpha_b}{K^2}\right) (1-\alpha b-\mu b K)$$

Now βc can be calculated from Eq 7.9 as:

$$\beta_c = \frac{0.5\sigma_{nc} t h'^2 \alpha_c^2 - M_{pj}}{M_{pc}} \tag{7.38}$$

The largest β_c value that also is less than the old βc value must have led to the true solution.

In order to have significant results from Eqs 7.35 and 7.37, the inequality of:

$$\left(\frac{1-\mu_i K}{2}\right)^2 - P_i \geq 0$$

must be satisfied. If this is not the case, μ_i must be adjusted so that

$$P_i \leq \left(\frac{1-\mu_i K}{2}\right)^2$$

is secured. Solving for μ_i the above equation leads to:

$$\mu i \leq \frac{1-2\sqrt{P_i}}{K} \qquad (7.39)$$

The highest possible μ_i value can be obtained using the equal sign. The value of P_i is a function of μ_i. Therefore μ_i can be calculated by a trial and error approach.

After such adjustments have been completed, α_i can be calculated by either of Eqs 7.35 and 7.37 and β_i can be calculated from Eqs 7.36 and 7.38 for beams and columns respectively.

7.13 Balancing Friction a I fill Boundary

Equilibrium of the infill (the condition to prevent infill rigid body rotation) has already discussed and led to Eq 7.16. As seen the forces transferred from the columns tend to rotate the infill clockwise. Eq 7.16

implies that the inequality of $1-\alpha_c-\mu_c K>=0$ must always be satisfied, otherwise the column-infill interactive forces tend to rotate the infill anti-clockwise which opposes the direction of the load. Therefore, if the above condition has been violated the coefficient of friction, μ_c, should be adjusted to a lesser value, μ_{cb}, defined as the interface balancing shear such that:

$$1-\alpha_c-\mu_{cb}K = 0 \tag{7.40}$$

As discussed also in Section 6.11 such an adjustment favours effectively the agreement between this proposed method and the finite element analysis. Combining Eq 7.40 with Eqs 7.9 and 7.13 leads to μ_{cb} as:

$$\mu_{cb} = \left[1-m_c \sqrt[4]{(1+3\mu_{cb}{}^2K^4)}\right]/K \tag{7.41}$$

where

$$m_c = \sqrt{\frac{2M_{pj}+2\beta_c M_{pc}}{f_c t h'^2}}$$

μ_{cb} can be calculated from Eq 7.41 by trial and error with a quick convergence. Alternatively it may be calculated using the chart introduced in the following section, by reading q_c which then must be entered into Eq 7.44 to give:

$$\mu_{cb} = \sqrt{\frac{q_c{}^4-1}{3K^4}} \tag{7.42}$$

7.14 Design Chart

As discussed earlier in this chapter, the value of α_c can be calculated from Eq 7.9 directly. In some cases,

α_c may be subjected to either or both of the following adjustments:

i) Adjusting μ_c value so as to maintain the infill equilibrium, Section 7.13

ii) Adjusting β_c value so as to reduce αc to $0.5K_2$ to meet the requirements for DC mode, Section 7.9.2.

Such adjustments can be carried out as described in Sections 7.9.2 and 7.13. Alternatively they may be worked out using the proposed chart given in Fig 7.7. Two non-dimentional parameters are involved in this chart defined as the column/infill strength parameter, m_c, as:

$$m_c = \sqrt{\frac{2M_{pj}+2\beta_c M_{pc}}{f_c t h'^2}} \qquad (7.43)$$

and the infill parameter of geometry, q_c as:

$$q_c = \sqrt[4]{1+3\mu_c{}^2 K^4} \qquad (7.44)$$

Comparison of these parameters with Eq 7.9 leads to α_c as:

$$\alpha c = m_c q_c \qquad (7.45)$$

This equation gives a series of m curves in the chart for m taking values from 0.05 to 0.7 which are plotted in α_c-q_c coordinates.

In order to simulat he infill balancing condition, μ_{cb} derived from Eq 7.40 must replace μ_c in Eq 7.44 leading to:

$$q_c = \sqrt[4]{1+3K^2(1-\alpha_c)^2} \qquad (7.46)$$

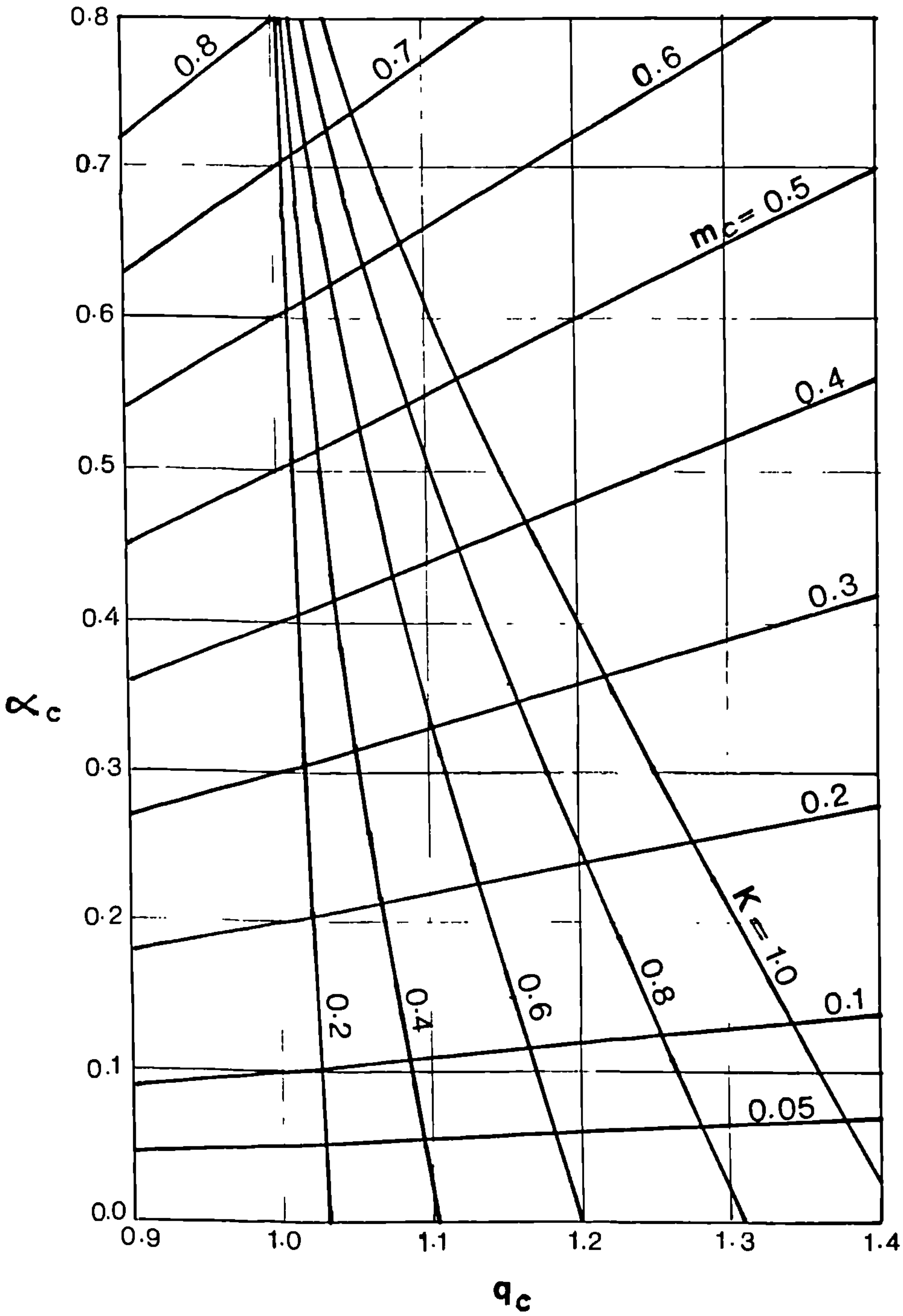

Figure 7.7 Chart for adjusting μ_c, β_c and α_c

This equation gives a series of K curves which are plotted in Fig 7.7. In order to specify the new state of an infilled frame for K taking values between 0.2 to 1.0 with DC mode of failure, a horizontal line at $\alpha_C = 0.5K_2$ must be drawn. Fig 7.8 illustrates the application of the chart. The arrows connecting the points marked by the same number indicate the adjustments procedure.

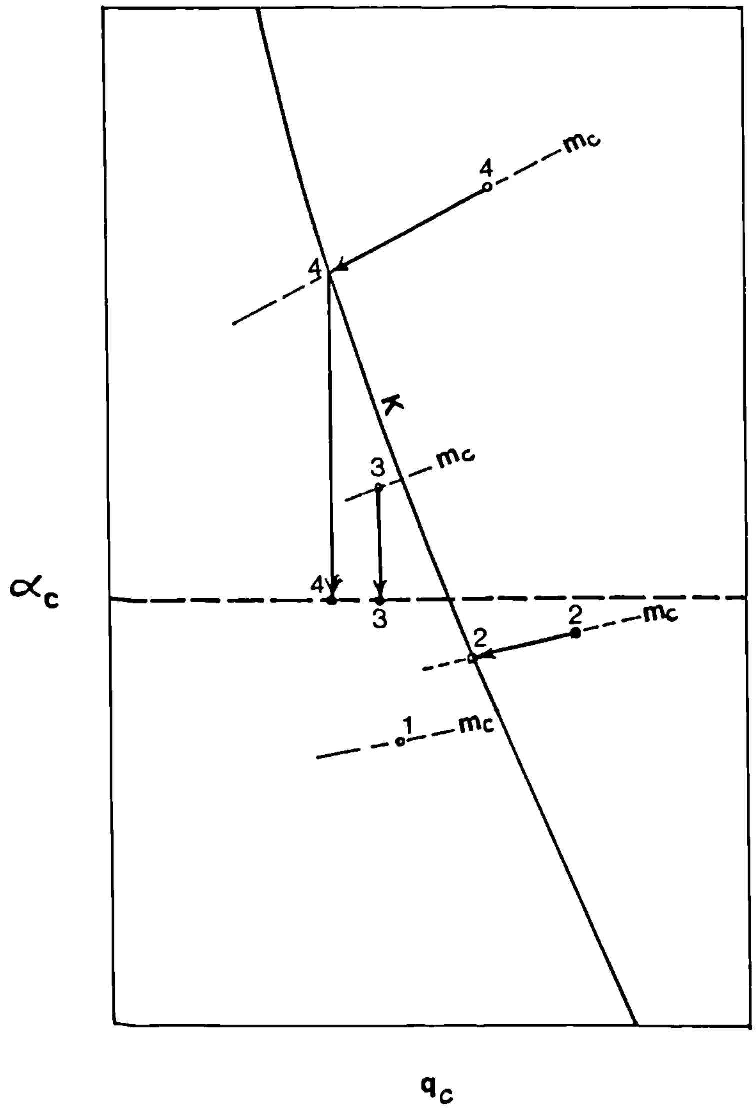

Figure 7.8 Application of The Chart

7.15 Frames Without Plastic Hinge at the Peak Load

The frame-infill interaction has been discussed in Section 7.2 where the beam and column ends were permitted to move and rotate independently at the loaded corners. The elastic analysis led to Eq 7.5 in terms of M_1 and M_j, Fig 7.2. The case when plastic hinges occur at the loaded corners, Eq 7.6, was taken as the normal case and was studied in detail in previous sections. Comparison of results of the proposed method with results of tests on infilled frames with very weak infill revealed, however, that such frames might not develop any plastic hinge at the collapse load and, the frame may behave in an elastic manner up to the peak load. This can be verified by assuming no change in the angle of the loaded corners of the frame. i.e.

$$\phi_c+\phi_b=0 \tag{7.47}$$

where ϕ_c and ϕ_b are the end rotations of the column and beam meeting at the loaded corners. Using the moment area method described in the standard text[99], these rotation angles can be derived and written as:

$$\begin{aligned} \phi_c &= -\ (1/4)M_1h' + C \\ \phi_b &= -\ (1/4)M_1l' + D \end{aligned} \tag{7.48}$$

where

$$C = (1/48)\sigma_{nc}th'3\alpha_c^2(6+3\alpha_c^2-8\alpha_c)\ +1.5K_c\Delta h_x$$

$$D = (1/48)\sigma_{nb}tl'3\alpha_b^2(6+3\alpha_b^2-8\alpha_b)\ +1.5K_b\Delta v_y$$

substituting for ϕ_c and ϕ_b from Eq 7.48 into Eq 7.47 and solving for M1 leads to;-

$$M_1 = 4(C+D)/(h'+l') \tag{7.49}$$

The M_1 value normally exceeds M_{pj} and the frame develops plastic hinges at the loaded corners. If however, $M_1 < M_{pj}$ the frame may not experience plasticity prior to the peak load. Therefore, M_{pj} must be replaced by M_1 in all previous equations in this chapter. This is a rare case and happens to only the infilled frames with very weak infill. Such frames undergo DC mode. As seen in Section 7.9.2, in DC mode α_c and/or α_b remain unchanged and are equal to $0.5k_2$. This indicates that M_1 can be calculated independently with no relation to the calculation of M_j, Eq 7.5.

7.16 Comparison Programme

In the following Sections the proposed method described in this chapter and the five previously existing methods described in chapter two, are compared with the experimental results from three different sources as well as with the finite element analysis carried out in the present work. The infilled frames subjected to comparison cover the variation of the following parameters.

i) Relative strength and stiffness of the frame and infill
ii) Aspect ratio of the panel, h'/l'
iii) Relative strength of the beams and columns.
iv) Pin-jointed and also semi-rigid jointed frames
v) Frame-infill lack-of-fit i ced by shrinkage, changes in the temperature and also poor workmanship.

As will be shown later compared with the previously existing methods, the estimations of the proposed method agree best with the actual results.

7.17 Results used in The Comparison Programme

7.17.1 The Finite Element Analysis Results

The infilled frames subjected to finite element analysis consisted of frames made of universal steel sections and square or rectangular infills with a variety of beam/column strength and stiffness combinations likely to be used in practice. A perfect fit was assumed for the frame/infill interfaces. These have been described in Chapter 6 and the results of the analysis are listed in Tables E.1 to E.9. Tables E.13(a) to E.21(a) also summarize the properties assumed for these infilled frames.

7.17.2 Experimental Results

There exists many experiments reported on model steel frames infilled by micro concrete walls. It was found convenient to use the test results from three different sources so that the effect of possible individual testing errors can be minimized in the process of the present comparison. The properties and the geometry of the test specimens are given in part (a) of Tables E.22 to E.39 in Appendix E. The following paragraphs describes these tests in more detail

Experiments of Saneinejad[29] are one of the series of tests chosen for comparison. These experiments consisted of two identical serı of 9 model 300x300mm square infilled frames loaded diagonally to complete destruction. The frames had been made of three types of solid rectangular steel sections, fully welded at the corners and infilled by micro concrete or sand-browning plaster mix with a variety of thicknesses to match the desired frame/infill strength and stiffness parameters. The results of the identical frames were averaged so that the testing errors are minimized. The infilled frames tested covered λh values ranging **3.6** to **15.0** and **m** values ranging **0.03** to **8.358.** The complete properties and geometry data of these series of tests, A1 to A9, are listed in Part (a) of Tables E.22 to E.30.

Types B, C and D of the tests carried out in the Building Research Station reported by Mainstone(9) (Figs 2.17 and 2.19), were also included into the present comparison. These series of model infilled frames had been made of micro-concrete infills combined with a weak frame, a strong frame and a strong frame with weak joints respectively. The reported compressive strength of the infills of type C frames included also the strength of the companion specimens of the frames subjected to repeated loading which showed much higher cracking strength, compared with the frames subject to only normal loading. Therefore the frames type C were excluded from the comparison scheme to avoid The difficulties in determining the strength of the infill. The complete properties and geometry data of these tests, M_1 to M_4, are listed in part (a) of Tables E.31 to E.34 in Appendix E.

Tests carried out by Stafford Smith(12) are the third series of tests included in the present comparison. These tests consisted of model square steel frames filled by 154x154x19mm micro concrete infill. The frames had been made of solid rectangular steel sections of 5 different thicknesses to cover the desired range for variation of λh. Five identical test specimens had been tested for each type, results of which have been averaged for use in this work. The complete list of the properties of these tests are listed in Tables E.35 to E.39.

In addition to the above descriptions the following assumptions were also made to complete the information needed:

i) The value of the co-efficient of friction at the frame-infill interfaces had not been reported by the original investigators. Therefore it was decided to take $\mu=0.45$ for all the test series. This value is slightly higher than the **0.41** reported by King et al[42] and also by Liauw et al[24], but it is lower that the **0.65** reported by Robbat et al[77].

ii) In the process of interpreting the compressive strength of the infill material it was decided to increase by 25% the result of the standard 100mm cube or cylindre compression tests, so as to cater for the effect of scaling-down[100] which applied to some of the test series under consideration.

iii) The compressive strength reported in Tables E.22 to E.39, σ_c, denotes the unconfined uniaxial compressive strength of the infill estimated as[32]:

$$\sigma_c = 0.95 f_c'$$

where the standard cylinder strength was taken as[32]:

$$f_c' = 0.8 f_{cu}$$

iv) Tensile strength for the infill material had not been reported by Mainstone[9] and Stafford smith[12]. Therefore the tensile splitting strength was taken as $0.12\sigma_c$ for the weak concrete used by Mainstone[9] and $0.10\sigma_c$ for the rather strong concrete used by Stafford Smith. These values agree with the values suggested by standard texts[32].

v) In order that a realistic comparison between the test results and the theoretical predictions can be made, the actual lack of fit induced as a result of shrinkage of the infill was estimated[32] to be equivalent to 2 millistrain in both the horizontal and vertical directions. For the sand-browning plaster infills, however, one millistrain was found to be the most appropriate value.

7.18 The Methods of Analysis Involved in Comparison

Five previously existing methods and also the newly proposed method of analysis were involved in the comparison programme. These methods are listed as follow:

SC The method which developed by Stafford Smith and Carter[13], Section 2.4.

SR Modification of SC method plus design recommendations established by Riddington and Stafford Smith[17], Section 2.6.

M The empirical method recommended by Mainstone[9], Section 2.5.

W The plastic design method developed by Wood[20], Section 2.7

W* Wood's method using the penalty factor, γ_p, proposed by Ma[96], Section 2.7.8.

L The plastic method of analysis developed by Liauw et al[25], Section 2.8

P The proposed method in the present work.

The infilled frames introduced in the previous section were analysed by the proposed method. The complete results are listed in Tables E.13(b) to E.39(b) in Appendix E. The results from all the methods concerned are listed in part (c) of these Tables. The section (d) of each Table compares the three most important results (the peak load, Hc, the cracking load, H_t, and the initial stiffness, K_0) of the frame in question, calculated from all the previous methods in a normalised format with respect to the test or finite element results. The normalised values have been written in percent format for simplicity and convenience. Program "ANALIF" was written in the BASIC language so that all the above mentioned calculations can be carried out using a micro computer. Some adjustments have been imposed to the predicted values so that a uniform and realistic comparison can be made between the methods in question. These are described in the following paragraphs.

In the SC method the ratio of f_t'/f_c' had been assumed to be $0.1f_c'$, Fig 2.10. The actual value of this ratio depends on the strength and water/cement ratio of the concrete[32]. Therefore, the offset of f_t'/f_c' from **0.1** has been adjusted by multiplying H_t to the adjusting factor of

$(f_t'/f_c')/0.1$. In this method the curves corresponding to 50% of the peak load in Fig 2.13 was adopted for calculating the diagonal stiffness of the infilled frames. This load limit being assumed to be the maximum load that may possibly occur during normal service loading.

Notice that as described in Chapter 2, the stiffness calculated from the M method refers to the stiffness of the infilled frame measured at the vicinity of the peak load on the load-deflection diagram. It is, however, the initial stiffness that is needed in practice whose value can be as high as double the value calculated by the M method. Therefore, the calculated stiffness values were doubled so that the results of stiffness, K_0, would be comparable with those calculated by the other methods.

The SR method had been based on the results obtained from finite element analysis of infilled frames with uniform infill even though it was developed specifically for masonry(17). Therefore it was concluded that it might also be used for concrete infill. This could be done by simply changing the multiplier **1.12** in Eq 2.36 to **1.68** (see Eqs 2.20 and 2.21). In this case, the cube strength of the infill must be used in the method as the compressive strength, because the calculation of the compressive failure was adapted from Mainstone's work(9).

The compressive strength used in **W** and **L** methods was taken as the cylinder strength, f_c'. The optional justification, Δf, has been accounted for using the analytical curves proposed by Wood(20), Fig 2.26.

7.19 Comparison of Peak Racking Load, H_c

7.19.1 General

The results related to H_c in part (d) of Tables E.13 to E.39 are listed in Table 7.2 so that the overall performance of each method relative to the others can be verified. The normalization has been so arranged that the value of 1.00 refers to a perfect agreement with the test or finite element results. The upper and lower maximum deviations and also the standard deviation relative to the reference value, 1.00, are also reported at the end of the table. In order to see the performance of each method when the experimental variations such as changes in material properties and workmanship are excluded, another set of deviations are also reported at the end of the table. These values comprise only the finite element analysis results, frames WMUR2 to WWUB2. As seen these latter values are smaller than the former values of deviation.

A graphical representation has also given in Fig 7.9 so that the accuracy of the methods under consideration can be visualized by one look. The value of unity represents a perfect match to the test or finite element results. Only a selective number of frames have been incorporated into the chart. These consisted of all the finite element examples, frames No. 1 to 9, and also 3 infilled frames with highest λh, frames No. 10 to No. 12. This selection of frames covered a wide range of λh, m, beam/column strength ratio and infill aspect ratio.

In the following sections the performance of each method of analysis will be discussed in detail.

Table 7.2 Comparison of The Collapse Racking Load, **Hc**

NO	Frame	lh	m	Hc(test)	Hc(calc.)/Hc(test or comp.)							
				KN	SC	SR	M	W	W*	L	P	P**
1	WMUR2	8.18	0.082	833.00	1.04	1.37	1.51	1.15	0.54	0.83	0.83	0.83
2	MMUR2	4.90	0.161	1098.00	1.31	1.60	1.68	1.01	0.60	0.87	0.92	0.92
3	SMUR2	3.34	0.161	1148.00	1.84	2.15	2.25	0.93	0.58	0.84	1.01	1.01
4	SWUR2	3.25	0.071	1038.00	2.09	2.43	2.47	0.81	0.40	0.81	0.94	0.94
5	WWUS2	8.27	0.186	679.00	1.26	1.08	1.22	0.96	0.63	0.95	0.96	0.96
6	MWUS2	4.96	0.186	747.00	1.91	1.55	1.61	1.17	0.57	0.86	1.05	1.05
7	SWUS2	3.38	0.186	879.00	2.38	1.84	1.91	1.00	0.49	0.73	0.95	0.95
8	SSUS2	3.65	1.496	1530.00	1.26	0.99	1.38	0.87	0.81	0.97	1.09	1.09
9	WWUB2	12.24	0.061	696.00	1.45	1.31	1.49	1.22	0.61	0.92	0.94	0.94
10	SSUSA1	3.60	8.358	2.31	0.97	0.76	1.16	2.43	2.29	2.13	0.95	0.95
11	SSUSA2	4.16	4.697	3.50	0.99	0.78	1.03	1.77	1.64	1.78	1.04	1.04
12	MMUSA3	5.39	2.435	2.28	0.95	0.78	0.92	1.36	1.23	1.41	1.12	1.12
13	SSUSA4	5.98	0.507	16.58	1.34	1.11	1.28	0.84	0.80	1.14	1.15	1.09
14	SSUSA5	6.91	0.284	25.49	1.35	1.14	1.29	0.81	0.70	1.05	1.00	0.98
15	SSUSA6	7.40	0.217	33.83	1.24	1.06	1.19	0.77	0.60	0.90	0.87	0.86
16	MMUSA7	8.44	0.186	11.56	1.56	1.30	1.51	1.03	0.80	1.20	1.15	1.11
17	MMUSA8	10.31	0.084	26.62	1.23	1.09	1.23	0.76	0.52	0.78	0.75	0.79
18	WWUSA9	14.96	0.030	22.76	1.24	1.14	1.32	0.72	0.45	0.68	0.66	0.82
19	WWUSM1	7.16	0.412	28.60	1.07	0.90	1.02	0.73	0.69	1.03	0.99	0.95
20	WWURM2	7.06	0.178	32.14	1.00	1.19	1.32	0.96	0.66	0.94	0.88	0.85
21	WWURM3	6.71	0.131	27.58	1.08	1.47	1.62	1.07	0.69	1.00	0.92	0.89
22	WWUSM4	3.32	0.328	64.20	1.29	1.00	1.09	0.41	0.34	0.55	0.86	0.79
23	W1USS	14.33	0.038	10.50	1.12	1.03	1.18	0.72	0.44	0.66	0.63	0.90
24	W2USS	10.69	0.085	12.60	1.25	1.11	1.26	0.84	0.55	0.82	0.79	0.93
25	M1USS	8.80	0.147	14.00	1.36	1.18	1.33	0.93	0.65	0.97	0.93	1.03
26	M2USS	6.60	0.334	19.82	1.29	1.08	1.23	0.80	0.69	1.04	0.99	1.03
27	S1USS	4.15	1.146	35.55	1.14	0.90	1.22	0.71	0.71	0.88	1.06	1.04
For all frames:												
	Deviations				-0.05	-0.24	-0.08	-0.59	-0.66	-0.45	-0.37	-0.21
					1.38	1.43	1.47	1.43	1.29	1.13	0.15	0.12
	Standard deviation				0.49	0.46	0.54	0.38	0.49	0.33	0.14	0.11
FOR F.E. results only:												
	Deviations				0.04	-0.01	0.22	-0.19	-0.60	-0.27	-0.17	-0.17
					1.38	1.43	1.47	0.22	-0.19	-0.03	0.09	0.09
	Standard deviation				0.80	0.79	0.87	0.14	0.46	0.16	0.08	0.08

Note: Forcalculating the standard deviation, the normalized values were compared with the normalized test values (1.0). ie.;

$$S = \left[\sum \sqrt{(Xi-1)^2}\right] / (N-1) \quad \text{(N=the number of samples)}$$

* Using Ma's penalty factor
** Using variable K1

Frame Nos. 1-9 FE, 10-18 Ref(29), 19-22 Ref(9), 23-27 Ref(12)

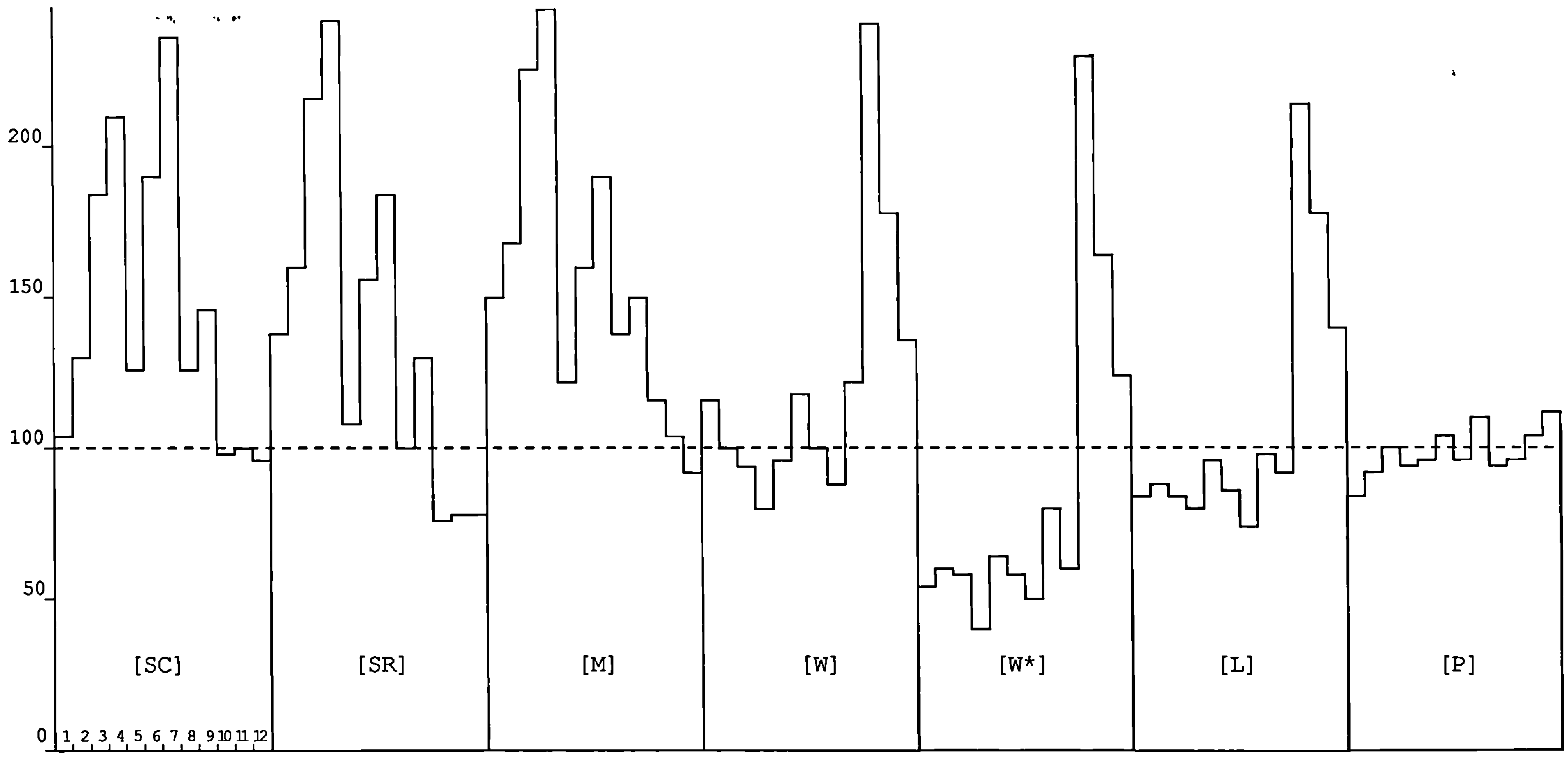

Figure 7.9 Comparison of Various Methods of Analysis with Finite Element and Test Results of Horizontal Collapse Load, **Hc**, Using Table 7.4

7.19.2 Methods Based on Stiffness Parameter λh

Methods SC, SR and M, introduced in Section 7.18, are all based on the stiffness parameter, λh. As discussed in Chapter 2 these methods are also based on the following assumptions.

i) Frame members behave in linear and elastic manner at all the stages of loading up to the peak load.
ii) Frame is uniform.

Amid the tests used for comparison in Table 7.2, the tests No. 10, to No. 12 were the only cases that satisfied the both assumptions. This was confirmed by the proposed method which accounts for both the elastic and plastic behaviour of the frame material. Comparison of M_1, M_{3c} and M_{3b} from part (b) of Tables E.22 to E.24, with M_{pj}, M_{pc} and M_{pb} respectively in these Tables, shows that the members of these frames remains in linear and elastic state up to the peak load. Therefore, it is not surprising to see a fairly good agreement between the predictions of SC method and the test results for these particular tests, the largest deviation was only 5% below the test value. The M method also leads to a consistent and good agreement with deviations ranging between -8 to +16. However, the SR method leads to consistently low values, because this method neglects the contribution of the frame, which is quite appreciable in these particular cases.

If either the above assumptions (i and ii) ceases to be met, the SC, SR and M methods lead to generally far over-estimated results. Infilled frames No. 1, 2, 5, 8, 9 ınd also No. 13 to No. 27 in Table 7.2, were made of almost ıniform members and, thus, satisfied the second assumption, ›ut they violate the first assumption and develop plastic .inges at the loaded corners before the peak load has been ·eached. Maximum deviation of predictions of the methods of C, SR and M reached to 56, 60 and 68% respectively. This s because the frame underwent yielding at the loaded orners and, thus, failed to take higher bending moments at hese sections, not being able to develop the length of ontact predicted by the elastic analysis used in SC method. uch discrepancy becomes more dramatic for infilled frames ith weak frame, e.g. frame 9 in Table 7.2. These frames evelop plastic hinges at a load level much lower than that f the peak.

Fig 2.10 shows that the SC method does not reflect he effect of rectangular infill on the compressive strength f the infill as much as it should since, it estimates an ven a narrower diagonal band width for infilled frames with igher **l'/h'** ratio. As a result of this the estimated peak ɔads have been shifted in the opposite direction to the ffect of the plasticity of the frame, resulting in, ɔparently, fairly accurate results for a few rectangular ıfilled frames, frames No. 1 and 20. As can be seen for ame 1 in Fig 7.1, such a counter balancing is not ɔnsistent for rectangular infilled frames. On the other ınd, the methods SR and M over-estimate the effect of ctangular infills. The infilled frames No. 4 and 7 in .g 7.2 have a similar frame and infill but different panel pect ratio. Therefore the inaccuracy of the three methods of SC, SR and M can be calculated respectively for frame No.4 having an aspect ratio of $\mathbf{h'/l'}$=0.5722 as:

100[(2.09/2.38)-1.00] = -12%

100[(2.43/1.84)-1.00] = +32%

100[(2.47/1.91)-1.00] = +29%

This comparison is not affected by experimental errors due to variation of properties of the materials and workmanship, because the source of comparison is a non-linear finite element analysis. Therefore the inaccuracies are purely due to the theoretical assumptions of the method in question.

Further study of this matter showed that the results from SC, SR and M methods would considerably improve if the strength of the infill were related to only the length of the smaller side of the infill. Assuming $\mathbf{h'<l'}$ this assumption leads to the peak diagonal load as:

$$\mathbf{R_{ic} = \sqrt{2}\,\alpha_c h' t f_c}$$

and for the peak racking load to:

$$\mathbf{H_{ic} = \sqrt{2}\,\cos\theta\alpha_c h' t f_c} \qquad (7.50)$$

α_c equals to a/h',Eq 2.6 , for SC method and equals to $\mathbf{W'_{ec}/w'}$, Eqs 2.14 and 2.20, for SR and M methods. The multiplier $\sqrt{2}$ adjusts $\mathbf{R_{ic}}$ to become identical to those predicted by the method in question for square infill, so that the values of α_c that has been proposed by the same method can be used in Eq 7.50 directly. Having implemented this modification the discrepancy of SC, SR and M methods (due to only converting from square to rectangular panel with the aspect ratio of **h′/l′=0.5722**) become:

$$100[(2.09/2.38)(\sqrt{2}/\sec 29.8)\ -1.00] \quad = +7.8\%$$

$$100[(2.43/1.84)(0.5\sqrt{2}/\cos 29.8)-1.00] = +7.6\%$$

$$100[(2.47/1.91)(0.5\sqrt{2}/\cos 29.8)-1.00] = +5.4\%$$

which are only slightly on the unsafe side.

The finite element analysis, Table 7.2, showed that non-uniformity of the frame, i.e. the beams being weaker than columns, has a significant effect on the peak load. Plastic resisting moment of the joints, $\mathbf{M_{pj}}$, would directly decrease if a weaker beam is chosen. This results in a comparatively shorter length of contact at the column-infill interfaces and therefore a relatively lower value for the peak racking load. However, the weakness of the beams are ignored by the SC, SR and M methods. Therefore, they predicted dramatically high values of peak loads for infilled frames with weak beams relative to the columns. As shown in Table 7.2, deviations of the predicted values of the peak loads from the actual values for frames No 3, 4, 6 and 7 ranged between +84 to +138%, +31 to +143% and +61 to 147% respectively. The maximum value of column/beam strength ratio defined as $\mathbf{M_{pc}/M_{pb}}$ was 16 for frames No 4 and
listed
7 in Table 7.2. Such high deviations imply that these methods should be considered inapplicable for non-uniform frames, or alternatively, the frames should be assumed that is made, uniformly, of members having strength and stiffness equal to that of the weaker member. This leads to considerablly under-estimated results for rectangular infilled frames which resist mainly on the column strength.

7.19.3 Wood Method (W)

As discussed in Chapter 2, Wood's method uses the strength parameter, **m**, and is based on the following major assumptions for the state of the infill and frame materials at the peak load:

i) Infill stress has reached to a simplified biaxial failure surface over the proposed stressed area.

ii) Frame has developed one of the proposed plastic collapse mechanism.

Although an experimentally based variable penalty factor γ_p, has been proposed by Wood to cater for the errors due to the simple assumptions made for the infill behaviour, there is still a question of whether this factor, alone, can reasonably do the job. In order to answer this question frames 10, 11 and 12 in Table 7.2, must be excluded from the comparison Table because they did not meet the second assumption which may have indirect effects on γ_p. These frames had very high **m** values (2.28 to 3.50) and will be discussed later. Although The remaining frames did not develop a plastic collapse mechanism at the peak load they partially met the second assumption by developing plastic hinges only at the loaded corners. Since this is generally the case, one may conclude that the proposed penalty factor, γ_p, actually accounts for also the reserved strength left in the frame at the peak load before it develops a complete plastic collapse mechanism. Having excluded the above mentioned three frames and also frame No 22 which had very weak joints relative to the strength of the beams and columns, the results from Wood's method deviated from the actual results ranging between -29% to +22%. The comparison included infilled frames with rectangular panels and frames with weak beams relative to the columns and also infilled frames having λh and m values covering a wide range. Considering the variations due changes of the properties of the materials and workmanship the above deviations prove that the W method predicts the peak load within a reasonably accurate range. Performance of the method can be judged in a more precise comparison by considering only the finite element analysis results which are independent of any inconsistency of material properties and workmanship. Such a comparison leads to deviations ranging between -19% to +22% with an standard deviation equals to 14%.

The W method, however, underestimates by 59% the collapse load of a semi-rigid frame (frame No. 22 in Table 7.2) with beams and columns 20 times stronger than the joints. Details of this frame including the plastic resisting moments of beams, columns and joints (M_{pb}, M_{pc} and M_{pJ}) are listed in Table E.34.

The method also over-estimated up to 143% the collapse load of the infilled frames with strong frame and very weak infill, frames 10 to 12 in Table 7.2. According to the results of the newly proposed method (Tables E.22(b), 23(b) and 24(b)), the frame members of these infilled frames behaved linear and elastic throughout the loading up to the peak load. Therefore, the above mentioned large deviation is because the second of the main assumptions of the method, mentioned earlier in this section, has been entirely violated.

The collapse loads also were calculated by W method using the uniform γ_p value proposed by Ma[96], section 2.78. As seen in Table 7.2, the results are generally low, thus, indicating that Ma presumably proposed a low and uniform γ_p such that, in no case, the value of the calculated collapse load exceeds the actual value.
Table 7.2 shows that except for frames No. 10 to 12 the Ma's proposed penalty factor leads to safe but uneconomical collapse loads.

7.19.4 Liauw Method (L)

As discussed in Chapter 2 the L method is independent of any penalty factor and uses only one of the strength parameters of $\mathbf{m_1}$, $\mathbf{m_2}$ or $\mathbf{m_3}$ and is based on the assumptions nearly similar to those of the W method, but assuming no shear stress at the frame-infill interfaces. However, finite element analysis, Table E.1 to E.12, showed that except for infilled frames with small aspect ratio, say $\mathbf{h'/l' < 0.5}$, the shear forces at the boundary of the infill over the length in contact, are significant. This is in favour of the strength of the infilled frame. On the other hand, the loss of strength due to lack of ductility of infill and assumption of development of a plastic collapse mechanism are unfavourable to the collapse load. But these may counter balance each other such that the final collapse load gets close to the actual value. In order to see if this is generally the case frames 10, 11, 12, 18, 22 and 23, Table 7.2, which might have created exceptional effects should be excluded from the comparison scheme (these frames will be discussed later). Having done this the deviations of the calculated values of the collapse load, from those of the actual and finite element analysis would be -27% to +20%. Excluding also the test results from the comparison so as to eliminate the errors due to changes of properties of the materials and workmanship, the range of deviations reduces to -27% to -3% with the standard deviation of 16%, Table 7.2. This shows that like the W method the L method also predicts the peak load within a reasonably accurate range for the group of the frames selected for comparison. Such an agreement also proves that the aforementioned counter effects is definitely the case.

Study of the method in predicting the collapse load of the infilled frame with semi-rigid joints, frame 22 in Table 7.2 shows that the L method underestimated 45% the collapse load. The estimated value was, however, 34% higher than that of the W method. This implies that like the W method the L method is incompatible with the infilled frames having semi-rigid joints.

Like the W method, the L method over-estimated greatly (113%) the collapse load of frames No. 10 to 12 in Table 7.2. The same discussion as made for the W method in previous section applies also the L method.

The L method predicted 32% and 34 % lower collapse loads for infilled frames 18 and 23. This is because of the assumption of the simple stress block in the loaded corners which will be discussed in the following section.

7.19.5 Proposed Method (P)

As discussed earlier in this Chapter, the proposed method uses linear elasticity theories with allowance for occurrence of plastic hinges at the loaded corners of the frame and is based on the following major assumptions at the peak load.

i) Infill stress has reached a simplified biaxial Von Mises criterion at either column or infill interfaces in the loaded corners.

ii) Infill has developed a specified (limited) strain in the loaded corners

iii) Frame may have developed plastic hinges at the loaded corners only, but no plastic collapse mechanism has occurred.

Contrary to the existing plastic methods the proposed method gives fairly accurate results for frames No. 10, 11 and 12. Because the method accounts for both the elastic and plastic behaviour of the frame, the deviations ranged between only -5 to +12%. These frames were found to be in an elastic state at the peak load. Unlike W and L methods the proposed method gives a relatively accurate result for the semi-rigid frame (frame No 22) with only -14% deviation, Table 7.2.

The proposed method gave results with deviations ranging between -17 to +15% for all the frames listed in Table 7.2, except those with small lengths of contact relative to the thickness of the infill. These were frames 17, 18, 23 and 24 which are listed in Table 7.3 in the order of the ratio of the length of contact, $\alpha_c h'$, to the thickness of the infill, t.

Table 7.3 Deviation of H_c(%) for Frames with Low α_c Value

No	Frame	α_c	$\alpha_c h'/t$	Deviations (%)	
				K_1=0.95	K_1, Eq 7.52
23	WIUSS	0.058	0.46	-37	-10
18	WWUA9	0.052	0.59	-34	-18
24	W2USS	0.086	0.69	-21	- 7
17	MMUSA8	0.086	1.21	-25	-21

As seen the smaller is this ratio, the lower is the predicted value of the peak load, relative to the actual value. This can be attributed to the infill confinement induced by the frame acting as solid platens over the regions in contact. Such a confinement produces an out-of-plane compressive stress and, thus, postpones the failure of the infill which is also subjected to biaxial compression in the plane of the infill. This additional strength is neglected in the proposed method as K_1 in Section 7.4 was taken as a constant value for all cases. However, this contribution is, indirectly, allowed for in W method, because Wood[20] used an empirical approach to establish the variation of the penalty fa r, γ_p. This can be accounted for also in the proposed method by relating the effective strength, f_c, to $\alpha_c h'/t$ value as follow .

The additional strength induced because of the confining effects of the platens in the test of a cylinder spesimen under uniaxial compression, has been studied by Gonnerman[101]. The proposed curve which has been reported also by Neville[42], has been converted by the author into a simple formula, relating the compressive strength to the height/diameter ratio of the cylinder as follows:

$$\frac{f_c}{f_c'} = \frac{0.217}{(h/d)-0.266} + 0.875 \qquad (7.51)$$

fc denotes the effective compressive strength of the specimen and f_c' is the standard cylinder compressive strength for $h/d=2.0$. Assuming that the effect of the $\alpha_c h'/t$ on the strength of the infill is similar to the effect of the h/d on the cylinder strength, h/d in Eq 7.51 may be replaced by $\alpha_c h'/t$ to give the effective compressive strength of the infill as:

$$f_c = k_1 f_c' \quad \text{where} \quad K_1 = \frac{0.217}{(\alpha_c h'/t)-0.266} + 0.875 \qquad (7.52)$$

K_1 from Eq 7.52 replaces the value proposed in Section 7.4.

Having imposed the modified K_1 value, deviations of the calculated values of H_c from the actual values reduce to the values given in the last column of Tables 7.2 and Table 7.3. As seen the deviations have decreased effectively. The range of deviation for all the frames listed in Table 7.2 becomes -21% to +12% and the standard deviation drops to 11% (see the last column of Table 7.2).

As can be seen from Table 7.2 and Fig 7.9, unlike the previously existing methods, the proposed method gives consistent and safe predictions for H_c over a wide range of γ_p and m values and for the practical range of panel proportion and frames with lack of fit and semi-rigid joints

7.20 Comparison of the Estimated Cracking Load, H_t

Table 7.4 and Fig 7.10(a) compare the normalized value of cracking load (ratio of the calculated to the test result) estimated by SC, SR, M and the proposed method, P. These results lead to standard deviations of 44, 28, 26 and 9% respectively. The W and L methods are not applicable for determination of the diagonal cracking load. The deviations shown in Table 7.4 are because of;

a) Variation of the strength of the infill relative to those of the companion specimens.
b) Errors due to the assumptions made in the method concerned.

In order to verify the errors due to only the theories, the results of the tests may be excluded from the comparison scheme, i.e. considering only the finite element analysis results. This leads to smaller deviations as given separately in Table 7.4 . These results also have been plotted in a bar chart, Fig 7.10(a), which also includes the results of the tests No. 10, 11 and 12 so that the comparison chart covers a wide range of λh and m values. As seen the results of the proposed method and the finite element agree remarkably well with each other with a standard deviation of only 3% showing that the theory that has been used in the proposed method s fairly realistic and, thus, reliable. The previously existing methods, however, do not follow any particular trend and give rather disappointing results with deviations up to 88%.

Table 7.4 Comparison of Diagonal Tension Load, **Ht**

No	Frame	λh	m	Ht(test) KN	Ht(calc.)/Ht(test or f.e.) SC	SR	M	W	L	P
2	MMUR2	4.90	0.161	1098.00	1.70	1.40	1.09			0.95
3	SMUR2	3.34	0.161	1101.00	1.78	1.40	1.27			0.95
4	SWUR2	3.25	0.071	1038.00	1.88	1.48	1.32			1.00
5	WWUS2	8.27	0.186	679.00	1.33	1.30	0.99			1.02
6	MWUS2	4.96	0.186	684.00	1.41	1.29	1.15			1.01
7	SWUS2	3.38	0.186	714.00	1.45	1.23	1.28			0.97
8	SSUS2	3.65	1.496	811.00	1.27	1.09	1.47			1.01
10	SSUSA1	3.60	8.358	2.00	1.04	0.87	0.76			0.86
11	SSUSA2	4.16	4.697	2.95	1.19	1.05	0.74			0.91
12	MMUSA3	5.39	2.435	1.96	1.40	1.28	0.70			1.01
13	SSUSA4	5.98	0.507	14.21	1.33	1.24	1.03			0.98
14	SSUSA5	6.91	0.284	23.97	1.35	1.32	1.01			1.03
15	SSUSA6	7.40	0.217	31.57	1.34	1.31	0.98			1.03
19	WWUSM1	7.16	0.412	26.80	1.05	1.02	0.82			0.80
22	WWUSM4	3.32	0.328	33.20	1.22	1.04	1.14			0.81
24	W2USS	10.69	0.085	13.30	1.29	1.31	1.10			1.03
25	M1USS	8.80	0.147	13.30	1.35	1.31	1.17			1.03
26	M2USS	6.60	0.334	13.30	1.40	1.31	1.32			1.03
27	S1USS	4.15	1.146	17.30	1.14	1.01	1.51			0.80
	For all frames: Deviations				0.04	-0.13	-0.30			-0.20
					0.88	0.48	0.51			0.03
	Standard deviation				0.44	0.28	0.26			0.09
	For F.E. analysis frames only: Deviations				0.27	0.09	-0.01			-0.05
					0.88	0.48	0.47			0.02
	Standard deviation				0.64	0.36	0.29			0.03

Note: For calculating the standard deviation, the normalized values were compared with the normalized test values (1.0). ie.;

$$s = \left[\sum \sqrt{(Xi-1)^2}\right] / (N-1) \quad \text{(N=the number of samples)}$$

Frame Nos. 1-9 FE, 10-18 Ref(29), 19-22 Ref(9), 23-27 Ref(12)

7.21 Comparison of the Estimated Initial Stiffness, K_0

Table 7.5 and Fig 7.10(b) compare the normalized value of the initial stiffness (ratio of the calculated to the test result) estimated by SC, SR, M and the proposed method resulting in standard deviations of 67%, 35%, 28% and 23% respectively. The deviations are because of:

a) Variation of the modulus of the infill relative to those of the companion specimens.
b) Errors due to the assumptions made in the method concerned.
c) Variation of the lack of fit induced by shrinkage of the infill.

Mainstone(9) found that the stiffness of an infilled frame subjected to racking load, is strongly affected by shrinkage of the infill, Fig 2.19. In order to eliminate such unknown error from the comparison table, only the results of finite element analysis may be brought into consideration as listed at the end of Table 7.5. By this approach the effects may be verified independently. As seen comparison of the results of the proposed method with the finite element analysis leads to reasonably accurate stiffnesses with standard deviation of 10% and deviations ranging -19% to +15%. Amid the previously existing methods, only the M method leads to rather consistent results with standa d deviation of 18%. The SC and SR methods leads to over and under estimations.

Fig 7.10(b) compares the performances of the methods under consideration. This comparison includes also frames No. 10 to 12 covering a wide range of λh value.

Table 7.5 Comparison of Stiffness, **KO**

No	Frame	λh	m	K0(test KNmm	K0(calc.)/K0(test or f.e.) SC	SR	M	W	L	P
1	WMUR2	8.18	0.082	192.60	1.72	1.01	1.03			0.96
2	MMUR2	4.90	0.161	211.10	1.94	0.92	0.99			1.04
3	SMUR2	3.34	0.161	238.20	1.88	0.82	1.03			0.97
4	SWUR2	3.25	0.071	234.60	1.91	0.83	1.04			0.97
5	WWUS2	8.27	0.186	187.90	1.34	0.69	0.81			1.10
6	MWUS2	4.96	0.186	210.33	1.38	0.61	0.76			1.01
7	SWUS2	3.38	0.186	246.60	1.26	0.52	0.75			0.81
8	SSUS2	3.65	1.496	299.30	1.04	0.43	0.71			1.11
9	WWUB2	12.24	0.061	150.50	1.50	0.86	0.89			1.15
10	SSUSA1	3.60	8.358	4.97	0.62	0.25	0.45			0.64
11	SSUSA2	4.16	4.697	4.96	1.07	0.45	0.68			1.07
12	MMUSA3	5.39	2.435	3.40	1.18	0.54	0.75			1.09
13	SSUSA4	5.98	0.507	15.71	1.28	0.61	0.82			1.08
14	SSUSA5	6.91	0.284	16.40	2.09	1.04	1.32			1.52
15	SSUSA6	7.40	0.217	23.90	1.88	0.94	1.15			1.24
16	MMUSA7	8.44	0.186	11.56	1.81	0.95	1.11			1.18
17	MMUSA8	10.31	0.084	23.66	1.91	1.03	1.13			0.95
18	WWUSA9	14.96	0.030	22.99	2.24	1.32	1.29			0.81
19	WWUSM1	7.16	0.412	22.85	1.48	0.74	0.92			0.93
20	WWURM2	7.06	0.178	26.74	1.73	0.91	1.04			0.73
21	WWURM3	6.71	0.131	25.34	1.89	1.05	1.04			0.60
22	WWUSM4	3.32	0.328	26.20	1.84	0.74	1.84			1.34
23	W1USS	14.33	0.038	25.90	1.63	0.88	0.87			0.62
24	W2USS	10.69	0.085	33.60	1.26	0.68	0.74			0.66
25	M1USS	8.80	0.147	38.50	1.15	0.59	0.68			0.71
26	M2USS	6.60	0.334	43.80	1.09	0.52	0.67			0.84
27	S1USS	4.15	1.146	48.60	1.08	0.47	0.72			1.19
	For all frames: Deviations				-0.38	-0.75	-0.55			-0.40
					1.24	0.32	0.84			0.52
	Standard deviation				0.67	0.35	0.28			0.23
	For F.E analysis only: Deviations				0.04	-0.57	-0.29			-0.19
					0.94	0.01	0.04			0.15
	Standard deviation				67	0.33	0.18			0.10

Note: For calculating the standard deviation, the normalized values were compared with the normalized test values (1 0). ie.;

$$S = [\Sigma \sqrt{(Xi-1)^2}] / (N-1)$$ (N=the number of samples)

Frame Nos. 1-9 FE, 10-18 Ref(29), 19-22 Ref(9), 23-27 Ref(12)

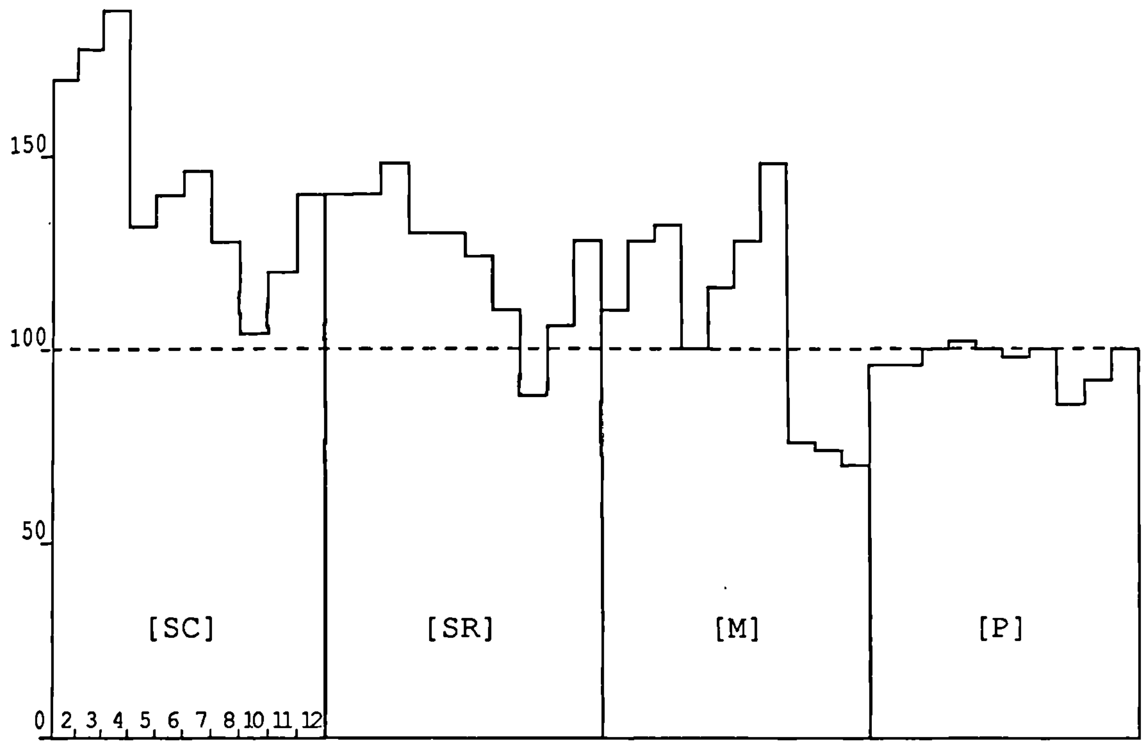

(a)

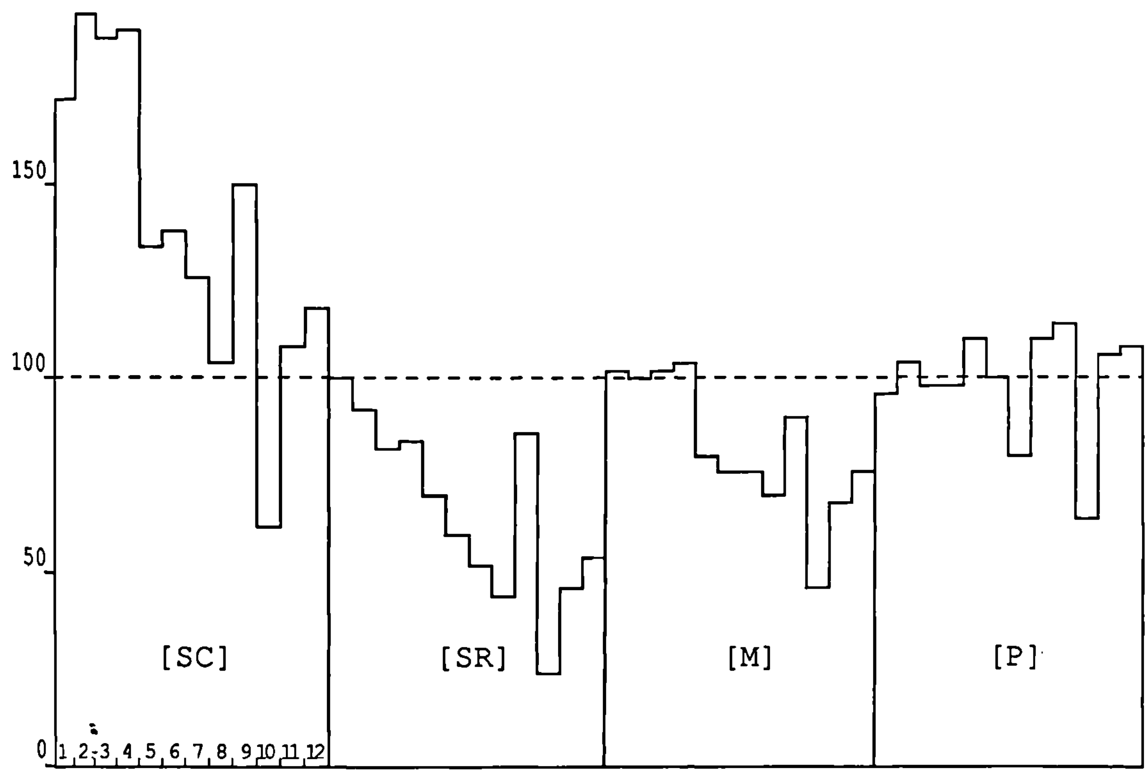

(b)

Figure 7.10 Comparison of various Methods of Analysis with Finite Element and test results using Tables 7.5 and 7.6; a) Cracking load, H_t, b) Stiffness, K_o

7.22 Comparison of Estimated Frame Bending Moments

Frame internal forces may not be easily obtained from experiment. Finite element analysis results, however, give these forces in full detail as listed in Tables E.1 to E.12 . For design purposes, the bending moments at the loaded and unloaded ends of the frame members and also the sagging or hogging bending moments somewhere within the span of the beams and columns are needed. Tables E.13(c) to E.21(c) list these moments (M1, M4, M3c and M3b) resulting from the finite element analysis computer program and the previously existing methods, if applicable, and the proposed method. These are rearranged into Tables 7.6 to 7.8 as follows:

Finite element analysis showed that all the frames analysed developed plastic hinges at the loaded corners of the frame at the peak load, i.e. M1=Mpj. Table 7.6 compares the predicted value of M1/Mpj ratio for all the methods under consideration. As seen the finite element analysis and also W, L and P methods permit occurrence of plastic hinges at the loaded corners. However, the other existing methods, (SC, SR and M methods) either are not applicable or give very scattered results with deviations between -89% to +242%.

Table 7.7 compares the ratio of M_4/M_{pj}. As seen, excluding the infilled frame No 8, SSUS2, the value of this ratio from the finite element analysis ranges 0.01 to 0.14. All the previously existing methods give dramatically over-estimated values. The proposed method, however, gives results generally within the same range as given by the finite element analysis, but over-estimates only the results for frames No. 6 and 8. A safe and economical value for M_4 may be taken as the higher of the two values of 0.2 M_{pj} and the calculated value using the proposed method.

Table 7.8 compares the ratio of the sagging or hogging bending moment of the column, M_{3c}, to the plastic resisting moment of the columns, M_{pc}, using the finite element results and the predicted values. As seen the previously existing methods are either not applicable or gave dramatically high values. The finite element analysis results gave M_{3c}/M_{pc} ratios ranging between 0 to 0.24 and the results from the proposed method fall within the range of 0.07 to 0.18. Therefore, 0.25 M_{pc} should be a safe estimate for M_{3c}. Similarly M_{3b} may be taken as $0.25M_{pb}$ rather than the values given by the proposed method.

Table 7.6 Comparison of bending moment at the loaded corners

No.	Frame	M_{pj} KNm	M_1/M_{pj}			
			SC	SR	M	W,L,P
1	WMUR2	72.37	N.a	1.10	0.25	1.00
2	MMUR2	142.00	"	0.93	0.43	1.00
3	SMUR2	142.00	"	1.20	0.56	1.00
4	SWUR2	62.35		3.42	0.54	1.00
5	WWUS2	62.35	"	0.98	0.24	1.00
6	MWUS2	62.35	"	1.22	0.46	1.00
7	SWUS2	62.35	"	1.66	0.60	1.00
8	SSUS2	501.60	"	0.23	0.86	1.00
9	WWUB2	62.35	"	2.00	0.11	1.00

Frame Nos. 1-9 FE, 10-18 Ref(29), 19-22 Ref(9), 23-27 Ref(12)

Table 7.7 Comparison of bending moment at unloaded corners

No.	Frame	M_4/M_{pj}						
		F.e	SC	SR	M	W	L	P
1	WMUR2	0.03	N.a	1.11	0.25	1.00	1.00	0.03
2	MMUR2	0.10	"	0.89	0.41	1.00	1.00	0.03
3	SMUR2	0.14	"	1.25	0.58	1.00	1.00	0.06
4	SWUR2	0.09	"	2.92	0.46	1.00	1.00	0.01
5	WWUS2	0.00	"	0.85	0.21	1.00	1.00	0.04
6	MWUS2	0.01	"	1.34	0.51	1.00	1.00	0.34
7	SWUS2	0.04	"	1.88	0.67	1.00	1.00	0.06
8	SSUS2	0.28	"	0.22	0.81	1.00	1.00	0.59
9	WWUB2	0.01	"	1.84	0.11	1.00	1.00	0.08

Frame Nos. 1–9 FE

Table 7.8 Comparison of column bending moment, M_{3c}

No.	Frame	M_{3c}/M_{pj}						
		F.e	SC	SR	M	W	L	P
1	WMUR2	0.24	0.00	N.a	N.a	1.00	1.00	0.17
2	MMUR2	0.20	0.00	"	"	1.00	0.77	0.16
3	SMUR2	0.15	0.00	"	"	1.00	0.49	0.15
4	SWUR2	0.14	0.00	"	"	1.00	0.45	0.16
5	WWUS2	0.00	0.00	"	"	1.00	0.96	0.17
6	MWUS2	0.04	0.00	"	"	1.00	0.57	0.15
7	SWUS2	0.07	0.00	"	"	1.00	0.34	0.15
8	SSUS2	0.17	0.00	"	"	<1.00	0.67	0.07
9	WWUB2	0.07	0.00	"	"	1.00	0.96	0.18

Frame Nos. 1–9 FE

7.23 Comparison of the Predicted Frame Axial Forces

Frame members are subjected to axial and shear forces. These forces may not be easily obtained from experiment. The finite element analysis, however, gives detailed information about the axial forces and their variations along the the frame members. Using Tables E.13(c) to E.21(c), Table 7.9 has been established and lists the ratio of the estimated/computed values of the columns axial forces for frames No 1 to 9. As seen all the previously existing methods resulted in either zero or extremely underestimated values for the column axial forces. The proposed method, however, leads to results with moderate deviations ranging generally between -19% and +11%. Infilled frame No. 8, SSUS2, having a very strong frame relative to the infill, developed a much lower than predicted shear force at the infill/column interface. Therefore, the estimated value of the column axial force has been 75% higher than the computed value of the column axial force induced by the shear forces transferred at the infill/column interface. For the same reason the column axial force is strongly dependent on the coefficient of friction of the frame/infill interfaces. Therefore, a safe design value for axial force should allow for possible variation of the co-efficient of friction and also the deviation of the estimation of the proposed method from the actual values.

7.24 Comparison of Estimated Frame Shear Forces

Estimation of shear force is very important for design purposes because the frame members have normally a limited shear capacity. Table 7.10 gives the ratios of calculated to computed values of column shear forces. Only proposed method gaves reasonable results with a standard deviation of 0.15.

Table 7.9 Comparison of Column Axial Force, N_{c1}

No.	Frame	N_{c1}	N_{c1}(calc.)/N_{c1}(comp.)					
		KN	SC	SR	M	W	L	P
1	WMUR2	104.56	0.00	0.00	0.07	0.00	0.00	0.96
2	MMUR2	146.00	0.00	0.00	0.17	0.00	0.00	1.09
3	SMUR2	206.64	0.00	0.00	0.17	0.00	0.00	1.00
4	SWUR2	224.80	0.00	0.00	0.05	0.00	0.00	0.81
5	WWUS2	256.40	0.00	0.00	0.04	0.00	0.00	0.99
6	MWUS2	314.90	0.00	0.00	0.07	0.00	0.00	1.01
7	SWUS2	428.20	0.00	0.00	0.07	0.00	0.00	1.11
8	SSUS2	463.10	0.00	0.00	0.65	0.00	0.00	1.75
9	WWUB2	267.30	0.00	0.00	0.01	0.00	0.00	0.95

Frame Nos. 1-9 FE

Table 7.10 Comparison of Column Shear Force, S_{c1}

No.	Frame	S_{c1}	S_{c1}(calc.)/S_{c1}(comp.)					
		KN	SC	SR	M	W	L	P
1	WMUR2	560.29	N.a	1.07	0.02	0.85	1.24	0.90
2	MMUR2	776.00	N.a	1.21	0.06	0.71	1.09	1.24
3	SMUR2	934.40	N.a	1.41	0.07	0.57	1.03	1.00
4	SWUR2	865.40	N.a	1.55	0.02	0.49	0.97	0.94
5	WWUS2	420.80	N.a	.93	0.02	0.78	1.53	0.94
6	MWUS2	521.70	N.a	1.18	0.04	0.84	1.23	0.95
7	SWUS2	690.40	N.a	1.25	0.04	0.64	0.93	0.97
8	SSUS2	914.60	N.a	0.88	0.33	0.72	0.68	1.24
9	WWUB2	423.00	N.a	1.15	0.01	1.01	1.52	0.80
Deviations:				-0.12 +0.55	-0.99 -0.67	-0.51 +0.01	-0.32 +0.53	-0.20 +0.24
Standard Deviations:				0.29	0.99	0.32	0.31	0.15

Frame Nos. 1-9 FE

7.25 Comments

The comparison described in Sections 7.16 to 7.24 revealed that all the previously existing methods failed to predict the strength and stiffness of infilled frames with consistently reasonable accuracy, if the strength parameter, **m**, varies between 0.04 to 8.4. This is mainly because they either do not allow for limited frame resisting moment (occurrence of plastic hinges), or limited infill ductility (crushing of the infill prior to the formation of a plastic collapse mechanism in frame).

These methods also failed to predict the frame forces within an acceptable range of accuracy. This is because of the same reason mentioned earlier and also because of the simplifications made in allowing for the shear forces transferred at the frame-infill interfaces.

The proposed method, however, provides all the information for design purposes within a reasonable range of accuracy. This is mainly because this method accounts for both the elastic and plastic behaviour and interactions of the three structural constituents, frame, infill and their interfaces.

The proposed method also is compatible with frames having semi-rigid or even pin joints. This leads to a simple design approach for semi-rigid or pin-jointed infilled frames in which the beams can be designed continuously using a plastic design approach whereas the columns maybe designed with the assumption of no sway and pin-jointed condition, saving the cost of the material and labour used in fully rigid connections. The possible bending moment developed in the frame members as a result of the frame infill interaction (0.25 Mpc and 0.25 Mpb for columns and beams respectively, Table 7.8) have a small effect on the shear and axial load capacity of the frame members(98).

CHAPTER EIGHT

Conclusions and Recommendations

8.1 Conclusions

The following sections contain the conclusions drawn from the present work.

8.1.1 Investigation Approach

The behaviour of infilled frames have been studied either experimentally or theoretically. The following conclusions on the application of these approaches can be made.

1) Using current test equipment, an experimental approach may not, alone, lead to all the necessary information for understanding the behaviour of infilled frames under in-plane loading. The experimental results (loads and deflections) may be strongly affected by testing approach and unintended changes of mechanical properties of the materials.

2) The theoretical analysis using the finite element method should be capable of providi g almost all the necessary information to assist in the understanding of the behaviour of infilled frames. But misleading results may be obtained from previous such analyses because of the simple assumptions made.

3) Theoretical investigation on the subject can usefully employ finite element analysis. Such an analysis must include reasonably accurate models for;

   a) non-linearity of materials and

   b) behaviour of frame/infill interfaces and

should prevent errors occurring due to:

   i) incompatible elements in the mesh subdivision.

   ii) unnecessary damages occurred to the material in the process of the finite element iterative solution using irrelevant acceleration procedures and simple material models

8.1.2 Present Finite Element Analysis

A non-linear finite element computer program has been developed to analyse plane structures under static loading. The method gave results which agreed fairly well with the actual results up to and beyond the peak load. The program has many advantages over other programs that have been written for analysis of infilled frames. The following conclusions can be made:

1) The mathematical models suggested for simulating the non-linear behaviour of materials are numerically stable and reasonably accurate.

2) The techniques used to achieve a fast convergence for

the finite element solution equations leads to satisfactory convergence without any significant unnecessary damage to the materials.

3) The proposed beam element accurately simulates the displacement function of the frame members involving axial, shear and flexural deformations.

4) The proposed interface element assists in obtaining detailed accurate stress distribution diagrams over the frame-infill interfaces in contact.

5) The proposed loading jack and support elements distribute the external load or reaction forces, uniformly, over the bearing surfaces. These elements also act as a spring to simulate a loading jack or platen, respectively, with limited flexibility in process of the proposed displacement increment approach used in the program.

6) The three proposed elements significantly improve the accuracy and performance of the analysis.

7) The proposed displacement increment approach assists in obtaining a complete load-deflection diagram for the structure, monitoring even such as diagonal cracking and corner crushing of the infill as well as the occurrence of the plastic hinges and p ssibly of formation of a plastic collapse mechanism. This extra information was found useful for understanding the behaviour of the infilled frames.

8.1.3 General Behaviour of Infilled Frames

Finite element analysis of infilled frames with practical range of strength and stiffness loaded monotonically to destruction, led to the following conclusions:

1) Three major states for the frame can be recognized;

i) At a load close to the peak load the infill is, partly, in a state of strain hardening in the loaded corners and remains linear elastic over the rest of the area, while the frame remains entirely in the elastic state. During the loading up to this load level, The frame-infill contact lengths remain almost constant. This state may be referred to as "elastic state."

ii) Increasing the load, the state of the infilled frame alters into the "elastoplastic state" as the frame initiates plasticity (yielding) at the loaded corners leading to formation of two plastic hinges at these points. The lengths of contact increase and excessive compressive strain in the loaded corners of the infill follows the peak load and the load then falls and eventually crushing of the infill in the loaded corners occurs. This state continues until further plastic hinges develop.

iii) At the limit of the elastoplastic state which is at a load considerably lower than the peak load where the infill has partially crushed, the frame initiates further plastic hinges followed by a plastic collapse mechanism. This may be termed "perfect plastic state"

2) Infill non-linearity which is associated with permanent strains (plasticity) starts at a load well below the peak load. This indicates that repetition of the load may result in gradual deterioration of the infill at a much higher rate than is normally seen in ordinary structures.

3) The major parameters affecting the normal stress acting at the frame-infill interfaces at the peak load, are as follows:

i) Square infills develop almost equal normal stress at the beam and column interfaces. The aspect ratio of the infill (h'/l') has a strong effect on distribution of the infill diagonal force to the beam and column interfaces in contact. Rectangular infills transfer much of the resulting diagonal force to the columns. The straightforward rule of dividing the diagonal force into the components acting normal to the beams and columns does not agree with the finite element results.

ii) The beam/column strength ratio has a strong effect on the beam/infill normal stress. This parameter, however, has almost no effect on the *column/infill* normal stress.

iii) The frame/infill strength ratio has no effect on the normal stress acting at the column/infill interface, but it has a significant effect on the normal stress acting at the beam/infill interface.

iv) Variation of the coefficient of friction of the frame-infill interfaces changes the normal stress acting at these surfaces. The lower the coefficient of friction is the higher the normal stress becomes.

4) Shear stresses at the frame/infill interfaces in contact are generally proportional to the normal stresses with the following additional considerations.

i) At peak load the shear stress developed at the beam-infill interface is almost equal to its maximum possible value, $\mu\sigma_{nb}$, and may not becomes less than $0.90\mu\sigma_{nb}$. Therefore it can be concluded that the state of the beam/infill interface remains slipping up to the peak load.

ii) Shear stress developed at the column-infill interface is strongly affected by the aspect ratio of the infill.

5) Diagonal compression failure of infilled frames occur as a result of the Biaxial compression failure of the infill material in the loaded corners.

6) Unless the infill is subjected to vertical load or it is somehow prestressed, the lengths of contact may not exceed one half of the infill dimension under consideration.

7) Diagonal cracking of the infill occurs as a result of the tensile failure of the infill at the central area. The cracking load must not be considered as the peak

load. The event of cracking is accompanied by an abrupt increase in diagonal deflection and slight increase in the frame/infill lengths of contact.

8) The infill cracking load is not much affected by the frame strength, but rather depends on the geometry and strength of the infill.

9) At the peak load, infilled frames mainly develop plastic hinges only at the loaded corners. Infilled frames with extremely weak infill, however, might not develop any plastic hinges at this load level.

10) Except in the loaded corners, Infilled frames under only diagonal loading develop insignificant axial forces in the frame members. However, these axial forces gradually become significant over the infill/frame lengths of contact.

11) The frame members are subjected to extremely high shear forces only in the vicinity of the loaded corners while at the peak load. This normally necessitates adding relatively heavy web stiffeners to the frame members in the loaded corners.

12) Force distribution within the frame is such that the maximum bending moment, shear and axial force all occur at the same point (loaded corner). Interaction of these forces may significantly reduce the resisting moment capacity of the frame members. Therefore extra care must be taken to cater for these shear and axial forces.

13) The previous test infilled frames whose frame members were made of hollow steel sections or reinforced concrete, may have failed by shear well before the apparent moment resisting of these members has reached.

8.1.4 Methods Based on Infill/Frame Stiffness Parameter

Comparison of the peak load calculated by the methods based on the infill/frame stiffness parameter, λh, proposed by Stafford Smith and Carter[13], Stafford Smith and Riddington[18] and Mainstone[9] with the proposed finite element analysis results and also the results from three experimental sources, led to the following conclusions.

1) As these methods rely on only the column stiffness they dramatically over estimate the peak load for infilled frames having weak beams relative to the columns. Results deviated from the actual values up to +147%.

2) For infilled frames with uniform frame members, these methods give still scattered results because they ignore the occurrence of the plastic hinges occurring at the loaded corners while at the peak load. This produced up to 68% deviation fr m the actual values.

3) These methods also give mixed results in allowing for variation of the aspect ratio of the infill. It is shown that these methods can be modified to cater for variation of this parameter.

4) These methods give fairly accurate predictions for the peak load for infilled frames with very strong and uniform frame members relative to the infill **($m>2.43$)**. Deviations from the actual values ranged -12% to +16%.

8.1.5 Wood's Plastic Method

Comparison of the peak load calculated by the plastic method proposed by Wood[20] with the proposed finite element analysis results and also the results from three experimental sources, led to the following conclusions.

1) Not including the frames discussed in clauses 2 and 3 below, the method predicts the peak load reasonably accurately with a standard deviation of 14%. The maximum deviations were -19% and +22%

2) The method, however, significantly underestimates the collapse load for semi-rigid frames. Up to 59% under-estimation was encountered.

3) Contrary to the methods based on λh, Wood's method leads to very high predictions for the infilled frames with weak infill and very strong frame. Deviations ranging +36% to +143% were obtained for infilled frames with **$m=2.43$** to **8.36** respectively. This is because the method assumes occurrence of a plastic collapse mechanism which was was not the case for these frames.

4) Excluding the frames discussed in clause 3 above the uniform and simplified γ_p value proposed by Ma[96]

gives safe but uneconomical collapse load. Excluding the frames discussed in clauses 2 and 3 above the standard deviation became 46%.

8.1.6 Liauw et al Plastic Method

Comparison of the peak load calculated by the plastic method proposed by Liauw et al (25) with the proposed finite element analysis results and also the results from three experimental sources led to the following conclusions.

1) This method ignores the beneficial effect of shear stress acting at the frame/infill interfaces in contact. The method also ignores the loss of strength due to lack of ductility of infill and formation of plastic hinges only at the loaded corners rather than development of a plastic collapse mechanism. These errors counter-balance and the method results in a reasonably accurate collapse load with deviations ranging -27% to -3% from the actual values and a standard deviation of 16%.

2) Similar conclusions as made in clauses 2 and 3 in Section 8.1.5 are applicable for this method.

3) Unlike Wood's method, this method leads to underestimated values for the collapse load of the infilled frames with a thick infill relative to the dimensions of the biaxially loaded corner blocks of the infill).

8.1.7 New Hand Method of Analysis

Because of the shortcomings of the existing methods, a new method was developed allowing for the limited infill ductility and also combined elastic and plastic deformations of the frame at the peak load. Comparison of the peak load calculated by the proposed method, with the proposed finite element analysis results and also the results from three experimental sources led to the following conclusions.

1) This method predicts the collapse load within a fairly accurate range for all the infilled frames studied. These include frames with non-uniform members and frames with semi-rigid and even pin joints and also frames with rectangular panels. None of these infilled frame types led to the calculated collapse load deviating more than -21% and +12% from the actual results. The standard deviation using this theory was only 8%.

2) The proposed method predicts fairly accurate the diagonal cracking load. Compared to the results of the proposed non-linear finite element analysis, the standard deviation became only 3%. The previously existing methods, however, give mixed results deviating from the actual values up to 88%.

3) All previous methods give scattered results for infilled frame stiffness. This may be attributed to the effects of shrinkage and lack of fit. The proposed

method however gives rather consistent results and has the advantage of being capable of adjusting the stiffness for variation of lack of fit and shrinkage.

4) The proposed method provides all the necessary information for design purpose including the deflection at the diagonal cracking and at the peak loads and also the internal forces of the frame members within a reasonable range of accuracy. This permits the inclusion of both the limit states of collapse and serviceability into the design criteria for infilled frames.

8.2 Recommendations for Future Work

8.2.1 Extension of Program NEPAL

The program NEPAL may be extended to carry out the following analyses:

1) Infilled frames with masonry infill can be included into the program. Such an analysis may be executed by the current version of the program taking, comparatively, much more CPU time than for a similar infilled frame with a uniform infill. Development of a super-element for masonry material as introduced in Section 3.9.7 was found to be significantly helpful in reducing the CPU time.

2) Although analysis of multi-bay and multi-storey infilled frames can be executed by the current version of the program such computations have been impractical

using the IBM mainframe computer in the Computing Centre of Sheffield University. This problem may be overcome by making some simplifications in the non-linear finite element solution procedure and reducing the number of nodes to reduce the CPU time. Alternatively one may wait and use a much faster computer that might become available sometime in the future

8.2.2 Experimental Investigation

The effects of load repetition and reversal are expected to be significant. Little information is available on this area and further experimental work would be valuable.

8.2.3 Application of Finite Element Analysis

The programme of this work involved finite element analysis on 12 infilled frame examples selected from most practical types and dimensions. The programme may be extended to cover also the following:

1) Panels with smaller aspect ratio, i.e. **$h'/l'<0.57$.**

2) Presence of gaps around the infill and also a gap only at the top of the wall. The experimental data reported by Riddington(34) may be used for comparison.

3) Frames with pin and semi-rigid joints .

4) Panels with opening of different size and position.

5) Masonry infill.

6) Reinforced concrete frame

7) Multi-bay and Multi-storey infilled frames.

8.2.4 Design Procedure

Application of the proposed method as a design approach is briefly described in section 7.24. This can be extended into more detail to conform with codes of practice for design of infilled frames using the safety factors involved.

REFERENCES

1 WOOD R H, "An Economical Design of Rigid Steel Frames for Multi-Storey Buildings". National Building Studies, Res. Paper No. 10, H M S O LONDON.

2 WOOD R H and GOODWIN E, "Degree of Finity Methods for Certain Sway Problems". Structure of Engineers, Vol 30,1952, pp 153.

3 BEAUFOY L A and DIWAN A F S, "Analysis of Continous Structures by The Stiffness Factors Method". Quart. J. Mech., Vol 2,1949, pp263.

4 CANDLER D B, "The Prediction of Critical Loads of Elastic Structures". PhD Thesis, Manchester Uni versity, 1955.

5 LIVESLY R K and CHANDLER D B, "Stability Functions for Structural Frameworks". Manchester University Press, 1956.

6 JOINT COMMITTEE (SECOND REPORT), "Fully-Rigid Multi-Storey Welded Steel Frames". Instn. Strut. Engrs, May 1971.

7 WOOD R H, "The Stability of Tall Buildings". Proc. Instn. Civ. Engrs., Vol 11, 1958, pp 69-102.

8 SAMAI M L, "Behaviour of Reinforced Concrete Frames with Lightweight Blockwork Infill Panels". PhD Thesis, The University of Sheffield, UK, 1984.

9 MAINSTONE R J, "On The Stiffness and Strengths of Infilled Frames". Proceeding Institution of Civil Engineers, Supplement (iv), paper 7360 S, 1971.

10 POLYAKOV S V, "On the Interaction Between Masonry Filler Walls and Enclosing Frame When Loaded in the Plane of The Wall". Earthquake Engineering, 1960. Earthquake Engineering Research Institute, San Francisco, 1960.

11 HOLMES M, "Steel Frames with Brickwork and Concrete Infilling". Proceedings Institution of Civil Engineers, Vol 19, August 1961, pp 473-478.

12 STAFFORD SMITH B, "Behaviour of Square Infilled Frames". Proceedings of American Society of Civil Engineers, Vol 92, February, 1966, pp 381-403.

13 STAFFORD SMITH B and CARTER C, "A Method of Analysis for Infill Frames". Proceedings Institution of Civil Engineers, Vol. 44, September, 1969.

14 HETENIY M, "Beam on Elastic Foundation". The University of Michigan Press, Ann Arbor.

15 KADIR M R and HENDRY A W, "Strength and Stiffness of Brickwork Infilled Frames Under Racking Load", Proc. of the British Ceramic Society, No 24, September, 1975, pp 215-233.

16 HOBBS B and SAMAI M L, "Behaviour of Reinforced Concrete Frames eith Lightweight Concrete Blockwork Infill Panels". Department of Civil and Structural Engineering, The University of Sheffield, England, September, 1984.

17 RIDDINGTON J R and STAFFORD SMITH B, "Analysis of Infilled Frames Subjected to Racking with Design Recommendations". The Structural Engineering, Vol 55, No 6, June, 1977, pp 263-268.

18 STAFFORD SMITH B and RIDDINGTON J R, "The design of Masonry Infilled Steel Frames for Bracing Structures". Structural Engineers, Vol 56B, March, 1978, pp 1-7.

19 MAINSTONE R J, "Supplementary Note on the Stiffness and Strength of Infilled Frames". Building Research Establishment, Current Paper C P 13/74, February, 1974.

20 WOOD R H, "Plastic, Composite Action and Collapse Design of Unreinforced Shear Wall Panels in Frames". Proceedings Institution of Civil Engineers, Part 2, Volume 65, June, 1978.

21 NIELSEN M P, "On the Strength of Reinforced Concrete Discs". Acta Polytechnic Scand., Civil Eng. Building Construction, Series 70, Copenhagen, Bulletin 2,1971.

22 MAY I M, "Determination of Collapse Loads for Unreinforced Panels With and Without Openings". Proc. Instn. Civ. Engrs., Part 2, Vol 71, March, 1981, pp 215-233.

23 MAINSTONE R J, SMITH D G E, SIMS P A C and WOOD R H, Discussion on Wood's paper(9), Proc. Instn. Civ. Engrs. Part 2, Vol 67, March 1979, pp 237-245

24 LIAUW T C and KWAN K H, "Non-Linear Analysis of Multi-story Infilled Frames". Proc. Instn. Civ. Engrs, Part 2, Vol 73, June, 1982, pp 441-454.

25 LIAUW T C and KWAN K H, "Plastic Theory of Non-Integral Infilled Frames". Proc. Civ. Engrs, Part 2, Vol 75, September, 1983, pp 379-396.

26 BARUA H K and MALLICK S K, "Behaviour of Mortar Infilled Steel Frames Under Latral Load". Building and Environmental, Vol 12, 1977.

27 MALLICK D V and SEVERN R T, "The Behaviour of Infilled Frames Under Static Loading". Proceeding Institution of Civil Engineers, Vol. 38, December, 1967, pp 639-656.

28 KADIR M R and HENDRY A W, "The Behaviour of Brickwork Infilled Frames Under Racking Load". Proc. 5th Int. Sympm. Load Bearing Brickwork, British Ceramic Research Association, London, 1975.

29 SANEINEJAD A, "Behaviour of Model Infilled Frames". MEng Dissertation, Department of Civil and Structural Engineering, The University of Sheffield, England, September, 1981.

30 KADIR M R A, "The Structural Behaviour of Masonry Infill Panels in Framed Structures". PhD thesis, Edinburg University, April, 1974.

31 HENDRY A W, "Structural Brickwork". McMillan, London, 1981.

32 NEVILLE A M. "Properties of Concrete". Third Edition, Pitman Publishing Limited, London.

33 LIAUW T C and KWAN K H, MAY I M and MA Y A and WOOD R H and SIMS P C A, Discussion on Reference 25, Proc. Instn. Civ. Engrs, Part 2, June, 1984, PP 279-286.

34 RIDDINGTON J R, "The Influence of Initial Gap on Infilled Frame Behaviour". Proc Instn Civ Engrs, Part 2, vol 77, September, 1984, PP 295-310.

35 DHANASEKAR M and PAGE A W, "The Influence of Brick Masonry Infill Properties on the Behaviour of Infilled Frames". Proc Instn Civ Engrs, Part 2, Vol 81, December, 1986, PP 593-605.

36 ZIENKIEWICZ O C, "The Finite Element Method". Third Edition, MacGraw-Hill, London.

37 SMITH I M, "Programming, The Finite Element Method". John Wiley & Son, 1982.

38 TIMOSHENKO S P and GOODIER J N, "Theory of Elasticity". Third Edition, McGraw-Hill, 1982.

39 CHEN W F, "Plasticity in Reinforced Concrete". McGraw-Hill, 1982.

40 MEYER C and BATHE K J. "Non-Linear Analysis of R.C. Structures in Practice". ASCE, Structural Division, vol 108, No ST7, July, 1982, pp 1605-1622.

41 GOODMAN R E, TAYLOR R L and A BREKKE T L, "A Model for The Mechanics of Jointed Rock". ASCE, Soil Mechanics and Foundations Division, May, 1968, pp 637-659.

42 KING G J W and PANDEY P C., "The Analysis of Infilled Frames Using Finite Elements". Proc. Instn. Civ.Engrs. Part 2, Vol. 65, Dec. 1978.

43 NAGFEO, NAG Finite Element (Subprograms). The University of Sheffield Computer Centre.

44 WILSON E L, TAYLOR R L, DOHERTY W P and GHABUSSI T, "Incompatible Displacement Models in Numerical and Computer Methods in Structural Mechanics". Academic Press 1973, pp 43-57 (ed ST Fenves et al).

45 VALANIS K C, "Theory of Viscoplasticity without a Yield Surface, i) General Theory; ii) Application to Mechanical Behaviour of Metals". Arch Mech, Vol 23, No 4, pp 517-551.

46 BAZANT Z P and BHAT P D, "Endocronic Theory of Inelasticity and Failure of Concrete". ASCE. Journal of the Engineering Mechanics Division, August, 1976, EM4, pp 701-722.

47 DARWIN D and PECKNOLD D A, "Non-Linear Biaxial Stress-Strain Low for Concrete". ASCE, Journal of Eng. Mechanics Division, April, 1977, EM2, pp 229-241.

48 GHONEIM AM and GHALI A, "Non Linear Analysis of Concrete Structures". Canadian Journal of Civil Engineering, Vol 9, No 3, September, 1982, pp 489-501.

49 DARWIN D and PECKNOLD D A, "Inelastic Model for Cyclic Biaxial Loading of Reinforced Concrete". Report, Structural Series, No. 409, University of Illinois at Urbana-Champaign.

50 WISCHERS G, "Application of Effect of Compressive Load on Concrete". Betontech, Ber., Nos. 2 and 3, Dusseldorf.

51 SAENZ L P, "Discussion". Journal American Concrete Institute, Vol 61, September, 1964, pp 1229-35.

52 SARGIN M, "Stress-Strain Relationship for Concrete and the Analysis of Structural Concrete Sections". Study No 4, Solid Mechanics Division, University of Waterloo, Ontario, 1971.

53 WANG P T, SHAH S P and NAAMAN A E, "Stress-Strain Curve of Normal and Lightweight Concrete in Compression". Journal American Concrete Institute, November 1978.

54 BARNARD P R. "Researches into the Complete Stress-Strain Curves for Concrete". Mag. Concrete Research, Vol 16, No 49, December 1964, pp 203-210

55 KUPFER H and HILSDROF K, "Behaviour of Concrete Under Biaxial Stresses". ACI Journal, August, 1969, pp 656-666.

56 HOBBS D W. "Strength and Deformation Properties of Plain Concrete Subjected to Combined Stress". Part 1, Cement and Concrete Association, Technical Report 42, 4 November, 1970.

57 HOBBS D W, POMEROY C D and NEWMAN, J B, "Design Stresses for Concrete Structures Subject to Multi-axial Stresses". The Structural Engineer, April, 1977, No 4, Vol 55, pp 151-164.

58 CORRASQUILLO L R, NILSON A H and SLATE F O, "Properties of High Strength Concrete Subjected to Short-term Load". ACI Journal, May-June 1981, pp 171-178.

59 SINHA B P, GERSTLE K H and TULIN L G, "Stress-Strain Relations for Concrete Under Cyclic Loading". Journal ACI, February, 1964, pp 195-211.

60 KARSAN I D and JIRSA J O, "Behaviour of Concrete Under Compressive Loadings". Journal ASCE, Structural Division, December, 1969.

61 MAHER A and DARWIN D, "Mortar Constituent of Concrete in Compression". ACI Journal, March-April 1982, pp 100-109.

62 SPOONER D C and DOUGILL J W, "A Quantitative Assessment of Damage Sustained in Concrete During Compressive Loading". Magazine of Concrete Research (London), Vol 27, No 92, September, 1975, pp 151-160.

63 COOK D J and CHINDAPRASIRT P, "Influence of Loading History Upon the Compressive Properties of Concrete Research, Vol 32, No 111, June, 1980, pp 89-100

64 COOK D J and CHINDAPRASIRT P, "Influence of Loading History Upon the Tensile Properties of Concrete". Magazine of Concrete Research, Vol 33, No 116, September, 1981.

65 TASUJI M, NILSON A H and SLATE F O, "Biaxial Stress-Strain Relationships for Concrete". Mag. Concrete Research, Vol 31, No 109, December, 1979.

66 EVANS R H and MARATHE M S, "Microcracking and Stress-Strain Curves for Concrete in Tension". Journal Material and Constructions, No 1, Jan-Feb 1968, pp 61-64.

67 SCANLON A, "Time Dependent Deflexion of Reinforced Concrete Slabs". PhD thesis, University of Alberta, Canada, 1971.

68 NAYAK G C and ZIENKIEWICZ O C, "Convenient Forms of Stress Invariants of Plasticity". Proc. Am Soc Civ Engrs Vol 98, 1972, pp 949-954.

69 DRUCKER D C and PRAGER W, "Soil Mechanics and Plastic Analysis or Limit Design". Q J Appl Math, Vol 10, 1952, pp 157-165

70 BALMER G G, "Shearing Strength of Concrete under High Triaxial Stress-Computation of Mohr's Envelope as a Curve". Bur Reclam Struct Res Lab Rep SP-23, 1949.

71 RICHART F E, BRANDTZAEG and BROWN L R, "A Study of the Failure of Concrete Under Combined Compressive Stress". Univ Ill, Eng Exp Stn, Bill 185, Urbana, 1928.

72 KHOO C L and HENDRY A W, "Strength Test on Brick and Mortar Under Complex Stresses for the Development of a Failure Criterion for Brickwork in Compression". Proceedings of the British Ceramic Society No 21, April, 1973, pp 51-66.

73 LIU T C Y, NILSON A H and SLAT F O, "Biaxial Stress-Strain Relations for Concrete". ASCE, Structural Division, May 1972, pp 1025-1034.

74 GERSTLE K H, "Simple Formulation of Biaxial Concrete Behaviour". ACI Journal, Jan-Feb, 1981, pp 62-68.

75 BAZANT Z P and TSUBAKI T, "Slip Dilatancy Model for Cracked Reinforced Concrete". J ASCE, Struct Div, September 1980, pp 1947-1966.

76 DIVAKAR M P, FATITIS A and SHAH S P, "Constitutive Model for Shear Transfer in Cracked Concrete." J ASCE, Vol 113, No 5, May, 1987, pp 1046-1062.

77 ROBBAT B G and RUSSELL H G, "Friction Coefficient of Steel on Concrete of Grout". J ASCE, Vol 111, No 3, March, 1985, pp 505-515.

78 DRYSDALE R G and HAMID A A, "Behaviour of Concrete Block Masonry Under Axial Compression". ACI Journal, June, 1979, pp 707-721.

79 PAGE A W, "Finite Element Model for Masonry". ASCE, Structural Divn., Vol 104, No ST8, August 1978, pp 1267-1285.

80 HAMID A A, DRYSDALE R G and HEIDEBRECHT A C, "Shear Strength of Concrete Masonry Joints". ASCE, Structural Division, Vol 105, No ST7, July, 1979, pp 1227-1240.

81 HEGEMIER G A, KRISHNAMOORTHY G, ISENGERG J and EQING RD. "Earthquake Response and Damage Prediction of Reinforced Concrete Masonry Multi-storey Buildings". Proc. Sixth World Conf. on Earthquake Engineering, pp 3013-3024.

82 FRANCIS A J, HORMAN C B and JEREMS E L, "The Effect of Joint Thickness and other Factors on the Compressive Strength of Brickwork". Proc. Second Int. Brick Masonry Conf. (Stoke-on-Trent), 1971.

83 ATKINSON R H and NOLAND J L, "A Proposed Failure Theory for Brick Masonry in Compression". Proc., 3rd Canadian Masonry Symposium, Edmonton, Canada, 1983, pp 5.1-5.17.

84 SCOTT MCNARY, DANIEL P and ABRAMS M, "Mechanics of Masonry in Compression". J ASCE, Struct. Div., Vol. 111, No. 4, April, 1985, pp 857-870.

85 SAMARASINGHE W, "The In-Plane Failure of Brickwork". PhD thesis, University of Edinburgh, 1980.

86 HENDRY A W, "A Note on the Strength of Brickwork in Combined Racking Shear and Compression". Proc. Br. Ceram. Assoc., Load Bearing Brickwork(b), Dec-Nov 1987, pp 47-52.

87 PAGE A W, "The Biaxial Compressive Strength of Brick Masonry". Proc. Instn. Civil Engineers, Part 2, Sept 1981, pp 893-906

88 DHANASEKAR M, PAGE A W and KLEEMAN P W. "The Failure of Brick Masonry Under Biaxial Stresses". Proc. Instn. Civ. Engrs., Part 2, Vol 79, June, 1985, pp 295-313.

89 HAMID A A and DRYSDALE R G, "Concrete Masonry Under Combined Shear and Compression Along the Mortar Joints". ACI Journal, Sept-Oct 1980, pp 314-320.

90 HAMID A A and DRYSDALE R G, "Proposed Failure Criteria for Concrete Block Masonry Under Biaxial Stresses". ASCE, Structural Division, Vol 107, No ST8, August 1981, pp 1675-1687.

91 ARGYRIS J H. "Vontinua and Discontinua". Proc., First Conf. Matrix Meth., Struct. Mech., Write-Patterson A.F.B., Ohio (1965).

92 SHARIFI P and POPOV E P, "Non-Linear Buckling Analysis of Sandwich Arches". J. Engng. Mech. Div., ASCE, Vol 97, No EMS, pp 1397-1412 (1971).

93 BERGAN P G, " Convergence Criteria for Interactive Processes, AIAA Journal, Vol 10, No 3, September, 1982, pp 489-501.

94 CRISFIELD M A, "A Fast Incremental/Iteractive Solution procedure that Handles Snap-through". J Computer and Structures, Vol. 13, No. 1-3, pp 55-62.

95 BRESLER B and SCORDELIS AC, "Shear Strength of Reinforced Concreter Beams-Series II". SESM Rep. No 64.2, University of California, Berkeley, 1964

96 MA Y A, "Unreinforced Shear Wall Panels in Frames." Ph.D. Thesis, Department of Engineering of The University of Warwick, September 1983.

97 KONG F K and EVANS R H, "Reinforced and Prestressed Concrete". Second edition, Thoms Nelson and Sons Ltd., 1980.

98 HORNE M R and MORRIS L J, "Plastic Design of Low-rise Frames". Granada Publishing Ltd., 1981.

99 "STEEL DESIGN MANUAL". Fourth edition(metric), Granada Publishing Ltd., 1972.

100 PAUL JOHNSON R, "Strength Tests on Scaled-Down Concretes Suitable for Models, with a Note on Mix Design". Magazine of Concrete Research, Vol. 14, No. 40, 1962.

101 GONNERMAN H F, "Effect of SIze and Shape of Test Specimen on Compressive Strength of Concrete". Proc. ASTM, 25, Part II, 1925, PP. 237-287.

APPENDIX A

Input Data for Program
NEPAL

A.1 General

NEPAL is a 2-D Finite Element computer program for non-linear and elastoplastic analysis of composite and also masonry plane structures.

In order to minimize the volume of input data, the structure must be divided into zones. Such zones must each be conformed by elements of the same type and size which are referred by their row and column order along Y and X (the global co-ordinate within the zone under consideration). Therefore data must be input for the zones rather than for the elements.

Nodes are numbered from left to right; along X direction, as shown in section A.4.

The data file for the computer program NEPAL is free formatted, ie each term must be separated by one or more spaces. The input data may be typed either in form of floating point or exponential mode. The numbers in the input file are either real or integer, signified here, by letters R and I respectively.

A.2 Input Data

A.2.1 Structure Geometry

```
I1
C1
I2   I3   I4
```

I1	=	The problem execution number
C1	=	Name of the example
I2	=	2 (see Section A.3.1)
I3	=	Total number of nodes
I4	=	Total number of zones

A.2.2 Zone Properties; one set for each zone

```
I1  I2  I3  I4  I5  I6  I7  R1  R2  R3  R4  R5  R6
```

I1	=	The zone order number
I2	=	An integer number to specify the zone element type (see section A.3.2)
I3	=	Structural type of the zone; 1 for frame 2 for uniform wall 3 for masonry wall 4 for interface 5 for loading jack mechanism 6 for support mechanism
I4	=	Reinforcement type; 0 for no reinforcement
I5,I6	=	Number of columns and rows of elements within the zone respectively; not to be more than 9
I7	=	Element code 0 for all cases except: 1 for a zone formed by 4-node beam elements 2 for a zone formed by 4-node column elements 3 for a zone formed by 5-node beam elements 4 for a zone formed by 5-node column elements 5 for a zone formed by 6-node beam elements 6 for a zone formed by 6-node column elements ijk for either a masonry wall or an interface zone (see Section A.3.3).
R1-R3	=	Dimensions of the zone in [mm] in x, y and z directions respectively
R4,R5	=	Lack of fit for a masonry wall or an interface in mm in X and Y directions respectively (see Section A.3.4)
R6	=	The total weight of the zone in Newton; input 0.0 when the effect of zonal weight is to be neglected

A.2.3 Zone Topology

I1 I2 .. .. I(n+2)

I1 = zone number
I2 = The total number of nodes, n, needed to determine the topology of the zone
I3-I(n+2) =Node numbers showing the topology of the zone; to be typed in the order as shown in Section A.4

A.2.4 Nodal Displacement Output Data

I1 I2 .. .. I(m+1)

I1 = m, the total number of nodes whose displacement values are to be output
I2-I(m+1) =The node numbers whose displacements desired to be output

A.2.5 Properties of The Materials

I

I = The total number of material types used in the structure

Then one dataset for each material type as follows:

I1 R1 R2 .. .. R10

a) For Brittle Materials:

I1 = Material type number
R1 = Initial modulus of elasticity (KN/mm^2)
R2 = Initial Poisson's ratio
R3 = Direct tensile strength (N/mm^2)
R4 = Unconfined compressive strength; 0.95Xfc' (N/mm^2)
R5 = 10^3X(strain at peak uniaxial compressive strength)
R6 = 'A' factor; Eq 4.36
Input 0; 'A' will be calculated automatically
R7 = 'C' factor; Eq 4.32
2 for mortar
3 for concrete
R8 = 'R' factor; Eq 4.58
input 0; 'R' will be set to 3.5 automatically
R9 = f_{bc}, ratio of equal biaxial/uniaxial strength
input 0; f_{bc} will be calculated by Eq 4.31
R10 = 'K' factor, specifying the tangent of the interlocking angle in cracked surfaces

b) For Ductile Materials (Steel):

I1,R1,R2 Same as (a)
R3,R4 = Direct tensile and compressive strength which must be the same (N/mm^2)
R5-R10 = 0

c) For Interfaces:

R1 = Normal stiffness of the interface, kn (KN/mm^3)
R2 = Shear stiffness of the interface, Ks (KN/mm^3)
R3 = Tensile bond strength (N/mm^2)
R4 = Shear bond strength (N/mm^2)
R5 = Shear stiffness after debonding, Ksru (Kn/mm^3)
R6-R7 = 0
R8 = τ_0, related to the yielding criterion (N/mm^2)
R9 = μ', slope of the yielding criterion
R10 = coefficient of friction of the interface

d) For Masonry Wall:

Four lines of material property data are to input as follows:
i) Masonry unit properties, are to be input Same as (a
ii) Masonry internal joints, are to be input Same as (c
iii) Masonry sides and bottom interfaces, are to be input Same as (c and
iV) Masonry top interface, are to be input Same as (c

e) For Loading Jack and Support Elements:

I1 R1

I1 = Material type number
R1 = Stiffness of the element (KN/mm^2)
For Support elements, a high value must be taken for R, say 10000 times the structure stiffness. A very high value also is hurmful and produces precision errors. For loading element a value equals 10 to 50 times the structure stiffness is relevant.

A.2.6 Reinforcement Properties Data

I

I = Total number of reinforcement arrangements within the structure;
I=0 shifts onto Section A.2.8

R1 R2 .. .. R7 .. R11 R12

```
R1  = E1 of link bars, Fig A.3
R2  = E2 "    "     "     "
R3  = E1 of main bars     "
R4  = E2 "    "     "     "
R5  = E1 of steel flanges in a steel beam
R6  = E2 "    "     "     "  "    "     "
R7  = Fy of link bars, Fig A.3
R8  = Fu "    "     "     "
R9  = Fy of main bars     "
R10 = Fu "    "     "     "
R11 = Fy of steel flanges
R12 = Fu "    "       "
```

Note: If any of bar types(link, main or steel flanges) not exists, its corresponding values must be assigned 0

A.2.7 Reinforcement Geometry; one set for each group

I R1 R2 .. .. R9 R10

```
I   = Reinforcement arrangement order number
R1  = RX1   percentage of bottom bars in X direction
R2  = RX2        "      "  top    "   " X     "
R3  = RY1        "      "  left   "   " Y     "
R4  = RY2        "      "  right  "   " Y     "
R5  = RLX        "      " uniformly distributed bars in X
R6  = RLY        "      "   "          "         "    " Y
R7  = X1R1 Absissa of the left main bars, Section A.4
R8  = X1R2    "     "  "  right  "    "          "
R9  = ETAR1   "     "  "  bottom "    "          "
R10 = ETAR2   "     "  "   top   "    "          "
```

A.2.8 Structural Restraint Data

I1 I2 I3

```
I1  = Degree of freedom per node
I2  = Total number of components of stress and strain
I3  = Total number of restrained nodes
```

I I1 I2 I3

I = Restrained node number

I1-I3 = Restraining condition of the node in X, Y, Z directions respectively as follows:

	Direction	Restraint	Free
I1	X	1	0
I2	Y	2	0
I3	Z	3	0

N.B. I3 must be ommitted when the degree of freedom of the structure is 2.

A.2.9 Loading Data

I

I = Number of loaded nodes. Input 0 to shifts onto section A.2.10.

Input one data set for each loaded node as follows:

I1 R1 R2 R3

I1 = Node number
R1 = Load in X direction (N)
R2 = " " Y " "
R3 = " " Z " "

A.2.10 Material Non-linearity Data

R1 I1 I2 R2 R3 I3

R1 = Acceptable norm for rate of convergence
I1,I3 = 0, 1 or 2 to select the tangent modulus of elasticity of brittle material and reinforcement respectively as follows:
0 to select the apparent tangent value
1 " " " unloading " "
2 " " " average of the above
I2 = 0, 1 or 2 to select the tangent value of the Poisson's ratio of brittle material as follows:
0 to select the apparent tangent value
1 " " " initial value
2 " " " average of the above
R2 = 0.0 to 1.0 to specify the rate of allowance for change in the Poisson's ratio
R3 = Crushing strain limit (as a ratio to the strain at peak stress). Input 0 or any value less than 1.0 then E_{max}= (3/ D)+1 will be set which allows yielding up to s=0.25 before concrete crushes.

A.2.11 Deflection Increment Characteristics Data

R1 R2 R3 I1 R4

R1 = Minimum deflection increment
R2 = Maximum " "
R3 = Specified maximum deflection
R4 = Specified early increments
I1 = Number of times R4 must be repeated

A.2.12 Output Results Characteristics Data

I R1 R2 .. .. .. Ri

I = i
R1-Ri = Deflections at which results are to be output

A.2.13 Iterations Characteristics Data

I1 I2 I3 I4 R1 I5 I6 R2 I7

I1 = Desired number of iterations
I2 = Specified maximum allowed number of iterations
I3 = Maximum CPU time allocated to the computation
I4 = 0 or 1; magnification of bond strength. set I4=1 to flag the magnifying process
R1 = Rate of reducing the stiffness of slipping interfaces to accelerate convergence(this option is not effective, input 0 for R1)
I5 = 0 or 1 to flag the choice of the interface mechanics as follows:
I5=0, interfaces undergo a parabolic tensile bond criterion and no yielding and gradual debonding is permitted.
I6 = 0 or 1, I6=0 flags unsymmetric equations solving
R2 = Rmu which is greater than unity and denotes the rate of reducing the coefficient of friction of an slipping joint. This option is not effective, input 1.0
I7 = Flag to select the desired choice of incremental [D] for slipping interface.
I7=0 [D] gripped will be taken
I7=1 Clamping routine willbe taken (very effective)
I7=2 Ks=0 will be set

A.3 Notes

A.3.1 Note 1 (see A.2.1)

I2 is the dimensionality of the problem. Since the computer program NEPAL deals with Plane problems only, I2 must be assigned 2.

A.3.2 Note 2 (see A.2.2)

a) Zones other than Loading Jack or Support

I2 is a 4-digit number 'ijkl' indicating the type of element and the arrangement of gaussian points within the elements of the zone. i and j are the number of nodes on the horizontal and vertical sides of the element respectively. To be compatible with NEPAL, the combination of i and j are limited to:

22 23 32 24 42 33

ij = 22 must be assigned to masonry, interface, 4-node isoparametric and also 4, 5 and 6-node beam and column elements. 'ij' values other than 22 may be assigned to other types of isoparametric elements only.

k and l are the number of columns and rows, respectively, of the gaussian points attributed to each element of the zone under consideration.

The following limitations must be born in mind:

i) Horizontal interface elements may not have more than one row and less than 2 columns of gaussian points.
ii) Vertical interface elements may not have more than one column and less than 2 rows of gaussian points.
iii) The maximum number of columns and rows of gaussian points are limited to 7 in this program.
iv) In order to prevent a possible singularity of the global stiffness matrix and malfunctionality of the solution, the minimum number of gaussian points is better to be limited to 2x2 for any type of element except for interface elements, see notes (i) and (ii)
v) 5 and 6-node beam and column elements must have more than 2 rows and columns of gaussian integration points, respectively.

b) Loading Jack and Support Elements:

I2 is a single digit number indicating the total number of nodes of the element.

A.3.3 Note 3 (see section A.2.2)

a) Masonry Wall

I7 is a 3-digit integer number, ijk, where i and j specify the number of columns and rows of the gaussian integration points, respectively, of each unit element located within any corner of the zone not more than two elements apart from the corner. It is important to specify a closer gaussian integration points for masonry unit elements located at the vicinity of the masonry wall corners because, these corners undergo a high stress gradient as a result of the diagonal load concentration.

i and j also specify the number of gaussian points of bed and head joints respectively on the entire masonry wall. k is the number of gaussian points of each boundary interface element of masonry.

b) Interface:

I7 is a 3-digit integer number, ijk, where i is 1 or 2 for horizontal or vertical interface zone respectively.
j is the order number of the node with a wide angle at the bottom or the left side of the zone and k is the order number of the node with a wide angle at the top or at the right side of the zone in a vertical or horizontal interface zone respectively.

If no wide angle corner exist, the value of j or k should be assigned to zero for the appropriate side of the interface. Fig. A.1 gives some examples.

c) Jack and Support

I7 must be assigned to 1 or 2 for a horizontal or vertical loading or support element respectively.

A.3.4 Note 4 (see A.2.2)

Lack of fit is applicable to an interface element only. For a uniform wall, lack of fit may be permitted for the boundary interfaces. However, in a masonry wall, since boundary interfaces are included with the wall, lack of fit must be attributed to the masonry wall zone. The lack of fit value assigned to the side interfaces of a masonry will splits between the two sides of the wall, but the value given to the horizontal interfaces will be given to the top interface only.

A.4 Infilled Frame Examples

A.4.1 Masonry Infilled R.C. Frame

Figures A.2 and A.3 show the elements of input data for one of the masonry infilled R.C. frame test series carried out by Samai[8]. The corresponding data list is given in table A.1.

A.4.2 Micro Concrete Infilled Steel Frame

Figure A.4 show the elements of input data for one of the micro concrete infilled steel frame test series carried out by Saneinejad[29]. The corresponding data list is given in table A.2.

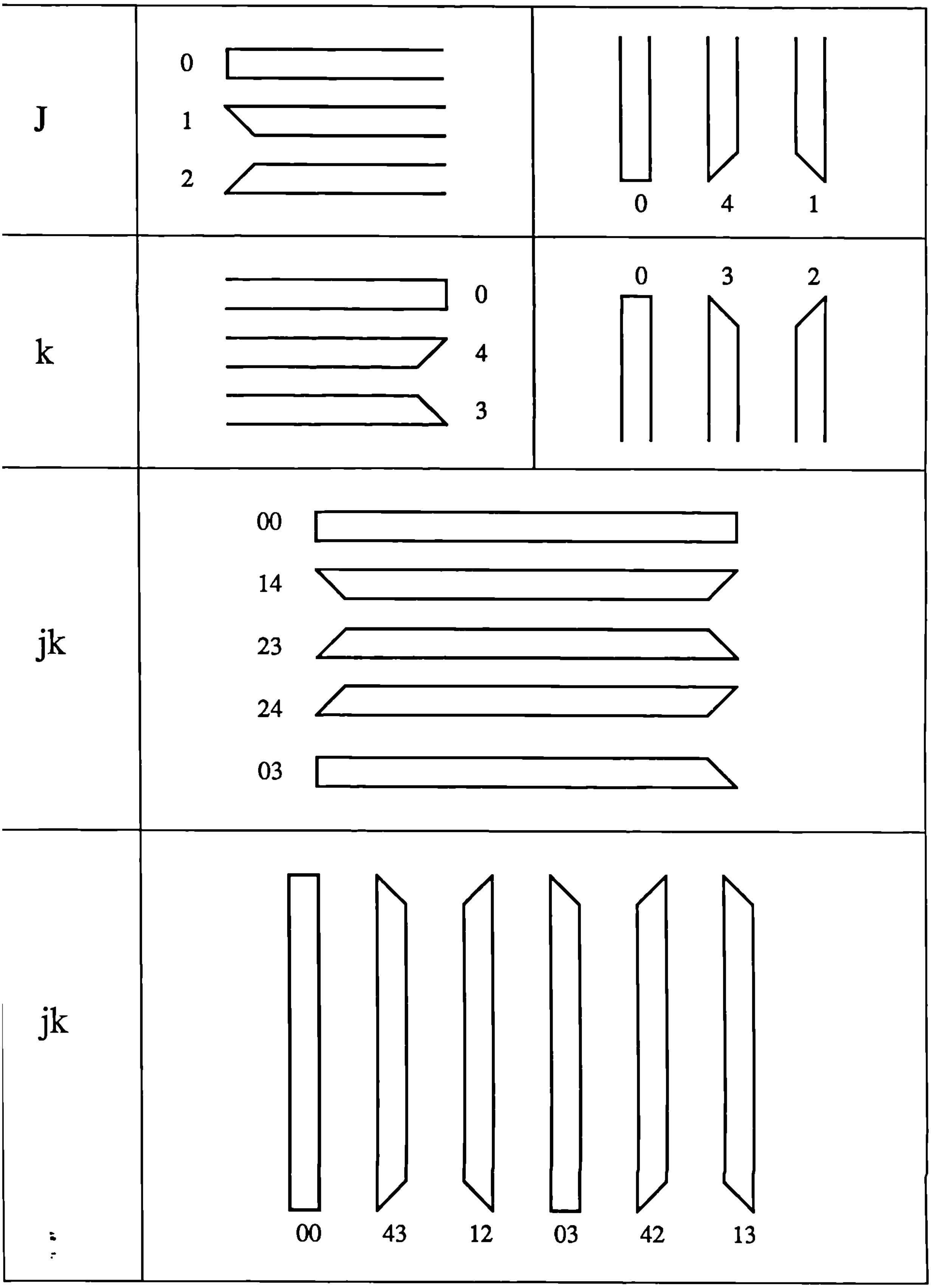

Figure A.1 Code Number for Geometry of Interface

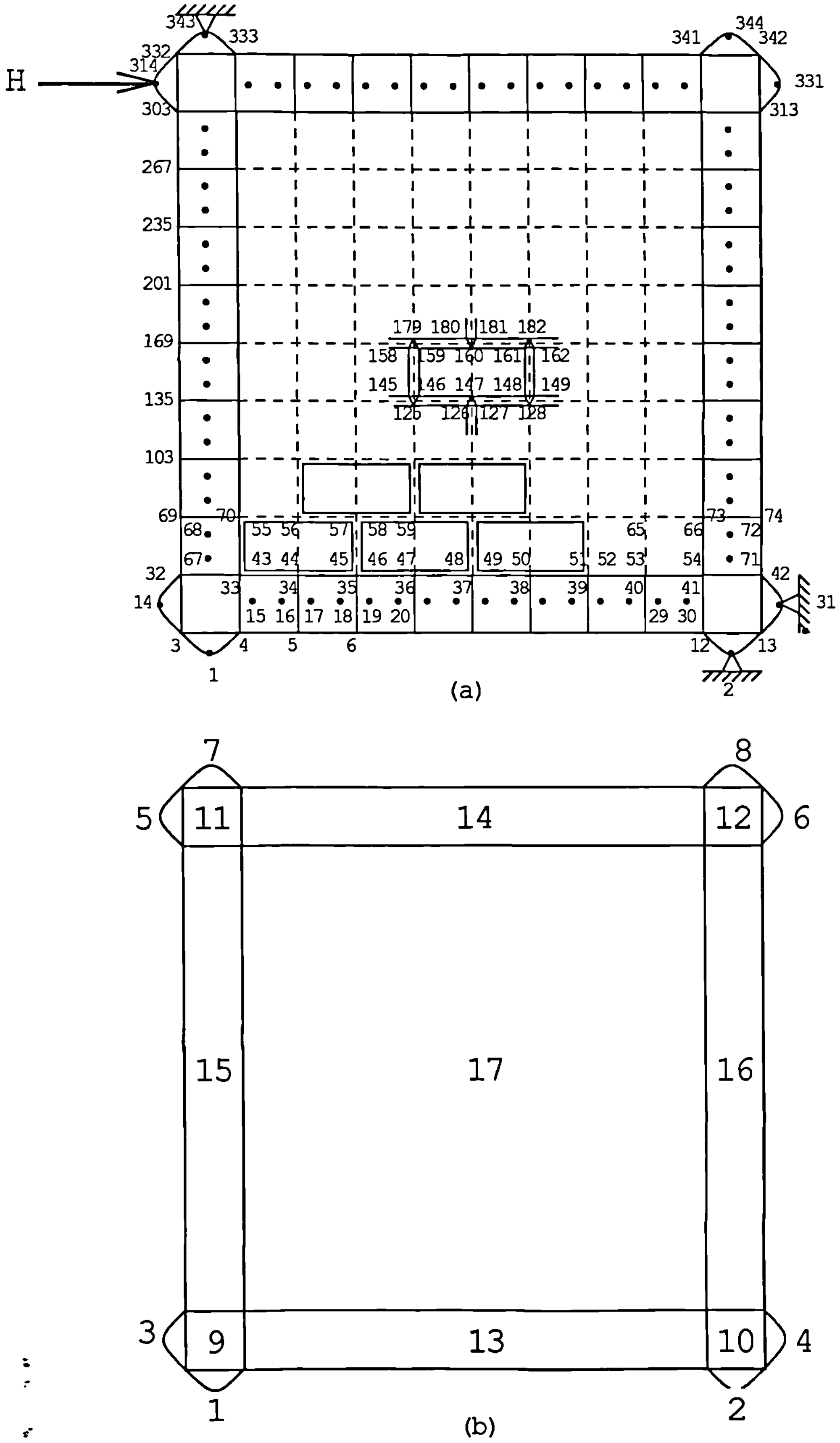

Figure A.2 R.C Masonry-infilled Frame Subdivision Lay-out; a) node numbering and b) zone numbering.

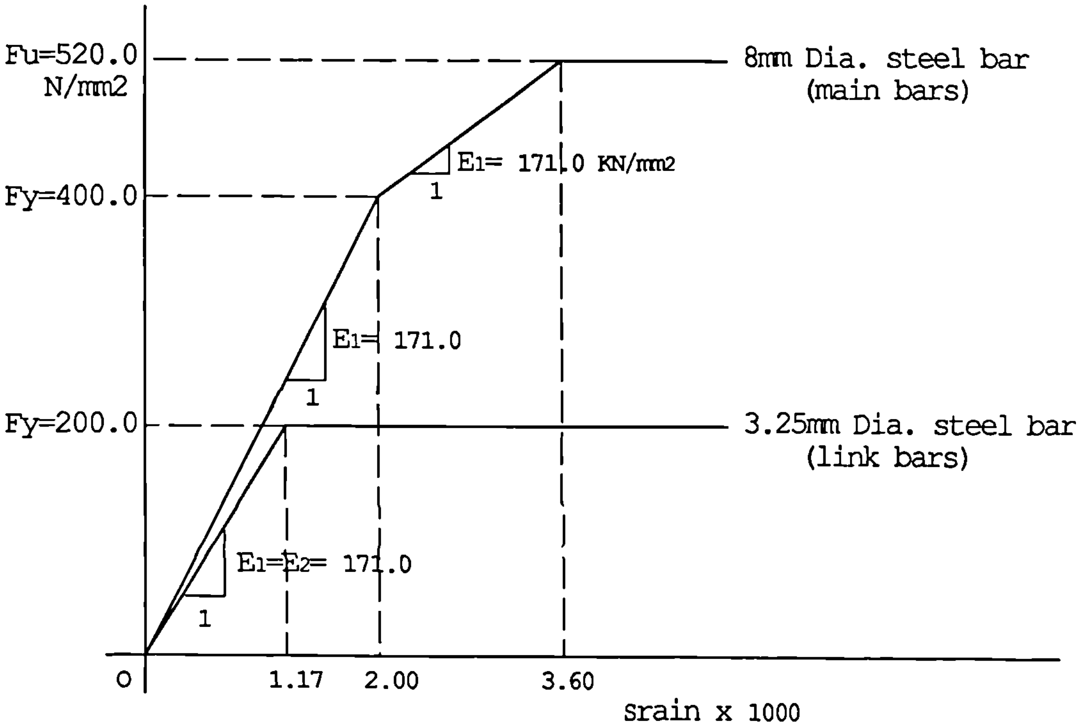

(a)

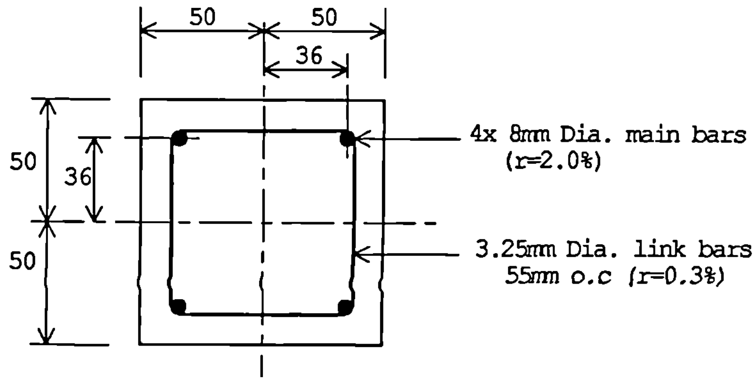

(b)

Figure A.3 Reinforcement Data of The Frame Tested by Samai(8); a) stress-strain characteristics and b) beam and column reinforcement geometry.

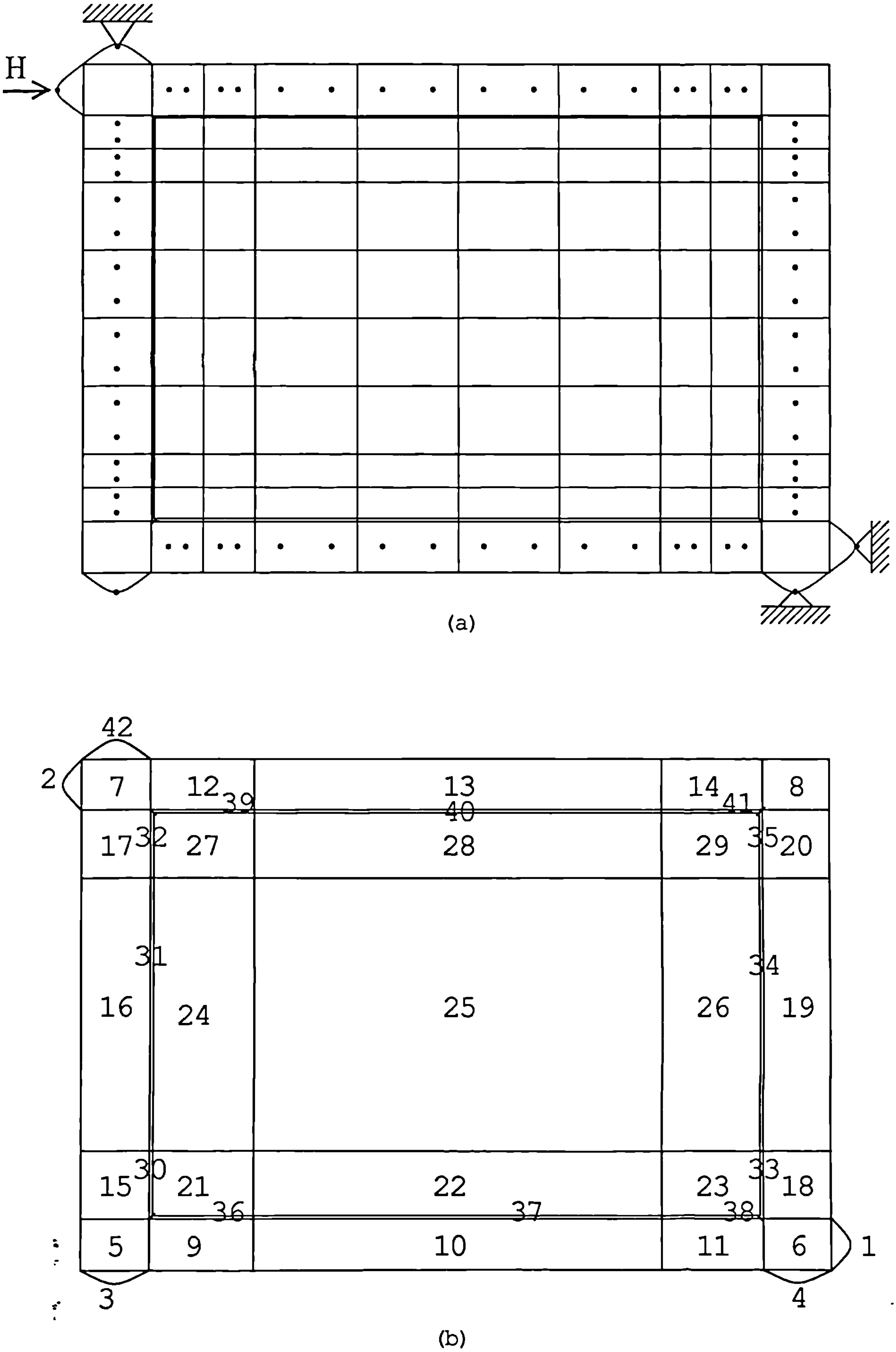

Figure A.4 Steel Concrete-infilled Frame Subdivision Lay-out; a) node numbering and b) zone numbering.

Table A.1 Data Listing for Reinforced Concrete Frame with lightweight Concrete Blockwork, Frame "IHW2" Tested by Samai[8]

```
 1
'IHW2'
 2  344   17
 1    3   6 0 1 1   2   0.0    0.0    0.0   0.0   0.0    0.0
 2    3   6 0 1 1   2   0.0    0.0    0.0   0.0   0.0    0.0
 3    3   6 0 1 1   1   0.0    0.0    0.0   0.0   0.0    0.0
 4    3   5 0 1 1   1   0.0    0.0    0.0   0.0   0.0    0.0
 5    3   6 0 1 1   1   0.0    0.0    0.0   0.0   0.0    0.0
 6    3   6 0 1 1   1   0.0    0.0    0.0   0.0   0.0    0.0
 7    3   6 0 1 1   2   0.0    0.0    0.0   0.0   0.0    0.0
 8    3   6 0 1 1   2   0.0    0.0    0.0   0.0   0.0    0.0
 9 2233 1 3 1 1   0 100.0  100.0  100.0   0.0   0.0    0.0
10 2233 1 3 1 1   0 100.0  100.0  100.0   0.0   0.0    0.0
11 2233 1 3 1 1   0 100.0  100.0  100.0   0.0   0.0    0.0
12 2233 1 3 1 1   0 100.0  100.0  100.0   0.0   0.0    0.0
13 2224 1 1 8 1   5 810.0  100.0  100.0   0.0   0.0    0.0
14 2224 1 1 8 1   5 810.0  100.0  100.0   0.0   0.0    0.0
15 2242 1 2 1 8   6 100.0  810.0  100.0   0.0   0.0    0.0
16 2242 1 2 1 8   6 100.0  810.0  100.0   0.0   0.0    0.0
17 2211 3 0 8 8 222 810.0  810.0   35.0   0.0   0.0  315.0
 1  3
    1    3    4
 2  3
    2   12   13
 3  3
   14   32    3
 4  3
   31   13   42
 5  3
  314  332  303
 6  3
  331  313  342
 7  3
  343  333  332
 8  3
  344  342  341
 9  2
    3   32
10  2
   12   41
11  2
  303  332
12  2
  312  341
13 18
    4   33   15   16   17   18   19   20   21   22   23   24   25   26
   27  28    29   30
14 18
  304   333 315 316 317 318 319 320 321 322 323 324 325
  326   327 328 329 330
```

Table A.1 (cont.)

```
15 25
   32    69 103 135 169 201 235 267 303  67  68 101 102
  133   134 167 168 199 200 233 234 265 266 271 272
16 25
   41    73 107 139 173 205 239 273 312  71  72 105 106
  137   138 171 172 203 204 237 238 269 270 301 302
17 34
   43    55  75  88 109 121 141 154 175 187 207
  220   241 253 275 288  33  70 104 136 170 202 236
  268   304  41  73 107 139 173 205 239 273 312
32
   33    35  37  39  41  43  45  48  51  54
  304   306 308 310 312 288 291 294  97 300
  104   170 236  88 154 220 107 173 239 100 166 232
 4
 1
 28.0  0.175   2.8  28.0   2.0    0.0  3.0  3.5  1.15  1.75
 3
 8.27  0.175   0.9   6.93  2.22   0.0  2.0  3.5  1.15  1.75
 0.25  0.1067  0.4   0.6   0.0533 0.0  0.0  1.25 0.025 1.20
 0.25  0.1067  0.1   0.15  0.0533 0.0  0.0  1.25 0.025 0.76
 0.25  0.1067  0.1   0.15  0.0533 0.0  0.0  1.25 0.025 0.76
 5
    500.0
 6
    10000000000.0
 3
171.0 171.0 200.0 90.22  0  0 200.0 200.0 400.0 520.0  0  0
 1     1.0  1.0  0.0  0.0  0.0  0.3  0.0  0.0  0.72  0.72
 2     0.0  0.0  1.0  1.0  0.3  0.0  0.72 0.72 0.0   0.0
 3     1.0  1.0  1.0  1.0  0.3  0.3  0.72 0.72 0.72  0.72
 2
 3
 8
     1        1   2
     2        1   2
    14        0   2
    31        1   2
   314        1   2
   331        0   2
   343        1   0
   344        1   0
   0
      0.002  0      0      1.0     0.0     0
     -0.05  -0.10 -15.0    2      -0.03
   7
         -0.035 -0.42  -0.9   -3.5   -4.8   -9.7     -13.5
   9     13    10     0    1.0  0  1   1.0   1
```

Table A.2 Data Listing for Steel Frame with Concrete Infill, Frame "SMUR2" analysed in this study.

```
1
'SMUR2'
2    222    42
5    2222 1 3 1 1   0  368.3  251.5   40.0  0.0  0.0  0.0
6    2222 1 3 1 1   0  368.3  251.5   40.0  0.0  0.0  0.0
7    2222 1 3 1 1   0  368.3  251.5   40.0  0.0  0.0  0.0
8    2222 1 3 1 1   0  368.3  251.5   40.0  0.0  0.0  0.0
9    2223 1 1 2 1   5  789.0  251.5   20.0  0.0  0.0  0.0
10   2223 1 1 4 1   5 3156.0  251.5   20.0  0.0  0.0  0.0
11   2243 1 1 2 1   5  789.0  251.5   20.0  0.0  0.0  0.0
12   2243 1 1 2 1   5  789.0  251.5   20.0  0.0  0.0  0.0
13   2223 1 1 4 1   5 3156.0  251.5   20.0  0.0  0.0  0.0
14   2223 1 1 2 1   5  789.0  251.5   20.0  0.0  0.0  0.0
15   2232 1 2 1 2   6  368.3  451.5   40.0  0.0  0.0  0.0
16   2232 1 2 1 4   6  368.3 1806.0   40.0  0.0  0.0  0.0
17   2234 1 2 1 2   6  368.3  451.5   40.0  0.0  0.0  0.0
18   2234 1 2 1 2   6  368.3  451.5   40.0  0.0  0.0  0.0
19   2232 1 2 1 4   6  368.3 1806.0   40.0  0.0  0.0  0.0
20   2232 1 2 1 2   6  368.3  451.5   40.0  0.0  0.0  0.0
21   2211 2 0 2 2   0  789.0  451.5  140.0  0.0  0.0  0.0
22   2211 2 0 4 2   0 3156.0  451.5  140.0  0.0  0.0  0.0
23   2222 2 0 2 2   0  789.0  451.5  140.0  0.0  0.0  0.0
24   2211 2 0 2 4   0  789.0 1806.0  140.0  0.0  0.0  0.0
25   2211 2 0 4 4   0 3156.0 1806.0  140.0  0.0  0.0  0.0
26   2211 2 0 2 4   0  789.0 1806.0  140.0  0.0  0.0  0.0
27   2222 2 0 2 2   0  789.0  451.5  140.0  0.0  0.0  0.0
28   2211 2 0 4 2   0 3156.0  451.5  140.0  0.0  0.0  0.0
29   2211 2 0 2 2   0  789.0  451.5  140.0  0.0  0.0  0.0
30   2221 4 0 2 1 120 789.0     0.0  140.0  0.0  0.0  0.0
31   2241 4 0 4 1 100 3156.0    0.0  140.0  0.0  0.0  0.0
32   2241 4 0 2 1 103 789.0     0.0  140.0  0.0  0.0  0.0
33   2241 4 0 2 1 110 789.0     0.0  140.0  0.0  0.0  0.0
34   2241 4 0 4 1 100 3156.0    0.0  140.0  0.0  0.0  0.0
35   2221 4 0 2 1 104 789.0     0.0  140.0  0.0  0.0  0.0
36   2212 4 0 1 2 240    0.0  451.5  140.0  0.0  0.0  0.0
37   2214 4 0 1 4 200    0.0 1806.0  140.0  0.0  0.0  0.0
38   2214 4 0 1 2 203    0.0  451.5  140.0  0.0  0.0  0.0
39   2214 4 0 1 2 210    0.0  451.5  140.0  0.0  0.0  0.0
40   2214 4 0 1 4 200    0.0 1806.0  140.0  0.0  0.0  0.0
41   2212 4 0 1 2 202    0.0  451.5  140.0  0.0  0.0  0.0
1       3 6 0 1 1   1    0.0    0.0    0.0  0.0  0.0  0.0
2       3 5 0 1 1   1    0.0    0.0    0.0  0.0  0.0  0.0
3       3 6 0 1 1   2    0.0    0.0    0.0  0.0  0.0  0.0
4       3 6 0 1 1   2    0.0    0.0    0.0  0.0  0.0  0.0
42      3 6 0 1 1   2    0.0    0.0    0.0  0.0  0.0  0.0
1    3
     30   13   41
2    3
  194  211  183
3    3
     1    3    4
4    3
     2   12   13
42   3
```

Table A.2 (cont.)

```
  222  211 212
5   2
    3   31
6   2
   12  40
7   2
  183  211
8   2
  192  220
9   6
    4   32  14  15  16  17
10 10
         6  34  18  19  20  21   22  23   24   25
11  6
   38   26  27  28  29

12  6
  184  212 195 196 197 198
13 10
  186  214 199 200 201 202 203 204  205   206
14  6
  190  218 207 208 209 210
15  7
   31   55  72  51  52  68  69
16 13
   72   89 106 123 140  85  86  102  103  119  120 136 137
17  7
  140  157 183 153 154 170 171
18  7
   40   66  83  53  5   70  71
19  13
   83  100 117 134 151  87  88  104  105  121  122 138 139
20  7
       151 168 192 155 156 172  173
21  3
   42   57  74
22  3
   44   59  76
23  3
   48   63  80
24  5
   74   91 108 125 142
25  5
   76   93 110 127 144
26  5
   80   97 114 131 148
27  3
  142  159 174
28  3
  144  161 176
29  3
  148  165 180
30  4
   32   42  34  44
31  4
```

Table A.2 (cont.)

```
   34   44  38  48
32  4
    38  48  40  50
33  4
   174 184 176 186
34  4
   176 186 180 190
35  4
  180  190 182 192
36  5
   32   56  73  42  74
37  7
   73   90 107 124 141  74 142
38  5
  141  158 184 142 174
39  5
   50   65  82  40  83
40  7
   82   99 116 133 150  83  151
41  5
  150  167 182 151 192
28
    3    4  12  13  40    41   50   65   82   99   116  133
  150  167 174 175  176  177  178  179  180  181  182
  183  184 192 211  212
5
2
 18.46 0.175  1.5   11.3   1.75 0.0   2.5  0.0     0.0   1.5
1
200.0  0.25   245.0 245.0  0.0  0.0   0.0  0.0     0.0   0.0
4
100.0  50.0   0.05  0.07   0.05 0.0  0.0  0.0     0.0   0.64
5
  10000.0
6
  1.0D+8
3
0.0 0.0 0.0 0.0 200.0 199.0 0.0 0.0 0.0 0.0 244.0 245.0
1 21.56 21.56  0.0    0.0   0  0    0.0 0.0    0.9658 0.9658
2  0.0   0.0  53.652 53.652 0  0 0.9354 0.9354 0.0    0.0
3 21.56 21.56 53.652 53.652 0  0 0.9354 0.9354 0.9658 0.9658
2
3
5
       1     1  0
       2     1  2
      30     1  2
     194     1  2
     222     1  2
0
 0.002   1      1      1.0    4.0    0
 0.1     0.15 150.0   10      0.2
11
 2.9  6.9  9.3  9.6  9.9  10.2  10.6  11.0  13.0  14.0  25.0
8   16  5150    0   0.0   0  1  1.0   1
```

APPENDIX B

Structure of Program NEPAL

The finite element computer Program 'NEPAL' is structured in the sense of Dijkstra described by Smith[37]. The main feature exibited by this program will be seen to be a nested structure and representations called 'structure charts', (rather than flow charts) will be used to describe their actions. The main features of these charts are:

i) The Block

Do this
Do that
Do the Other

This will be used for the outermost level of each structure chart. Within a block, the indicated actions are to be performed separately.

ii) The Choice

QUESTION?

Answer 1	Answer 2	Answer 3
Action 1	Action 2	Action 3

This corresponds to the if..... then..... else kind of construct.

iii) The Loop; This comes in various forms, but it will usually concern with 'DO' loop.

For i from 1 to n
ACTION (To be repeated n times)

Using these notations the main structure of program 'NEPAL' has illustrated in Table B.1. The variable names sre listed in Table B.2 and the way data must be input is described in Appendix A. the listing of the program is filed with the University of Sheffield.

Table B.1 The Structure Charts of Program 'NEPAL'

START

Input data, output data
Form [B] matrices and store them into workfile
Calculate the half band width of the global stiffness matrix

For all elements

Determine the element properties

For all Gaussian pointos of the element

Read [B] from workfile 'BEES'
Form [D]
Form element tangent stiffness matrix [ELK]

Assemble [ELK] with the Global system tangent Stiffness matrix [SYSK]

INC = 0

For all increments up to 'DELTA'

CONV = 0
Apply deflexion increment 'DEF'
ITR = 0

For all iterations up to Convergence

Update iteration counter ITR, (ITR = ITR + 1)
Solve the equations to obtain changes in the structure nodal displacements

convergence achieved?

Yes	No
CONV = 1	

Calculate total nodal displacements 'NODIS'
Zero [UBNF] and [SYSK]
Include internally applied loads into [UBNF]

Table B.1 Cont.

For all elements

Calculate the element properties
Zero [ELK]
Calculate element nodal total displacement
'ELDIS'

For all Gaussian integration points

Read [B] from the workfile, 'BEES'

Calculate the total strains at the Gaussain
point, [TSTRN]
Read the old state of the G.P from array 'STATE'
Deduct the previously occurred plastic strains
Read the old mechanical properties of G.P. from
[ULOAD], cracks angles and unloading modulus
Determine the new state of the material
Calculate the current stresses [STRS]
Form Tangent [D]
Transform [D] into Global co-ordinates

CONV?

CONV = 1	CONV = 0
output results	continue

Include the effect of [STRS] into [EQNF]
Include the contribution of G.P. into [ELK]

Update [UBNF] ([UBNF] = [UBNF] - [EQNF])
Include [ELK] with [SYSK]

STOP

END

Table B.2 List Of Variable Names Used in Program 'NEPAL'

Integer Variables:

ADDRES	A flagging integer
COMB	A flagging integer
CONV	A flagging integer-To flag for convergence
DIF	Maximum freedom order difference within an element
DIMEN	Dimensionality DIMEN = 2 for 2-D structures
DIRECT	Direction 1 for x and 2 for y
DITR	Desired number of iterations
DOFEL	Total No. of degrees of displacement freedom of the element
DOFNOD	Degree of freedom per node
ETBAR	Specifier for the way the tangent modulus of the reinforcing bars should be chosen
ETVAL	The same as ETBAR but for other materials
FDM	Freedom order number
GH	Element Gaussian point counter (by column)
GV	Element Gaussian point counter (by row)
HBAND	Half Band-width of the global stiffness matrix
HNN	Number of nodes on each horizontal side of an element
INC	Deflection increment counter
ITEST	ITEST remain zero when no error is faced. ITEST>0 notifies that an error has discovered by one of the program Libraries.
ITR	Iteration counter
JNBE	Recording order number of B matrix of the Jack element within the workfile 'BEES'
JNEL	Jack element order number
JNNEL	Another Jack element order number when it has 5 nodes
JNZ	The Jack element zone number
LAM	Direction number LAM = 1 Horizontal interface or adjusting element LAM = 2 Vertical " " LAM = 0 Ordinary element
LODNOD	Number of externally loaded nodes
MAXITR	Specified maximum number of iterations
MAJOR	State of major crack or interface

State	Ordinary material	Interface
0	Intact	Fully bonded
1	Gripped	Partially bonded
2	Interlocked	Debonded
3	Open	N.A

MINOR	State of minor crack or interfaces

State	Ordinary material	Interface
0	Intact	Gripped or elastic
1	Gripped	Debonding or slip
2	N.A	Yielding
3	Open	Open

MAX	Order number of the principal direction having the most tensile stress

Table B.2 Cont.

MIN	Order number of the principal direction having the least tensile stress
NBE	Recording order number of B matrices in file 'BEES'
NEL	The element order number
NNEL	Another element order number when the element has 5 or more nodes (Up to 10 modes are allowed)
NETYP	Number of types of element within a zone
NE	Element type number within the current zone
NGPH	Number of columns in Mesh of the element Gaussian points
NGPV	Number of rows in Mesh of the element Gaussian points
NMTYP	Number of types of material used in the structure
NODEL	Number of nodes per element
NQP	Total number of Gaussian point per element other than reinforcement
NQPRX	Number of columns in Mesh of the element reinforcement Gaussian points
NQPRY	Number of rows in Mesh of the element reinforcement Gaussian points
NRSLT	Number of times that a detailed output or results is wanted
NRTYP	Number of types of reinforcement in the structure
NUCONV	Specifier for convergence of the Poisson's ratio NUCONV = 0 not converged NUCONV = 1 converged
NUMSS	Number of terms in the stress or strain vector
NUTVAL	Specifier for the choice of the Tangent poisson's ratio
Z	Zone counter
NM	Material counter
PLAST	An ordinary material state specifier
PRINT	If PRINT=0 results will not output at the current iteration If PRINT=1 results will output
QUAD	The order number of Gaussian points
RESNOD	Total number of restraint nodes
SIGN	Taking values of +1 or -1 to indicate a + or - value
STRESS	STRESS = 0 OR 1 to specify whether the stress transformation matrix is required
SUBINC	Number of Current Subincrement(if applicable)
TOTDOF	Total number of displacement freedoms within the global system
TOTEL	Total number of elements within the system
TOTNOD	Total number of nodes within the system
TOTZON	Total number of zones within the system
TQUAD	Total number of Gaussian points within the system other than the reinforcement GPs

Table B.2 Cont.

TRQUAD	Total number of Reinforcement Gaussian points within the system
TSINC	Specified total number of subincrements(if applicable)
VNN	Number of nodes on each vertical side of an element Array Size Names (Integer)

Integer Array Size Names:

DD	Maximum expected Number of co-ordinate directions subjected to integration and derivation
FE	Maximum expected number of displacement freedom per element
FN	Maximum expected nodal displacement freedom
GG	Maximum expected rows or colums of Gaussian points within an element
GGG	Dimension of array GAUSS ,GGG = 2
SS	Maximum expected number of stress components
MFDM	Maximum expected displacement freedom within the system
NN	Maximum expected number of nodes per element
QQ	Maximum expected total number of Gaussian points within the system (other than reinforcement Gaussian points)
RQ	Maximum expected number of reinforcement Gaussia points within the system
ZZ	Maximum expected total number of zones

NB, Single letter integers, usually I, J etc. used as simple counters are not listed.
Multiple letter integers beginning with I and J, for example IELTOP, are the reference size of the appropriate array, ELTOP in this case.
e.g. ELTOP (IELTOP, JELTOP)

Double Precision Variables:

ALFA	Ratio of the most tensile to the most compressive equivalent uniaxial strain
ANGLE	angle
DEF	The total current deflection
DELTA	The total specified deflection up to which the analysis should be carried on
DET	Determinant of Jacobian matrix-multiplier to obtain the element stiffness matrix
EADJ	Modulus of elasticity of a loading Jack or support element
EMAX	Specified maximum straining ratio at which the material loses all its strength crushes
E0	Initial modulus of elasticity
EE	Secant modulus at ehe crest of the unconfined uniaxial stress-strain curve

Table B.2 Cont.

ES	Secant modulus at the crest of the stress-strain curve
EP	Plastic straining ratio
EPE	Plastic straining ratio after unloading
EPR	Plastic straining ratio at the current stress level
EPSC	Strain at the peak unconfined uniaxial stress
ER	Current straining ratio
ERR	Degree of inaccuracy
ET	Tangent modulus
ETA	Normalized co-ordinate (vertical)
ETAR1	Abcissa of botton reinforcement
ETAR2	Abcissa of top reinforcement
EUL	Unloading modulus
EULC	Unloading modulus at peak unconfined uniaxial stress
FA	A
FBC	f_{bc}
FC	C
FD	D
FDD	D
FG	g
FM	m
FNU	related To the Poisson's ratio
FR	R
GAMA	Angle of the major crack to x direction
GAMA2	Angle of minor crack to major crack directions
KH	Horizontal weight of Gaussian point for numerical integration
KT	Breadth of the element for numerical integration
KV	Vertical weight of Gaussian point for numerical integration
KN	Normal stiffness of an interface
KS	Tangential stiffness of an interface
FIRSTD	Specified first deflection increment
MINDEF	Specified allowed minimum deflection increment
MAXDEF	Specified allowed maximum deflection increment
MAXNRM	Maximum inaccuracy found in calculation of the the norm of the convergence
MU	Co-efficient of friction
NORM	Norm of convergence
NORMS	Acceptable norm of convergence
NU	The Poisson's ratio
NU0	The initial Poisson's ratio
NUT	Tangential Poisson's ratio
NUVAR	Specifier for allowance for variation of Poisson's ratio NUVAR = 0 to 1.0
RCT	Compressive to tensile strength of brittle material
REF	Reference for convergence
RLX	Steel ratio (horizontal link bars)
RLY	Steel ratio (vertical link bars)

Table B.2 Cont.

RTC	Tensile to compressive strength of material
RX1	Steel ratio (horizontal or bottom bar)
RX2	Steel ratio (horizontal or top bar)
RY1	Steel ratio (vertical or left bar)
RY2	Steel ratio (vertical or right bar)
RUL	Ratio of unloading
SBOND	Shear bond strength of an interface
SEP2	Cracking strain (secondary cracks)
SLIP2	Slip at the secondary cracks
SHEAR	The absolute value of shearing strain
SIGMAC	Unconfined uniaxial compressive strength
SIGMAT	Direct tensile strength
SNC	Ratio of strain at thepeak stress to that of the unconfined uniaxial test
SSC	Ratio of stress at the peak stress to that of the unconfined uniaxial test
STRNSL	Slip strain at the major cracks
STRNSP	Separation at major crack
SUBDEF	Subdeflection
TBOND	Tensile bond strength
TETA	Angle of the least tensile principal stress directions to x direction
TOTDEF	Current total deflection
TSDEF	Total subdeflection increment
X1	Normalized co-ordinate
X1R1	Abcissa of vertical or left reinforcement
X1R2	Abcissa of vertical or right reinforcement

Integer Arrays:

NF(INF,FN)	Holds the nodal freedom order numbers
NODEF(INODEF)	Holds the node numbers whose displacements are desired to be output
RESTR(IRESTR,JRESTR)	Holds restraint nodes and their restrainment situation
RSTAT(RQ)	Holds the states of reinforcement at the element reinforcement Gaussian points
STATE(QQ)	Holds the state of material at the Gaussian points
STEER(FE)	Holds the element nodes order numbers
ZPROP(ZZ,JZPROP)	Holds the zones properties
ZTOP(ZZ,JZTOP)	Holds the zones topology
A(28)	Array used by subroutine timdat in purpose of calculating the CP time
ELTOP(IELTOP,JELTOP)	Holds the topology of all the elements ELTOP (NEL, 5) = 10 * NZ + NE ELTOP (NEL, 6) = 100 * Q + P ELTOP (NEL, 1....4) = Element nodes order numbers when NODE < 4 ELTOP (NNEL, 1...6) = Element nodes order numbers when NODE > 4

Table B.2 Cont.

Double Precision Arrays:

B(SS,FE)	Strain displacement matrix, [B]
BT(FE,SS)	Transpose of [B]
BTDB(FE,FE)	$[B]^T[D][B]$
BTS(FE)	Product of B^T and stress vector
D(SS,SS)	Elasticity matrix (tangent), $[D_t]$
DI	Initial $[D_t]$
DB	[D][B]
DT	[D][T]
EBAR (6)	Holds the modulus of steel bars
ELDIS(FE)	Element nodal displacements vector
ELK(FE,FE)	Holds the element stiffness matrix
EQNF(FE)	Holds the element equivalent nodal force vector
EPSB(6)	A vector
EPSBP(3)	A vector
EUS(3)	Equivalent uniaxial strain vector
EUSEL(3)	Elastic equivalent uniaxial strain vector
GEOM(NN,DIMEN)	Geometry of the element nodes
GDER(DIMEN,10)	Holds the element shape functions Derivatives

APPENDIX C

Proposed 3-D Equivalent 4-node Plane Element

A symmetry plane is attributed to any plane element having a uniform finite thickness, Fig 3.7. When an element is perfectly plane and subjected to a set of out-of-plane forces acting symmetrically about its symmetry plane, the resulting out-of-plane displacements are also symmetric about this plane. Under such a loading condition The symmetry plane remains stationary. Therefore it may be called the reference plane of the element.

Taking advantage of existence of such a reference plane an 8-node solid element whose thickness forms the thickness of the plane element, may be assigned only four nodes at the corners of the reference plane as shown in Fig 3.7.

Assuming a linear variation for lateral displacement of The lateral surfaces of the element, the linear shape founctions of 4-node isoparametric element, Eq 3.23, can also be proposed for the lateral displacement of these surfaces as follows:

$$N_i=(1/4)(1+\xi\xi_i)(1+\eta\eta_i) \qquad (C.1)$$

The 3-D displacement functions of the proposed element may now be written in matrix form as:

$$\begin{bmatrix} u \\ v \\ w \end{bmatrix} = \begin{bmatrix} N_1 & 0 & 0 & . & . & . & N_4 & 0 & 0 \\ 0 & N_1 & 0 & . & . & . & 0 & N_4 & 0 \\ 0 & 0 & N_1 & . & . & . & 0 & 0 & N_4 \end{bmatrix} \begin{bmatrix} X_1 \\ Y_1 \\ Z_1 \\ .. \\ Z_4 \\ Y_4 \\ Z_4 \end{bmatrix} \quad \text{(C.2)}$$

or: $\{e\} = [N]\{a\}$

Z_1 to Z_4 denote the out-of-plane changes in thickness of the element at nodes **1** to **4** respectively and **w** designates the change of thickness of the element at an arbitrary point within the area of the element.

As shown in Fig 3.7, the strain components of an arbitrary point within the reference plane and also at the corresponding points on either lateral surfaces of the element, can be worked out as given in Table C.1.

Table C.1 Strain Distribution in the Plane 3-D Equivalent Element

Strain	reference plane	side surface	Mean values
εx	$\partial u/\partial x$	$\partial u/\partial x$	$\partial u/\partial x$
εy	$\partial v/\partial y$	$\partial v/\partial y$	$\partial v/\partial y$
εz	$(w/2)/(t/2)$	$(w/2)/(t/2)$	w/t
γxy	$\partial u/\partial y+\partial v/\partial x$	$\partial u/\partial y+\partial v/\partial x$	$\partial u/\partial y+\partial v/\partial x$
γyz	0	$\partial(w/2)/\partial y$	$(1/4)\partial w/\partial y$
γzx	0	$\partial(w/2)/\partial x$	$(1/4)\partial w/\partial xy$

In this table, **t** denotes the thickness of the element. In order to avoid any integration in **z** direction, only the mean values of the strain produced on the reference plane and the lateral surfaces may be used. This procedure is equivalent to a numerical integration over two gaussian points located at **(1/4)t** apart from the reference plane. The relations listed in Table C.1 can be written in matrix form as:

$$\begin{bmatrix} \varepsilon x \\ \varepsilon y \\ \varepsilon z \\ \gamma xy \\ \gamma yz \\ \gamma zx \end{bmatrix} = \begin{bmatrix} \partial/\partial x & 0 & 0 \\ 0 & \partial/\partial y & 0 \\ 0 & 0 & 1/t \\ \partial/\partial y & \partial/\partial x & 0 \\ 0 & 0 & (1/4)\,\partial/\partial y \\ 0 & 0 & (1/4)\,\partial/\partial xy \end{bmatrix} \begin{bmatrix} u \\ v \\ w \end{bmatrix}.$$

or: $$\{\varepsilon\} = [L]\{e\} \qquad \text{(C.3)}$$

Substituting for **{e}** from Eqs C.2, the element **[B]** matrix can be obtained as follows:

$$\{\varepsilon\} = [L][N]\{a\}$$

Defining:

$$[B] = [L][N]$$

Hence:

$$\{\varepsilon\} = [B]\{a\}$$

The stiffness matrix of the element can be formed by the standard procedure described in Section 3.4.5

APPENDIX D

Proposed Beam Element

D.1 General

The development of the beam element has been briefly reviewed in Chapter 3. As a compromise between accuracy and economy it appears that the 6-node rectangular element developed by Wilson et al[44] is the best, to date, available 2D beam element. However this element has the following disadvantages:

i) Since the curvature induced by bending is controlled by internal independent shape functions (**N_5** and **N_6** vide Section 3.11.2), the element is a **C_0** continuity element i.e. the slope continuity is violated between the element in question and the adjacent ones.

ii) The parabolic bending shape functions, **N_5** and **N_6**, are not compatible with curvature of a beam involving a point of inflexion.

iii) The element is not compatible with the shear deformation and does not account for the parabolic shear strain distribution developed across the beam.

A new element has therefore been developed, as discussed in Section 3.11.3. The proposed element is a **C_1** continuity element, i.e the slope continuity is maintained,

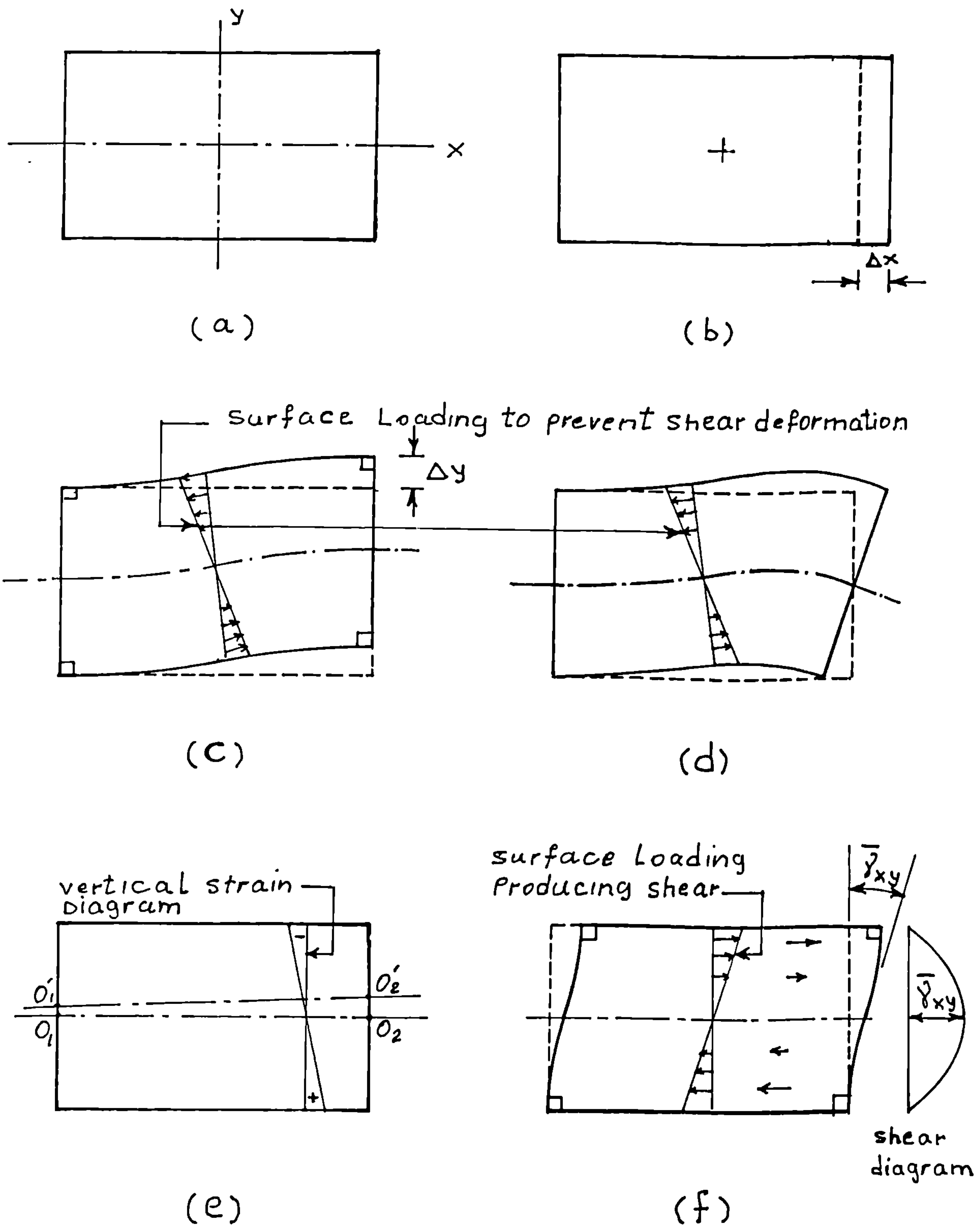

Figure D.1 Deformation of a Beam Segment under Arbitrary Forces; (a) geometry, (b) axial deformation, (c,d) shear-free bending, (e) relative displacement of the neutral axis and (f) pure shear and is fully compatible with shear deformation and also permits a parabolic shear strain distribution to develop across the beam. The algorithm of this element is given in the following sections.

D.2 Proposed Rectangular C_1 Beam Element

D.2.1 The General Concept

A beam segment is shown in Fig D.1(a). When the beam is arbitrary loaded, this segment of the beam would deform and its configuration mode would generally be limited to the modes shown in Fig D.1 or combinations of them. In order to relate such configuration modes to certain nodal displacements, four principal corner nodes may be assigned to this element each having two in plane degrees of freedom. Displacement of these nodes should, independently, force the element to deform into a mode that first, the "functional completeness" (vide Zienkiewicz[36], pp 33) is satisfied and second; the slope continuity is maintained between the adjacent elements so that the curvature induced by bending is continuously followed. Such modes were indeed possible to introduce as illustrated in Fig D.2, but they can only produce shear-free configurations shown in Fig D.1(b), (c) and (d). In such shear-free modes of displacement, shear strain is somehow restrained, say by a field of surface forces, and the displacement contours remain perpendicular. Obviously by combining the nodal displacements shown in Fig D.2 all the shear-free modes of configuration (visualized in Fig D.1(b,c,d)) can be simulated.

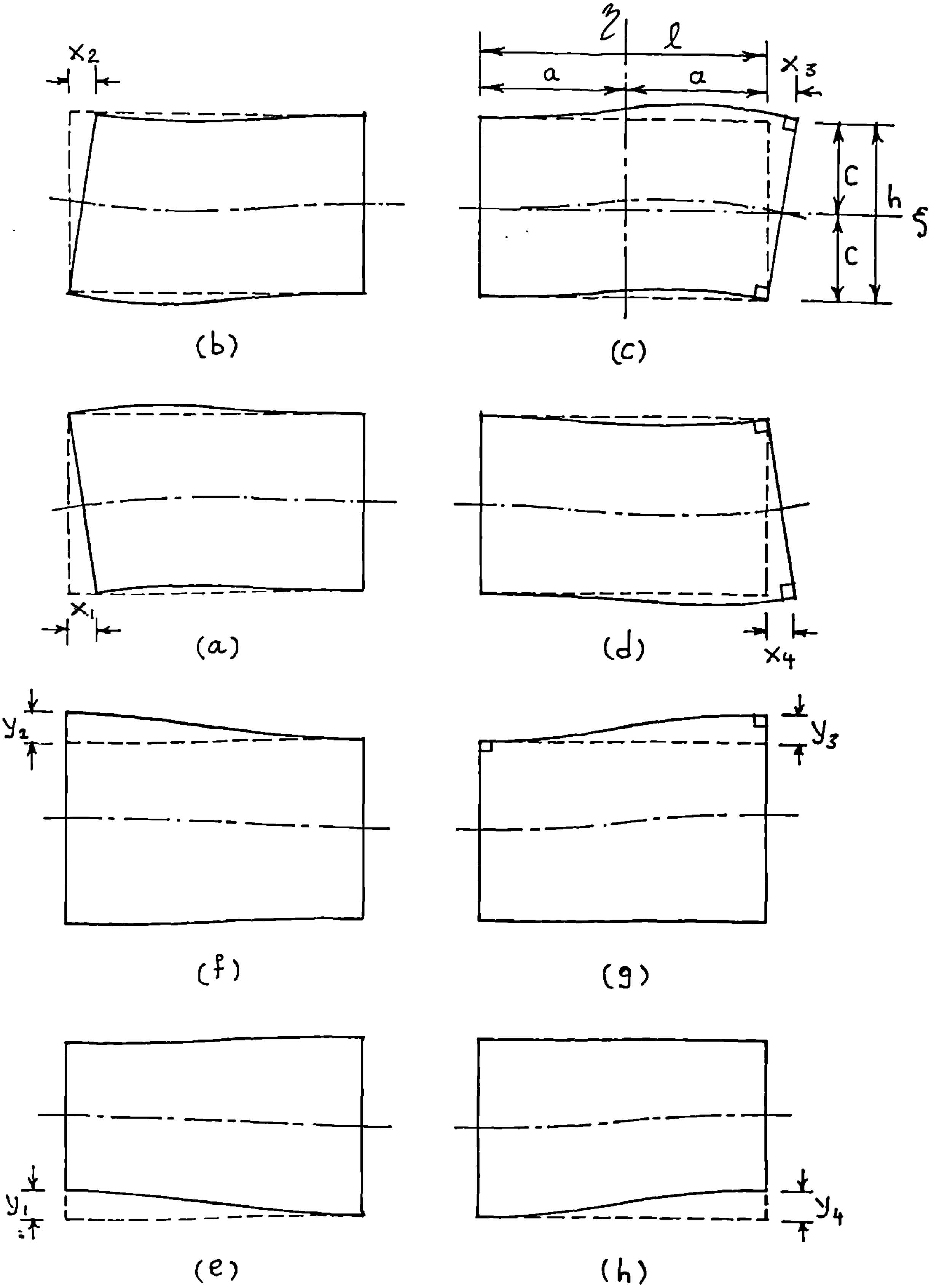

Figure D.2 Modes of Deformation of The Proposed Beam Element Resulting from Nodal Displacements; (a,b,c,d) horizontal nodal displacements and (e,f,g,h) vertical nodal displacements

In order that the beam element simulate The shear deformation, it requires additional degrees of freedom. This will be discussed in Section D.2.4. The shear-free shape functions for displacement of the corner nodes are derived in the following sections.

D.2.2 Shape Functions for Horizontal Nodal Displacements

Consider node 3 of the element in Fig D.2(c) while this node has taken unit displacement in the positive direction of **x**. The left hand side of the element, while remaining straight has rotated, clockwise, causing the top and bottom faces of the beam to move upwards producing a curve containing a point of inflexion.

Displacement of an arbitrary point, $\mathbf{P}(\xi,\eta)$, within the element is a function of the local normalized coordinates, ξ and η ie:

$$
\begin{aligned}
\mathbf{N_{u}X3} &= \mathbf{F_1}(\xi,\eta) \\
\mathbf{N_{v}X3} &= \mathbf{F_2}(\xi,\eta)
\end{aligned}
\tag{D.1}
$$

where $\mathbf{N_{u}X3}$ and $\mathbf{N_{v}X3}$, namely the shape functions for horizontal displacement of node 3, signify the horizontal and vertical displacements respectively of point **P** resulted from unit displacement of node 3 in **x** direction. At the remote ends of the element, $\mathbf{N_{u}X3}$ and $\mathbf{N_{v}X3}$ must satisfy the following conditions:

For $\xi=-1$:

$$\mathbf{N_{u}X3} = 0 \quad \text{and} \quad \mathbf{N_{v}X3} = 0$$

Hence:

$$N_uX3 = (1+\xi)P_1$$

$$N_vX3 = (1+\xi)P_2$$

For $\xi=+1$, F_1 is a linear function of η and $N_vX3=0$. Hence:

$$N_uX3 = (1 + \xi)(f_1\eta + f_2) \qquad (D.3)$$

$$N_vX3 = (1 + \xi)(1 - \xi)f_3 \qquad (D.4)$$

where f_1 and f_2 are functions of ξ only. Now the element strain components can be examined using the chain rule of differentiation as follows:

$$\varepsilon_x = (\partial N_uX3/\partial\xi)(\partial\xi/\partial x) = (1/a)(\partial N_uX3/\partial\xi) \qquad (D.5)$$

$$\varepsilon_y = (\partial N_vX3/\partial\eta)(\partial\eta/\partial y) = (1/c)(\partial N_vX3/\partial\eta) \qquad (D.6)$$

$$\gamma_{xy} = (\partial N_uX3/\partial\eta)(\partial\eta/\partial y) + (\partial N_vX3/\partial\xi)(\partial\xi/\partial x)$$

$$= (1/c)(\partial N_uX3/\partial\eta) + (1/a)(\partial N_vX3/\partial\xi) \qquad (D.7)$$

It must be mentioned that the terms involving $\partial\xi/\partial y$ or $\partial\eta/\partial x$ have zero value. Substituting for N_vX3 into Eq D.6 results in:

$$\varepsilon_y = (1/c)(1-\xi^2)(\partial f_3/\partial\eta)$$

Since the depth of the beam remains constant for any value of ξ, ε_y equals to zero requiring that $\partial f_3/\partial\eta$ becomes zero. Therefore f_3 is also a function of ξ only.

Substituting for N_uX3 and N_vX3 from Eq D.3 and D.4, respectively, into Eq D.7 and equating it to zero gives:

$$\gamma_{xy} = (1/a)\left[(1-\xi^2)(\partial f_3/\partial \xi) - 2\xi f_3\right] + (1/c)(1+\xi) f_1 = 0 \qquad \text{(D.8)}$$

The first and the third terms of Eq D.8 would become zero if ξ takes the value -1.0 requiring also the second term of this equation to become zero for the same value of ξ, ie:

$$f_3 = A(1+\xi) \qquad \text{(D.9)}$$

where **A** is assumed to be a constant so that N_{vX3} have one point of inflexion. Substituting for f_3 from Eq D.9 into Eq D.8 and solving for f_1 gives:

$$f_1 = (c/a)A(3\xi-1) \qquad \text{(D.10)}$$

Substituting for f_1 from Eq D.10 into Eq D.3 gives:

$$N_{uX3} = (1+\xi)\left[(c/a)A(3\xi-1)\xi + f_2\right]$$

For ξ=+1 and η=0, N_{uX3} must become 0.5. This requires that:

$$f_2 = 1/4 + B(1-\xi) \qquad \text{(D.11)}$$

Substituting for f_1 and f_2 from Eq D.10 and D.11 into Eq D.3, N_{uX3} becomes:

$$N_{uX3} = (1+\xi)\left[(c/a)A(3\xi-1)\eta+1/4+B(1-\xi)\right] \qquad \text{(D.12)}$$

For ξ=+1 and η=+1, N_{uX3} should become +1. Applying this condition, A results in:

$$A = (1/8)(a/c) \qquad \text{(D,13)}$$

Substituting for A from Eq D.13 into Eq D.12, N_{uX3} may be derived as follows:

$$N_{uX3} = (1/8)(1+\xi)\left[(3\xi-1)\eta + 2 + B'(1-\xi)\right] \qquad \text{(d.14)}$$

The nodal displacement under consideration is a combination of a uniform axial tensile displacement and the left end rotation as shown in Fig D.1(b) and (d) respectively. The former deformation produces a tensile longitudinal stress and the latter produces no stress along the beam on its centre line. Therefore, for all the points on the centre line of the element, ε_x must have a constant value for the above combination. This condition allows the value of **B'** to be determined as follows:

$$\varepsilon_x = (1/a)(\partial N_{uX3}/\partial\xi) \quad = \quad \text{a Constant value}$$

or:

$$\varepsilon_x = (1/4)\left[(1/a) - B'\xi\right] = \quad \text{a Constant value}$$

ie:

$$B' = 0$$

Substituting for **B'**, Eq D.14 becomes:

$$N_{uX3} = (1/8)(1+\xi)\left[\eta(3\xi-1)+2\right] \qquad \text{(D.15)}$$

Substituting for **A** from Eq D.13 into Eq D.9 and also substituting for f_3 from Eq D.9 into Eq D.4 leads to the following expression giving N_{vX3} in terms of ξ. (D.16)

$$N_{vX3} = (1/8)(a/c)(1-\xi^2)(1+\xi)$$

Using the same procedure as used above, the shape functions for horizontal displacement of the other 3 nodes can be derived. These shape functions may generally be expressed as follows:

$$N_{uxi} = (1/8)(1+\xi_i\xi)\left[\eta_i\eta(3\xi_i\xi-1) +2\right] \qquad (D.17)$$

$$N_{vxi} = (1/8)(1/\gamma)\xi_i\eta_i(1+\xi_i\xi)(1-\xi^2) \qquad (D.18)$$

where γ is the aspect ratio of the beam given as:

$$\gamma = c/a = h/l \qquad (D.19)$$

The index **i** denotes the order number of the node in question and ξ_i and η_i are the normalized coordinates of node **i** taking either values of +1 or -1.

D.2.3 Shape Functions for Vertical Nodal Displacements

Consider node 3 of the element in Fig D.2(g) while this node has taken unit displacement in **y** direction. The left side of the element, while remaining straight, has uniformly stretched upwards and only the top side of the element has moved away producing a curve having a point of inflexion. The horizontal and vertical displacement shape functions for such a nodal displacement may be expressed as:

$$N_{uY3} = F_3(\xi,\eta) \qquad (D.20)$$

$$N_{vY3} = F_4(\xi,\eta) \qquad (D.21)$$

These functions must satisfy the boundary conditions; ie. for either ξ=-1 or η=-1, N_{vY3} must become zero. These conditions require that:

$$N_{vY3} = (1+\xi)(1+\eta)Q \qquad (D.22)$$

Since the displacement contours are perpendicular (shear-free deformation), the top face of the element at $\xi=\pm1$ must have zero slope. ie:

$$\partial \mathbf{Nv}/\partial\xi = 0$$

or: $$(1+\eta)\left[(1+\xi)(\partial Q1/\partial\xi) + Q1\right] = 0 \quad (\text{for } \xi=\pm1) \tag{D.23}$$

The first term of the above equation becomes zero for $\xi=-1$. Therefore, the second term must also become zero for the same value of ξ. This condition requires that:

$$Q1 = P1(1+\xi) \tag{D.24}$$

where $\mathbf{P1}$ is a linear function of ξ so that $\mathbf{N_{v}Y3}$ becomes a function of third degree in ξ. This is a necessary condition for this function as to have one point of inflexion. Now $\mathbf{P1}$ can be written as:

$$P1 = A\xi + B \tag{D.25}$$

Substituting for $\mathbf{P1}$ and $\mathbf{Q1}$ from Eq D.25 and Eq D.24 respectively into Eq D.23 and setting ξ equal to +1 and Eq D.23 to zero, $\mathbf{B}$ can be derived in terms of $\mathbf{A}$ as follows:

$$B = -2A$$

And Eq D.22 becomes:

$$N_{v}Y3 = (1+\xi)^2(1+\eta)(\xi-2)A$$

For $\xi=+1$ and $\eta=+1$ the value of $\mathbf{N_{v}Y3}$ must become unity. Hence, $\mathbf{A}=1/8$ and $\mathbf{N_{v}Y3}$ becomes:

$$N_{v}Y3 = (1/8)(1+\xi)^2(1+\eta)(2-\xi) \tag{D.26}$$

The boundary conditions for horizontal displacements require that:

$$N_{uY3} = 0 \qquad \text{(for } \xi = \pm 1\text{)}$$

$$N_{vY3} = 0 \qquad \text{(for } \eta = -1\text{)}$$

Hence:

$$N_{uY3} = (1-\xi^2)(1+\eta)Q_2 \tag{D.27}$$

Enforcing a zero shear strain all over the element using Eq D.27, Eq D.26 and Eq D.7 the following equation results:

$$(1/4)(1/a)(1+\eta)(1+\xi)(2-\xi) - (1/8)(1/a)(1+\eta)(1+\xi)^2 + (1/c)(1-\xi^2)\left[Q_2+(\partial Q_2/\partial\eta)(1+\eta)\right] = 0 \tag{D.28}$$

For $\eta=-1$ the first, second and fourth terms of the above equation become zero. Therefore, the third term must also become zero for the same value of η i.e:

$$Q_2 = D(1+\eta) \tag{D.29}$$

Substituting for Q_2 from Eq D.29 into Eq D.28 solving for **D** the above equation gives:

$$D = -(3/16)(c/a)$$

Substituting for **D** from the above into Eq D.29 and also substituting for Q_2 from Eq D.29 into Eq D.27, leads to the shape function for horizontal displacement of node 3 as follows:

$$N_{uY3} = -(3/16)(c/a)(1+\eta)^2(1-\xi^2)$$

The shape functions for vertical displacement of the other 3 nodes can be derived by the same procedure as used for node 3. This allows all these shape functions to be written in only two general expressions as follows:

$$N_{uYi} = -\xi_i \eta_i (3/16) \gamma (1-\xi^2)(1+\eta_i \eta)^2 \tag{D.30}$$

$$N_{vYi} = (1/8)(1+\xi_i \xi)^2 (1+\eta_i \eta)(2-\xi_i \xi) \tag{D.31}$$

where γ is the aspect ratio of the beam given by Eq D.19.

D.2.4 Proposed Shape Functions for Shear Deformation

The shape functions for displacements of corner nodes of the element, illustrated in Fig D.2, only produce the horizontal and vertical strains. The equilibrating shear forces are, therefore, taken by, say, a set of frictional stresses acting on both side surfaces of the element preventing the element from taking the shear deformation shown in Fig D.1(c and d). Such a restraint may be attributed to an imaginary internal node. Displacement of such an internal node must be independent of the other nodal displacements involved in the element. i.e, displacement of the proposed fifth node must produce no displacement at the corners of the element. Such a condition can be met by combining the pure shear mode of deformation shown in Fig D.1(f) and the shear-free deformation of the modes shown in Fig D.2(b) and (c) imposed in the opposite direction. This combination is illustrated in Fig D.3 where $\mathbf{X_5}$, shown in Fig D.3(c), may be considered as the displacement of the imaginary internal node whose location is not a matter of importance. The displacement shape function of the above combination can be obtained by a superimposition as given below:

$$N_{uX5} = N_{u(a)} - (N_{uX2}+N_{uX3}) \qquad (D.32)$$

$$N_{vX5} = N_{v(a)} - (N_{vX2}+N_{vX3}) \qquad (D.33)$$

where $N_{u(a)}$ and $N_{v(b)}$ denote the horizontal and vertical displacement shape functions, respectively, of the pure shear deformation shown in Fig D.3(a) or Fig D.1(f). These are derived as follows:

For $\eta=-1$, $N_{u(a)}$ must become zero. Hence,

$$N_{u(a)} = (1+\eta)Q_3 \qquad (D.34)$$

where Q_3 is a function of η only since variation of ξ does not affect the horizontal displacement of the point in question. Since the strain variation across the beam is parabolic, shear strain at $\eta=\pm1$ is zero. Hence,

for $\eta=\pm1$:

$$\gamma_{xy} = \partial N_{u(a)}/\partial y = 0$$

i.e:

$$\gamma_{xy} = (1/c)\left[Q_3 + (1+\eta)(\partial Q_3/\partial\eta)\right] = 0 \qquad (D.35)$$

Since the second term of the above equation becomes zero for $\eta=-1$, its first term should also become zero for the same value of η. This follows that:

$$Q_3 = P_3(1+\eta) \qquad (D.36)$$

where P_3 is a linear function of η because γ_{xy} is a parabolic function of η. Substituting for Q from Eq D.36 into Eq D.35 and simplifying leads to:

$$(1+\eta)(2P_3) + (1+\eta)^2(\partial P_3/\partial\eta) = 0 \quad (\text{for } \eta=\pm1)$$

Allowing for $\eta=+1$ gives:

$$P_3 + (\partial P_3/\partial\eta) = 0 \tag{D.37}$$

Setting:

$$P_3 = A\eta + B \tag{D.38}$$

and substituting for P_3 from Eq D.38 into Eq D.37 and solving for **B** gives:

$$B = -2A$$

Substituting for value of **B** from the above equation and P_3 from Eq D.38 and Q_3 from Eq D.36 into Eq D.34 leads to:

$$N_{u(a)} = A(1+\eta)^2(\eta-2)$$

This function should equal to +1 for $\eta=+1$. This boundary condition requires that:

$$A = -1/4$$

Hence:

$$N_{u(a)} = (1/4)(1+\eta)^2(2-\eta) \tag{D.39}$$

The shape function for the vertical displacement, **u**, is simply determined as:

$$N_{v(a)} = 0 \tag{D.40}$$

Notice that the standard finite element formulation (vide Eq 3.11) requires that the external work done by the forces applied to the nodal points is equal to the total strain energy absorbed by the element. Since the proposed shear deformation of Eq D.39 resulted from a set of frictional forces acting over the area of element, calculation of the external energy as a direct product of the imaginary nodal displacement, $\mathbf{X_5}$, and the corresponding nodal force, $\mathbf{F_{X5}}$, is not applicable. The external energy (due to such shearing deformation) may, however, be calculated as follows:

$$\mathbf{W} = \int_{\mathbf{A}} \mathbf{qudA}$$

Where $\mathbf{q}$ denotes the function of the surface frictional stresses as shown in Figs D.1(f) and D.3(a) and $\mathbf{u}$ is the horizontal displacement function of the element induced by these surface stresses given by Eq D.39. Examination of the beam element showed that in order to avoid such an integration, Eq D.39 may be adjusted by simply dividing it by 1.2. This adjustment is an exact necessary and sufficient allowance for the effect of the above integral for beam elements of any material and geometry. Therefore equation D.39 becomes:

$$N_{u(a)} = (1/4.8)(1+\eta)^2(2-\eta) \qquad \text{(D.41)}$$

Now the shearing displacement shape functions can be derived from Eq D.32 and Eq D.33 using Eqs D.41, D.40, D.17, and Eq D.18 to give:

$$N_{uX5} = (1/24)(-5\eta^3-18\eta\xi^2+21\eta-2) \qquad \text{(D.42)}$$

$$N_{vX5} = -(1/4)(1/\gamma)\xi(1-\xi^2) \qquad \text{(D.43)}$$

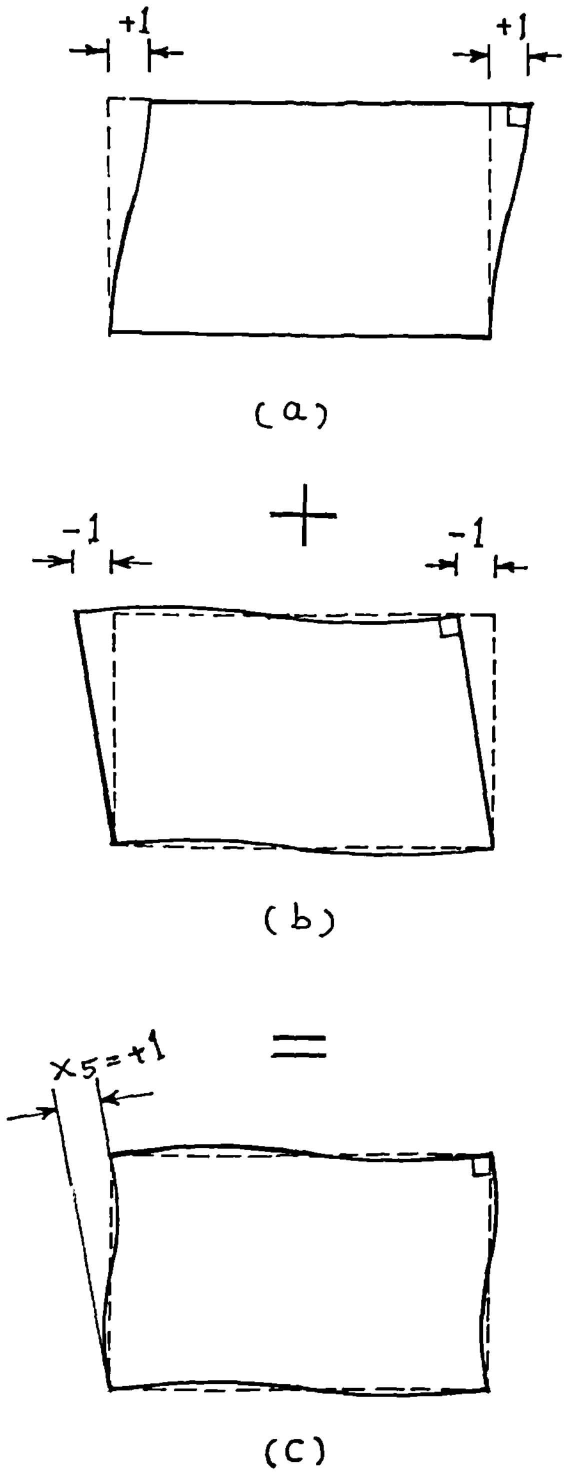

Figure D.3 Deformation of The Proposed Beam Flement Due to Displacement of The Proposed Fictitous 5th Node (a)pure shear, (b)shear-free bending and (c)combination of a and b as the 5th node displacement

D.2.5 Proposed Shape Function for Relative Displacement of the Centre Line of the Beam

In addition to the deformation discussed in Sections D.2.2 to D.2.4, when the beam segment is subjected to bending, another deformation mode is expected to occur as shown in Fig D.1(e). This mode consists of displacement of the centre line of the beam relative to its top and bottom sides as a result of the effect of the Poisson's ratio and the bending stress diagram across the beam. Such deformation can be controlled by two more degrees of freedom operating at the remote ends and immediately inside the element as shown in Fig. D.4. Since the bending stress is linearly distributed across the beam, the strain diagram resulting from such stresses may also be taken as linear as shown in Fig D.4(a) and (b). Consequently, the vertical displacement function must be parabolic because it is the integral of the vertical strain. The shape function for the left node (node 5) may, therefore, be expressed as:

$$N_{vy5} = (1-\xi)P$$

where $P(\eta)$ is a parabolic function of η. The factor $(1-\xi)$ permits this function to take the value of zero at the other end of the element. At the left hand side of the element, the value of the function must also become zero for $\eta=\pm 1$ and it must become unity for $\eta=0$. These require that the above shape function to be expressed as:

$$N_{vy5} = (1/2)(1-\xi)(1-\eta^2) \qquad \text{(D.44)}$$

Using the same procedure, the shape function for the vertical displacement of node 6 results in:

$$N_{vY6} = (1/2)(1+\xi)(1-\eta^2) \tag{D.45}$$

Since the vertical displacements of the fictitious nodes, Y_5 and Y_6, produce no horizontal displacement, therefore:

$$N_{uY5} = 0 \quad \text{and} \quad N_{uY6} = 0 \tag{D.46}$$

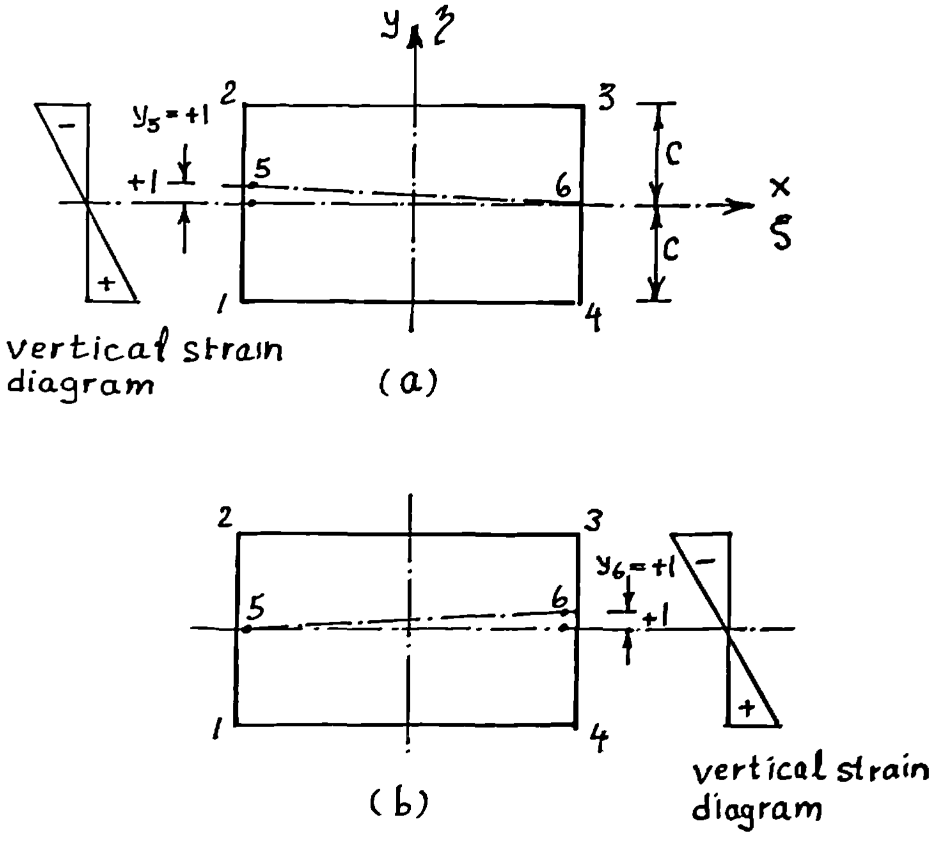

Figure D.4 Displacement of Centre Line of a Beam Due to Effect of the Poisson's Ratio; (a) left end moment, node 5, and (b) right end moment, node 6

D.2.6 The Proposed Beam Element Stiffness Matrix

The shape functions of the proposed beam element given in Sections D.2.2 to D.2.5 can be packed into Eq 3.5 to form **N** matrix. The **B** matrix of the element can then be generated from Eq 3.7. This matrix can be used in Eq 3.11 to form the element **K** matrix. Notice that the eleventh degree of freedom of the element, $\mathbf{X_6}$, is redundant and must be set restrained so that singularity of the stiffness matrix is prevented. The non-zero terms of the 3X12 [B] matrix are listed for the principal axis of the element as follows:

$$B_{1,1} = +(1/4)(1/a)(\eta-1-3\xi\eta)$$
$$B_{1,2} = +(3/8)(c/a^2)\xi(1-\eta)^2$$
$$B_{1,3} = -B_{1,1} - (1/2)(1/a)$$
$$B_{1,4} = -(3/8)(c/a^2)\xi(1+\eta)^2$$
$$B_{1,5} = -B_{1,1} + (1/2)(1/a)\eta$$
$$B_{1,6} = -B_{1,4}$$
$$B_{1,7} = -B_{1,5} + (1/2)(1/a)$$
$$B_{1,8} = -B_{1,2}$$
$$B_{1,9} = -(3/2)(1/a)\xi\eta$$
$$B_{2,2} = -(1/8)(1/c)(1-\xi)^2(2+\xi)$$
$$B_{2,4} = -B_{2,2}$$
$$B_{2,6} = +(1/8)(1/c)(1+\xi)^2(2-\xi)$$
$$B_{2,8} = -B_{2,6}$$
$$B_{2,10} = -(1/c)\eta(1-\xi)$$
$$B_{2,12} = -(1/c)\eta(1+\xi)$$
$$B_{3,9} = +(5/8)(1/c)(1-\eta^2)$$
$$B_{3,10} = -(1/2)(1/a)(1-\eta^2)$$
$$B_{3,12} = +(1/2)(1/a)(1-\eta^2)$$

APPENDIX E

Comparison Tables

This appendix deals with the comparison programme discussed in Chapters 6 and 7. Tables E.1 to E.12 list the complete results for all the marked stations and for all the frames analysed. The following symbols and abbreviations have relation to frame forces:

TB and BB	denote the top and bottom beams respectively.
LC and RC	designate left and right columns respectively
e	is the distance from the point of maximum moment to the loaded corner.
M2	refers to the maximum moment within the span of the member.
M3	denotes the moment at the point of frame-infill separation.

The following symbols and abbreviations have relation to the stresses and strains in the loaded corners and also in the central area of the infill:

σ_1 and σ_2	denote the most compressive and tensile principal stresses at the designated points respectively.
R_s and R_e	denote the ratio of stress to strength and also the ratio of strain to strain

corresponding to peak stress respectively.

C and R — appearing next to **Re**, designate whether the infill has cracked or crushed respectively.

TC and BC — denote the outer most sampling points at the top and bottom loaded corners respectively.

TM and BM — denote the sampling points with the highest stress in the top and bottom loaded corners respectively.

CM — denotes the point at the centre of the infill

The following symbols and abbreviations have relation to the forces at the frame-infill interfaces in contact:

a — denotes the length of contact. Ratios $\mathbf{a/l_1}$ and $\mathbf{a/h_1}$ denote the ratio of the length of contact to the length of the corresponding frame members.

b — designates the distance of the centroid of the normal forces, acting at the interface in question, for the loaded corner of the infill.

c — denotes the length over which the infill has separated measured from the loaded corner of the infill.

C and **F** — denote the total normal and shear forces, respectively, transferred from frame to the infill through the contact surface of the frame member under consideration.

The stations specified as; working, crack, peak, post peak and ultimate in the first column of Tables E.1 to E.12, correspond to the stations 1 to 5 shown on the corresponding load deflection diagrams, Figs 6.3 to 6.7.

Tables E.13 to E.39 list the results of the analysis of 27 finite element examples and tests of infilled frames computed by program "ANALIF" using the previously existing and also the proposed methods of analysis. The following abbreviations and symbols represent the methods and the finite element or test series data used in the comparison programme:

SC	The Stafford Smith and Carter method(13).
SR	The Stafford Smith and Riddington method(18).
M	The Mainstone empirical method(9).
W	The Wood plastic method[20].
W*	The Wood method using the penalty factor proposed by Ma[96].
L	The Liauw et al plastic method[25].
P	The author's proposed method
FE	The finite element examples, comparison Tables E.13 to E.21.
A	The test carried out by Saneinejad[29], comparison Tables E.22 to E.30.
M	The test carried out in the Building Research Station reported by Mainstone[9], comparison Tables E.31 to E.34.
SS	The test carried out by Stafford Smith[12], comparison Tables E.,35 to E.39.

Table E.1 F.E Analysis of Infilled Frame 'WMUR2' under Horizontal Forces Compared with Available Methods (* See text for symbol)

F.E ANALYSIS

Beginning of frame plasticity: Hp = 790.0 KN, Δp = 6.27 MM

At infill Cracking: Ht = N.A (Not cracked)

At Peak Load: Hc = 833.0 KN, Δc = 7.57 MM

On Plastic Plateau: Hu = 439.0 KN

INTERFACE: Gh = 0, σtb = .05, Kn = 100, μ = .64; Gv = 0 mm, σSb = .07 N/mm2, Ks = 50 KN/mm3, Ksru = .05 KN/mm3

STEEL FRAME: E = 200 KN/mm2, FY = 245 N/mm2, Kf = 2.3967 KN/mm, Hou = 102.3 KN

FRAME MEMBERS	A	I	Me	Mp	d	tw*
UB 254x146x31	71.99	5852	114	142	251.5	20
UC 152X152X23	62.4	1768	56.84	72.37	152.4	30

UNIFORM INFILL: Size: 4734X2709X140 mm, l/h = 1.75, σt = 1.5, σc = 11.3 N/mm2, εc = .00175, E = 18.46 KN/mm2

Stations and LOADS (H KN, Δ mm)	*	a/l' a/h'	b/l' b/h'	c/l' c/h'	C KN	F KN	N1 KN	N2 KN	e/l' e/h'	S1 KN	S2 KN	M1 KN.M	M2 KN.M	M3 KN.M	M4 KN.M
WORKING	BB	0.278	0.055	N.A	-232.74	132.91	-135.69	-2.78	1.000	233.32	0.58	-44.44	2.08	0.10	2.08
H = 472	TB	0.278	0.055	N.A	-232.67	132.90	-135.68	-2.78	1.000	233.25	0.58	44.45	-2.08	-0.10	-2.08
Δ = 2.45	LC	0.088	0.033	N.A	-335.28	64.26	1058.74	1123.00	0.088	332.97	-2.31	19.63	-5.29	-5.29	0.40
	RC	0.088	0.033	N.A	-335.26	64.18	-52.96	11.22	0.088	332.95	-2.31	-19.63	5.29	5.30	-0.41
CRACK (NA)															
PEAK LOAD	BB	0.424	0.076	N.A	-397.94	254.29	-268.36	-14.07	1.000	400.22	2.28	-113.78	7.29	1.08	7.29
H = 833	TB	0.424	0.075	N.A	-398.08	254.36	-268.46	-14.10	1.000	400.36	2.28	113.75	-7.29	-1.07	-7.29
Δ = 7.57	LC	0.126	0.067	0.004	-568.21	141.32	-104.42	36.90	0.134	560.18	-8.03	73.24	-16.83	-17.12	1.90
	RC	0.126	0.067	0.004	-568.33	141.48	-104.56	36.92	0.134	560.29	-8.04	-73.25	16.85	17.13	-1.91
POST PEAK	BB	0.288	0.113	0.048	-261.81	167.56	-190.40	-22.84	1.000	265.67	3.86	-125.96	11.43	-1.58	11.43
H = 623	TB	0.308	0.086	N.A	-312.12	121.09	-120.09	0.99	1.000	314.57	2.45	115.63	-7.53	0.49	-7.53
Δ = 10.49	LC	0.140	0.074	0.004	-509.53	106.30	-63.10	43.20	0.138	503.29	-6.24	76.30	-15.75	-15.88	-1.35
	RC	0.202	0.127	0.047	-454.65	189.63	-112.00	77.63	0.174	431.86	-22.79	-91.76	39.58	38.10	-11.15
ULTIMATE	BB	0.188	0.126	0.078	-180.09	111.64	-133.59	-21.95	1.000	189.13	9.04	-111.09	25.01	-9.74	25.01
H = 439	TB	0.292	0.093	N.A	-246.05	32.84	-0.34	32.50	1.000	247.88	1.83	107.43	-5.67	0.45	-5.67
Δ = 14.78	LC	0.100	0.066	0.019	-435.81	45.80	-17.89	27.91	1.000	438.31	2.50	71.19	-10.16	-4.07	-10.16
	RC	0.296	0.209	0.159	-362.20	177.74	-64.44	113.30	0.277	318.18	-44.02	-93.83	66.15	62.10	-21.85

Stations	*	σ1 N/mm2	σ2 N/mm2	Rs	Re	*
WORKING	BC	-1.82	-12.21	0.971	0.724	
	BM	-1.82	-12.21	0.971	0.724	
	TC	-1.82	-12.21	0.971	0.724	
	TM	-1.82	-12.21	0.971	0.724	
	CM	0.53	-1.99	0.417	0.226	
PEAK LOAD	BC	-3.92	-8.78	0.625	2.550	
	BM	-3.84	-13.33	0.992	0.834	
	TC	-3.92	-8.78	0.625	2.550	
	TM	-3.84	-13.33	0.992	0.834	
	CM	1.00	-3.30	0.758	0.479	
POST PEAK	BC	0.00	0.00	0.000	0.000	R
	BM	-4.39	-13.59	0.999	1.078	
	TC	-2.62	-5.64	0.401	3.207	
	TM	0.80	-8.10	0.946	0.846	
	CM	0.92	-2.53	0.680	0.441	
ULTIMATE	BC	0.00	0.00	0.000	0.000	R
	BM	1.22	-3.74	0.913	0.819	
	TC	-2.14	-5.13	0.368	3.153	
	TM	-3.44	-11.29	0.835	1.057	
	CM	0.85	-1.80	0.605	0.401	

Table E.2 F.E Analysis of Infilled Frame 'MMUR2' under Horizontal Forces Compared with Available Methods (* See text for symbols)

F.E ANALYSIS

Beginning of frame plasticity:	At infill Cracking:	At Peak Load:	On Plastic Plateau:
H_p = 949.0 KN Δ_p = 5.62 MM	H_t= 1098.0 KN Δ_t= 7.92 MM	H_c= 991.9 KN (1098.0) Δ_c= 9.82 MM (7.99)	H_u= 700.0 KN

INTERFACE: G_n = 0, σ_{tb}= .05, Kn = 100, μ = .64; G_v = 0 mm, σ_{Sb}= .07 N/mm2, Ks = 50 KN/mm3, Ksru= .05 KN/mm3

STEEL FRAME: E = 200 KN/mm2, FY= 245 N/mm2, Kf = 5.417 KN/mm, Hou= 192.2 KN

FRAME MEMBERS:	A	I	Me	Mp	d	tw*
UB 254x146x31	71.99	5852	114	142	251.5	20
UC 254X254X73	151.1	13731	264.9	321	254	35

UNIFORM INFILL: Size: 4734X2709X140 mm l/h=1.75; σ_t = 1.5, σ_c = 11.3 N/mm2; ε_c = .00175, E = 18.46 KN/mm2

Stations and LOADS H KN Δ mm	*	a/l' a/h'	b/l' b/h'	c/l c/h	C KN	F KN	N1 KN	N2 KN	e/l' e/h'	S1 KN	S2 KN	M1 KN.M	M2 KN.M	M3 KN.M	M4 KN.M
WORKING	BB	0.247	0.058	N.A	-271.92	163.30	-162.46	0.84	1.000	273.93	2.01	-57.73	5.72	-1.44	5.72
H = 645.9	TB	0.247	0.058	N.A	-271.92	163.30	-162.46	0.84	1.000	273.93	2.01	57.73	-5.72	1.44	-5.72
Δ = 3.06	LC	0.151	0.055	N.A	-491.50	121.53	-109.41	12.12	0.150	483.27	-8.23	31.80	-21.81	-22.03	-3.11
	RC	0.151	0.055	N.A	-491.50	121.53	-109.41	12.12	0.150	483.27	-8.23	-31.80	21.81	22.03	3.11
CRACKING	BB	0.290	0.070	N.A	-497.19	317.78	-318.96	-1.18	1.000	502.24	5.05	-134.73	14.20	-2.78	14.20
H = 1090	TB	0.290	0.070	N.A	-497.19	317.78	-318.96	-1.18	1.000	502.24	5.05	134.73	-14.20	2.78	-14.20
Δ = 7.71	LC	0.187	0.094	N.A	-796.54	186.80	-144.80	42.00	0.173	769.54	-27.00	101.67	-64.90	-64.25	-4.79
	RC	0.187	0.094	N.A	-796.54	186.80	-144.80	42.00	0.173	769.54	-27.00	-101.67	64.90	64.25	4.79
PEAK LOAD	BB	0.402	0.093	N.A	-447.88	286.50	-269.96	16.54	0.343	446.53	-1.35	-145.84	13.25	12.89	9.06
H = 991.5	TB	0.402	0.093	N.A	-447.87	286.49	-269.95	16.54	0.343	446.52	-1.35	145.85	-13.25	-12.89	-9.06
Δ = 9.75	LC	0.335	0.103	N.A	-746.27	157.32	-141.92	15.40	0.288	721.28	-24.99	111.96	-54.39	-53.01	-8.01
	RC	0.335	0.103	N.A	-746.26	157.30	-141.89	15.41	0.290	722.26	-24.00	-114.63	52.57	51.23	8.01
POST PEAK	BB	0.410	0.101	N.A	-438.01	280.33	-257.45	22.88	0.343	436.25	-1.77	-155.79	15.00	14.45	9.51
H = 960.7	TB	0.410	0.101	N.A	-438.07	280.36	-257.48	22.88	0.343	436.30	-1.77	155.81	-15.00	-14.45	-9.51
Δ = 11.43	LC	0.334	0.122	0.002	-737.34	154.17	-133.87	20.30	0.294	703.04	-34.30	122.87	-71.99	-70.16	-8.27
	RC	0.334	0.122	0.002	-737.39	154.23	-133.93	20.30	0.294	703.09	-34.30	-122.80	72.00	70.15	8.27
ULTIMATE	BB	0.410	0.115	N.A	-361.56	186.43	-123.31	63.12	0.341	358.20	-3.35	-149.86	18.55	17.52	8.15
H = 710.0	TB	0.156	0.139	0.078	-309.02	182.19	-159.27	22.92	0.444	308.85	-0.18	161.85	-17.57	14.87	-17.11
Δ = 14.00	LC	0.364	0.220	0.083	-634.34	207.60	-112.45	95.15	0.319	550.34	-84.00	131.88	-148.35	-136.29	8.45
	RC	0.339	0.137	0.005	-617.19	75.32	-63.12	12.20	0.306	586.59	-30.60	-121.61	71.90	69.46	14.63

Stations	*	σ1 N/mm2	σ2 N/mm2	Rs	Re	*
WORKING	BC	-2.76	-12.74	0.977	0.746	
	BM	-2.76	-12.74	0.977	0.746	
	TC	-2.76	-12.74	0.977	0.746	
	TM	-2.76	-12.74	0.977	0.746	
	CM	0.68	-2.54	0.531	0.297	
CRACKING	BC	-4.77	-11.16	0.798	2.010	
	BM	-5.27	-13.72	0.990	1.200	
	TC	-4.77	-11.16	0.798	2.010	
	TM	-5.27	-13.72	0.990	1.200	
	CM	1.34	-3.81	0.993	0.936	
PEAK LOAD	BC	-4.14	-9.62	0.687	2.350	
	BM	-4.52	-12.92	0.942	1.450	
	TC	-4.14	-9.62	0.687	2.350	
	TM	-4.33	-13.22	0.970	1.351	
	CM	0.00	-5.08	0.450	0.473	C
POST PEAK	BC	-3.15	-6.57	0.466	3.143	
	BM	-4.26	-13.07	0.960	1.408	
	TC	-3.15	-6.57	0.465	3.144	
	TM	-4.26	-13.08	0.960	1.408	
	CM	0.00	-4.96	0.439	0.468	C
ULTIMATE	BC	-2.19	-4.16	0.293	3.943	
	BM	-0.40	-11.89	0.871	1.340	
	TC	0.00	0.00	0.000	0.000	R
	TM	-2.90	-9.27	0.683	1.415	
	CM	0.00	-4.71	0.417	0.456	C

Table E.3 F.E Analysis of Infilled Frame 'SMUR2' under Horizontal Forces Compared with Available Methods (* See text for symbols)

F.E ANALYSIS

Beginning of frame plasticity: H_p = 1105.0 KN, Δ_p = 6.34 MM

At infill Cracking: H_t = 1101 KN, Δ_t = 6.84 MM

At Peak Load: H_c = 1148 KN, Δ_c = 10.95 MM

On Plastic Plateau: H_u = 0.0 KN

STATIONS and LOADS

INTERFACE: G_h = 0, σ_{tb}= 0.05, K_n = 100, μ = 0.64; G_v = 0 mm, σ_{Sb}= 0.07 N/mm2, K_s = 50 KN/mm3, K_{sru}= 0.05 KN/mm3

STEEL FRAME: E = 200 KN/mm2, FY= 245 N/mm2, Kf = 6.74 KN/mm, Hou= 199.7 KN

FRAME MEMBERS:	A	I	Me	Mp	d	tw*
UB 254x146x31	71.99	5852	114	142	251.5	20
UC 356X368X177	305.4	63630	846.6	999.4	368.3	40

UNIFORM INFILL: Size: 4734X2709X140 mm, l/h=1.75; σ_t = 1.5, σ_c = 11.3 N/mm2; ε_c = .00175, E = 18.46 KN/mm2

H KN Δ mm	*	a/l' a/h'	b/l b/h	c/l' c/h'	C KN	F KN	N1 KN	N2 KN	e/l' e/h'	S1 KN	S2 KN	M1 KN.M	M2 KN.M	M3 KN.M	M4 KN.M
WORKING	BB	0.196	0.054	N.A	-242.22	143.02	-126.25	16.77	1.000	271.84	29.62	-175.71	8.00	-104.77	8.00
H = 686.0	TB	0.196	0.054	N.A	-242.22	143.02	-126.25	16.77	1.000	271.84	29.62	175.71	-8.00	104.77	-8.00
Δ = 2.88	LC	0.184	0.071	N.A	-577.30	151.73	-152.86	-1.13	0.170	559.40	-17.90	24.27	-50.01	-49.73	-10.16
	RC	0.184	0.071	N.A	-577.30	151.73	-152.86	-1.13	0.170	559.40	-17.90	-24.27	50.01	49.73	10.16
CRACKING	BB	0.177	0.056	N.A	-502.32	290.89	-250.29	40.60	1.000	509.52	7.20	-111.11	19.42	-8.64	19.42
H = 1101	TB	0.177	0.056	N.A	-502.31	290.85	-250.25	40.60	1.000	509.51	7.20	111.12	-19.42	8.64	-19.42
Δ = 6.84	LC	0.281	0.108	N.A	-893.84	127.70	-129.54	-1.84	0.254	851.13	-42.71	97.93	-107.63	-107.55	-24.40
	RC	0.281	0.108	N.A	-893.69	127.54	-129.53	-1.99	0.254	851.08	-42.61	-97.93	107.37	107.42	24.46
PEAK LOAD	BB	0.329	0.086	N.A	-469.40	299.84	-217.27	82.57	1.000	472.17	2.77	-147.81	19.37	10.55	19.37
H = 1148	TB	0.327	0.088	N.A	-457.20	291.90	-213.96	77.94	1.000	459.76	2.57	147.44	-19.35	-11.18	-19.35
Δ = 10.95	LC	0.472	0.151	N.A	-1021.68	212.32	-206.64	5.68	0.333	934.38	-87.30	114.58	-173.99	-152.87	-28.01
	RC	0.471	0.152	N.A	-1018.73	207.94	-194.19	13.75	0.331	931.05	-87.68	-117.65	173.58	150.81	25.25
POST PEAK	BB	0.323	0.090	N.A	-453.51	288.97	-196.15	92.82	1.000	456.50	3.00	-151.16	20.90	11.30	20.90
H = 1140	TB	0.298	0.097	N.A	-422.11	268.02	-184.58	83.44	1.000	424.65	2.54	150.70	-20.70	-12.26	-20.70
Δ = 11.93	LC	0.459	0.158	N.A	-1054.08	244.45	-236.93	7.52	0.335	955.28	-98.80	108.63	-197.09	-175.09	-30.32
	RC	0.459	0.158	N.A	-1041.10	225.11	-205.08	20.03	0.329	943.97	-97.13	-116.51	193.13	168.04	25.66

Station	*	σ1 N/mm2	σ2 N/mm2	Rs	Re	*
WORKING	BC	-2.40	-12.27	0.951	0.649	
	BM	-2.40	-12.27	0.951	0.649	
	TC	-2.40	-12.27	0.951	0.649	
	TM	-2.40	-12.27	0.951	0.649	
	CM	0.68	-2.66	0.534	0.301	
CRACKING	BC	-6.71	-13.43	0.950	1.447	
	BM	-0.94	-12.00	1.000	0.974	
	TC	-6.71	-13.43	0.950	1.447	
	TM	-0.94	-12.00	1.000	0.974	
	CM	1.36	-3.64	0.997	0.950	
PEAK LOAD	BC	-4.34	-10.22	0.731	2.212	
	BM	-2.89	-13.05	0.999	1.063	
	TC	-4.39	-10.39	0.743	2.172	
	TM	-1.75	-12.39	0.989	1.203	
	CM	0.00	-4.61	0.400	0.408	C
POST PEAK	BC	-3.84	-931.00	0.668	2.410	
	BM	-3.72	-13.30	0.993	1.168	
	TC	-3.90	-9.62	0.691	2.332	
	TM	-1.18	-11.77	0.965	1.374	
	CM	0.00	-4.30	0.390	0.336	C

Table E.4 F.E Analysis of Infilled Frame 'SWUR2' under Horizontal Forces Compared with Available Methods (* See text for symbols)

F.E ANALYSIS

Beginning of frame plasticity:
Hp = 952.0 KN
Δp = 5.49 MM

At infill Cracking:
Ht = 1038.0 KN
Δt = 8.32 MM

At Peak Load:
Hc = 928.0 KN (1038.0)
Δc = 9.45 MM (8.32)

On Plastic Plateau:
Hu = 0.0 KN

STATIONS and LOADS

INTERFACE: Gh = 0, σtb= .05, Kn = 100, μ = .64; Gv = 0 mm, σSb= .07 N/mm2, Ks = 50 KN/mm3, Ksru= .05 KN/mm3

STEEL FRAME: E = 200 KN/mm2, FY= 245 N/mm2, Kf = 2.35 KN/mm, Hou= 88.10 KN

FRAME MEMBERS:	A	I	Me	Mp	d	tw*
UB 178x102x19	45.2	1797	49.52	62.35	177.8	18
UC 356X368X177	305.4	63630	846.6	999.4	368.3	40

UNIFORM INFILL: Size: 4734X2709X140 mm l/h=1.75, σt = 1.5, σc = 11.3 N/mm2, εc = .00175, E = 18.46 KN/mm2

H KN Δ mm	*	a/l a/h	b/l' b/h'	c/l' c/h'	C KN	F KN	N1 KN	N2 KN	e/l' e/h'	S1 KN	S2 KN	M1 KN.M	M2 KN.M	M3 KN.M	M4 KN.M	*	σ1 N/mm2	σ2 N/mm2	Rs	Re	*
WORKING	BB	0.170	0.031	N.A	-189.96	105.92	-84.83	21.09	1.000	190.72	0.76	-19.87	2.22	-0.76	2.22	BC	-2.43	-12.29	0.952	0.652	
H = 610.0	TB	0.170	0.031	N.A	-189.96	105.92	-84.83	21.09	1.000	190.72	0.76	19.87	-2.22	0.76	-2.22	BM	-2.43	-12.29	0.952	0.652	
Δ = 2.60	LC	0.179	0.066	N.A	-544.25	153.42	-154.18	-0.76	0.164	523.16	-21.09	8.34	-51.19	-51.13	-4.24	TC	-2.43	-12.29	0.952	0.652	
	RC	0.179	0.066	N.A	-544.25	153.42	-154.18	-0.76	0.164	523.16	-21.09	-8.34	51.19	51.13	4.24	TM	-2.43	-12.29	0.952	0.652	
																CM	-2.39	0.58	0.463	0.253	
CRACKING	BB	0.112	0.041	N.A	-351.86	224.95	-168.71	56.24	1.000	353.68	1.82	-51.87	5.43	-2.24	5.43	BC	-5.22	-12.42	0.889	1.707	
H = 1012	TB	0.112	0.041	N.A	-351.86	224.95	-168.71	56.24	1.000	353.69	1.82	51.87	-5.43	2.24	-5.43	BM	-4.11	-13.46	0.996	1.134	
Δ = 6.46	LC	0.199	0.101	N.A	-900.08	217.97	-219.08	-1.11	0.171	843.48	-56.60	42.02	-136.57	-133.45	-10.57	TC	-5.22	-12.42	0.889	1.707	
	RC	0.199	0.101	N.A	-900.07	217.97	-219.09	-1.11	0.171	843.47	-56.60	-42.01	136.57	133.45	10.57	TM	-4.11	-13.46	0.996	1.134	
																CM	1.09	-3.91	0.841	0.560	
PEAK LOAD	BB	0.176	0.054	N.A	-335.13	197.40	-114.37	83.03	1.000	335.90	0.77	-66.49	5.29	2.30	5.29	BC	-3.69	-9.11	0.654	2.455	
H = 926.0	TB	0.176	0.054	N.A	-335.12	197.42	-114.39	83.03	1.000	335.88	0.77	66.50	-5.29	-2.30	-5.29	BM	-2.33	-12.63	0.985	1.245	
Δ = 9.31	LC	0.489	0.139	N.A	-899.34	194.30	-188.31	5.99	0.310	812.02	-87.32	56.15	-163.88	-131.86	-11.01	TC	-3.69	-9.11	0.654	2.455	
	RC	0.489	0.139	N.A	-899.35	194.27	-188.28	5.99	0.310	812.03	-87.32	-56.15	163.88	131.86	11.01	TM	-2.33	-12.63	0.985	1.245	
																CM	0.00	-5.56	0.492	0.492	C
POST PEAK	BB	0.166	0.064	N.A	-304.54	194.91	-87.41	107.50	1.000	304.67	0.13	-71.06	4.88	4.38	4.88	BC	-2.79	-6.04	0.429	3.306	
H = 889.0	TB	0.166	0.064	N.A	-304.55	194.91	-87.41	107.50	1.000	304.67	0.13	71.07	-4.88	-4.38	-4.88	BM	-2.66	-11.57	0.880	1.729	
Δ = 10.93	LC	0.540	0.162	N.A	-909.24	198.31	-198.43	-0.13	0.309	801.74	-107.50	84.82	-186.27	-119.46	14.46	TC	-2.79	-6.04	0.429	3.306	
	RC	0.540	0.162	N.A	-909.24	198.32	-198.44	-0.13	0.309	801.74	-107.50	-84.88	186.28	119.58	-14.46	TM	-2.66	-11.57	0.880	1.729	
																CM	0.00	-5.74	0.508	0.500	C
ULTIMATE	BB	0.172	0.083	N.A	-229.49	138.29	-5.29	133.00	0.178	229.35	-0.14	-72.35	5.67	5.67	5.12	BC	0.00	0.00	0.000	0.000	R
H = 734.0	TB	0.174	0.085	N.A	-234.98	142.90	-5.90	137.00	0.178	234.45	-0.53	74.39	-6.55	-6.56	-4.49	BM	-3.59	-9.79	0.710	2.278	
Δ = 12.48	LC	0.426	0.199	0.078	-861.25	181.41	-181.27	0.14	0.318	728.25	-133.00	52.84	-266.62	-223.88	-16.92	TC	0.00	0.00	0.000	0.000	R
	RC	0.435	0.201	0.078	-866.32	186.90	-186.36	0.53	0.318	729.32	-137.00	-49.80	273.94	226.13	16.57	TM	-2.79	-9.42	0.699	2.233	
																CM	0.00	-5.39	0.477	0.484	C

Table E.5 F.E Analysis of Infilled Frame 'WWUS2' under Horizontal Forces Compared with Available Methods (See text for symbols)

F.E ANALYSIS

Beginning of frame plasticity:	At infill Cracking:	At Peak Load:	On Plastic Plateau:
Hp = 635.0 KN Δp = 4.94 MM	Ht = 679.0 KN Δt = 5.95 MM	Hc = 635.0 KN (679.0 KN) Δc = 8.17 MM (5.95 MN)	Hu = 0.0 KN

STATIONS and LOADS	INTERFACE	STEEL FRAME	UNIFORM INFILL
	Gh = 0, Gv = 0 mm σtb= .05, σSb= .07 N/mm2 Kn = 100, Ks = 50 KN/mm3 μ = .64, Ksru= .05 KN/mm3	E = 200 KN/mm2 FY = 245 N/mm2 Kf = 1.9 KN/mm Hou= 86.8 KN FRAME MEMBERS: A, I, Me, Mp, d, tw* UB 178x102x19: 45.2, 1797, 49.52, 62.35, 177.8, 18 UC 152X152X23: 62.4, 1768, 56.84, 72.37, 152.4, 30	Size: 2709X2709X140 mm l/h=1.00 σt = 1.5, σc = 11.3 N/mm2 εc = .00175, E = 18.46 KN/mm2

H KN Δ mm	*	a/l' a/h'	b/l' b/h'	c/l' c/h'	C KN	F KN	N1 KN	N2 KN	e/l' e/h'	S1 KN	S2 KN	M1 KN.M	M2 KN.M	M3 KN.M	M4 KN.M	*	σ1 N/mm2	σ2 N/mm2	Rs	Re	*
WORKING	BB	0.166	0.037	N.A	-207.34	73.77	-73.78	-0.01	1.000	207.49	0.14	-13.84	0.68	0.35	0.68	BC	-2.93	-11.01	0.827	0.419	
H = 280.0	TB	0.166	0.037	N.A	-207.34	73.77	-73.78	-0.01	1.000	207.49	0.14	13.84	-0.68	-0.35	-0.68	BM	-2.93	-11.01	0.827	0.419	
Δ = 1.49	LC	0.086	0.032	N.A	-205.70	74.62	-74.76	-0.14	1.000	205.72	0.01	11.34	-0.69	-0.66	-0.69	TC	-2.93	-11.01	0.827	0.419	
	RC	0.086	0.032	N.A	-205.70	74.62	-74.76	-0.14	1.000	205.72	0.01	-11.34	0.69	0.66	0.69	TM	-2.93	-11.01	0.827	0.419	
																CM	0.54	-1.69	0.410	0.222	
CRACKING	BB	0.161	0.068	N.A	-429.68	259.94	-258.68	1.26	0.161	428.96	-0.72	-54.32	1.66	1.65	0.00	BC	-5.12	-11.70	0.834	1.892	
H = 679.0	TB	0.161	0.068	N.A	-429.68	259.94	-258.68	1.26	0.161	428.96	-0.72	54.32	-1.66	-1.65	-0.00	BM	-5.47	-13.84	0.997	1.075	
Δ = 5.95	LC	0.145	0.064	N.A	-420.76	256.36	-256.36	0.00	0.161	420.76	-0.00	53.13	-0.00	-0.00	-0.00	TC	-5.12	-11.70	0.834	1.892	
	RC	0.145	0.064	N.A	-420.76	256.36	-256.36	0.00	0.161	420.76	-0.00	-53.13	0.00	0.00	0.00	TM	-5.47	-13.84	0.997	1.075	
																CM	1.36	-3.58	1.000	0.980	
PEAK LOAD	BB	0.281	0.097	N.A	-419.75	258.98	-230.71	28.27	0.504	409.63	-10.12	-63.67	9.76	5.34	-3.66	BC	-3.63	-9.75	0.706	2.284	
H = 635.0	TB	0.496	0.098	N.A	-415.98	254.82	-227.50	27.32	0.496	406.13	-9.85	64.82	-9.79	-12.32	3.24	BM	-1.73	-12.39	0.990	1.191	
Δ = 8.17	LC	0.162	0.085	N.A	-414.20	247.96	-234.51	13.45	0.333	407.46	-6.74	59.54	-10.83	-4.89	1.14	TC	-3.43	-9.33	0.676	2.383	
	RC	0.162	0.084	N.A	-410.56	245.74	-231.02	14.72	0.333	404.29	-6.27	-58.93	10.19	4.11	-0.93	TM	-2.54	-12.20	0.940	1.506	
																CM	0.00	-6.92	0.610	0.540	C

Table E.6 F.E Analysis of Infilled Frame 'MWUS2' under Horizontal Forces Compared with Available Methods (See text for symbols)

F.E ANALYSIS

Beginning of frame plasticity:	At infill Cracking:	At Peak Load:	On Plastic Plateau:
Hp = 684.0 KN Δp = 4.16 MM	Ht= 684.0 KN Δt= 4.16 MM	Hc= 747.0 KN Δc= 8.00 MM	Hu = 0.0 KN

STATIONS and LOADS	INTERFACE	STEEL FRAME	UNIFORM INFILL
	Gh = 0, Gv = 0 mm σtb= .05, σSb = .07 N/mm2 Kn = 100, Ks = 50 KN/mm3 μ = .64, Ksru = .05 KN/mm3	E = 200 KN/mm2 FY = 245 N/mm2 Kf = 3.57 KN/mm Hou= 90.0 KN FRAME MEMBERS: A I Me Mp d tw* UB 178x102x19 45.2 1797 49.52 62.35 177.8 18 UC 254X254X73 151.1 13731 264.9 321 254 35	Size: 2709X2709X140 mm l/h=1.00 σt = 1.5 σc = 11.3 N/mm2 εc = .00175 E = 18.46 KN/mm2

H KN / Δ mm	*	a/l' a/h'	b/l' b/h'	c/l' c/h'	C KN	F KN	N1 KN	N2 KN	e/l' e/h'	S1 KN	S2 KN	M1 KN.M	M2 KN.M	M3 KN.M	M4 KN.M
WORKING	BB	0.165	0.041	N.A	-253.64	97.96	-98.16	-0.20	1.000	254.51	0.87	-19.85	2.05	0.09	2.05
H = 387.0	TB	0.165	0.041	N.A	-253.64	97.96	-98.16	-0.20	1.000	254.51	0.87	19.85	-2.05	-0.09	-2.05
Δ = 1.84	LC	0.188	0.056	N.A	-288.23	121.29	-122.16	-0.87	1.000	288.23	0.00	28.14	-0.00	0.00	-0.00
	RC	0.188	0.056	N.A	-288.23	121.29	-122.16	-0.87	1.000	288.23	0.00	-28.14	0.00	-0.00	0.00
CRACKING	BB	0.163	0.059	N.A	-400.14	224.01	-224.04	-0.03	1.000	401.80	1.66	-43.67	4.43	0.67	4.43
H = 684.0	TB	0.163	0.059	N.A	-400.14	224.01	-224.04	-0.03	1.000	401.80	1.66	43.67	-4.43	-0.67	-4.43
Δ = 4.16	LC	0.184	0.074	N.A	-460.20	263.20	-264.86	-1.66	1.000	460.23	0.03	58.43	-0.00	0.07	-0.00
	RC	0.184	0.074	N.A	-460.20	263.20	-264.86	-1.66	1.000	460.23	0.03	-58.43	0.00	-0.07	0.00
PEAK LOAD	BB	0.381	0.098	N.A	-419.74	267.74	-224.97	42.77	0.494	412.48	-7.26	-68.22	9.25	9.12	-0.36
H = 747.0	TB	0.381	0.098	N.A	-419.74	267.74	-224.97	42.77	0.494	412.48	-7.26	68.22	-9.25	-9.12	0.36
Δ = 8.00	LC	0.747	0.116	N.A	-540.42	317.73	-314.94	2.79	0.343	521.73	-18.69	78.49	-28.63	-12.82	-0.00
	RC	0.747	0.116	N.A	-540.43	317.73	-314.94	2.79	0.343	521.74	-18.69	-78.49	28.63	12.82	0.00
POST PEAK	BB	0.179	0.121	0.078	-315.03	184.91	-173.64	16.96	0.178	315.02	-8.95	-73.48	13.70	13.70	0.78
H = 523.0	TB	0.181	0.102	N.A	-353.57	183.41	-129.57	53.84	0.492	345.93	-7.64	61.49	-9.31	-8.32	0.81
Δ = 10.46	LC	0.186	0.119	N.A	-407.32	171.17	-164.10	8.81	0.538	393.91	-16.81	70.29	-19.20	-5.11	-1.17
	RC	0.322	0.207	0.078	-389.05	201.96	-194.99	6.97	0.399	349.88	-39.17	-82.38	63.66	64.42	3.80

H KN / Δ mm	*	σ1 N/mm2	σ2 N/mm2	Rs	Re	*
WORKING	BC	-3.28	-11.69	0.872	0.479	
H = 387.0	BM	-3.28	-11.69	0.872	0.479	
Δ = 1.84	TC	-3.28	-11.69	0.872	0.479	
	TM	-3.28	-11.69	0.872	0.479	
	CM	0.71	-2.44	0.548	0.307	
CRACKING	BC	-5.99	-13.95	0.997	1.081	
H = 684.0	BM	-5.99	-13.95	0.997	1.081	
Δ = 4.16	TC	-5.99	-13.95	0.997	1.081	
	TM	-5.99	-13.95	0.997	1.081	
	CM	1.36	-3.55	0.998	0.939	
PEAK LOAD	BC	-3.60	-9.44	0.682	2.367	
H = 747.0	BM	-1.96	-12.61	0.999	1.074	
Δ = 8.00	TC	-3.60	-9.44	0.682	2.367	
	TM	-1.96	-12.61	0.999	1.074	
	CM	0.00	-6.48	0.574	0.518	C
POST PEAK	BC	0.00	0.00	0.000	0.000	R
H = 523.0	BM	-4.09	-12.55	0.921	1.492	
Δ = 10.46	TC	-2.80	-5.72	0.405	2.930	
	TM	-3.67	-10.97	0.803	0.849	
	CM	0.00	-5.15	0.456	0.460	C

Table E.7 F.E Analysis of Infilled Frame 'SWUS2' under Horizontal Forces Compared with Available Methods (*See text for symbols)

F.E ANALYSIS

Beginning of frame plasticity:	At infill Cracking:	At Peak Load:	On Plastic Plateau:
Hp = 591.0 KN Δp = 4.21 MM	Ht = 714.0 KN Δt = 3.69 MM	Hc = 879.0 KN Δc = 7.92 MM	Hu = 480.0 KN

STATIONS and LOADS	INTERFACE	STEEL FRAME	UNIFORM INFILL
	Gh = 0 Gv = 0 mm σtb= .05 σSb= .07 N/mm2 Kn = 100 Ks = 50 KN/mm3 μ = .64 Ksru= .05 KN/mm3	E = 200 KN/mm2 FY= 245 N/mm2 Kf = 4.31 KN/mm Hou= 94.0 KN FRAME MEMBERS: A, I, Me, Mp, d, tw* UB 178x102x19: 45.2, 1797, 49.52, 62.35, 177.8, 18 UC 356X368X177: 305.4, 63630, 846.6, 999.4, 368.3, 40	Size: 2709X2709X140 mm 1/h=1.00 σt = 1.5 σc = 11.3 N/mm2 εc = .00175 E = 18.46 KN/mm2

H KN Δ mm	*	a/l' a/h'	b/l' b/h'	c/l' c/h'	C KN	F KN	N1 KN	N2 KN	e/l' e/h'	S1 KN	S2 KN	M1 KN.M	M2 KN.M	M3 KN.M	M4 KN.M	*	σ1 N/mm2	σ2 N/mm2	Rs	Re	*
WORKING	BB	0.166	0.040	N.A	-212.66	80.73	2646.27	2727.00	1.000	213.63	0.97	-16.19	2.09	-0.10	2.09	BC	-2.92	-10.48	0.783	0.369	
H = 365.0	TB	0.166	0.040	N.A	-212.66	80.73	2646.27	2727.00	1.000	213.63	0.97	16.19	-2.09	0.10	-2.09	BM	-2.92	-10.48	0.783	0.369	
Δ = 1.48	LC	0.332	0.074	N.A	-284.38	126.30	-127.27	-0.97	0.341	284.10	-0.27	30.55	-2.78	-2.79	-2.29	TC	-2.92	-10.48	0.783	0.369	
	RC	0.332	0.074	N.A	-284.38	126.30	-127.27	-0.97	0.341	284.10	-0.27	-30.55	2.78	2.79	2.29	TM	-2.92	-10.48	0.783	0.369	
																CM	0.64	-1.96	0.494	0.273	
CRACKING	BB	0.188	0.072	N.A	-298.17	144.55	-127.85	16.70	1.000	299.15	0.99	-43.63	4.04	1.86	4.04	BC	-4.44	-11.37	0.820	0.831	
H = 504.0	TB	0.188	0.072	N.A	-298.17	144.55	-127.85	16.70	1.000	299.15	0.99	43.63	-4.04	-1.86	-4.04	BM	-4.44	-11.37	0.820	0.831	
Δ = 3.78	LC	0.514	0.154	N.A	-354.97	94.56	-95.54	-0.99	0.458	338.27	-16.70	79.65	-28.30	-27.70	-5.70	TC	-4.44	-11.37	0.820	0.831	
	RC	0.514	0.154	N.A	-354.97	94.56	-95.54	-0.99	0.458	338.27	-16.70	-79.65	28.30	27.70	5.70	TM	-4.44	-11.37	0.820	0.831	
																CM	0.00	-3.39	0.300	0.387	C
PEAK LOAD	BB	0.300	0.099	N.A	-400.89	255.66	-188.76	66.90	0.292	396.37	-4.52	-70.23	10.70	10.97	2.40	BC	-3.49	-8.52	0.611	2.595	
H = 879.0	TB	0.300	0.099	N.A	-400.89	255.66	-188.76	66.90	0.292	396.37	-4.52	70.23	-10.70	-10.97	-2.40	BM	-2.62	-12.94	1.000	1.035	
Δ = 7.92	LC	0.523	0.142	N.A	-728.04	413.96	-428.20	-14.24	0.423	690.43	-37.61	81.90	-78.96	-68.66	-20.10	TC	-3.49	-8.52	0.611	2.595	
	RC	0.523	0.142	N.A	-728.04	413.96	-428.20	-14.24	0.423	690.43	-37.61	-81.90	78.96	68.66	20.10	TM	-2.62	-12.94	1.000	1.035	
																CM	0.00	-7.57	0.670	0.573	C
POST PEAK	BB	0.169	0.112	0.046	-361.07	230.73	-153.48	77.25	0.493	356.04	-5.04	-70.90	10.79	10.48	4.13	BC	0.00	0.00	0.000	0.000	R
H = 708.0	TB	0.170	0.111	0.045	-361.41	231.30	-154.89	76.41	0.492	356.48	-4.93	70.89	-10.73	-10.71	-4.22	BM	-2.26	-12.40	0.968	0.764	
Δ = 10.45	LC	0.583	0.179	N.A	-602.09	302.52	-307.31	-4.79	0.449	552.52	-49.57	87.40	-80.28	-71.31	-15.35	TC	0.00	0.00	0.000	0.000	R
	RC	0.584	0.176	N.A	-601.51	307.53	-307.72	-0.19	0.442	554.08	-47.43	-87.21	81.55	68.02	14.57	TM	-4.41	-13.42	0.985	1.009	
																CM	0.00	-6.92	0.608	0.537	C
ULTIMATE	BB	0.282	0.215	0.078	-249.07	83.55	-5.91	77.64	0.487	223.13	-25.94	-71.70	30.47	20.92	-4.06	BC	0.00	0.00	0.000	0.000	R
H = 491.0	TB	0.162	0.144	0.078	-327.50	209.66	-73.86	135.80	0.468	316.75	-10.75	76.06	-19.33	-5.46	-4.11	BM	0.00	-8.08	0.715	2.160	
Δ = 15.5	LC	0.460	0.251	0.129	-495.23	170.38	-144.44	25.94	0.334	417.59	-77.64	97.27	-119.47	-100.15	1.94	TC	0.00	0.00	0.000	0.000	R
	RC	0.761	0.295	0.161	-621.47	244.88	-234.13	10.75	0.361	485.67	-135.80	-70.26	179.85	102.25	14.20	TM	-3.53	-11.53	0.852	1.530	
																CM	0.00	-4.00	0.348	0.403	C

Table E.8 F.E Analysis of Infilled Frame 'SSUS2' under Horizontal Forces Compared with Available Methods (* See text for symbols)

F.E ANALYSIS

Beginning of frame plasticity: H_p = 1446.0 KN, Δ_p = 9.61 MM

At infill Cracking: H_t = 811.0 KN, Δ_t = 3.15 MM

At Peak Load: H_c = 1530.0 KN, Δ_c = 10.97 MM

On Plastic Plateau: H_u = 0.0 KN

STATIONS and LOADS

INTERFACE: G_h = 0, G_v = 0 mm; σ_{tb}= .05, σ_{Sb}= .07 N/mm2; Kn = 100, Ks = 50 KN/mm3; μ = .64, Ksru= .05 KN/mm3

STEEL FRAME: E = 200 KN/mm2, FY= 245 N/mm2, Kf = 36.03 KN/mm, Hou= 707.0 KN

FRAME MEMBERS	A	I	Me	Mp	d	tw*
UB 406X178X74	152.7	34151	405.4	501.6	412.8	25
UC 356X368X177	305.4	63630	846.6	999.4	368.3	40

UNIFORM INFILL: Size: 2709X2709X140 mm, l/h=1.00; σ_t = 1.5, σ_c = 11.3 N/mm2; ε_c = .00175, E = 18.46 KN/mm2

H KN Δ mm	*	a/l' a/h'	b/l' b/h'	c/l' c/h'	C KN	F KN	N1 KN	N2 KN	e/l' e/h'	S1 KN	S2 KN	M1 KN.M	M2 KN.M	M3 KN.M	M4 KN.M	*	σ1 N/mm2	σ2 N/mm2	Rs	Re	*
WORKING	BB	0.332	0.087	N.A	-289.45	128.90	-145.92	-17.02	1.000	308.29	18.84	-64.72	27.69	-6.39	27.69	BC	-2.64	-8.62	0.637	0.251	
H = 443.0	TB	0.332	0.087	N.A	-289.45	128.90	-145.92	-17.02	1.000	308.29	18.84	64.72	-27.69	6.39	-27.69	BM	-2.64	-8.62	0.637	0.251	
Δ = 1.48	LC	0.331	0.085	N.A	-279.74	122.07	-140.91	-18.84	1.000	296.76	17.02	60.20	-27.65	3.21	-27.65	TC	-2.64	-8.62	0.637	0.251	
	RC	0.331	0.085	N.A	-279.74	122.07	-140.91	-18.84	1.000	296.76	17.02	-60.20	27.65	-3.21	27.65	TM	-2.64	-8.62	0.637	0.251	
																CM	0.69	-2.25	0.487	0.268	
CRACKING	BB	0.337	0.100	N.A	-491.25	257.95	-293.92	-35.97	1.000	530.98	39.73	-128.61	58.79	-12.53	58.79	BC	-3.74	-12.11	0.895	0.515	
H = 805.0	TB	0.337	0.100	N.A	-491.25	257.95	-293.92	-35.97	1.000	530.98	39.73	128.61	-58.79	12.53	-58.79	BM	-3.74	-12.11	0.895	0.515	
Δ,= 3.10	LC	0.337	0.099	N.A	-475.17	246.11	-285.84	-39.73	1.000	511.14	35.97	120.86	-58.69	5.90	-58.69	TC	-3.74	-12.11	0.895	0.515	
	RC	0.337	0.099	N.A	-475.17	246.11	-285.84	-39.73	1.000	511.14	35.97	-120.86	58.69	-5.90	58.69	TM	-3.74	-12.11	0.895	0.515	
																CM	1.33	-3.85	0.991	0.880	
PEAK LOAD	BB	0.506	0.208	N.A	-1023.99	621.02	-610.16	10.86	1.000	1084.38	60.39	-472.24	139.50	58.66	139.50	BC	-5.82	-13.40	0.956	1.427	
H = 1525	TB	0.506	0.208	N.A	-1023.85	620.79	-609.93	10.86	1.000	1084.24	60.39	472.24	-139.50	-58.66	-139.50	BM	-5.59	-13.81	0.992	0.965	
Δ = 10.9	LC	0.547	0.295	N.A	-925.43	402.75	-463.14	-60.39	0.509	914.57	-10.86	483.03	-167.27	-166.23	-152.90	TC	-5.82	-13.40	0.956	1.427	
	RC	0.547	0.295	N.A	-925.15	402.61	-463.00	-60.39	0.509	914.29	-10.86	-482.53	167.27	166.23	152.90	TM	-5.59	-13.81	0.992	0.965	
																CM	0.00	-7.77	0.669	0.548	C

Table E.9 F.E Analysis of Infilled Frame 'WWUB2.1' under Horizontal Forces Compared with Available Methods (* See text for symbols)

F.E ANALYSIS

Beginning of frame plasticity: Hp = 644.0 KN, Δp = 5.49 MM

At infill Cracking: Ht= N.A (Not cracked)

At Peak Load: Hc = 696.0 KN, Δc = 6.96 MM

On Plastic Plateau: Hu= 400.0 KN

STATIONS and LOADS

INTERFACE: Gh = 0, Gv = 0 mm; σtb= .05, σSb = .07 N/mm2; Kn = 100, Ks = 50 KN/mm3; μ = .64, Ksru= .05 KN/mm3

STEEL FRAME: E = 200 KN/mm2, FY= 245 N/mm2, Kf = .38 KN/mm, Hou= 50 KN

FRAME MEMBERS:	A	I	Me	Mp	d	tw*
UB 178x102x19	45.2	1797	49.52	62.35	177.8	18
UC 152X152X23	62.4	1768	56.84	72.37	152.4	30

UNIFORM INFILL: Size: 4734X4734X140 mm l/h=1.00; σt = 1.5, σc = 11.3 N/mm2; εc = .00175, E = 18.46 KN/mm2

H KN Δ mm	*	a/l' a/h'	b/l' b/h'	c/l' c/h'	C KN	F KN	N1 KN	N2 KN	e/l' e/h'	S1 KN	S2 KN	M1 KN.M	M2 KN.M	M3 KN.M	M4 KN.M	*	σ1 N/mm2	σ2 N/mm2	Rs	Re	*
WORKING	BB	0.086	0.027	N.A	-282.38	144.03	-143.74	0.30	0.095	282.16	-0.22	-21.62	0.92	0.93	-0.02	BC	-4.07	-13.19	0.974	0.725	
H = 423.0	TB	0.086	0.027	N.A	-282.38	144.03	-143.74	0.30	0.095	282.16	-0.22	21.62	-0.92	-0.93	0.02	BM	-4.07	-13.19	0.974	0.725	
Δ = 2.81	LC	0.058	0.023	N.A	-278.73	142.72	-142.50	0.22	0.053	278.43	-0.30	18.34	-1.34	-1.33	-0.01	TC	-4.07	-13.19	0.974	0.725	
	RC	0.058	0.023	N.A	-278.73	142.72	-142.50	0.22	0.053	278.43	-0.30	-18.34	1.34	1.33	0.01	TM	-4.07	-13.19	0.974	0.725	
																CM	0.52	-1.26	0.397	0.214	
CRACK (NA)																					
PEAK LOAD	BB	0.090	0.042	N.A	-430.19	272.04	-270.71	1.33	0.096	429.08	-1.11	-57.58	3.82	3.85	-0.90	BC	-4.41	-10.01	0.714	2.266	
H = 696.0	TB	0.090	0.042	N.A	-430.19	272.04	-270.71	1.33	0.096	429.08	-1.11	57.58	-3.82	-3.85	0.90	BM	-5.78	-13.83	0.991	1.193	
Δ = 7.13	LC	0.083	0.039	N.A	-424.31	268.40	-267.29	1.11	0.083	422.98	-1.33	53.01	-4.87	-4.87	0.87	TC	-4.41	-10.01	0.714	2.266	
	RC	0.083	0.039	N.A	-424.31	268.40	-267.29	1.11	0.083	422.98	-1.33	-53.01	4.87	4.87	-0.87	TM	-5.78	-13.83	0.991	1.193	
																CM	0.84	-2.08	0.641	0.377	
POST PEAK	BB	0.101	0.053	0.004	-379.60	236.77	-234.07	2.70	0.114	377.47	-2.13	-66.98	6.52	6.69	-2.37	BC	-2.48	-5.37	0.382	3.453	
H = 604.0	TB	0.103	0.056	0.006	-377.09	241.33	-238.82	2.51	0.115	374.80	-2.30	69.31	-7.22	-7.38	2.33	BM	-5.41	-13.19	0.946	1.320	
Δ = 9.84	LC	0.106	0.054	N.A	-366.06	232.72	-230.59	2.13	0.115	363.37	-2.70	65.58	-8.93	-9.07	2.29	TC	-2.25	-5.00	0.356	3.691	
	RC	0.103	0.051	N.A	-370.73	230.24	-227.95	2.30	0.114	368.22	-2.51	-63.03	8.16	8.33	-2.28	TM	-3.31	-13.22	0.999	0.937	
																CM	0.68	-1.86	0.522	0.314	
ULTIMATE	BB	0.101	0.054	0.005	-298.37	109.99	-105.31	4.68	0.112	295.94	-2.43	-58.54	6.35	6.54	-3.74	BC	-2.73	-4.16	0.293	3.198	
H = 397.0	TB	0.117	0.093	0.076	-247.74	155.50	-152.25	3.25	0.117	242.20	-5.54	73.91	-18.28	-18.28	4.76	BM	-4.95	-9.64	0.680	1.097	
Δ = 12.50	LC	0.156	0.086	0.059	-248.43	157.89	-155.46	2.43	0.116	243.75	-4.68	70.72	-15.95	-15.10	3.51	TC	0.00	0.00	0.000	0.000	R
	RC	0.106	0.053	N.A	-293.97	107.67	-102.14	5.54	0.114	290.72	-3.25	-55.27	8.64	8.82	-4.89	TM	-2.81	-11.79	0.896	1.660	
																CM	0.49	-1.20	0.373	0.235	

Table E.10 F.E Analysis of Infilled Frame 'WMUR2NF' under Horizontal Forces Compared with Available Methods (* See text for symbols)

F.E ANALYSIS

Beginning of frame plasticity:	At infill Cracking:	At Peak Load:	On Plastic Plateau:
Hp = 596.6 KN Δp = 5.06 MM	Ht = N.A (Not cracked)	Hc = 620.4 KN Δc = 6.06 MM	Hu = 0.0 KN

INTERFACE: Gh = 0, σtb= .05, Kn = 100, μ = .64; Gv = 0, σSb= .07, Ks = 50, Ksru= .05; mm, N/mm2, KN/mm3, KN/mm3

STEEL FRAME: E = 200 KN/mm2, FY= 245 N/mm2, Kf = 2.4 KN/mm, Hou= 102.3 KN

FRAME MEMBERS:	A	I	Me	Mp	d	tw*
UB 254x146x31	71.99	5852	114	142	251.5	20
UC 152X152X23	62.4	1768	56.84	72.37	152.4	30

UNIFORM INFILL: Size: 4734X2709X140 mm l/h=1.75; σt = 1.5, σc = 11.3 N/mm2; εc = .00175, E = 18.46 KN/mm2

STATIONS and LOADS H KN Δ mm	*	a/l' a/h'	b/l' b/h'	c/l' c/h'	C KN	F KN	-N1 KN	-N2 KN	e/l' e/h'	S1 KN	S2 KN	M1 KN.M	M2 KN.M	M3 KN.M	M4 KN.M	*	σ1 N/mm2	σ2 N/mm2	Rs	Re *
WORKING	BB	0.076	0.043	N.A	-235.30	0.00	2.45	2.45	1.000	235.77	0.47	-47.84	1.74	-12.57	1.74	BC	-1.90	-12.01	0.950	0.651
H = 365.2	TB	0.076	0.043	N.A	-235.30	0.00	2.45	2.45	1.000	235.77	0.47	47.84	-1.74	12.57	-1.74	BM	-1.90	-12.01	0.950	0.651
Δ = 2.08	LC	0.077	0.025	N.A	-370.10	0.00	14.51	14.51	0.077	367.65	-2.45	19.58	-5.41	-5.41	0.71	TC	-1.90	-12.01	0.950	0.651
	RC	0.077	0.025	N.A	-370.10	0.00	14.51	14.51	0.077	367.65	-2.45	-19.58	5.41	5.41	-0.71	TM	-1.90	-12.01	0.950	0.651
																CM	0.43	-1.57	0.337	0.180
CRACK (NA)																				
PEAK LOAD	BB	0.231	0.062	N.A	-409.82	0.00	8.68	8.68	1.000	411.87	2.05	-123.27	6.58	-0.89	6.58	BC	-4.23	-7.36	0.517	2.934
H = 593.0	TB	0.231	0.062	N.A	-409.82	0.00	8.68	8.68	1.000	411.87	2.05	123.27	-6.58	0.89	-6.58	BM	-6.80	-13.61	0.962	1.398
Δ = 7.26	LC	0.093	0.060	0.008	-610.31	0.00	52.62	52.62	0.107	601.64	-8.68	79.00	-18.41	-18.84	2.49	TC	-4.23	-7.36	0.517	2.934
	RC	0.093	0.060	0.008	-610.31	0.00	52.62	52.62	0.107	601.64	-8.68	-79.00	18.41	18.84	-2.49	TM	-6.80	-13.61	0.962	1.398
																CM	0.73	-2.58	0.563	0.322
POST PEAK	BB	0.216	0.068	N.A	-386.97	0.00	10.81	10.81	1.000	388.84	1.87	-126.99	6.09	-0.85	6.09	BC	-3.16	-5.12	0.360	3.667
H = 555.1	TB	0.216	0.068	N.A	-386.97	0.00	10.81	10.81	1.000	388.84	1.87	126.99	-6.09	0.85	-6.09	BM	-4.75	-13.69	0.998	1.079
Δ = 8.46	LC	0.139	0.072	0.001	-576.74	0.00	52.51	52.51	0.137	565.93	-10.81	85.45	-22.19	-22.19	3.02	TC	-3.16	-5.12	0.360	3.667
	RC	0.139	0.072	0.001	-576.74	0.00	52.51	52.51	0.137	565.93	-10.81	-85.44	22.19	22.19	-3.02	TM	-4.75	-13.69	0.998	1.079
																CM	0.71	-2.44	0.547	0.313
ULTIMATE	BB	0.292	0.096	N.A	-166.15	0.00	39.58	39.58	0.278	166.12	-0.03	-74.82	0.86	0.86	0.76	BC	0.00	0.00	0.000	0.000 R
H = 212.0	TB	0.170	0.116	0.078	-163.04	0.00	0.34	0.34	1.000	166.98	3.95	94.67	-13.43	2.08	-13.43	BM	-3.17	-7.69	0.552	1.031
Δ = 12.08	LC	0.028	0.250	0.003	-251.63	0.00	38.72	38.72	0.324	212.05	-39.58	80.73	-52.71	64.93	17.53	TC	0.00	0.00	0.000	0.000 R
	RC	0.148	0.094	0.041	-251.63	0.00	37.86	37.86	0.160	251.29	-0.34	-55.88	7.87	7.89	7.09	TM	-1.22	-3.83	0.282	0.168
																CM	0.39	-1.14	0.296	0.175

Table E.11 F.E Analysis of Infilled Frame 'SMUR2NF' under Horizontal Forces Compared with Available Methods (See text for symbols)

F.E ANALYSIS

Beginning of frame plasticity:	At infill Cracking:	At Peak Load:	On Plastic Plateau:
Hp = 885.0 KN Δp = 5.39 MM	Ht= N.A (Not cracked)	Hc = 922.4 KN Δc = 7.18 MM	Hu = 0.0 KN

STATIONS and LOADS

INTERFACE: Gh = 0, σtb= .05, Kn = 100, μ = .64; Gv = 0 mm, σSb = .07 N/mm2, Ks = 50 KN/mm3, Ksru= .05 KN/mm3

STEEL FRAME: E = 200 KN/mm2 FY= 245 N/mm2 Kf = 6.74 KN/mm Hou= 199.7 KN

FRAME MEMBERS:	A	I	Me	Mp	d	tw*
UB 254x146x31	71.99	5852	114	142	251.5	20
UC 356X368X177	305.4	63630	846.6	999.4	368.3	40

UNIFORM INFILL: Size: 4734X2709X140 mm 1/h=1.75; σt = 1.5, σc = 11.3 N/mm2; εc = .00175, E = 18.46 KN/mm2

H KN Δ mm	*	a/l' a/h'	b/l' b/h'	c/l' c/h'	C KN	F KN	N1 KN	N2 KN	e/l' e/h'	S1 KN	S2 KN	M1 KN.M	M2 KN.M	M3 KN.M	M4 KN.M
WORKING	BB	0.185	0.037	N.A	-353.29	0.00	20.08	20.08	1.000	355.61	2.32	-66.10	7.06	-1.88	7.06
H = 616.9	TB	0.185	0.037	N.A	-353.29	0.00	20.08	20.08	1.000	355.61	2.32	66.10	-7.06	1.88	-7.06
Δ = 2.90	LC	0.189	0.065	N.A	-657.03	0.00	-2.32	-2.32	0.170	636.95	-20.08	51.49	-54.71	-54.12	-10.01
	RC	0.189	0.065	N.A	-657.03	0.00	-2.32	-2.32	0.170	636.95	-20.08	-51.49	54.71	54.12	10.01
CRACK (NA)															
PEAK LOAD	BB	0.162	0.057	N.A	-524.74	0.00	58.26	58.26	1.000	529.96	5.22	-149.08	16.62	-4.09	16.62
H = 922.4	TB	0.162	0.057	N.A	-524.74	0.00	58.26	58.26	1.000	529.96	5.22	149.08	-16.62	4.09	-16.62
Δ = 7.18	LC	0.289	0.109	N.A	-1038.87	0.00	-5.22	-5.22	0.257	980.61	-58.26	123.37	-138.81	-137.06	-24.91
	RC	0.289	0.109	N.A	-1038.87	0.00	-5.22	-5.22	0.257	980.61	-58.26	-123.37	138.81	137.06	24.91
POST PEAK	BB	0.161	0.069	N.A	-480.49	0.00	96.04	96.04	1.000	486.01	5.52	-163.66	19.50	-2.42	19.50
H = 847.1	TB	0.161	0.069	N.A	-480.49	0.00	96.04	96.04	1.000	486.01	5.52	163.66	-19.50	2.42	-19.50
Δ = 9.52	LC	0.332	0.152	N.A	-1039.22	0.00	-5.52	-5.52	0.289	943.18	-96.04	134.56	-209.06	-206.39	-32.60
	RC	0.332	0.152	N.A	-1039.22	0.00	-5.52	-5.52	0.289	943.18	-96.04	-134.56	209.06	206.39	32.60
ULTIMATE	BB	0.162	0.110	0.078	-285.43	0.00	124.4	124.40	1.000	291.63	6.21	-153.01	24.42	-0.21	24.42
H = 513.3	TB	0.162	0.110	0.078	-285.43	0.00	124.4	124.40	1.000	291.63	6.21	153.07	-24.42	0.21	-24.42
Δ = 12.26	LC	0.372	0.244	0.139	-762.01	0.00	-6.21	-6.21	0.322	637.61	-124.40	126.45	-261.97	-252.80	-41.20
	RC	0.372	0.244	0.139	-762.02	0.00	-6.21	-6.21	0.322	637.62	-124.40	-126.39	261.97	252.81	41.20

Station	*	σ1 N/mm2	σ2 N/mm2	Rs	Re	*
WORKING	BC	-5.09	-13.27	0.958	0.659	
	BM	-5.09	-13.27	0.958	0.659	
	TC	-5.09	-13.27	0.958	0.659	
	TM	-5.09	-13.27	0.958	0.659	
	CM	0.64	-2.58	0.513	0.284	
PEAK LOAD	BC	-6.12	-9.90	0.695	2.324	
	BM	-5.92	-13.97	1.000	1.053	
	TC	-6.12	-9.90	0.695	2.324	
	TM	-5.92	-13.97	1.000	1.053	
	CM	1.15	-3.30	0.861	0.631	
POST PEAK	BC	-3.64	-4.73	0.338	3.802	
	BM	-5.50	-13.70	0.985	1.250	
	TC	-3.64	-4.73	0.338	3.802	
	TM	-5.50	-13.70	0.985	1.250	
	CM	1.26	-3.36	0.925	0.685	
ULTIMATE	BC	0.00	0.00	0.000	0.000	R
	BM	0.95	-7.64	0.982	0.942	
	TC	0.00	0.00	0.000	0.000	R
	TM	0.93	-7.60	0.970	0.940	
	CM	1.15	-2.48	0.825	0.632	

Table E.12 F.E Analysis of Infilled Frame 'SWUR2NF' under Horizontal Forces Compared with Available Methods (See text for symbols)

F.E ANALYSIS

Beginning of frame plasticity:
Hp = 742.0 KN
Dp = 4.21 MM

At infill Cracking:
Ht = N.A (Not cracked)

At Peak Load:
Hc = 841.0 KN
Δc = 6.12 MM

On Plastic Plateau:
Hu= 0.0 KN

STATIONS and LOADS

INTERFACE

Gh = 0 Gv = 0 mm
σtb= .05 σSb= .07 N/mm2
Kn = 100 Ks = 50 KN/mm3
μ = .64 Ksru= .05 KN/mm3

H KN / Δ mm	*	a/l' a/h'	b/l' b/h'	c/l' c/h'	C KN	F KN
WORKING	BB	0.062	0.021	N.A	-319.31	0.00
H = 565.0	TB	0.062	0.021	N.A	-319.31	0.00
Δ = 2.66	LC	0.188	0.060	N.A	-608.20	0.00
	RC	0.188	0.060	N.A	-608.20	0.00
CRACK (NA)						
PEAK LOAD	BB	0.090	0.035	N.A	-474.99	0.00
H = 838.0	TB	0.090	0.035	N.A	-474.99	0.00
Δ = 6.48	LC	0.199	0.093	N.A	-948.04	0.00
	RC	0.199	0.093	N.A	-948.04	0.00
POST. (NA)						
ULTIMATE	BB	0.358	0.229	0.111	-92.15	0.00
H = 142.0	TB	0.159	0.059	0.011	-92.19	0.00
Δ = 10.60	LC	0.047	0.246	0.003	-220.31	0.00
	RC	0.358	0.233	0.125	-220.38	0.00

STEEL FRAME

E = 200 KN/mm2 FY= 245 N/mm2 Kf = 2.35 KN/mm Hou = 88.10 KN

FRAME MEMBERS:	A	I	Me	Mp	d	tw*
UB 178x102x19	45.2	1797	49.52	62.35	177.8	18
UC 356X368X177	305.4	63630	846.6	999.4	368.3	40

H KN / Δ mm	N1 KN	N2 KN	e/l' e/h'	S1 KN	S2 KN	M1 KN.M	M2 KN.M	M3 KN.M	M4 KN.M
WORKING	21.45	21.45	1.000	319.57	0.26	-31.27	1.53	0.38	1.53
H = 565.0	21.45	21.45	1.000	319.57	0.26	31.27	-1.53	-0.38	-1.53
Δ = 2.66	-0.26	-0.26	0.167	586.75	-21.45	37.96	-51.24	-50.67	-3.49
	-0.26	-0.26	0.167	586.75	-21.45	-37.96	51.24	50.67	3.49
CRACK (NA)									
PEAK LOAD	55.00	55.00	0.089	474.58	-0.41	-73.86	3.95	3.94	2.18
H = 838.0	55.00	55.00	0.089	474.58	-0.41	73.86	-3.95	-3.94	-2.18
Δ = 6.48	0.41	0.41	0.171	893.04	-55.00	81.80	-129.43	-126.36	-6.99
	0.41	0.41	0.171	893.04	-55.00	-81.80	129.43	126.36	6.99
POST. (NA)									
ULTIMATE	47.50	47.50	0.313	77.09	-15.06	-43.79	33.08	30.48	-15.27
H = 142.0	31.25	31.25	1.000	95.15	2.96	29.69	-10.03	1.77	-10.03
Δ = 10.60	15.06	15.06	0.475	172.81	-47.50	31.89	-52.01	10.28	13.82
	-2.96	-2.96	0.318	189.13	-31.25	-41.19	70.77	67.67	13.35

UNIFORM INFILL

Size: 4734X2709X140 mm l/h=1.75
σt = 1.5 σc = 11.3 N/mm2
εc = .00175 E = 18.46 KN/mm2

H KN / Δ mm	*	σ1 N/mm2	σ2 N/mm2	Rs	Re	*
WORKING	BC	-5.15	-13.35	0.963	0.676	
H = 565.0	BM	-5.15	-13.35	0.963	0.676	
Δ = 2.66	TC	-5.15	-13.35	0.963	0.676	
	TM	-5.15	-13.35	0.963	0.676	
	CM	0.56	-2.36	0.454	0.247	
CRACK (NA)						
PEAK LOAD	BC	-6.54	-9.77	0.688	2.348	
H = 838.0	BM	-8.00	-14.21	0.999	1.064	
Δ = 6.48	TC	-6.54	-9.77	0.688	2.348	
	TM	-8.00	-14.21	0.999	1.064	
	CM	0.88	-3.41	0.690	0.413	
POST. (NA)						
ULTIMATE	BC	0.00	0.00	0.000	0.000	R
H = 142.0	BM	-0.01	-3.44	0.303	0.617	
Δ = 10.60	TC	0.00	0.00	0.000	0.000	R
	TM	-0.59	-5.68	0.465	1.441	
	CM	0.55	-1.08	0.384	0.361	

Table E.13 Analysis of Infilled Frame WMUR2

a) Data

General data:	Frame Data:	Infill Data
μ =0.640	E = 200.00 KN/mm2	σc=11.300 N/mm2
K1=1.000	Mpc= 72.37 KNm	σt= 1.350
K2=0.667	Mpb= 142.00	E =18.460 KN/mm2
Ke=2.750	Mpj= 72.37	εc= 0.00175
β =0.200	LFT=0.00 (strain)	lxhxt=4734x2709x140 mm

b) Results using the proposed method

				Column	Beam
Hc	= 688.00 KN		α =	0.126	0.142
Ht	= 1041.39		β =	0.200	0.200
Huf	= 106.86		σn =	10.622	3.192 N/mm2
Δh	= 7.476 mm		τ =	2.226	2.043
Δhx	= 3.267		N1 =	-100.05	-185.92 KN
K0	= 184.05 KN/mm		N2 =	6.46	6.14
Kc	= 92.03		S1 =	502.07	293.65
Mode	= CC		S2 =	-6.14	-6.46
Mj	= -2.17 KNm		M1 =	-72.37	-72.37 KNm
Q	= -0.0175		M2 =	12.39	24.11
$\sigma nb0$	= 7.569 N/mm2		M3 =	12.37	24.06
w'	= 4702 mm		M4 =	-2.17	-2.17

c) Table of Comparison

	FE Test	SC	SR	M	W	W*	L	P
Hc	833.00	864.60	1120.31	1257.67	957.81	451.64	693.44	688.00
Ht	N.a	1733.10	1538.93	1014.26				1041.39
K0	192.60	330.97	194.69	198.86				184.05
Nc	104.56	0.00	0.00	7.67	0.00	0.00	0.00	100.05
Nb	268.46	0.00	0.00	13.40	0.00	0.00	0.00	185.92
Sc	560.29		597.58	13.40	478.90	225.82	693.44	502.07
Sb	400.36		*341.96*	7.67	*274.05*	*129.22*	*396.81*	*293.65*
M1	73.24	0.00	80.94	18.15	72.37	72.37	72.37	72.37
M3c	17.13	0.00			72.37	72.37	72.37	12.37
M3b	1.08	0.00			142.00	142.00	< 66.67	24.06
M4	1.90	0.00	80.94	18.15	72.37	72.37	72.37	2.17
Mode	CC				CC	CC	m1=0.154	CC
		λh= 8.18		Q=0.022	mn=0.016		m2=0.328	
		α = 0.192			0.082		m3=0.190	

d) Table of Comparison, (Calculated/Test values) X 100

	FE Test	SC	SR	M	W	W*	L	P
Hc	833.00	104	135	151	115	54	83	83
K0	192.60	172	101	103				96

Note: N.a= Not applicable, N.r= Not recorded

* using the Ma's penalty factor

Table E.14 Analysis of Infilled Frame MMUR2

a) Data

General data:	Frame Data:	Infill Data
μ =0.640	E = 200.00 KN/mm2	σc=11.300 N/mm2
K1=1.000	Mpc= 321.00 KNm	σt= 1.350
K2=0.667	Mpb= 142.00	E =18.460 KN/mm2
Ke=2.750	Mpj= 142.00	εc= 0.00175
β =0.200	LFT=0.00 (strain)	lxhxt=4734x2709x140 mm

b) Results using the proposed method

			Column	Beam
Hc = 1010.09 KN		α =	0.194	0.170
Ht = 1041.39		β =	0.200	0.200
Huf = 209.67		σn =	10.622	3.773 N/mm2
Δh = 9.173 mm		τ =	2.226	2.415
Δhx = 3.029		N1 =	-158.94	-249.25 KN
K0 = 220.22 KN/mm		N2 =	5.19	22.28
Kc = 110.11		S1 =	760.83	419.08
Mode= CC		S2 =	-22.28	-5.19
Mj = 3.85 KNm		M1 =	-142.00	-142.00 KNm
Q = -0.0422		M2 =	52.64	24.26
$\sigma nb0$= 7.569 N/mm2		M3 =	52.47	24.23
w' = 4702 mm		M4 =	3.85	3.85

c) Table of Comparison

	FE Test	SC	SR	M	W	W*	L	P
Hc	1098.00	1443.35	1758.92	1844.59	1103.77	660.72	959.66	1010.09
Ht	1098.00	1866.42	1538.93	1200.43				1041.39
K0	211.10	408.84	194.69	209.49				220.22
Nc	146.00	0.00	0.00	24.51	0.00	0.00	0.00	158.94
Nb	322.00	0.00	0.00	42.84	0.00	0.00	0.00	249.25
Sc	776.00		938.09	42.84	551.89	330.36	959.66	760.83
Sb	506.00		536.81	24.51	315.81	189.05	549.16	419.08
M1	136.00	0.00	127.06	58.02	142.00	142.00	142.00	142.00
M3c	65.00	0.00			321.00	321.00	<247.73	52.47
M3b	2.80	0.00			142.00	142.00	< 80.23	24.23
M4	14.30	0.00	127.06	58.02	142.00	142.00	142.00	3.85
Mode	CC				CC	CC	m1=0.276	CC
		λh= 4.90		Q=0.049	mn=0.031		m2=0.377	
		α = 0.32			m =0.161		m3=0.213	

d) Table of Comparison, (Calculated/Test values) X 100

	FE Test	SC	SR	M	W	W*	L	P
Hc	1098.00	131	160	168	101	60	87	92
Ht	1098.00	170	140	109				95
K0	211.10	194	92	99				104

Note: N.a= Not applicable, N.r= Not recorded
* using the Ma's penalty factor

Table E.15 Analysis of Infilled Frame SMUR2

a) Data

General data:	Frame Data:	Infill Data
μ =0.640	E = 200.00 KN/mm2	σc=11.300 N/mm2
K1=1.000	Mpc= 999.40 KNm	σt= 1.350
K2=0.667	Mpb= 142.00	E =18.460 KN/mm2
Ke=2.750	Mpj= 142.00	εc= 0.00175
β =0.200	LFT=0.00 (strain)	lxhxt=4734x2709x140 mm

b) Results using the proposed method

			Column	Beam
Hc = 1163.45 KN		α =	0.250	0.156
Ht = 1041.39		β =	0.200	0.200
Huf = 209.67		σn =	10.622	4.487 N/mm2
Dh = 10.023 mm		τ =	2.226	2.872
Dhx = 1.988		N1 =	-207.19	-225.62 KN
K0 = 232.15 KN/mm		N2 =	4.13	70.52
Kc = 116.08		S1 =	937.84	458.58
Mode= CC		S2 =	-70.52	-4.13
Mj = 8.83 KNm		M1 =	-142.00	-142.00 KNm
Q = -0.1081		M2 =	153.73	25.37
$\sigma nb0$= 7.569 N/mm2		M3 =	152.06	25.36
w' = 4702 mm		M4 =	8.83	8.83

c) Table of Comparison

	FE Test	SC	SR	M	W	W*	L	P
Hc	1148.00	2117.69	2464.65	2586.34	1065.60	660.72	959.66	1163.45
Ht	1101.00	1955.30	1538.93	1400.26				1041.39
K0	238.20	447.78	194.69	244.26				232.15
Nc	206.64	0.00	0.00	34.82	0.00	0.00	0.00	207.19
Nb	217.30	0.00	0.00	60.85	0.00	0.00	0.00	225.62
Sc	934.40		1314.48	60.85	532.80	330.36	959.66	937.84
Sb	472.20		752.20	34.82	304.89	189.05	549.16	458.58
M1	147.80	0.00	178.05	82.42	142.00	142.00	142.00	142.00
M3c	152.90	0.00			999.40	999.40	<491.62	152.06
M3b	11.20	0.00			142.00	142.00	< 80.23	25.36
M4	19.40	0.00	178.05	82.42	142.00	142.00	142.00	8.83
Mode	CC				CC	CC	m1=0.433	CC
		λh= 3.34		Q=0.049	mn=0.031		m2=0.377	
		α = 0.47			m =0.161		m3=0.213	

d) Table of Comparison, (Calculated/Test values) X 100

	FE Test	SC	SR	M	W	W*	L	P
Hc	1148.00	184	215	225	93	58	84	101.
Ht	1101.00	178	140	127				95
K0	238.20	188	82	103				97

Note: N.a= Not applicable, N.r= Not recorded
* using the Ma's penalty factor

Table E.16 Analysis of Infilled Frame SWUR2

a) Data

General data:	Frame data:	Infill data
μ =0.640	E = 200.00 KN/mm2	σc=11.300 N/mm2
K1=1.000	Mpc= 999.40 KNm	σt= 1.350
K2=0.667	Mpb= 62.35	E =18.460 KN/mm2
Ke=2.750	Mpj= 62.35	εc= 0.00175
β =0.200	LFT=0.00 (strain)	lxhxt=4734x2709x140 mm

b) Results using the proposed method

			Column	Beam
Hc = 978.71 KN		α =	0.219	0.083
Ht = 1041.39		β =	0.200	0.200
Huf = 92.06		σn =	10.622	6.908 N/mm2
Δh = 8.605 mm		τ =	2.226	4.421
Δhx = 1.852		N1 =	-182.36	-169.53 KN
K0 = 227.47 KN/mm		N2 =	2.72	73.94
Kc = 113.73		S1 =	809.18	377.71
Mode= CC		S2 =	-73.94	-2.72
Mj = -0.43 KNm		M1 =	-62.35	-62.35 KNm
Q = -0.1313		M2 =	157.81	11.40
$\sigma nb0$= 7.569 N/mm2		M3 =	155.97	11.40
w' = 4702 mm		M4 =	-0.43	-0.43

c) Table of Comparison

	FE Test	SC	SR	M	W	W*	L	P
Hc	1038.00	2171.76	2519.94	2562.20	844.88	416.31	842.05	978.71
Ht	1038.00	1955.30	1538.93	1370.50				1041.39
K0	234.60	447.78	194.69	242.82				227.47
Nc	224.80	0.00	0.00	12.09	0.00	0.00	0.00	182.36
Nb	173.10	0.00	0.00	21.13	0.00	0.00	0.00	169.53
Sc	865.40		1343.97	21.13	422.44	208.15	842.05	809.18
Sb	362.90		769.08	12.09	241.74	119.11	481.86	377.71
M1	53.25	0.00	182.04	28.62	62.35	62.35	62.35	62.35
M3c	137.00	0.00			999.40	999.40	<448.17	155.97
M3b	2.30	0.00			62.35	62.35	< 46.64	11.40
M4	5.60	0.00	182.04	28.62	62.35	62.35	62.35	0.43
Mode	CC				CC	CC	m1=0.417	CC
		λh= 3.25		Q=0.017	mn=0.013		m2=0.250	
		α = 0.483			m =0.071		m3=0.187	

d) Table of Comparison, (Calculated/Test values) X 100

	FE Test	SC	SR	M	W	W*	L	P
Hc	1038.00	209	243	247	81	40	81	94.
Ht	1038.00	188	148	132				100
K0	234.60	191	83	104				97

Note: N.a= Not applicable, N.r= Not recorded
* using the Ma's penalty factor

Table E.17 Analysis of Infilled Frame WWUS2

a) Data

General data:	Frame data:	Infill data
μ =0.640	E = 200.00 KN/mm2	σc=11.300 N/mm2
K1=1.000	Mpc= 72.37 KNm	σt= 1.350
K2=0.667	Mpb= 62.35	E =18.460 KN/mm2
Ke=2.750	Mpj= 62.35	εc= 0.00175
β =0.200	LFT=0.00 (strain)	lxhxt=2709x2709x140 mm

b) Results using the proposed method

			Column	Beam
Hc = 649.34 KN		α =	0.141	0.141
Ht = 691.20		β =	0.200	0.200
Huf = 92.06		σn =	7.569	7.569 N/mm2
Δh = 6.280 mm		τ =	4.844	4.844
Δhx = 3.166		N1 =	-252.78	-252.05 KN
K0 = 206.79 KN/mm		N2 =	5.44	6.17
Kc = 103.40		S1 =	397.30	398.03
Mode= CC		S2 =	-6.17	-5.44
Mj = -2.27 KNm		M1 =	-62.35	-62.35 KNm
Q = -0.0187		M2 =	12.13	12.40
$\sigma nb0$= 7.569 N/mm2		M3 =	12.10	10.40
w' = 3831 mm		M4 =	-2.27	-2.27

c) Table of Comparison

	FE Test	SC	SR	M	W	W*	L	P
Hc	679.00	854.40	735.96	828.33	655.06	426.95	643.64	649.34
Ht	679.00	905.10	880.64	671.99				691.20
K0	187.90	251.98	129.22	152.60				206.79
Nc	256.40	0.00	0.00	9.54	0.00	0.00	0.00	252.78
Nb	258.70	0.00	0.00	9.54	0.00	0.00	0.00	252.05
Sc	420.80		392.51	9.54	327.53	213.47	643.64	397.30
Sb	429.00		392.51	9.54	327.53	213.47	643.64	398.03
M1	54.32	0.00	53.17	12.92	62.35	62.35	62.35	62.35
M3c	0.00	0.00			72.37	72.37	< 69.45	12.10
M3b	1.65	0.00			62.35	62.35	62.35	10.40
M4	0.00	0.00	53.17	12.92	62.35	62.35	62.35	2.27
Mode	CC				CC	CC	m1=0.149	CC
		λh= 8.27		Q=0.024	mn=0.041		m2=0.143	
		α = 0.19			m =0.186		m3=0.187	

d) Table of Comparison, (Calculated/Test values) X 100

	FE Test	SC	SR	M	W	W*	L	P
Hc	679.00	126	108	122	96	63	95	96
Ht	679.00	133	130	99				102
K0	187.90	134	69	81				110

Note: N.a= Not applicable, N.r= Not recorded
* using the Ma's penalty factor

Table E.18 Analysis of Infilled Frame MWUS2

a) Data

General data:	Frame data:	Infill data
μ =0.640	E = 200.00 KN/mm2	σc=11.300 N/mm2
K1=1.000	Mpc= 321.00 KNm	σt= 1.350
K2=0.667	Mpb= 62.35	E =18.460 KN/mm2
Ke=2.750	Mpj= 62.35	εc= 0.00175
β =0.200	LFT=0.00 (strain)	lxhxt=2709x2709x140 mm

b) Results using the proposed method

			Column	Beam
Hc = 784.99 KN		α =	0.180	0.180
Ht = 691.20		β =	0.200	0.200
Huf = 92.06		σn =	7.569	7.569 N/mm2
Δh = 7.406 mm		τ =	4.844	4.844
Δhx = 0.895		N1 =	-319.00	-298.65 KN
K0 = 211.98 KN/mm		N2 =	12.35	31.40
Kc = 105.99		S1 =	486.34	503.35
Mode= CC		S2 =	-31.40	-12.35
Mj = -20.99 KNm		M1 =	-62.35	-62.35 KNm
Q = -0.0741		M2 =	49.25	57.19
$\sigma nb0$= 7.569 N/mm2		M3 =	48.73	6.46
w′ = 3831 mm		M4 =	-20.99	-20.99

c) Table of Comparison

	FE Test	SC	SR	M	W	W*	L	P
Hc	747.00	1426.32	1155.32	1202.08	877.28	426.95	643.64	784.99
Ht	684.00	966.65	880.64	786.76				691.20
K0	210.33	290.75	129.22	159.85				211.98
Nc	314.90	0.00	0.00	23.38	0.00	0.00	0.00	319.00
Nb	225.00	0.00	0.00	23.38	0.00	0.00	0.00	298.65
Sc	521.70		616.17	23.38	438.64	213.47	643.64	486.34
Sb	412.50		616.17	23.38	438.64	213.47	643.64	503.35
M1	68.20	0.00	83.46	31.67	62.35	62.35	62.35	62.35
M3c	12.80	0.00			321.00	321.00	<182.88	48.73
M3b	9.10	0.00			62.35	62.35	62.35	6.46
M4	0.36	0.00	83.46	31.67	62.35	62.35	62.35	20.99
Mode	CC				CC	CC	m1=0.251	CC
		λh= 4.96		Q=0.040	mn=0.041		m2=0.143	
		α =0.317			m =0.186		m3=0.187	

d) Table of Comparison, (Calculated/Test values) X 100

	FE Test	SC	SR	M	W	W*	L	P
Hc	747.00	191	155	161	117	57	86	105
Ht	684.00	141	129	115				101
K0	210.33	138	61	76				101

Note: N.a= Not applicable, N.r= Not recorded
* using the Ma's penalty factor

Table E.19 Analysis of Infilled Frame SWUS2

a) Data

General data:	Frame data:	Infill data
μ =0.640	E = 200.00 KN/mm2	σc=11.300 N/mm2
K1=1.000	Mpc= 999.40 KNm	σt= 1.350
K2=0.667	Mpb= 62.35	E =18.460 KN/mm2
Ke=2.750	Mpj= 62.35	εc= 0.00175
β =0.200	LFT=0.00 (strain)	lxhxt=2709x2709x140 mm

b) Results using the proposed method

			Column	Beam
Hc = 831.71 KN		α =	0.260	0.153
Ht = 691.20		β =	0.200	0.200
Huf = 92.06		σn =	7.569	6.226 N/mm2
Δh = 8.289 mm		τ =	4.844	3.985
Δhx = 1.905		N1 =	-473.83	-158.68 KN
K0 = 200.69 KN/mm		N2 =	3.28	72.46
Kc = 100.34		S1 =	673.03	357.87
Mode= CC		S2 =	-72.46	-3.28
Mj = 3.58 KNm		M1 =	-62.35	-62.35 KNm
Q = -0.1484		M2 =	151.38	11.12
σnb0= 7.569 N/mm2		M3 =	148.90	11.11
w' = 3831 mm		M4 =	3.58	3.58

c) Table of Comparison

	FE Test	SC	SR	M	W	W*	L	P
Hc	879.00	2092.71	1618.88	1680.68	877.28	426.95	643.64	831.71
Ht	714.00	1031.81	880.64	915.13				691.20
K0	246.60	310.13	129.22	186.13				200.69
Nc	428.20	0.00	0.00	30.91	0.00	0.00	0.00	473.83
Nb	188.80	0.00	0.00	30.91	0.00	0.00	0.00	158.68
Sc	690.40		863.40	30.91	438.64	213.47	643.64	673.03
Sb	396.40		863.40	30.91	438.64	213.47	643.64	357.87
M1	70.20	0.00	116.95	41.86	62.35	62.35	62.35	62.35
M3c	68.70	0.00			999.40	999.40	<342.72	148.90
M3b	11.00	0.00			62.35	62.35	62.35	11.11
M4	2.40	0.00	116.95	41.86	62.35	62.35	62.35	3.58
Mode	CC				CC	CC	m1=0.417	CC
		λh= 3.38		Q=0.038	mn=0.041		m2=0.143	
		α = 0.464			m =0.186		m3=0.187	

d) Table of Comparison, (Calculated/Test values) X 100

	FE Test	SC	SR	M	W	W*	L	P
Hc	879.00	238	184	191	100	49	73	95.
Ht	714.00	145	123	128				97
K0	246.60	126	52	75				81

Note: N.a= Not applicable, N.r= Not recorded
* using the Ma's penalty factor

Table E.20 Analysis of Infilled Frame SSUS2

a) Data

General data:	Frame data:	Infill data
μ =0.640	E = 200.00 KN/mm2	σc=11.300 N/mm2
K1=1.000	Mpc= 999.40 KNm	σt= 1.350
K2=0.667	Mpb= 501.60	E =18.460 KN/mm2
Ke=2.750	Mpj= 501.60	εc= 0.00175
β =0.200	LFT=0.00 (strain)	lxhxt=2709x2709x140 mm

b) Results using the proposed method

			Column	Beam
Hc = 1665.04 KN		α =	0.333	0.219
Ht = 815.82		β =	-0.047	-0.628
Huf = 740.64		σn =	7.980	7.569 N/mm2
Δh = 9.988 mm		t =	4.619	4.844
Δhx = 5.039		N1 =	-809.97	-529.48 KN
K0 = 333.39 KN/mm		N2 =	-226.23	-127.17
Kc = 166.70		S1 =	1135.56	854.84
Mode= DC		S2 =	127.17	226.23
Mj = 298.01 KNm		M1 =	-501.60	-501.60 KNm
Q = 0.1803		M2 =	75.53	-156.80
σnb0= 7.569 N/mm2		M3 =	68.29	-180.63
w' = 3831 mm		M4 =	298.01	298.01

c) Table of Comparison

	FE Test	SC	SR	M	W	W*	L	P
Hc	1530.00	1935.17	1511.38	2109.75	1325.63	1235.63	1490.63	1665.04
Ht	811.00	1031.81	880.64	1192.73				815.82
K0	299.30	310.13	129.22	212.08				333.39
Nc	463.10	0.00	0.00	299.31	0.00	0.00	0.00	809.97
Nb	610.20	0.00	0.00	299.31	0.00	0.00	0.00	529.48
Sc	914.60		805.94	299.31	662.82	617.82	1490.63	1135.56
Sb	1084.40		805.94	299.31	662.82	617.82	1490.63	854.84
M1	472.20	0.00	109.16	405.42	501.60	501.60	501.60	501.60
M3c	166.20	0.00			<999.40	<999.40	<666.94	68.29
M3b	58.70	0.00			<501.60	<501.60	<408.94	180.63
M4	139.50	0.00	109.16	405.42	501.60	501.60	501.60	298.01
Mode	DC				S	S	m1=0.496	DC
		λh= 3.65		Q=0.396	mn=0.329		m2=0.406	
		α = 0.43			m =1.496		m3=0.331	

d) Table of Comparison, (Calculated/Test values) X 100

	FE Test	SC	SR	M	W	W*	L	P
Hc	1530.00	126	99	138	87	81	97	109.
Ht	811.00	127	109	147				101
K0	299.30	104	43	71				111

Note: N.a= Not applicable, N.r= Not recorded
* using the Ma's penalty factor

Table E.21 Analysis of Infilled Frame WWUB2

a) Data

General data:	Frame data:	*Infill data*
μ =0.640	E = 200.00 KN/mm2	σc=11.300 N/mm2
K1=1.000	Mpc= 72.37 KNm	σt= 1.350
K2=0.667	Mpb= 62.35	E =18.460 KN/mm2
Ke=2.750	Mpj= 62.35	εc= 0.00175
β =0.200	LFT=0.00 (strain)	lxhxt=4734x4734x140 mm

b) Results using the proposed method

			Column	Beam
Hc = 653.35 KN		α =	0.080	0.080
Ht = 1207.88		β =	0.200	0.200
Huf = 52.68		σn =	7.569	7.569 N/mm2
Δh = 7.565 mm		τ =	4.844	4.844
Δhx = 3.813		N1 =	-254.47	-254.05 KN
K0 = 172.73 KN/mm		N2 =	3.75	4.17
Kc = 86.37		S1 =	399.30	399.71
Mode= CC		S2 =	-4.17	-3.75
Mj = -5.30 KNm		M1 =	-62.35	-62.35 KNm
Q = -0.0126		M2 =	12.88	13.04
$\sigma nb0$= 7.569 N/mm2		M3 =	12.86	11.04
w' = 6695 mm		M4 =	-5.30	-5.30

c) Table of Comparison

	FE Test	SC	SR	M	W	W*	L	P
Hc	696.00	1008.94	910.91	1039.10	852.28	426.95	643.65	653.35
Ht	N.a	1518.40	1538.93	1025.47				1207.88
K0	150.50	226.14	129.22	134.44				172.73
Nc	267.30	0.00	0.00	2.78	0.00	0.00	0.00	254.47
Nb	270.70	0.00	0.00	2.78	0.00	0.00	0.00	254.05
Sc	423.00		485.82	2.78	426.14	213.48	643.65	399.30
Sb	429.10		485.82	2.78	426.14	213.48	643.65	399.71
M1	57.60	0.00	114.99	6.59	62.35	62.35	62.35	62.35
M3c	4.90	0.00			72.37	72.37 <	69.80	12.86
M3b	3.90	0.00			62.35	62.35	62.35	11.04
M4	0.90	0.00	114.99	6.59	62.35	62.35	62.35	5.30
Mode	CC				CC	CC	m1=0.085	CC
		λh=12.24		Q=0.005	mn=0.013		m2=0.082	
					m =0.061		m3=0.173	

d) Table of Comparison, (Calculated/Test values) X 100

	FE Test	SC	SR	M	W	W*	L	P
Hc	696.00	145	131	149	122	61	92	94
K0	150.50	150	86	89				115

Note: N.a= Not applicable, N.r= Not recorded
* using the Ma's penalty factor

Table E.22 Analysis of Infilled Frame SSUSA1

a) Data

General data:	Frame data:	Infill data:
μ =0.450	E =175.0000 KN/mm2	σc= 1.160 N/mm2
K1=1.000	Mpc= 0.3540 KNm	σt= 0.240
K2=0.667	Mpb= 0.3540	E = 1.800 KN/mm2
Ke=2.750	Mpj= 0.3540	εc= 0.0011
β =0.200	LFT= 0.0010 Strain	lxhxt=300x300x14.05 mm

b) Results using the proposed method

					Column	Beam	
Hc =	2.201	KN		α =	0.3329	0.3333	
Ht =	1.727			β =	-0.7865	-0.8112	
Huf =	4.720			σn =	1.0787	0.9515	N/mm2
Δh =	1.377	mm		τ =	0.2463	0.1616	
Δhx =	0.739			N1 =	-0.6049	-0.4572	KN
K0 =	3.197	KN/mm		N2 =	-0.2593	-0.2302	
Kc =	1.598			S1 =	1.7437	1.5960	
Mode=	DC			S2 =	0.2302	0.2593	
Mj =	0.0446	KNm		M1 =	-0.1000	-0.1000	KNm
Q =	0.2645			M2 =	N.a	N.a	
σnb0=	1.113	N/mm2		M3 =	-0.0014	-0.0073	
w' =	424.0	mm		M4 =	0.0446	0.0446	

c) Table of Comparison

	A Test	SC	SR	M	W	W*	L	P
Hc	2.3100	2.2378	1.7447	2.6911	5.6184	5.2847	4.9226	2.2009
Ht	2.0000	2.0744	1.7400	1.5115				1.7268
K0	4.9700	3.0980	1.2645	2.2143				3.1966
Nc	N.r	0.0000	0.0000	0.4732	0.0000	0.0000	0.0000	0.6049
Nb	N.r	0.0000	0.0000	0.4732	0.0000	0.0000	0.0000	0.4572
Sc	N.r		0.9305	0.4732	2.8092	2.6424	4.9226	1.7437
Sb	N.r		0.9305	0.4732	2.8092	2.6424	4.9226	1.5960
M1	N.r	0.0000	0.0140	0.0710	0.3540	0.3540	0.3540	0.1000
M3c	N.r	0.0000			<0.3540	<0.3540	<0.3540	0.0014
M3b	N.r	0.0000			<0.3540	<0.3540	0.3540	0.0073
M4	N.r	0.0000	0.0140	0.0710	0.3540	0.3540	0.3540	0.0446
Mode	DC				S	S	m1=0.959	DC
		λh= 3.60		Q=0.542	mn=1.839		m2=0.959	
					m =8.358		m3=1.086	

d) Table of Comparison, (Calculated/Test values) X 100

	A Test	SC	SR	M	W	W*	L	P
Hc	2.3100	97	76	116	243	229	213	95
Ht	2.0000	104	87	76				86
K0	4.9700	62	25	45				64

Note: N.a= Not applicable, N.r= Not recorded
* using the Ma's penalty factor

Table E.23 Analysis of Infilled Frame SSUSA2

a) Data

General data:	Frame data:	Infill data
μ =0.450	E =175.0000 KN/mm2	σc= 1.160 N/mm2
K1=1.000	Mpc= 0.3540 KNm	σt= 0.240
K2=0.667	Mpb= 0.3540	E = 1.800 KN/mm2
Ke=2.750	Mpj= 0.3540	εc= 0.0011
β =0.200	LFT= 0.0010 Strain	lxhxt=300x300x25 mm

b) Results using the proposed method

				Column	Beam
Hc =	3.642	KN	α =	0.3327	0.3327
Ht =	2.673		β =	-0.6781	-0.6774
Huf =	4.720		σn =	0.9149	0.9149 N/mm2
Δh =	1.376	mm	τ =	0.4117	0.4117
Δhx =	0.688		N1 =	-1.1931	-1.1931 KN
K0 =	5.292	KN/mm	N2 =	-0.1656	-0.1657
Kc =	2.646		S1 =	2.4488	2.4489
Mode=	DC		S2 =	0.1657	0.1656
Mj =	0.0375	KNm	M1 =	-0.1262	-0.1262 KNm
Q =	0.1001		M2 =	N.a	N.a
$\sigma nb0$=	0.915	N/mm2	M3 =	0.0043	0.0043
w' =	424.0	mm	M4 =	0.0375	0.0375

c) Table of Comparison

	A Test	SC	SR	M	W	W*	L	P
Hc	3.5000	3.4477	2.7347	3.6179	6.2044	5.7249	6.2425	3.6419
Ht	2.9500	3.5002	3.0960	2.1776				2.6732
K0	4.9600	5.2875	2.2500	3.3977				5.2917
Nc	N.r	0.0000	0.0000	0.4416	0.0000	0.0000	0.0000	1.1931
Nb	N.r	0.0000	0.0000	0.4416	0.0000	0.0000	0.0000	1.1931
Sc	N.r		1.4585	0.4416	3.1022	2.8624	6.2425	2.4488
Sb	N.r		1.4585	0.4416	3.1022	2.8624	6.2425	2.4489
M1	N.r	0.0000	0.0219	0.0662	0.3540	0.3540	0.3540	0.1262
M3c	N.r	0.0000			<0.3540	<0.3540	<0.3540	0.0043
M3b	N.r	0.0000			<0.3540	<0.3540	<0.3540	0.0043
M4	N.r	0.0000	0.0219	0.0662	0.3540	0.3540	0.3540	0.0375
Mode	DC				S	S	m1=0.719	DC
		λh= 4.16		Q=0.323	mn=1.033 m =4.697		m2=0.719 m3=0.683	

d) Table of Comparison, (Calculated/Test values) X 100

	A Test	SC	SR	M	W	W*	L	P
Hc	3.5000	99	78	103	177	164	178	104.
Ht	2.9500	119	105	74				91
K0	4.9600	107	45	68				107

Note: N.a= Not applicable, N.r= Not recorded
* using the Ma's penalty factor

Table E.24 Analysis of Infilled Frame MMUSA3

a) Data

General data:	Frame data:	Infill data:
μ =0.450	E =200.0000 KN/mm2	σc= 1.160 N/mm2
K1=1.000	Mpc= 0.1490 KNm	σt= 0.240
K2=0.667	Mpb= 0.1490	E = 1.800 KN/mm2
Ke=2.750	Mpj= 0.1490	εc= 0.0011
β =0.200	LFT= 0.0010 Strain	lxhxt=300x300x20.3 mm

b) Results using the proposed method

				Column	Beam	
Hc =	2.550	KN	α =	0.3327	0.3327	
Ht =	1.973		β =	-0.3790	-0.3786	
Huf =	1.987		σn =	0.9149	0.9149	N/mm2
Δh =	1.376	mm	τ =	0.4117	0.4117	
Δhx =	0.688		N1 =	-0.7651	-0.7652	KN
K0 =	3.705	KN/mm	N2 =	0.0691	0.0691	
Kc =	1.853		S1 =	1.7848	1.7849	
Mode=	DC		S2 =	-0.0691	-0.0691	
Mj =	-0.0001	KNm	M1 =	-0.0719	-0.0719	KNm
Q =	-0.0514		M2 =	0.0139	0.0139	
$\sigma nb0$=	0.915	N/mm2	M3 =	0.0137	0.0137	
w' =	424.0	mm	M4 =	-0.0001	-0.0001	

c) Table of Comparison

	A Test	SC	SR	M	W	W*	L	P
Hc	2.2800	2.1621	1.7689	2.0877	3.0993	2.8026	3.2229	2.5500
Ht	1.9600	2.7388	2.5140	1.3670				1.9732
K0	3.4000	4.0194	1.8270	2.5590				3.7051
Nc	N.r	0.0000	0.0000	0.1041	0.0000	0.0000	0.0000	0.7651
Nb	N.r	0.0000	0.0000	0.1041	0.0000	0.0000	0.0000	0.7652
Sc	N.r		0.9434	0.1041	1.5497	1.4013	3.2229	1.7848
Sb	N.r		0.9434	0.1041	1.5497	1.4013	3.2229	1.7849
M1	N.r	0.0000	0.0142	0.0156	0.1490	0.1490	0.1490	0.0719
M3c	N.r	0.0000			<0.1490	<0.1490	<0.1490	0.0137
M3b	N.r	0.0000			<0.1490	<0.1490	<0.1490	0.0137
M4	N.r	0.0000	0.0142	0.0156	0.1490	0.1490	0.1490	0.0001
Mode	DC				S	S	m1=0.518	DC
		λh= 5.39		Q=0.111	mn=0.536		m2=0.518	
					m =2.435		m3=0.434	

d) Table of Comparison, (Calculated/Test values) X 100

	A Test	SC	SR	M	W	W*	L	P
Hc	2.2800	95	78	92	136	123	141	112.
Ht	1.9600	140	128	70				101
K0	3.4000	118	54	75				109

Note: N.a= Not applicable, N.r= Not recorded
* using the Ma's penalty factor

Table E.25 Analysis of Infilled Frame SSUSA4

a) Data

General data:	Frame data:	Infill data:
μ =0.450	E =175.0000 KN/mm2	σc=32.200 N/mm2
K1=1.000	Mpc= 0.3540 KNm	σt= 4.100
K2=0.667	Mpb= 0.3540	E =23.000 KN/mm2
Ke=2.750	Mpj= 0.3540	εc= 0.002
β =0.200	LFT= 0.0020 Strain	lxhxt=300x300x8.35 mm

b) Results using the proposed method

					Column	Beam	
Hc	=	19.093	KN	α =	0.2110	0.2110	
Ht	=	13.865		β =	0.2000	0.2000	
Huf	=	4.720		σn =	25.3969	25.3970	N/mm2
Δh	=	2.242	mm	τ =	11.4286	11.4286	
Δhx	=	1.121		N1 =	-5.8552	-5.8553	KN
K0	=	17.032	KN/mm	N2 =	0.1850	0.1850	
Kc	=	8.516		S1 =	13.2377	13.2378	
Mode=		CC		S2 =	-0.1850	-0.1850	
Mj	=	0.0153	KNm	M1 =	-0.3540	-0.3540	KNm
Q	=	-0.0190		M2 =	0.0592	0.0592	
σnb0=		25.397	N/mm2	M3 =	0.0591	0.0591	
w'	=	424.0	mm	M4 =	0.0153	0.0153	

c) Table of Comparison

	A Test	SC	SR	M	W	W*	L	P
Hc	16.5800	22.2391	18.4251	21.2511	13.8522	13.2625	18.8357	19.0930
Ht	14.2100	18.8821	17.6653	14.6601				13.8652
K0	15.7100	20.1653	9.6025	12.8276				17.0319
Nc	N.r	0.0000	0.0000	0.7550	0.0000	0.0000	0.0000	5.8552
Nb	N.r	0.0000	0.0000	0.7550	0.0000	0.0000	0.0000	5.8553
Sc	N.r		9.8267	0.7550	6.9261	6.6312	18.8357	13.2377
Sb	N.r		9.8267	0.7550	6.9261	6.6312	18.8357	13.2378
M1	N.r	0.0000	0.1474	0.1132	0.3540	0.3540	0.3540	0.3540
M3c	N.r	0.0000			<0.3540	<0.3540	<0.3540	0.0591
M3b	N.r	0.0000			0.3540	0.3540	<0.3540	0.0591
M4	N.r	0.0000	0.1474	0.1132	0.3540	0.3540	0.3540	0.0153
Mode	CC				SR	SR	m1=0.236	CC
		λh= 5.98		Q=0.076	mn=0.111		m2=0.236	
					m =0.507		m3=0.222	

d) Table of Comparison, (Calculated/Test values) X 100

	A Test	SC	SR	M	W	W*	L	P	P**
Hc	16.5800	134	111	128	84	80	114	115	109
Ht	14.2100	133	124	103				98	98
K0	15.7100	128	61	82				108	101

Note: N.a= Not applicable, N.r= Not recorded
* Using the Ma's penalty factor, ** Allowing for variable K1

Table E.26 Analysis of Infilled Frame SSUSA5

a) Data

General data:	Frame data:	Infill data:
μ =0.450	E =175.0000 KN/mm2	σc=32.200 N/mm2
K1=1.000	Mpc= 0.3540 KNm	σt= 4.100
K2=0.667	Mpb= 0.3540	E =23.000 KN/mm2
Ke=2.750	Mpj= 0.3540	εc= 0.00200
β =0.200	LFT= 0.0020 Strain	lxhxt=300x300x14.9 mm

b) Results using the proposed method

				Column	Beam	
Hc =	25.590	KN	α =	0.1579	0.1579	
Ht =	24.741		β =	0.2000	0.2000	
Huf =	4.720		σn =	25.3969	25.3970	N/mm2
Δh =	2.059	mm	τ =	11.4286	11.4286	
Δhx =	1.030		N1 =	-7.8643	-7.8643	KN
K0 =	24.856	KN/mm	N2 =	0.2044	0.2044	
Kc =	12.428		S1 =	17.7260	17.7261	
Mode=	CC		S2 =	-0.2044	-0.2044	
Mj =	0.0095	KNm	M1 =	-0.3540	-0.3540	KNm
Q =	-0.0157		M2 =	0.0612	0.0612	
σnb0=	25.397	N/mm2	M3 =	0.0611	0.0611	
w' =	424.0	mm	M4 =	0.0095	0.0095	

c) Table of Comparison

	A Test	SC	SR	M	W	W*	L	P
Hc	25.4900	34.3354	28.9455	32.7788	20.6882	17.7163	26.7084	25.5903
Ht	23.9700	32.3979	31.5224	24.3100				24.7415
K0	16.4000	34.2700	17.1350	21.5752				24.8556
Nc	N.r	0.0000	0.0000	0.7022	0.0000	0.0000	0.0000	7.8643
Nb	N.r	0.0000	0.0000	0.7022	0.0000	0.0000	0.0000	7.8643
Sc	N.r		15.4376	0.7022	10.3441	8.8582	26.7084	17.7260
Sb	N.r		15.4376	0.7022	10.3441	8.8582	26.7084	17.7261
M1	N.r	0.0000	0.2316	0.1053	0.3540	0.3540	0.3540	0.3540
M3c	N.r	0.0000			0.3540	<0.3540	<0.3540	0.0611
M3b	N.r	0.0000			0.3540	0.3540	0.3540	0.0611
M4	N.r	0.0000	0.2316	0.1053	0.3540	0.3540	0.3540	0.0095
Mode	CC				CC	SR	m1=0.177	CC
		λh= 6.91		Q=0.045	mn=0.062 m =0.284		m2=0.177 m3=0.198	

d) Table of Comparison, (Calculated/Test values) X 100

	A Test	SC	SR	M	W	W*	L	P	P*
Hc	25.4900	135	114	129	81	70	105	100	98
Ht	23.9700	135	132	101				103	103
K0	16.4000	209	104	132				152	147

Note: N.a= Not applicable, N.r= Not recorded
* Using the Ma's penalty factor, ** Allowing for variable K1

Table E.27 Analysis of Infilled Frame SSUSA6

a) Data

General data:	Frame data:	Infill data:
μ =0.450	E =175.0000 KN/mm2	σc=32.200 N/mm2
K1=1.000	Mpc= 0.3540 KNm	σt= 4.100
K2=0.667	Mpb= 0.3540	E =23.000 KN/mm2
Ke=2.750	Mpj= 0.3540	εc= 0.00200
β =0.200	LFT= 0.0020 Strain	lxhxt=300x300x19.5 mm

b) Results using the proposed method

				Column	Beam
Hc =	29.320	KN	α =	0.1381	0.1381
Ht =	32.380		β =	0.2000	0.2000
Huf =	4.720		σn =	25.3969	25.3970 N/mm2
Dh =	1.985	mm	τ =	11.4286	11.4286
Dhx =	0.993		N1 =	-9.0190	-9.0190 KN
K0 =	29.535	KN/mm	N2 =	0.2115	0.2115
Kc =	14.767		S1 =	20.3008	20.3009
Mode=	CC		S2 =	-0.2115	-0.2115
Mj =	0.0073	KNm	M1 =	-0.3540	-0.3540 KNm
Q =	-0.0142		M2 =	0.0621	0.0621
σnb0=	25.397	N/mm2	M3 =	0.0620	0.0620
w' =	424.0	mm	M4 =	0.0073	0.0073

c) Table of Comparison

	A Test	SC	SR	M	W	W*	L	P
Hc	33.8300	42.0125	35.7043	40.2672	25.9261	20.2674	30.5542	29.3198
Ht	31.5700	42.3999	41.2542	30.8852				32.3798
K0	23.9000	44.8500	22.4250	27.5401				29.5350
Nc	-1.0000	0.0000	0.0000	0.6790	0.0000	0.0000	0.0000	9.0190
Nb	-1.0000	0.0000	0.0000	0.6790	0.0000	0.0000	0.0000	9.0190
Sc	-1.0000		19.0423	0.6790	12.9631	10.1337	30.5542	20.3008
Sb	-1.0000		19.0423	0.6790	12.9631	10.1337	30.5542	20.3009
M1	-1.0000	0.0000	0.2856	0.1019	0.3540	0.3540	0.3540	0.3540
M3c	-1.0000	0.0000			0.3540	0.3540	<0.3540	0.0620
M3b	-1.0000	0.0000			0.3540	0.3540	0.3540	0.0620
M4	-1.0000	0.0000	0.2856	0.1019	0.3540	0.3540	0.3540	0.0073
Mode	CC				CC	CC	m1=0.154	CC
		λh= 7.40		Q=0.035	mn=0.048 m =0.217		m2=0.154 m3=0.191	

d) Table of Comparison, (Calculated/Test values) X 100

	A Test	SC	SR	M	W	W*	L	P	P**
Hc	33.8300	124	106	119	77	60	90	87	86
Ht	31.5700	134	131	98				103	103
K0	23.9000	188	94	115				124	123

Note: N.a= Not applicable, N.r= Not recorded
* Using the Ma's penalty factor, ** Allowing for variable K1

Table E.28 Analysis of Infilled Frame MMUSA7

a) Data

General data:	Frame data:	Infill data:
μ =0.450	E =200.0000 KN/mm2	σc=32.200 N/mm2
K1=1.000	Mpc= 0.1490 KNm	σt= 4.100
K2=0.667	Mpb= 0.1490	E =23.000 KN/mm2
Ke=2.750	Mpj= 0.1490	εc= 0.002
β =0.200	LFT= 0.0020 Strain	lxhxt=300x300x9.55 mm

b) Results using the proposed method

				Column	Beam
Hc =	13.283	KN	α =	0.1280	0.1280
Ht =	15.858		β =	0.2000	0.2000
Huf =	1.987		σn =	25.3969	25.3969 N/mm2
Δh =	1.947	mm	τ =	11.4286	11.4286
Δhx =	0.973		N1 =	-4.0804	-4.0804 KN
K0 =	13.646	KN/mm	N2 =	0.1105	0.1105
Kc =	6.823		S1 =	9.2025	9.2025
Mode=	CC		S2 =	-0.1105	-0.1105
Mj =	-0.0034	KNm	M1 =	-0.1490	-0.1490 KNm
Q =	-0.0164		M2 =	0.0256	0.0256
$\sigma nb0$=	25.397	N/mm2	M3 =	0.0256	0.0256
w' =	424.0	mm	M4 =	-0.0034	-0.0034

c) Table of Comparison

	A Test	SC	SR	M	W	W*	L	P
Hc	11.5600	18.0315	15.0619	17.5076	11.9334	9.2018	13.8723	13.2829
Ht	N.a	20.3498	20.2040	14.3445				15.8578
K0	11.5600	20.8668	10.9825	12.8770				13.6461
Nc	N.r	0.0000	0.0000	0.1807	0.0000	0.0000	0.0000	4.0804
Nb	N.r	0.0000	0.0000	0.1807	0.0000	0.0000	0.0000	4.0804
Sc	N.r		8.3033	0.1807	5.9667	4.6009	13.8723	9.2025
Sb	N.r		8.3033	0.1807	5.9667	4.6009	13.8723	9.2025
M1	N.r	0.0000	0.1245	0.0271	0.1490	0.1490	0.1490	0.1490
M3c	N.r	0.0000			0.1490	0.1490	<0.1490	0.0256
M3b	N.r	0.0000			0.1490	0.1490	0.1490	0.0256
M4	N.r	0.0000	0.1245	0.0271	0.1490	0.1490	0.1490	0.0034
Mode	CC				CC	CC	m1=0.143	CC
		λh= 8.44		Q=0.021	mn=0.041		m2=0.143	
					m =0.186		m3=0.187	

d) Table of Comparison, (Calculated/Test values) X 100

	A Test	SC	SR	M	W	W*	L	P
Hc	11.5600	156	130	151	103	80	120	115
K0	11.5600	181	95	111				118

Note: N.a= Not applicable, N.r= Not recorded
* Using the Ma's penalty factor, ** Allowing for variable K1

Table E.29 Analysis of Infilled Frame MMUSA8

a) Data

General data:	Frame data:	Infill data:
μ =0.450	E =200.0000 KN/mm2	σc=32.200 N/mm2
K1=1.000	Mpc= 0.1490 KNm	σt= 4.100
K2=0.667	Mpb= 0.1490	E =23.000 KN/mm2
Ke=2.750	Mpj= 0.1490	εc= 0.002
β =0.200	LFT= 0.0020 Strain	lxhxt=300x300x21.25 mm

b) Results using the proposed method

				column	Beam
Hc =	19.913	KN	α =	0.0858	0.0858
Ht =	35.286		β =	0.2000	0.2000
Huf =	1.987		σn =	25.3969	25.3969 N/mm2
Dh =	1.772	mm	τ =	11.4286	11.4286
Dhx =	0.886		N1 =	-6.1364	-6.1364 KN
K0 =	22.475	KN/mm	N2 =	0.1151	0.1151
Kc =	*11.238*		*S1* =	*13.7770*	*13.7770*
Mode=	CC		S2 =	-0.1151	-0.1151
Mj =	-0.0047	KNm	M1 =	-0.1490	-0.1490 KNm
Q =	-0.0114		M2 =	0.0268	0.0268
$\sigma nb0$=	25.397	N/mm2	M3 =	0.0268	0.0268
w' =	424.0	mm	M4 =	-0.0047	-0.0047

c) Table of Comparison

	A Test	SC	SR	M	W	W*	L	P
Hc	26.6200	32.8510	29.0529	32.8397	20.2750	13.7262	20.6931	19.9134
Ht	N.a	44.3568	44.9565	29.7355				35.2856
K0	23.6600	45.2094	24.4375	26.8375				22.4754
Nc	N.r	0.0000	0.0000	0.1635	0.0000	0.0000	0.0000	6.1364
Nb	N.r	0.0000	0.0000	0.1635	0.0000	0.0000	0.0000	6.1364
Sc	N.r		15.4949	0.1635	10.1375	6.8631	20.6931	13.7770
Sb	N.r		15.4949	0.1635	10.1375	6.8631	20.6931	13.7770
M1	n.r	0.0000	0.2324	0.0245	0.1490	0.1490	0.1490	0.1490
M3c	N.r	0.0000			0.1490	0.1490	<0.1490	0.0268
M3b	N.r	0.0000			0.1490	0.1490	0.1490	0.0268
M4	N.r	0.0000	0.2324	0.0245	0.1490	0.1490	0.1490	0.0047
Mode	CC				CC	CC	m1=0.096	CC
		λh=10.31		Q=0.010	mn=0.018		m2=0.096	
					m =0.084		m3=0.176	

d) Table of Comparison, (Calculated/Test values) X 100

	A Test	SC	SR	M	W	W*	L	P	P**
Hc	26.6200	123	109	123	76	52	78	75	79
K0	23.6600	191	103	113				95	101

Note: N.a= Not applicable, N.r= Not recorded
* Using the Ma's penalty factor, ** Allowing for variable K1

Table E.30 Analysis of Infilled Frame WWUSA9

a) Data

General data:	Frame data:	Infill data:
μ =0.450	E =197.0000 KN/mm2	σc=32.200 N/mm2
K1=1.000	Mpc= 0.0670 KNm	σt= 4.100
K2=0.667	Mpb= 0.0670	E =23.000 KN/mm2
Ke=2.750	Mpj= 0.0670	εc= 0.002
β =0.200	LFT= 0.0020 Strain	lxhxt=300x300x26.4 mm

b) Results using the proposed method

				Column	Beam
Hc =	14.938	KN	α =	0.0516	0.0516
Ht =	43.837		β =	0.2000	0.2000
Huf =	0.893		σn =	25.3969	25.3969 N/mm2
Dh =	1.608	mm	τ =	11.4286	11.4286
Dhx =	0.804		N1 =	-4.6136	-4.6136 KN
K0 =	18.583	KN/mm	N2 =	0.0589	0.0589
Kc =	9.292		S1 =	10.3244	10.3244
Mode=	CC		S2 =	-0.0589	-0.0589
Mj =	-0.0043	KNm	M1 =	-0.0670	-0.0670 KNm
Q =	-0.0078		M2 =	0.0125	0.0125
$\sigma nb0$=	25.397	N/mm2	M3 =	0.0125	0.0125
w' =	424.0	mm	M4 =	-0.0043	-0.0043

c) Table of Comparison

	A Test	SC	SR	M	W	W*	L	P
Hc	22.7600	28.1223	26.0076	30.0600	16.3682	10.2593	15.4665	14.9380
Ht	N.a	55.1068	55.8518	32.7897				43.8372
K0	22.9900	51.6120	30.3600	29.6967				18.5834
Nc	N.r	0.0000	0.0000	0.0375	0.0000	0.0000	0.0000	4.6136
Nb	N.r	0.0000	0.0000	0.0375	0.0000	0.0000	0.0000	4.6136
Sc	N.r		13.8707	0.0375	8.1841	5.1297	15.4665	10.3244
Sb	N.r		13.8707	0.0375	8.1841	5.1297	15.4665	10.3244
M1	N.r	0.0000	0.2081	0.0056	0.0670	0.0670	0.0670	0.0670
M3c	N.r	0.0000			0.0670	0.0670	<0.0670	0.0125
M3b	N.r	0.0000			0.0670	0.0670	0.0670	0.0125
M4	N.r	0.0000	0.2081	0.0056	0.0670	0.0670	0.0670	0.0043
Mode	CC				CC	CC	m1=0.058	CC
		λh=14.96		Q=0.003	mn=0.007		m2=0.058	
					m =0.030		m3=0.170	

d) Table of Comparison, (Calculated/Test values) X 100

	A Test	SC	SR	M	W	W*	L	P	P**
Hc	22.7600	124	114	132	72	45	68	66	82
K0	22.9900	224	132	129				81	104

Note: N.a= Not applicable, N.r= Not recorded
* Using the Ma's penalty factor, ** Allowing for variable K1

Table E.31 Analysis of Infilled Frame WWUSM1

a) Data

General data:	Frame data:	Infill data:
μ =0.450	E =200.0000 KN/mm2	σc=18.240 N/mm2
K1=1.000	Mpc= 0.6100 KNm	σt= 2.190
K2=0.667	Mpb= 0.6100	E =18.000 KN/mm2
Ke=2.750	Mpj= 0.6100	εc= 0.00175
β =0.200	LFT= 0.0020 Strain	lxhxt=387x387x18.75 mm

b) Results using the proposed method

				Column	Beam
Hc =	28.213	KN	α =	0.1904	0.1904
Ht =	21.453		β =	0.2000	0.2000
Huf =	6.305		σn =	14.3863	14.3863 N/mm2
Dh =	2.646	mm	τ =	6.4738	6.4738
Dhx =	1.323		N1 =	-8.6415	-8.6415 KN
K0 =	21.323	KN/mm	N2 =	0.3010	0.3010
Kc =	10.661		S1 =	19.5712	19.5712
Mode=	CC		S2 =	-0.3010	-0.3010
Mj =	0.0055	KNm	M1 =	-0.6100	-0.6100 KNm
Q =	-0.0209		M2 =	0.1000	0.1000
$\sigma nb0$=	14.386	N/mm2	M3 =	0.0998	0.0998
w' =	547.0	mm	M4 =	0.0055	0.0055

c) Table of Comparison

	M Test	SC	SR	M	W	W*	L	P
Hc	28.6000	30.4935	25.8141	29.1622	20.9309	19.6349	29.4669	28.2128
Ht	26.8000	28.0919	27.3328	22.0073				21.4531
K0	22.8500	33.7500	16.8750	20.9772				21.3228
Nc	N.r	0.0000	0.0000	0.5520	0.0000	0.0000	0.0000	8.6415
Nb	N.r	0.0000	0.0000	0.5520	0.0000	0.0000	0.0000	8.6415
Sc	N.r		13.7675	0.5520	10.4654	9.8175	29.4669	19.5712
Sb	N.r		13.7676	0.5520	10.4654	9.8175	29.4669	19.5712
M1	N.r	0.0000	0.2664	0.1068	0.6100	0.6100	0.6100	0.6100
M3c	N.r	0.0000			<0.6100	<0.6100	<0.6100	0.0998
M3b	N.r	0.0000			0.6100	0.6100	<0.6100	0.0998
M4	N.r	0.0000	0.2664	0.1068	0.6100	0.6100	0.6100	0.0055
Mode	CC				SR	SR	m1=0.213	CC
		λh= 7.16		Q=0.039	mn=0.091 m =0.412		m2=0.213 m3=0.212	

d) Table of Comparison, (Calculated/Test values) X 100

	M Test	SC	SR	M	W	W*	L	P	P**
Hc	28.6000	107	90	102	73	69	103	99	95
Ht	26.8000	105	102	82				80	80
K0	22.8500	148	74	92				93	89

Note: N.a= Not applicable, N.r= Not recorded,
* Using the Ma's penalty factor, ** Allowing for variable K1

Table E.32 Analysis of Infilled Frame WWURM2

a) Data

General data:	Frame data:	Infill data:
μ =0.450	E =200.0000 KN/mm2	σc=19.000 N/mm2
K1=1.000	Mpc= 0.6100 KNm	σt= 2.280
K2=0.667	Mpb= 0.6100	E =18.600 KN/mm2
Ke=2.750	Mpj= 0.6100	εc= 0.00175
β =0.200	LFT= 0.0020 Strain	lxhxt=591x387x18.75 mm

b) Results using the proposed method

				Column	Beam
Hc	= 28.144	KN	α =	0.1701	0.1701
Ht	= 31.264		β =	0.2000	0.2000
Huf	= 6.305		σn =	18.0202	7.7269 N/mm2
Δh	= 2.894	mm	τ =	3.4771	3.4771
Δhx	= 1.145		N1 =	-4.0786	-6.2285 KN
K0	= 19.448	KN/mm	N2 =	0.2130	0.3252
Kc	= 9.724		S1 =	21.9156	14.3508
Mode	= CC		S2 =	-0.3252	-0.2130
Mj	= -0.0039	KNm	M1 =	-0.6100	-0.6100 KNm
Q	= -0.0226		M2 =	0.1007	0.1007
σnb0	= 14.986	N/mm2	M3 =	0.1006	0.1006
w'	= 648.0	mm	M4 =	-0.0039	-0.0039

c) Table of Comparison

	M Test	SC	SR	M	W	W*	L	P
Hc	32.1400	32.1981	38.0919	42.3259	30.9615	21.1375	30.2111	28.1441
Ht	N.r	47.0589	43.4562	31.7254				31.2638
K0	26.7400	46.3766	24.4087	27.7078				19.4484
Nc	N.r	0.0000	0.0000	0.3167	0.0000	0.0000	0.0000	4.0786
Nb	N.r	0.0000	0.0000	0.4837	0.0000	0.0000	0.0000	6.2285
Sc	N.r		20.3157	0.4837	15.4808	10.5688	30.2111	21.9156
Sb	N.r		13.3032	0.3167	10.1372	6.9207	19.7829	14.3508
M1	N.r	0.0000	0.3931	0.0936	0.6100	0.6100	0.6100	0.6100
M3c	N.r	0.0000			0.6100	0.6100	0.6100	0.1006
M3b	N.r	0.0000			0.6100	0.6100	<0.6100	0.1006
M4	N.r	0.0000	0.3931	0.0936	0.6100	0.6100	0.6100	0.0039
Mode	CC				CC	CC	m1=0.209	CC
		λh= 7.06		Q=0.023	mn=0.037		m2=0.319	
					m =0.178		m3=0.210	

d) Table of Comparison, (Cal ated/Test values) X 100

	M Test	SC	SR	M	W	W*	L	P	
Hc	32.1400	100	119	132	96	66	94	88	85
K0	26.7400	173	91	104				73	70

Note: N.a= Not applicable, N.r= Not recorded
* Using the Ma's penalty factor, ** Allowing for variable K1

Table E.33 Analysis of Infilled Frame WWURM3

a) Data

General data:	Frame data:	Infill data:
μ =0.450	E =200.0000 KN/mm2	σc=16.720 N/mm2
K1=1.000	Mpc= 0.6100 KNm	σt= 2.000
K2=0.667	Mpb= 0.6100	E =17.600 KN/mm2
Ke=2.750	Mpj= 0.6100	εc= 0.00175
β =0.200	LFT= 0.0020 Strain	lxhxt=794x387x18.75 mm

b) Results using the proposed method

					Column	Beam
Hc	=	25.240 KN		α =	0.1781	0.1781
Ht	=	31.662		β =	0.2000	0.2000
Huf	=	6.305		σn =	16.4405	3.9057 N/mm2
Δh	=	3.301 mm		τ =	1.7576	1.7576
Δhx	=	1.082		N1 =	-2.1095	-4.3281 KN
K0	=	15.294 KN/mm		N2 =	0.1615	0.3314
Kc	=	7.647		S1 =	20.9123	10.1928
Mode	=	CC		S2 =	-0.3314	-0.1615
Mj	=	-0.0062 KNm		M1 =	-0.6100	-0.6100 KNm
Q	=	-0.0256		M2 =	0.0993	0.0993
σnb0	=	13.187 N/mm2		M3 =	0.0992	0.0992
w′	=	696.0 mm		M4 =	-0.0062	-0.0062

c) Table of Comparison

	M Test	SC	SR	M	W	W*	L	P
Hc	27.5800	29.8381	40.5024	44.6838	29.5646	19.0707	27.5367	25.2404
Ht	N.r	58.7044	51.2130	32.6378				31.6620
K0	25.3400	47.9975	26.6653	26.3774				15.2942
Nc	N.r	0.0000	0.0000	0.2168	0.0000	0.0000	0.0000	2.1095
Nb	N.r	0.0000	0.0000	0.4448	0.0000	0.0000	0.0000	4.3281
Sc	N.r		21.6013	0.4448	14.7823	9.5353	27.5367	20.9123
Sb	N.r		10.5286	0.2168	7.2050	4.6476	13.4215	10.1928
M1	N.r	0.0000	0.4180	0.0861	0.6100	0.6100	0.6100	0.6100
M3c	N.r	0.0000			0.6100	0.6100	<0.6100	0.0992
M3b	N.r	0.0000			0.6100	0.6100	<0.6100	0.0992
M4	N.r	0.0000	0.4180	0.0861	0.6100	0.6100	0.6100	0.0062
Mode	CC				CC	CC	m1=0.222	CC
		λh= 6.71		Q=0.020	mn=0.024		m2=0.456	
					m =0.131		m3=0.216	

d) Table of Comparison, (Cal ated/Test values) X 100

	M Test	SC	SR	M	W	W*	L	P	P**
Hc	27.5800	108	147	162	107	69	100	92	89
K0	25.3400	189	105	104				60	58

Note: N.a= Not applicable, N.r= Not recorded, using P from Ma's work
* Using the Ma's penalty factor, ** Allowing for variable K1

Table E.34 Analysis of Infilled Frame WWUSM4

a) Data

General data:	Frame data:	Infill data:
m =0.450	E =200.0000 KN/mm2	sc=22.960 N/mm2
K1=1.000	Mpc= 12.2000 KNm	st= 2.760
K2=0.667	Mpb= 12.2000	E =20.600 KN/mm2
Ke=2.750	Mpj= 0.6100	ec= 0.00175
b =0.200	LFT= 0.0020 Strain	lxhxt=387x387x18.75 mm

b) Results using the proposed method

			Column	Beam
Hc =	55.155	KN	α = 0.3327	0.3327
Ht =	27.037		β = 0.1807	0.1806
Huf =	6.305		σn = 18.1090	18.1091 N/mm2
Dh =	3.142	mm	τ = 8.1491	8.1491
Dhx =	1.571		N1 =-15.5532	-15.5544 KN
K0 =	35.113	KN/mm	N2 = 4.1220	4.1215
Kc =	17.557		S1 = 39.6008	39.6021
Mode=	SDC		S2 = -4.1215	-4.1220
Mj =	0.6100	KNm	M1 = -0.6100	-0.6100 KNm
Q =	-0.1300		M2 = 1.6993	1.6995
$\sigma nb0$=	18.109	N/mm2	M3 = 1.6743	1.6744
w' =	547.0	mm	M4 = 0.6100	0.6100

c) Table of Comparison

	M Test	SC	SR	M	W	W*	L	P
Hc	64.2000	82.8169	63.9283	70.2333	26.5684	22.0294	35.4605	55.1552
Ht	33.2000	40.3600	34.4469	37.9161				27.0368
K0	24.7200	48.2813	19.3125	45.4205				35.1134
Nc	N.r	0.0000	0.0000	0.0000	0.0000	0.0000	0.0000	15.5532
Nb	N.r	0.0000	0.0000	0.0000	0.0000	0.0000	0.0000	15.5544
Sc	N.r		34.0951	0.0000	13.2842	11.0147	35.4605	39.6008
Sb	N.r		34.0951	0.0000	13.2842	11.0147	35.4605	39.6021
M1	N.r	0.0000	0.6597	0.0000	0.6100	0.6100	0.6100	0.6100
M3c	N.r	0.0000			12.2000<	12.2000<	12.2000	1.6743
M3b	N.r	0.0000			12.2000	12.2000<	12.2000	1.6744
M4	N.r	0.0000	0.6597	0.0000	0.6100	0.6100	0.6100	0.6100
Mode	DC				CC	SR	m1=0.615	SDC
		λh= 3.32		Q=0.099	mn=0.072		m2=0.615	
					m =0.328		m3=0.203	

d) Table of Comparison, (Calculated/Test values) X 100

	M Test	SC	SR	M	W	W*	L	P
Hc	64.2000	129	100	109	41	34	55	86 79
Ht	33.2000	122	104	114				81 81
K0	26.2000	184	74	184				134 130

Note: N.a= Not applicable, N.r= Not recorded, using P from Ma's work
* Using the Ma's penalty factor, ** Allowing for variable K1

Table E.35 Analysis of Infilled Frame W1USS

a) Data

General data:	Frame data:		Infill data:
μ =0.450	E =200.0000	KN/mm2	σc=35.200 N/mm2
K1=1.000	Mpc= 0.0170	KNm	σt= 3.500
K2=0.667	Mpb= 0.0170		E =24.000 KN/mm2
Ke=2.750	Mpj= 0.0170		εc= 0.00200
β =0.200	LFT= 0.0020	Strain	lxhxt=152x152x19 mm

b) Results using the proposed method

				Column	Beam	
Hc =	6.667	KN	α =	0.0577	0.0577	
Ht =	13.682		β =	0.2000	0.2000	
Huf =	0.446		σn =	27.7631	27.7630	N/mm2
Δh =	0.833	mm	τ =	12.4934	12.4934	
Δhx =	0.416		N1 =	-2.0579	-2.0579	KN
K0 =	16.015	KN/mm	N2 =	0.0297	0.0297	
Kc =	8.007		S1 =	4.6095	4.6095	
Mode=	CC		S2 =	-0.0297	-0.0297	
Mj =	-0.0011	KNm	M1 =	-0.0170	-0.0170	KNm
Q =	-0.0088		M2 =	0.0031	0.0031	
σnb0=	27.763	N/mm2	M3 =	0.0031	0.0031	
w' =	216.0	mm	M4 =	-0.0011	-0.0011	

c) Table of Comparison

	SS Test	SC	SR	M	W	W*	L	P
Hc	10.5000	11.7316	10.7938	12.4384	7.5699	4.5838	6.9103	6.6674
Ht	N.a	17.1990	17.4315	13.2803				13.6817
K0	25.9000	42.1800	22.8000	22.6001				16.0146
Nc	N.r	0.0000	0.0000	0.0182	0.0000	0.0000	0.0000	2.0579
Nb	N.r	0.0000	0.0000	0.0182	0.0000	0.0000	0.0000	2.0579
Sc	N.r		5.7567	0.0182	3.7850	2.2919	6.9103	4.6095
Sb	N.r		5.7567	0.0182	3.7850	2.2919	6.9103	4.6095
M1	N.r	0.0000	0.0439	0.0014	0.0170	0.0170	0.0170	0.0170
M3c	N.r	0.0000			0.0170	0.0170	<0.0170	0.0031
M3b	N.r	0.0000			0.0170	0.0170	0.0170	0.0031
M4	N.r	0.0000	0.0439	0.0014	0.0170	0.0170	0.0170	0.0011
Mode	CC				CC	CC	m1=0.065	CC
		λh=14.33		Q=0.003	mn=0.008		m2=0.065	
					m =0.038		m3=0.171	

d) Table of Comparison, (Calculated/Test values) X 100

	SS Test	SC	SR	M	W	W*	L	P	P**
Hc	10.5000	112	103	118	72	44	66	63	90
K0	25.9000	163	88	87				62	92

Note: N.a= Not applicable, N.r= Not recorded, using P from Ma's work
* Using the Ma's penalty factor, ** Allowing for variable K1

Table E.36 Analysis of Infilled Frame W2USS

a) Data

General data:	Frame data:	Infill data:
μ =0.450	E =200.0000 KN/mm2	σc=35.200 N/mm2
K1=1.000	Mpc= 0.0383 KNm	σt= 3.500
K2=0.667	Mpb= 0.0383	E =24.000 KN/mm2
Ke=2.750	Mpj= 0.0383	εc= 0.002
β =0.200	LFT= 0.0020 Strain	lxhxt=152x152x19 mm

b) Results using the proposed method

				Column	Beam	
Hc =	9.974	KN	α =	0.0866	0.0866	
Ht =	13.682		β =	0.2000	0.2000	
Huf =	1.005		σn =	27.7631	27.7630	N/mm2
Δh =	0.902	mm	τ =	12.4934	12.4934	
Δhx =	0.451		N1 =	-3.0720	-3.0720	KN
K0 =	22.115	KN/mm	N2 =	0.0614	0.0614	
Kc =	11.057		S1 =	6.9019	6.9019	
Mode=	CC		S2 =	-0.0614	-0.0614	
Mj =	-0.0017	KNm	M1 =	-0.0383	-0.0383	KNm
Q =	-0.0122		M2 =	0.0069	0.0069	
σnb0=	27.763	N/mm2	M3 =	0.0068	0.0068	
w' =	216.0	mm	M4 =	-0.0017	-0.0017	

c) Table of Comparison

	SS Test	SC	SR	M	W	W*	L	P
Hc	12.6000	15.7281	13.9706	15.8175	10.5776	6.8802	10.3722	9.9739
Ht	13.3000	17.1990	17.4315	14.5856				13.6817
K0	33.6000	42.1800	22.8000	24.7489				22.1146
Nc	N.r	0.0000	0.0000	0.0688	0.0000	0.0000	0.0000	3.0720
Nb	N.r	0.0000	0.0000	0.0688	0.0000	0.0000	0.0000	3.0720
Sc	N.r		7.4510	0.0688	5.2888	3.4401	10.3722	6.9019
Sb	N.r		7.4510	0.0688	5.2888	3.4401	10.3722	6.9019
M1	N.r	0.0000	0.0568	0.0052	0.0383	0.0383	0.0383	0.0383
M3c	N.r	0.0000			0.0383	0.0383	<0.0383	0.0068
M3b	N.r	0.0000			0.0383	0.0383	0.0383	0.0068
M4	N.r	0.0000	0.0568	0.0052	0.0383	0.0383	0.0383	0.0017
Mode	CC				CC	CC	m1=0.097	CC
		λh=10.69		Q=0.009	mn=0.019		m2=0.097	
					m =0.085		m3=0.176	

d) Table of Comparison, (Calculated/Test values) X 100

	SS Test	SC	SR	M	W	W*	L	P	P**
Hc	12.6000	125	111	126	84	55	82	79	93
Ht	13.3000	129	131	110				103	103
K0	33.6000	126	68	74				66	80

Note: N.a= Not applicable, N.r= Not recorded, using p from Ma's work
* Using the Ma's penalty factor, ** Allowing for variable K1

Table E.37 Analysis of Infilled Frame M1USS

a) Data

General data:	Frame data:	Infill data:
μ =0.450	E =200.0000 KN/mm2	σc=35.200 N/mm2
K1=1.000	Mpc= 0.0660 KNm	σt= 3.500
K2=0.667	Mpb= 0.0660	E =24.000 KN/mm2
Ke=2.750	Mpj= 0.0660	εc= 0.00200
β =0.200	LFT= 0.0020 Strain	lxhxt=152x152x19 mm

b) Results using the proposed method

				Column	Beam
Hc =	13.062	KN	α =	0.1137	0.1137
Ht =	13.682		β =	0.2000	0.2000
Huf =	1.732		σn =	27.7631	27.7630 N/mm2
Dh =	0.960	mm	τ =	12.4934	12.4934
Dhx =	0.480		N1 =	-4.0174	-4.0174 KN
K0 =	27.208	KN/mm	N2 =	0.0960	0.0960
Kc =	13.604		S1 =	9.0449	9.0449
Mode=	CC		S2 =	-0.0960	-0.0960
Mj =	-0.0014	KNm	M1 =	-0.0660	-0.0660 KNm
Q =	-0.0145		M2 =	0.0115	0.0115
σnb0=	27.763	N/mm2	M3 =	0.0115	0.0115
w′ =	216.0	mm	M4 =	-0.0014	-0.0014

c) Table of Comparison

	SS Test	SC	SR	M	W	W*	L	P
Hc	14.0000	19.1080	16.5810	18.6556	13.0599	9.0317	13.6158	13.0622
Ht	13.3000	17.9156	17.4315	15.6072				13.6817
K0	38.5000	44.4600	22.8000	26.3646				27.2081
Nc	N.r	0.0000	0.0000	0.1668	0.0000	0.0000	0.0000	4.0174
Nb	N.r	0.0000	0.0000	0.1668	0.0000	0.0000	0.0000	4.0174
Sc	N.r		8.8432	0.1668	6.5299	4.5159	13.6158	9.0449
Sb	N.r		8.8432	0.1668	6.5299	4.5159	13.6158	9.0449
M1	N.r	0.0000	0.0674	0.0127	0.0660	0.0660	0.0660	0.0660
M3c	N.r	0.0000			0.0660	0.0660	<0.0660	0.0115
M3b	N.r	0.0000			0.0660	0.0660	0.0660	0.0115
M4	N.r	0.0000	0.0674	0.0127	0.0660	0.0660	0.0660	0.0014
Mode	CC				CC	CC	m1=0.127	CC
		λh= 8.80		Q=0.018	mn=0.032		m2=0.127	
					m =0.147		m3=0.183	

d) Table of Comparison, (Calculated/Test values) X 100

	SS Test	SC	SR	M	W	W*	L	P	P**
Hc	14.0000	136	118	133	93	65	97	93	103
Ht	13.3000	135	131	117				103	103
K0	38.5000	115	59	68				71	80

Note: N.a= Not applicable, N.r= Not recorded, using P from Ma's work
* Using the Ma's penalty factor, ** Allowing for variable K1

Table E.38 Analysis of Infilled Frame M2USS

a) Data

General data:	Frame data:	Infill data
μ =0.450	E =200.0000 KN/mm2	σc=35.200 N/mm2
K1=1.000	Mpc= 0.1500 KNm	σt= 3.500
K2=0.667	Mpb= 0.1500	E =24.000 KN/mm2
Ke=2.750	Mpj= 0.1500	εc= 0.00200
β =0.200	LFT= 0.0020 Strain	lxhxt=152x152x19 mm

b) Results using the proposed method

				Column	Beam
Hc =	19.655	KN	α =	0.1714	0.1714
Ht =	13.682		β =	0.2000	0.2000
Huf =	3.937		σn =	27.7631	27.7630 N/mm2
Δh =	1.071	mm	τ =	12.4934	12.4934
Δhx =	0.535		N1 =	-6.0377	-6.0377 KN
K0 =	36.720	KN/mm	N2 =	0.1635	0.1635
Kc =	18.360		S1 =	13.6169	13.6169
Mode=	CC		S2 =	-0.1635	-0.1635
Mj =	0.0051	KNm	M1 =	-0.1500	-0.1500 KNm
Q =	-0.0164		M2 =	0.0258	0.0258
$\sigma nb0$=	27.763	N/mm2	M3 =	0.0257	0.0257
w' =	216.0	mm	M4 =	0.0051	0.0051

c) Table of Comparison

	SS Test	SC	SR	M	W	W*	L	P
Hc	19.8200	25.4839	21.3626	24.3115	15.8999	13.6158	20.5267	19.6546
Ht	13.3000	18.6322	17.4315	17.6117				13.6817
K0	43.8000	47.8800	22.8000	29.2473				36.7200
Nc	N.r	0.0000	0.0000	0.6216	0.0000	0.0000	0.0000	6.0377
Nb	N.r	0.0000	0.0000	0.6216	0.0000	0.0000	0.0000	6.0377
Sc	N.r		11.3934	0.6216	7.9499	6.8079	20.5267	13.6169
Sb	N.r		11.3934	0.6216	7.9499	6.8079	20.5267	13.6169
M1	N.r	0.0000	0.0868	0.0474	0.1500	0.1500	0.1500	0.1500
M3c	N.r	0.0000			0.1500	<0.1500	<0.1500	0.0257
M3b	N.r	0.0000			0.1500	0.1500	0.1500	0.0257
M4	N.r	0.0000	0.0868	0.0474	0.1500	0.1500	0.1500	0.0051
Mode	CC				CC	SR	m1=0.192	CC
		λh= 6.60		Q=0.054	mn=0.074		m2=0.192	
					m =0.334		m3=0.203	

d) Table of Comparison, (Calculated/Test values) X 100

	SS Test	SC	SR	M	W	W*	L	P	P**
Hc	19.8200	129	108	123	80	69	104	99	103
Ht	13.3000	140	131	132				103	103
K0	43.8000	109	52	67				84	88

Note: N.a= Not applicable, N.r= Not recorded, using p from Ma's work
* Using the Ma's penalty factor, ** Allowing for variable K1

Table E.39 Analysis of Infilled Frame S1USS

a) Data

General data:	Frame data:	Infill data:
m =0.450	E =200.0000 KN/mm2	σc=35.200 N/mm2
K1=1.000	Mpc= 0.5140 KNm	σt= 3.500
K2=0.667	Mpb= 0.5140	E =24.000 KN/mm2
Ke=2.750	Mpj= 0.5140	εc= 0.002
β =0.200	LFT= 0.002 Strain	lxhxt=152x152x19 mm

b) Results using the proposed method

				Column	Beam
Hc	= 37.570	KN	α =	0.3173	0.3173
Ht	= 13.897		b =	0.2000	0.2000
Huf	= 13.491		σn =	27.7631	27.7630 N/mm2
Δh	= 1.304	mm	τ =	12.4934	12.4934
Δhx	= 0.652		N1 =	-11.7699	-11.7699 KN
K0	= 57.603	KN/mm	N2 =	-0.2907	-0.2907
Kc	= 28.801		S1 =	25.8000	25.8000
Mode	= CC		S2 =	0.2907	0.2907
Mj	= 0.1471	KNm	M1 =	-0.5140	-0.5140 KNm
Q	= 0.0157		M2 =	N.a	N.a
σnb0	= 27.763	N/mm2	M3 =	0.1169	0.1169
w′	= 216.0	mm	M4 =	0.1471	0.1471

c) Table of Comparison

	SS Test	SC	SR	M	W	W*	L	P
Hc	35.5500	40.4869	32.1053	43.3065	25.2632	25.2632	31.3277	37.5699
Ht	17.3000	19.7072	17.4315	26.0367				13.8968
K0	48.6000	52.4400	22.8000	34.8474				57.6027
Nc	N.r	0.0000	0.0000	5.6006	0.0000	0.0000	0.0000	11.7699
Nb	N.r	0.0000	0.0000	5.6006	0.0000	0.0000	0.0000	11.7699
Sc	N.r		17.1228	5.6006	12.6316	12.6316	31.3277	25.8000
Sb	N.r		17.1228	5.6006	12.6316	12.6316	31.3277	25.8000
M1	N.r	0.0000	0.1305	0.4268	0.5140	0.5140	0.5140	0.5140
M3c	N.r	0.0000			<0.5140	<0.5140	<0.5140	0.1169
M3b	N.r	0.0000			<0.5140	<0.5140	<0.5140	0.1169
M4	N.r	0.0000	0.1305	0.4268	0.5140	0.5140	0.5140	0.1471
Mode	CC				S	S	m1=0.355	CC
		λh= 4.15		Q=0.349	mn=0.252		m2=0.355	
					m =1.146		m3=0.293	

d) Table of Comparison, (Calculated/Test values) X 100

	SS Test	SC	SR	M	W	W*	L	P	P**
Hc	35.5500	114	90	122	71	71	88	106	104
Ht	17.3000	114	101	151				80	80
K0	48.6000	108	47	72				119	116

Note: N.a= Not applicable, N.r= Not recorded, using p from Ma's work
* Using the Ma's penalty factor, ** Allowing for variable K1

APPENDIX F

Constitutive Formulation for Masonry

F.1 General

The finite element representation of masonry has briefly been discussed in Section 3.9. Of the element types studied, the 4-node element made of the proposed plane-stress equivalent material, representing both the units and the joints, separated by interface elements, Fig 3.9, was found to be the most economical, practical and simplest available choice. The proposed 2-D material facilitates the possibility of simulating the masonry behaviour beyond its peak stress. Such a representation constitutes two distinct stiffness and strength contributors as follows:

i) The proposed plane-stress masonry equivalent material

which must (on the basis of plane stress-strain constitutive relationship) simulate the combined 3-D mechanical behaviour of masonry units and mortar joints while assuming the interface of the equivalent material elements remain intact.

ii) The interfaces of the proposed equivalent material elements. These line elements are assumed to pass through the midplane of the bed and head joints. Such interfaces must simulate all the inelastic behaviour of the joints such as debonding, slip and separation.

The following sections deal with analysing the 3-D mechanical behaviour of masonry so as to determine a set of mechanical properties for the proposed masonry equivalent material and the interfaces in order to operate in plane stress system with the same planar strengths and stiffnesses as those of the masonry.

F.2 Masonry under Uniaxial Compression

F.2.1 Mechanics of Masonry in Compression

Masonry is composed of two materials with, normally, quite different properties; relatively soft cement-lime mortar and stiff bricks or blocks, Fig F.1.

When subjected to uniaxial compression, since mortar is more flexible, it tries to expand laterally more than the bricks. Because the mortar and brick are bonded together the mortar is therefore subjected to lateral confining stresses as shown in Fig F.1. Conversely, the masonry units are subjected to tangential edge forces producing an internal state of stresses which consists of lateral tension coupled with axial compression. When masonry units are rather slender, the edge forces will be concentrated nonuniformly over a short distance from the edge of the unit as shown in Fig F.1(b). This has been concluded also in the 3rd paragraph of Section 3.2.3. The distribution of edge forces has been studied also by Khoo et al[72].

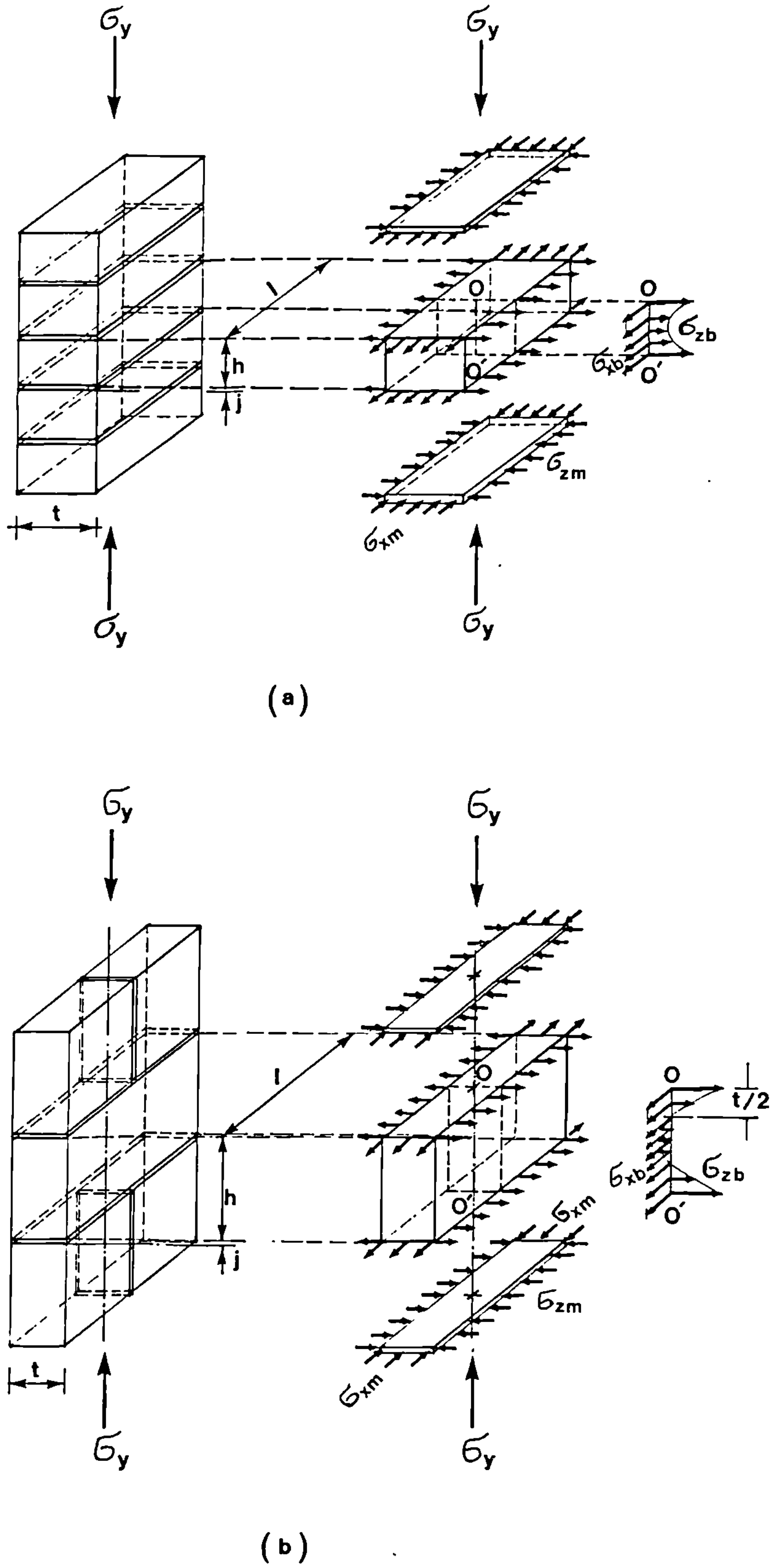

Figure F.1 Stress Distribution within The Components of Masonry under Uniaxial Compression; (a) brickwork and (b) blockwork

Experiments of Khoo et al[72] on mortar and brick showed that mortar in masonry undergoes significant non-linearity and plasticity with no sign of crushing while bricks remain almost linear and elastic before failing by vertical cracks or spalling. Two categories of failure theory have been established for masonry (with emphasis on brickwork) using either the stiffness or strength parameters of the unit and joint materials. These and a newly proposed method are discussed in the following sections.

F.2.2 Compressive Strength of Masonry using the Stiffness Parameters of Masonry Materials

The elasticity equations for joint and unit, Fig F.1, can be combined with equations of equilibrium between the two masonry constituents. This combination results in the lateral stresses as a function of vertical stress, σ_y, as follows:

$$\sigma_{xb} = \sigma_{zb} = \frac{\nu_b - \nu_m\left(\dfrac{E_b}{E_m}\right)}{(1-\nu_b) + (1-\nu_m)\left(\dfrac{E_b}{E_m}\right)\left(\dfrac{h}{j}\right)}\,\sigma_y \qquad \text{(F.1)}$$

where $\mathbf{E}$ and ν values are the secant elastic modulus and the Poisson's ratio of the indicated material at the stress level in question, subscripts $\mathbf{b}$ and $\mathbf{m}$ indicate the unit and the joint material respectively. This equation was first derived by Francis et al[82] in 1971. Combination of this equation with a linear tension-compression failure criterion for brick, Fig 4.26, leads to the uniaxial compressive strength of masonry written as:

$$\sigma_{bw} = \left[\frac{1}{\sigma_{cb}} + \frac{1}{\sigma_{tb}} \cdot \frac{\nu_b - \nu_m\left(\frac{E_b}{E_m}\right)}{(1-\nu_b) + (1-\nu_m)\left(\frac{E_b}{E_m}\right)\left(\frac{h}{j}\right)} \right]^{-1} \tag{F.2}$$

where σ_{cb} and σ_{tb} are the unconfined uniaxial compressive and direct tensile strengths of the masonry unit respectively.

In 1983, a similar formula to Eq F.1 was suggested by Atkinson(83) for incremental changes of stresses in which the **E** and ν terms were replaced by E_t and ν_t so as to indicate the tangential values. These values were considered to be functions of the current stresses. Scott McNary et al(84) found that the strength predictions resulting from the above incremental method are roughly 30% lower than corresponding experimental results.

The author believes that this discrepancy is likely to be due to assuming a uniform Poisson's ratio in all directions. If however this is rectified, Eq F.1 in its incremental form becomes:

$$\Delta\sigma_{zb} = \frac{\nu^*_{zyb} - \nu^*_{zym}\left(\frac{E_{tb}}{E_{tm}}\right)}{(1-\nu^*_{zxb}) + (1-\nu^*_{zxm})\left(\frac{E_{tb}}{E_{tm}}\right)\left(\frac{h_e}{j}\right)} \Delta\sigma_y \tag{F.3}$$

where h_e is an effective height of the masonry unit, to be taken as the smaller of **h** or **t** so that the effect of slender masonry units on the lateral displacement equilibrium is accounted for, Fig F.1. ν^*_{zxb} and ν^*_{zxm} are almost constant and equal to their initial values, ν_b and ν_m, respectively. This can be verified from Eq 4.64 and the fact that σ_{zb} approximately equals σ_{xb}

Combining the secant version of Eq F.3 with a linear tension-compression failure criterion leads to Eq F.4 as follows:

$$\sigma_{bw} = \left[\frac{1}{\sigma_{cb}} + \frac{1}{\sigma_{tb}} \frac{\nu_b - \nu_m\left(\frac{E_b}{E_m}\right)}{(1-\nu_{b0}) + (1-\nu_{m0})\left(\frac{E_b}{E_m}\right)\left(\frac{h_e}{j}\right)} \right]^{-1} \tag{F.4}$$

This proposed equation replaces Eq F.2. A rough comparison of the masonry strength calculated by Eq F.4 and the experiments of Scott McNary et al[84] leads to a fair agreement, within only $\pm$10% difference. An accurate comparison was not possible since the modulus of elasticity and the Poisson's ratio of brick had not been reported by Scott McNary et al[84].

F.2.3 Compressive Strength of Masonry using the Strength Parameters of Masonry Materials

An alternative approach to deriving masonry strength was proposed in 1969, by Hildorf[85]. In this method the multiaxial compression failure criterion of mortar and a simplified compression-tension failure criterion for brick were combined. This approach was taken up by Khoo et al(72) who, experimentally, established and refined the two failure criteria for brick and mortar as follows:

$$\frac{\sigma_y}{\sigma_{cb}} = 1 - \left(\frac{\sigma_{zb}}{\sigma_{tb}}\right)^{0.546} \tag{F.5}$$

$$\frac{\sigma_y}{\sigma_{cm}} = 1 + 2.91\left(\frac{\sigma_{zm}}{\sigma_{cm}}\right)^{0.805} \tag{F.6}$$

where σ_{cm} denotes the unconfined uniaxial compressive strength of mortar. They derived a failure criterion for compressive strength of brickwork by combining these equations with the equilibrium condition of the unit-joint interface forces *as shown in Fig F.1(a) and written as* follows:

$$\sigma_{zb} = -\frac{J}{h}\,\sigma_{zm} \tag{F.7}$$

This approach agreed fairly well with the experimental results(78) and seems to be more convenient than Eq F.4, because only the strength parameters of the masonry components are involved.

In the following section this approach is generalized so as to be applicable to all types of masonry including blockwork.

F.2.4 Proposed Generalized Approach for predicting the Compressive Strength of Masonry

The approach described in Section F.2.3 can be generalized by replacing the compression-tension failure criteria of brick Eq F.5 with the proposed compression-tension failure criteria for brittle materials, Eq 4.35, as follows:

$$\left(\frac{\sigma_y}{\sigma_{cb}}\right)^2 + \left(\frac{\sigma_{zb}}{\sigma_{tb}}\right)^2 + A\left(\frac{\sigma_y}{\sigma_{cb}}\right)\left(\frac{\sigma_{zb}}{\sigma_{tb}}\right) = 1 \tag{F.8}$$

The value of **A** can be adjusted to fit the masonry unit material in question. For a typical solid fired brick **A** = 5 gives the best agreement with the experiments of Khoo et al[72]. For concrete block masonry, **A** can be adjusted to fit the experimental data of the block material. If such data are not available, **A** can be calculated from Eq 4.36. The value of **A** varies from 0.25 to about 0.5 for weak to strong blocks.

The effect of non-uniform tensile stress distribution within the masonry unit may also be accounted for by replacing **h** in Eq F.7 by the effective height of the unit, h_e, and writing:

$$\sigma_{zb} = - \frac{J}{h_e} \sigma_{zm} \tag{F.9}$$

where h_e is to be taken as the smaller of **t** and **h**, Fig F.1.

Combination of Eqs. F.6, F.8 and F.9 leads to the failure criteria of masonry in compression as follows.

$$\left(\frac{\sigma_{bw}}{\sigma_{cb}}\right)^2 + AK\frac{\sigma_{bw}}{\sigma_{cb}} + K^2 = 1$$

or

$$\frac{\sigma_{bw}}{\sigma_{cb}} = -0.5AK + \sqrt{0.25A^2K^2 + (1-K^2)} \qquad (F.10)$$

where

$$K = \frac{\sigma_{zb}}{\sigma_{tb}} = 0.2653\alpha\beta\left[\left(\frac{\sigma_{bw}}{\sigma_{cb}}\right)\frac{1}{\beta} - 1\right]^{1.2422} \qquad (F.11)$$

and

$$\alpha = \left(\left|\frac{\sigma_{cb}}{\sigma_{tb}}\right|\right)\frac{J}{h_e} \qquad \text{and} \qquad \beta = \frac{\sigma_{cm}}{\sigma_{cb}} \qquad (F.12)$$

The compressive strength of masonry, σ_{bw}, can be calculated from Eq F.10 and Eq F.11 using a simple trial and error procedure or, using a more advanced numerical approach, such as the Newton-Raphson method. The above criterion has been plotted in Figs F.2(a to e). These charts can be used directly or to obtain the first estimate for the numerical approach chosen.

The proposed equations agree well with the actual behaviour of brickwork since they lead to an almost identical criterion to the fairly reliable criterion proposed by Khoo et al(72). Table F.1 compares the proposed theoretical prediction (Eqs F.10 and F.11) and the experimental values of strength of brickwork tested by Scott McNary et al(84).

The charts in Fig F.2 show that for concrete block masonry the mortar/unit strength ratio has only a small effect on the strength of masonry. Such an effect is insignificant for β taking a value of 0.6 or higher. This fact discredits the simplified assumption of the tendency of the mortar to squeeze out of the bed-joints of blockwork in compression. This has been concluded also by Drysdale(78).

Table F.1 Comparison of The Proposed Calculated with Experimental Compressive Strength of Brickwork.

Strength N/mm²			α	β	Brickwork Strength N/mm²	
Brick		Mortar				
σ_{cb}	σ_{tb}	σ_{cm}			Calc.	Test (84)
60.0	6.0	36.0	2.0	0.6	48.4	48.2
		19.7		0.328	38.9	40.9
		9.5		0.158	32.0	32.5
		3.9		0.065	26.9	29.9
41.0	4.1	36.0		0.878	38.9	37.7
		19.7		0.48	30.4	34.7
		9.5		0.232	24.1	27.0
		3.9		0.095	19.7	19.7

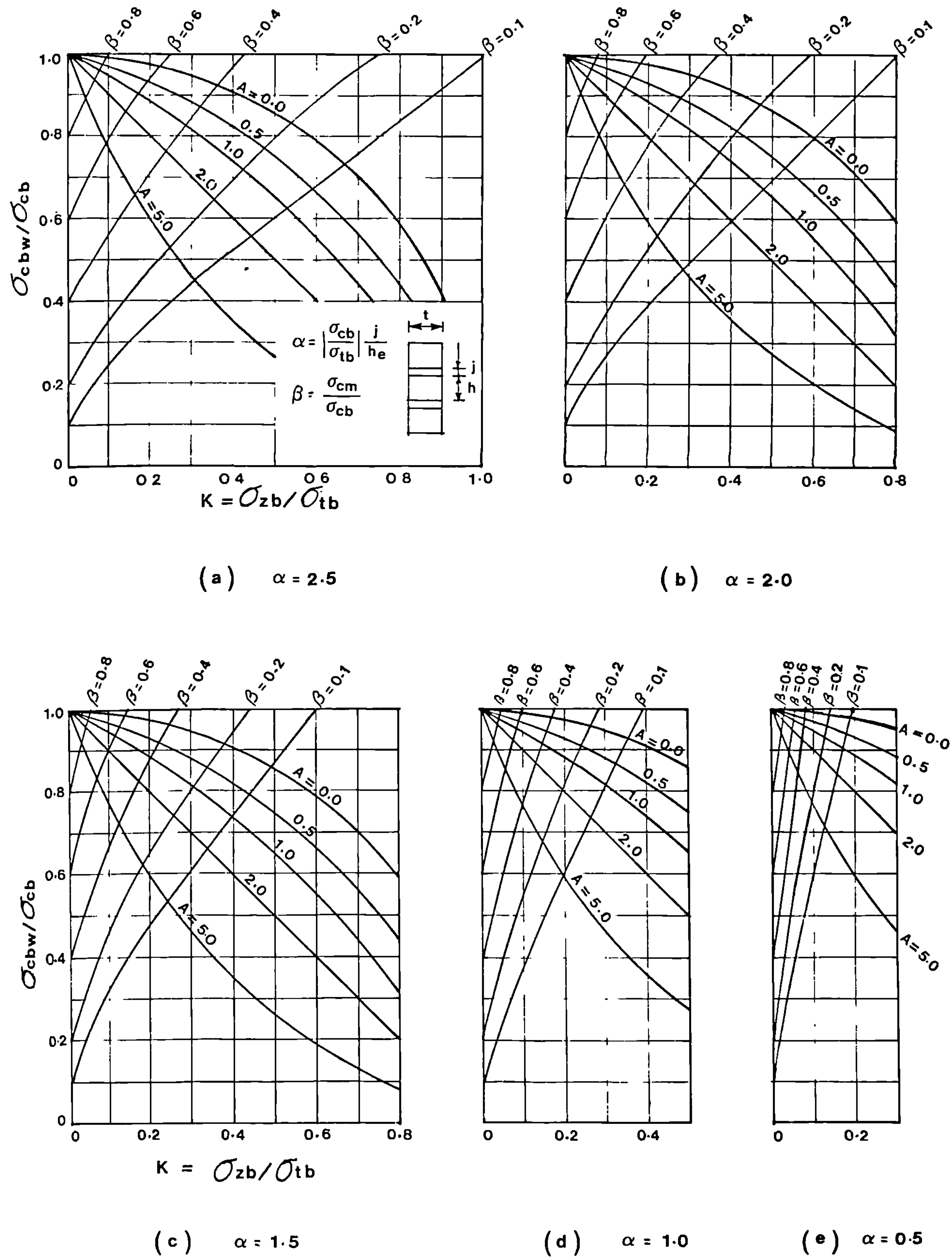

Figure F.2 Charts to Estimate the Compressive Strength of Masonry; (a) α=2.5, (b) α= 2.0, (c) α=1.5, (d) α=1.0 and (e) α=0.5.

F.2.5 Stress-strain Relationship of Masonry under Uniaxial Compression

Compression tests on brickwork have shown that its typical stress-strain curve is parabolic(31), Fig F.2. Only three major parameters: σ_{bw}, E_{bw} and ε_{cbw} are needed so that the unconfined uniaxial stress-strain curve of a given type of brickwork or blockwork can be calculated. These may be obtained either directly from a uniaxial unconfined test on masonry or can be calculated using the elastoplastic constitutive formulation proposed in the following sections.

a) Initial Modulus of elasticity, E_{bw}

The modulus of elasticity of masonry may be calculated theoretically assuming the joints and the units are under multiaxial stresses, but the approach is neither simple nor accurate. Mortar joints are bonded to masonry units and are normally under tensile stresses developed radially, within the plane of the joint, as a result of shrinkage. Such tensile stresses prevent the confining stresses from developing within the unit at early stages of loading. Therefore a realistic tangential modulus of elasticity may be calculated on the basis of adding up the flexibility of the masonry units and the bed-joints as follows:

$$\frac{h + J}{E_{bw}} = \frac{J}{E_m} + \frac{h}{E_b}$$

Hence

$$E_{bw} = \frac{h + j}{j/E_m + h/E_b} \qquad (F.13)$$

b) Compressive Strength, σ_{bw}

The compressive strength of masonry can be calculated from Eq F.10 and F.11 or directly from the charts in Fig F.2.

c) Strain at the Peak Uniaxial Compressive Stress, ε_{cbw}

The masonry vertical strain corresponding to the peak compressive stress, ε_{cbw}, may be obtained from a displacement controlled unconfined compressive test. Alternately, if the mechanical properties of mortar and unit are known or can be estimated, the strain at peak load, ε_{cbw}, can be calculated by summing the contribution for the units and the mortar joints as follows:

$$\varepsilon_{cbw} = \frac{h\varepsilon_{cu} + J\varepsilon_{cj}}{h + J} \qquad (F.14)$$

Where ε_{cu} and ε_{cj} are the strains at the peak stress normal to the bed-joints for unit and bed-joint materials respectively while they are bonded together. They can also be calculated in terms of the peak vertical and lateral stresses by use of the constitutive formulation proposed for brittle materials (Eqs. 4.57 to 4.62). The lateral stresses within the masonry unit and mortar joint are calculated from Eq F.11 and F.9 respectively.

F.3 Masonry Subjected to In-plane Stresses

F.3.1 Historical Review

The behaviour of masonry under in-plane stresses has been studied in the past by many researchers (79,81,86,88,89,90). There has been a number of attempts to develop failure criteria for masonry to be used in the Finite Element analysis. Page[(79)], 1978, incorporated his experimental data on model brickwork into a finite element analysis of a masonry wall on a beam up to the occurrence of the first crack. In 1981, Hamid et al[(90)] established a set of criteria for failure of grouted and ungrouted blockwork taking into consideration the anisotropic nature of the composite material. Dhanasekar et al[(88)], 1985, developed a set of criteria for failure of brickwork masonry using the experimental data provided by Page[(87)]. Since each of the above attempts was specific to a particular masonry type and material properties, a new formulation has been established for the present study described in the following sections.

F.3.2 General Considerations

The following modes have been observed and classified for failure of brickwork under biaxial stresses[(79)], Fig F.3.

i) cracking of masonry units.

ii) lateral splitting of masonry units

iii) plastic shear deformation of bed joints

iv) bond failure at unit-joint interfaces followed by slip and/or separation

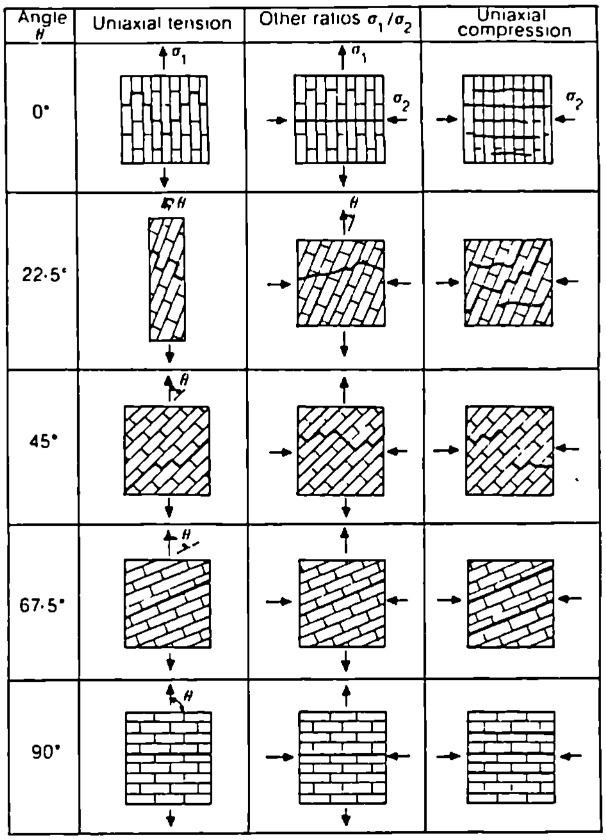

(a)

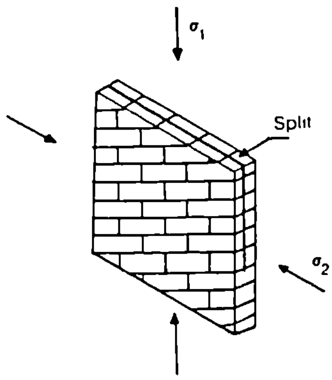

(b)

Figure F.3 Modes of Failure of Masonry in Biaxial Tests; (a) biaxial loading and (b) biaxial compression (after Dhanasekar et al[88])

These failure modes reveal that at least three failure criteria must be sought with respect to the three masonry strength contributors; masonry unit, joint and the joint-unit interface. The third and fourth classified failure modes have been discussed in Section 4.10. The first two failure modes, however, must be studied while assuming the third and fourth modes (interface failure) are somehow prevented.

Determination of the strengths of the elements of masonry while subjected to plane stresses are a very complex problem to deal with theoretically. Previous attempts have been purely empirical and covered only a limited range of masonry types and properties. With some simplifications, however, it has been possible to use an analytical approach to develop a set of proposed criteria for failure of a wide range of masonry types and properties, step by step from a simple to more general and complicated plane stress loading examples as follows.

F.3.3 Masonry under Compression and Shear

Assume a masonry element subjected to compression and shear, σ_n and τ, as shown in Fig F.4(b). If the masonry units and mortar joints are independently free to move laterally, their failure criterion in the σ_n - τ plane can be derived as described below.

The failure criterion of brittle materials in terms of principal compression-tension stresses is given by Eq 4.35. This equation may be divided by σ_c^2 throughout and rearranged to give:-

$$\left(\frac{\sigma_3}{\sigma_c}\right)^2 + \left(\frac{\sigma_c}{\sigma_t}\right)^2\left(\frac{\sigma_1}{\sigma_c}\right)^2 + A\left(\frac{\sigma_c}{\sigma_t}\right)\left(\frac{\sigma_1}{\sigma_c}\right)\left(\frac{\sigma_3}{\sigma_c}\right) = 1 \qquad (F.15)$$

where σ_c and σ_t denote the unconfined compressive and direct tensile strengths respectively and σ_1 and σ_3 are the most tensile and the most compressive principal stresses respectively. According to the principles of the Mohr circle, Fig F.4(d), the principal stresses can be related to σ_n and τ as:

$$\frac{\sigma_3}{\sigma_n} = 1/2 + \sqrt{1/4 + B^2} \qquad (F.16)$$

$$\frac{\sigma_1}{\sigma_n} = 1/2 - \sqrt{1/4 + B^2} \qquad (F.17)$$

where:

$$B = \left|\frac{\tau}{\sigma_n}\right| = \frac{R\tau}{-\sigma_n} \qquad (F.18)$$

Substituting for σ_3 and σ_1 from Eqs. F.16 and F.17 into Eq F.15 leads to:

$$\frac{\sigma_n}{\sigma_c} = \left[0.5+B^2+\sqrt{0.25+B^2} + \gamma^2\left(0.5+B^2-\sqrt{0.25+B^2}\right) + A\gamma B^2\right]^{-0.5} \qquad (F.19)$$

where:

$$\gamma = \left|\frac{\sigma_c}{\sigma_t}\right| \qquad (F.20)$$

The shear strength corresponding to $\sigma_n=0$, ie. τ_0, can also be calculated by dividing Eq F.19 by B^2 and putting the $1/B$ terms to zero to lead to:

$$\left|\frac{\tau_0}{\sigma_c}\right| = \left(1 + \gamma^2 + A\gamma\right)^{-0.5} \tag{F.21}$$

The above criterion, Eq F.19, is plotted by broken lines in Fig F.4(a) for the unit and mortar of a brickwork example.

Now consider that the masonry units and mortar joints are laterally confined by each other by frictional resistance of their interfacing planes. This requires that the proposed failure criteria to be modified. The modified failure surfaces must satisfy the following conditions:

i) The masonry units and joints when the masonry wall is under pure shear (i.e. σ_n=0) are not subjected to any confinement. They behave like two separate materials under the applied shear stress. Therefore the shear strength of the masonry components in question at σ_n=0 equals the shear strength of the same material in the unconfined situation, τ_{0b} and τ_{0m} in Fig F.4(a).

ii) When the masonry wall is subjected to normal stress only (i.e. τ= 0) its components, unit and joint, may be assumed to fail at the same stress level by tensile cracking and compression respectively. The uniaxial compressive strength of masonry, σ_{bw}, applies for this case. The uniaxial compressive strength of masonry has already been discussed in Section F.2.4.

The curves representing the failure criterion of the confined masonry unit and joint may still be simulated by Eq F.20. But the corresponding **A** values must be adjusted so as to satisfy the conditions set up above. The failure surfaces are then written as:

a) For Masonry unit:

$$\frac{\sigma_n}{\sigma_{bw}} = \left[0.5+B^2+\sqrt{0.25+B^2} + \gamma^2_{bm}\left(0.5+B^2-\sqrt{0.25+B^2}\right)+A_{bm}\gamma_{bm}B^2\right]^{-0.5} \tag{F.22}$$

b) For joints:

$$\frac{\sigma_n}{\sigma_{bw}} = \left[0.5+B^2+\sqrt{0.25+B^2} + \gamma^2_{mm}\left(0.5+B^2-\sqrt{0.25+B^2}\right)+A_{mm}\gamma_{mm}B^2\right]^{-0.5} \tag{F.23}$$

where,

$$\gamma_{bm} = \left|\sigma_{bw}/\sigma_{tb}\right| \quad \text{and} \quad \gamma_{mm} = \left|\sigma_{bw}/\sigma_{tm}\right|$$

The adjusted **A** values, A_{bm} and A_{mm} can be determined by allowing for a very small value for σ_n and substituting for $\tau=\tau_{0b}$ and $\tau=\tau_{0m}$ from Eq F.21 into Eqs F.22 and F.23 respectively as follows:

$$A_{bm} = \frac{1}{\gamma_{bm}}\left[\left(\frac{\sigma_{bw}}{\sigma_{cb}}\right)^2(1+\gamma_b^2+A_b\gamma_b) - 1\right] - \gamma_{bm} \tag{F.24}$$

$$A_{mm} = \frac{1}{\gamma_{mm}}\left[\left(\frac{\sigma_{bw}}{\sigma_{cm}}\right)^2(1+\gamma_m^2+A_m\gamma_m) - 1\right] - \gamma_{mm} \tag{F.25}$$

The **A** values for the brickwork example shown in Fig F.4 become:

$A_{bm} = 3.0618$ and $A_{mm} = 0.482$

The confined brick and mortar failure criteria, Eq F.22 and F.23, are represented by the dash-dot curves in Fig F.4(a). The lower of the two criteria is highlighted by a heavy solid line so as to indicate the lower bound for strength. As shown these criteria characterize the two failure modes; masonry unit cracking and bed joint shear plasticity or yielding. The transition of these failure modes can be determined by combining
Eq F.22 and F.23 or combining their equivalents written for principal stresses using the format of Eq F.15, and use of the appropriate **A** and γ values from Eqs F.24 and F.25. Such a manipulation leads to the following conclusion:

i) If $|\sigma_1/\sigma_3|<\gamma$ masonry is potentially subjected to the joint yielding mode

ii) If $|\sigma_1/\sigma_3|>\gamma$ masonry is potentially subjected to the unit cracking failure mode

where:

$$\gamma = \frac{A_{bm}\gamma_{bm} - A_{mm}\gamma_{mm}}{\gamma_{mm}^2 - \gamma_{bm}^2} \qquad (F.26)$$

and σ_1 and σ_3 are the tensile and compressive principal stresses in the plane of the wall respectively.

The typical masonry unit-joint interface failure criterion is also shown in Fig F.4(a). As can be seen, the bed joint yielding mode is normally overruled by at least one of the interface inelastic events such as: debonding, slip and/or separation so that the joint yielding failure mode is restricted only to the shaded triangle shown in Fig F.4(a). Therefore the joint yielding mode may be ignored prticularly for blockwork masonry having only a small mortar and block compressive strength difference. Should one, however, desire to bring the joint yielding mode into account, this effect may be included in the adjacent interface mechanical behaviour model as discussed in Section 4.10.

This simplification reduces the masonry failure criterion to Eq F.22 while subjected to combined normal and shear stresses in the σ_n-τ plane. Such a simplified criterion may be written in the format of Eq F.15 in terms of the in-plane principal stresses as follows:

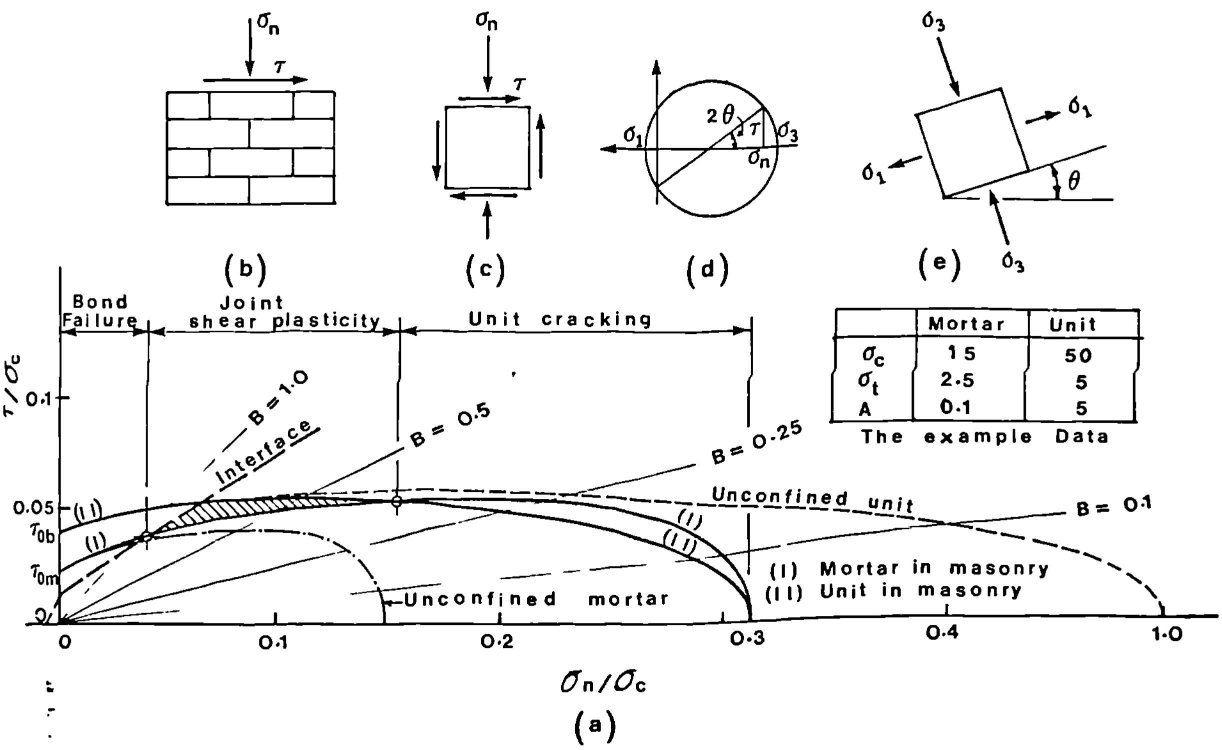

	Mortar	Unit
σ_c	15	50
σ_t	2.5	5
A	0.1	5

The example Data

Figure F.4 Masonry Subjected to Compression and Shear; (a) masonry failure criteria, (b) loading, (c) stresses, (d) Mohr circle and (e) principal stresses

$$\left(\frac{\sigma_{min}}{\sigma_{bw}}\right)^2 + \gamma_{bm}^2\left(\frac{\sigma_{max}}{\sigma_{bw}}\right)^2 + A_{bm}\gamma_{bm}\left(\frac{\sigma_{min}}{\sigma_{bw}}\right)\left(\frac{\sigma_{max}}{\sigma_{bw}}\right) = 1 \qquad (F.27)$$

where σ_{min} and σ_{max} are the compressive and tensile principal peak stresses respectively. The graphical representation of this equation is shown in Figs F.5(a,b,c).

F.3.4 Masonry under Biaxial Compression

Page[87] showed that brickwork under biaxial compression fails suddenly by splitting in a plane parallel to the free surface of the specimen at mid-thickness regardless of the bed joint angle, Fig F.3(a). However he observed that change of the orientation angle of the bed joints with respect to the applied principal stresses would alter the mode of failure from lateral splitting to one of the joint or interface failure modes only when one principal stress was very dominant.

From a complete series of biaxial tests on full scale grouted concrete masonry, Hegemier et al[81] found that the influence of the bed joint angle was insignificant and the behaviour essentially isotropic.

As shown on Figs F.5(a,b,c), the experiments of Page[87] imply that a failure criterion surface must take a bulb shape and the magnitude of the strength under equal biaxial compression is independent of the bed joint orientation. These led the author to propose Eq 4.30 as the masonry failure criterion in biaxial compression as well.

Considering the very limited experimental data available, setting $\overline{f_{bc}}$ equals unity should safely fit all types of masonry. Therefore Eq 4.30 reduces to:

$$\sigma_1^2 + \sigma_2^2 - \sigma_2\sigma_1 = \sigma_{bw}^2 \tag{F.28}$$

where σ_1 and σ_2 are the in-plane biaxial peak compressive principal stresses. Eqs. F.27 and F.28 are plotted in Figs F.5(a,b,c) to generate the complete failure criterion of masonry under plane stresses provided that the joint-unit interface failure is prevented.

F.4 Examination of the Proposed Failure Criteria

A complete failure criterion for masonry can be constructed using the following:

i) Cracking of masonry units, Eq F.27

ii) Lateral splitting of masonry units, Eq F.28 and Fig F.3(b),

iii) Plastic shear failure of bed joints, Eq 4.170

iv) *Joint-unit interface failure;*

-shear bond failure, Eq 4.168

-Tensile bond failure, Eq 4.171

These proposed failure surfaces are compared with the experimental data reported by Page[87] and others[88] in Figs F.5 to F.7 showing a good agreement. Since the proposed criterion claims to be applicable to all types of masonry, further experiments based on a variety of masonry types are needed to examine the proposed criterion further. This is not, however, possible in the current investigation.

F.5 Determination of The Stiffness Properties of Masonry Components

As discussed in Section F.1, the finite element representation of masonry required that masonry be defined as a combination of the units made of the proposed masonry masonry-equivalent material and the interfaces of these units, Fig 3.9. These two components have, each, their own specific failure criteria listed in Section F.4. They also have their own stiffness properties as determined below.

Interfaces have zero thickness. Therefore, they have, theoretically, zero flexibility - especially when they are bonded. But for the sake of economy in obtaining an acceptable convergence within a reasonable number of iterations, these interfaces must have some flexibility so that the inelastic displacements due to debonding can numerically be developed. This may simply be achieved by allowing for a small amount of flexibility for all bonded interfaces and deducting the same from the total flexibility of masonry leading to:

$$E_{ju} = \left[\frac{1}{E_{bw}} - \frac{1}{(J + h)\ K_n} \right]^{-1} \tag{F.29}$$

$$\varepsilon_{cju} = \varepsilon_{cbw} - \frac{\sigma_{bw}}{(J + h) K_n} \tag{F.30}$$

where E_{ju} and ε_{cju} denote the adjusted initial tangent modulus and the strain at peak uniaxial stress respectively for the proposed equivalent material. E_{bw} and ε_{cbw} are given by Eqs. F.13, F.14. K_n denotes the prescribed normal stiffness of the interface.

The masonry joint-unit interfaces must be given a shearing flexibility in proportion to their normal flexibility. Since the source of the interface flexibility is ordinary brittle material (mortar), the relation of the shearing and normal stiffness may be established according to the elasticity theory formulation as follows:

$$K_{s0} = \frac{K_n}{2(1 + \nu_m)} \tag{F.31}$$

where ν_m denotes the Poisson's ratio of mortar and K_{s0} signifies the shear stiffness of the interface.

To the proposed flexibility, some additional flexibility *must be added should* the *i*nterface debond and become looser. As mentioned in Section 4.10.3.2, Table 4.2 may be used as a guide if no reliable experimental data is available for this purpose.

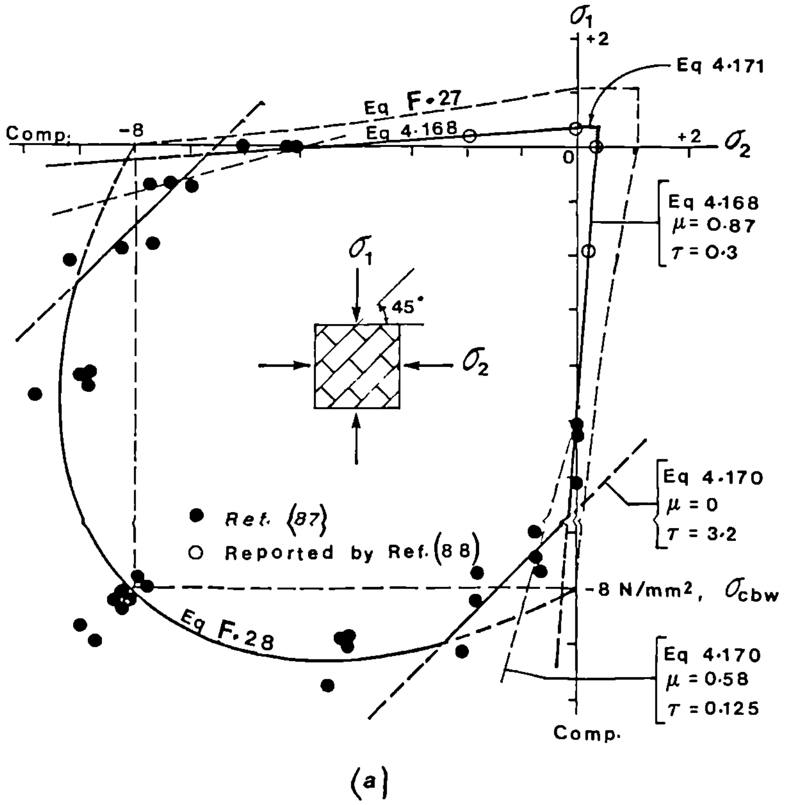

(a)

Figure F.5 Comparison of the Proposed Masonry Failure Criteria with Experimental Data; θ=45.

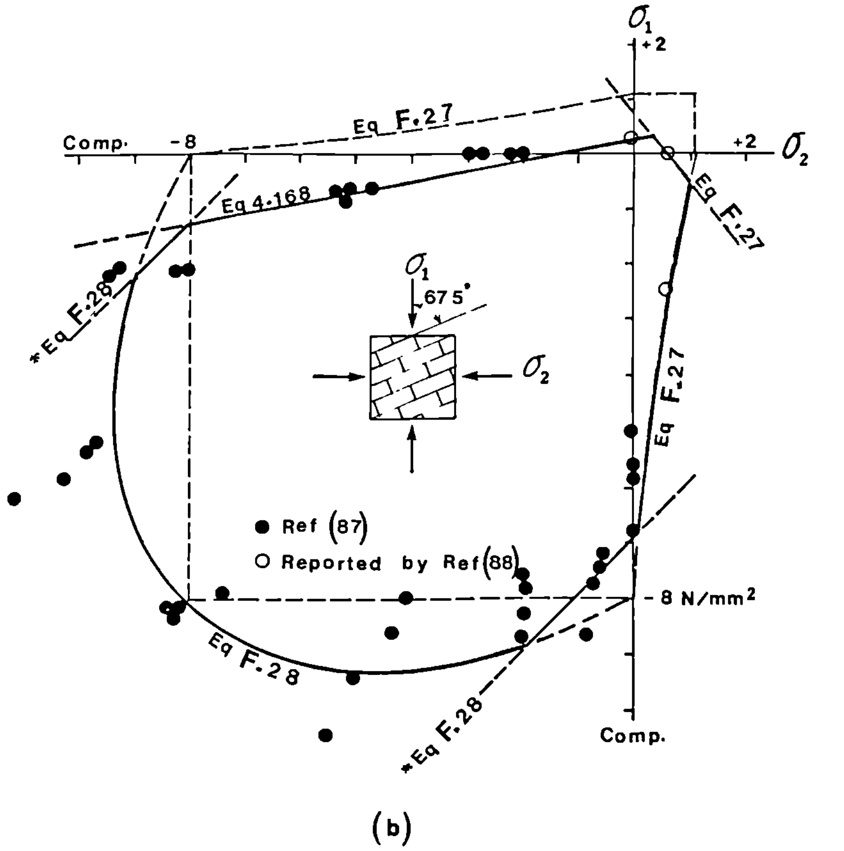

(b)

Figure F.6 Comparison of the Proposed Masonry Failure Criteria with Experimental Data; θ=67.5.

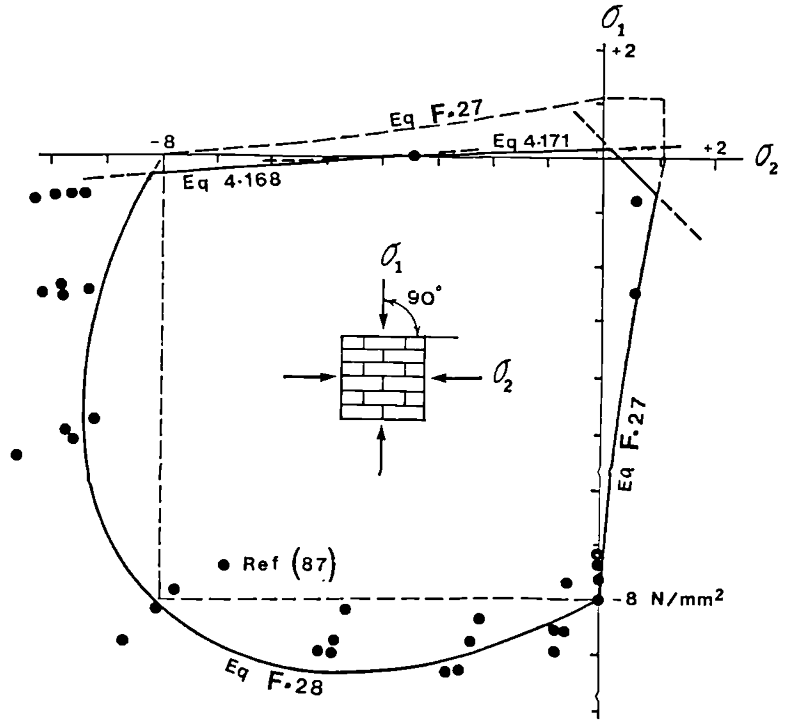

(c)

Figure F.7 Comparison of the Proposed Masonry Failure Criteria with Experimental Data; θ=67.5.